PhD-FSTC-2018-35
The Faculty of Sciences, Technology and Communication

# DISSERTATION

Presented on 25/04/2018 in Luxembourg

to obtain the degree of

# DOCTEUR DE L'UNIVERSITÉ DU LUXEMBOURG

# EN SCIENCES DE L'INGÉNIEUR

by

## Seyed Amin Sajadi Alamdari
Born on 21 September 1984 in Tabriz (Iran)

# STOCHASTIC MODEL PREDICTIVE CONTROL FOR ECO-DRIVING ASSISTANCE SYSTEMS IN ELECTRIC VEHICLES

## Defence committee:

Dr-Ing. Holger Voos, Dissertation Supervisor
*Professor, Université du Luxembourg*

Dr-Ing. Mohamed Darouach
*Professor, Université de Lorraine*

Dr. Ing. Jean-Régis Hadji-Minaglou, Vice-Chairman
*Professor, Université du Luxembourg*

Dr. Francesco Viti, Chairman
*Associate Professor, Université du Luxembourg*

Dr. Meng Wang
*Assistant Professor, Delft University of Technology*

# University of Luxembourg

## Doctoral Thesis

# Stochastic Model Predictive Control for Eco-Driving Assistance Systems in Electric Vehicles

*Author:*

Seyed Amin Sajadi Alamdari

*Supervisors:*

Prof. Dr.-Ing. Holger Voos

Prof. Dr. Mohamed Darouach

Prof. Dr.-Ing. Jean-Régis Hadji-Minaglou

*A thesis submitted in fulfilment of the requirements*
*for the degree of Doctor of Philosophy in Engineering*

*in the*

Automation & Robotics Research Group
Interdisciplinary Centre for Security, Reliability and Trust

June 2018

# Declaration of Authorship

I, Seyed Amin SAJADI ALAMDARI, declare that this thesis titled, 'Stochastic Model Predictive Control for Eco-Driving Assistance Systems in Electric Vehicles' and the work presented in it are my own. I confirm that:

- This work was done wholly or mainly while in candidature for a research degree at this University.

- Where any part of this thesis has previously been submitted for a degree or any other qualification at this University or any other institution, this has been clearly stated.

- Where I have consulted the published work of others, this is always clearly attributed.

- Where I have quoted from the work of others, the source is always given. With the exception of such quotations, this thesis is entirely my own work.

- I have acknowledged all main sources of help.

- Where the thesis is based on work done by myself jointly with others, I have made clear exactly what was done by others and what I have contributed myself.

Signed:

Date:

14 June 2018, Grand Duchy of Luxembourg

*"There was the Door to which I found no key; There was the Veil through which I might not see."*

Omar Khayyam, 1048-1131

# *Abstract*

Doctor of Philosophy in Engineering

## Stochastic Model Predictive Control for Eco-Driving Assistance Systems in Electric Vehicles[1]

by Seyed Amin Sajadi Alamdari

Electric vehicles are expected to become one of the key elements of future sustainable transportation systems. The first generation of electric cars are already commercially available but still, suffer from problems and constraints that have to be solved before a mass market might be created. Key aspects that will play an important role in modern electric vehicles are range extension, energy efficiency, safety, comfort as well as communication. An overall solution approach to integrating all these aspects is the development of advanced driver assistance systems to make electric vehicles more *intelligent*. Driver assistance systems are based on the integration of suitable sensors and actuators as well as electronic devices and software-enabled control functionality to automatically support the human driver. Driver assistance for electric vehicles will differ from the already used systems in fuel-powered cars such as electronic stability programs, adaptive cruise control etc. in a way that they must support energy efficiency while the system itself must also have a low power consumption. In this work, an eco-driving functionality as the first step towards those new driver assistance systems for electric vehicles will be investigated. Using information about the internal state of the car, navigation information as well as advanced information about the environment coming from sensors and network connections, an algorithm will be developed that will adapt the speed of the vehicle automatically to minimize energy consumption. From an algorithmic point of view, a stochastic model predictive control approach will be applied and adapted to the special constraints of the problem. Finally, the solution will be tested in simulations as well as in first experiments with a commercial electric vehicle in the SnT Automation & Robotics Research Group (SnT ARG).

---

# *Acknowledgements*

I have had the opportunity to meet, work with, and learn from a number of distinguished people who I have been impacted and indebted during my PhD. The accomplishment of this exciting and challenging journey would not be possible without their support, patience, and encouragement.

Seyed Amin Sajadi Alamdari
*Grand Duchy of Luxembourg, 2018*

# Contents

# List of Figures

# List of Tables

# Abbreviations

*Dedicated to my family, teachers, and friends . . .*

*for their love, patience, and encouragement.*

# Chapter 1

# Introduction

This thesis presents Risk-sensitive Nonlinear Model Predictive Control (RSNMPC) for Ecological Driving (Eco-driving) Advanced Driver Assistance System (ADAS) in the Battery Electric Vehicle (BEV). This chapter is structured as follows. Section 1.1 presents the research context, followed by research challenges and the motivations to conduct this study are given in Section 1.2. Section 1.3 presents the aim and scope of this study, followed by the scientific and practical contributions are presented in Section 1.4. Finally, the outline of the thesis is presented in Section 1.5.

## 1.1 Context of the Study

Development of Internal Combustion Engine (ICE) vehicles is one of the considerable achievements of modern technology. Power, performance, and the travel range of vehicles have improved tremendously with the advancement of technology to a level that they have even reshaped the city sprawl and the way people live today (Eskandarian, 2012). Like most of the other technologies, modern technology of vehicles is also associated with its own challenges in safety, energy requirement, and environmental impacts. A large number of ICE vehicles in use lead to serious problems for the environment and human life around the world. Air pollution and global warming are instances of problems of predominant concern. For instance, vehicles are responsible for around 12% of total European Union (EU) emissions of carbon dioxide ($CO_2$), given that $CO_2$ is the focal greenhouse gas contributing to environmental contamination and global warming (*European Commission* 2018).

It is now well recognised that BEV have one of the most promising powertrain technology for the predictable future transportations. A BEV uses one or more electric motors

for propulsion and electricity as the only source of propulsion energy.  The BEV has relatively interesting features in comparison to ICE vehicle alternatives.  First of all, the efficiency of the BEVs is far better than the ICE vehicles.  The BEV roughly have 80% to 95% efficiency while the ICE vehicles have 10% to 25% efficiency which means that only 1/4 maximum of the available energy are transferred to the wheels of the vehicle. Additionally, the BEVs offer the same or even better performance in comparison to the ICE vehicles, thanks to high torque at low speed of the electric motor.  Furthermore, the BEVs offer the opportunity to use different renewable energy resources.  Despite the fact that power plants have a contribution to carbon emissions, there are still different choices of getting true zero-emission electric from renewable energy sources.

Driving tactics play an important role in controlling the BEV.  Strategic decision making, manoeuvring and regulating the vehicle makes the driving a complex task.  Shaping the driving behaviour and the required skills to control a vehicle depends on many factors such as driver's age, perception and reaction capabilities, psychological abilities along with experiences.  Thanks to the rapid development of information and communication technologies, Intelligent Transportation System (ITS) can be applied in the field of road transportation and enhance the efficiency of transportation.  ITS are defined as systems that use computers, controls, communications, and various automation technologies in order to enhance safety, throughput, and efficiency of transportation while reducing energy consumption and environmental impact (Eskandarian, 2012).  In order to enhance safety, comfort, and efficiency of driving, driver assistance systems are designed to support the driver.  Interest in ADAS among a wide range of ITS applications has increased in recent years.  The ADAS refers mainly to the vehicle handling functions that an intelligent vehicle provides either autonomously or supports the driver to execute a trip including planning and reaching from origin to destination safer, more efficient, and with less harmful environmental impacts (Eskandarian, 2012).

The term *intelligent* vehicle refers to cover a specific level of machine intelligence in the scope of ADAS context.  The ADAS deals with the environment in terms of sensing and responding, the vehicle in terms of sensing and actuating electromechanical systems, and most importantly the driver in terms of augmenting information, enhancing sensing capabilities, and assisting in control functions (Eskandarian, 2012).  Autonomous and semi-autonomous ADAS are capable of sensing their environment and control the vehicle. In these vehicles, a variety of techniques are used to detect surroundings of the vehicles. Modern control systems interpret the sensory information to identify appropriate control actions.  Nowadays, available ADAS for ICE vehicles are mainly low-level closed-loop feedback control functionalities used to improve driving safety and comfort level such as the Anti-lock Brake System (ABS) or the Electronic Stability Control (ESC) (Ulsoy et al., 2012).  However, there is a trend to take over also more complex cognitive tasks of

the driver, leading to semi-autonomous driving such as Adaptive Cruise Control (ACC) and fully autonomous vehicles (Campbell et al., 2010). Cruise Control (CC), ACC and Cooperative Adaptive Cruise Control (CACC) systems are the well-established ADAS applications that automate the throttle and brake control of the vehicle to retain the pre-set longitudinal velocity while maintaining a safe distance from the preceding vehicles. The fundamental benchmark of autonomous ADAS applications are the ACC systems. The vehicle equipped with the ACC system regulates the velocity and relative distance to the preceding vehicle based on the driver's preference which can improve the driving experience and enhance traffic flow. The ACC system uses an onboard RAdio Detection And Ranging (RADAR) to measure the relative distance to the preceding vehicle in traffic and a control algorithm determines the proper throttle and brake actuation to regulate the velocity and the relative distance to the preceding vehicle. The handling and safety of road vehicles can be improved by modern control technologies.

Control technologies of the ADAS play an important role in safety and efficiency of the intelligent vehicles. There are multiple design objectives in the ADAS controller design which some of these objectives are contradictory. For instance, the trade-off challenge between the reference tracking and the control input effort. In addition, the ADAS controller has hard constraints such as actuators limit and soft constraints such as safety limits that need to be considered. The only advanced control methodology, which has made a significant impact on industrial control engineering, is predictive control (Maciejowski, 2002). The main reasons for its success are handling multivariable control problem, taking account of actuator limitations, and operating the system close to constraints. The Model Predictive Control (MPC) is a control framework that usually results in a constrained Optimal Control Problem (OCP) to optimise multiple performance criteria under different design constraints (Eskandarian, 2012).

The main components in a conventional MPC are the system model dynamics, a value function, the system constraints, a state estimator, and an algorithm to solve the OCP. A mathematical model of the process is used to formulate the OCP and to predict the effects of the future control inputs. Due to the computational complexity of the OCP, the MPC has been applied mainly for *slow* dynamic systems, such as the chemical and process industry. During the last decades, however, several developments including modern computing hardware have allowed using these methods also for *fast* dynamic systems with a growing interest for automotive applications (Re et al., 2010). Meanwhile, requirements on intelligent vehicles in terms of safety, efficiency, and performance have experienced a similar increase. The MPC seems a suitable method to exploit the potentials of modern concepts and to fulfil the automotive requirements since most of them can be stated in the form of a constrained Multi-Input Multi Output (MIMO) OCP and the MPC provides an approximate solution of this class of problems (Re et al., 2010).

## 1.2    Problem statement and Motivation

Battery is the core component of an Electric Vehicle (EV). The BEVs have limited onboard energy capacity, which limits their cruising range on a single charge. This limitation is also known as *range anxiety*, which generally reduce the share of BEVs in the automotive market. The recent and future performance improvement of the battery technology will be definitely a game changer. Great investigations and endeavour with the aim of elaborating performance of battery to meet the BEV's requirements have been initiated. The current EV battery has relatively low energy density, which directly affects the maximum all-electric drive range of the EV (Yong et al., 2015). However, most of these advances have failed to commercialise and are not foreseen to become available in near future. Despite the fact that ranges are being extended, the BEVs still are not able to reach the same opportunities offered by ICEs, especially for long-haul trips. Therefore, in addition to battery research, current research and development of the BEVs remarkably focus on various ways of saving energy consumption that lead to extending the cruising range of BEVs.

Improvement of performance and energy efficiency is a challenging task where three energy conversion steps are generally investigated for the energy efficiency of the transportation. The grid level improvement known as *grid-to-tank*, which converts stationary distribution nodes to an onboard storage. Considering the component level or the system control level, *tank-to-wheels* efficiency can improve propelling the vehicle by converting the onboard energy to mechanical energy. The *wheels-to-distance* enhancement, considers the influence of the vehicle parameters and the driving strategies, which is in support and motivation of this study. Environmentally friendly vehicles and ecological driving are highly demanding for efficient utilisation of energy resources and reduction of energy consumption in road networks (Md Abdus Samad Kamal et al., 2013). A wide variety of factors such as the driving style, the BEV energy consumption characteristic map, its aerodynamic drag, the road slope with upcoming curves, traffic speed limits, the road visibility, dynamic of traffic flow, temperature, as well as weather conditions have a significant impact on the energy consumption of the BEV. The goal of Eco-driving is to adapt the driving strategy to an energy-aware driving strategy.

Apart from performance efficiency considerations, traffic and transportation are a major cause of safety and environmental problems. The total number of road traffic deaths worldwide remains high at 1.25 million per year with the highest road traffic fatality rates in low-income countries indicated by World Health Organization (WHO). A total of 26, 100 people died in 2015 from road traffic injuries in the EU reported by the European Commission. For every death on Europe roads, there are an estimated 4 permanently disabling injuries such as damage to the brain or spinal cord, 8 serious injuries and

50 minor injuries (*European Commission* 2018). Many lives have been saved thanks the introduction of different automotive ADAS. Moreover, energy requirements and environmental impacts are another major challenge that the transportation system is facing. Encouraging drivers towards Eco-driving can reduce energy consumption. In order to achieve the energy efficient driving strategy, a driver has to consider different factors such as the BEV dynamics, its energy consumption characteristic map, the road slopes, the road curves, and the traffic situations in an anticipated driving manner. However, drivers do not always and under all circumstances drive ecologically. Moreover, driver's Eco-driving mental workload is still high which may lead to their distraction (Rouzikhah et al., 2013). On the one hand, utilising automatic ADAS can support drivers in various driving tasks.

The anticipatory driving based ADAS applications can reduce the energy consumption by predicting earlier the possible situations. The ADAS applications have a high potential to improve the safety and efficiency of the transportation network. However, there are several challenges in ADAS applications such as design and development of control methods and impact of ADAS on transportation efficiency. For instance, the ACC systems for the BEVs are incapable of *ecologically* regulating the velocity and relative distance to the preceding vehicle which leads to an increased energy consumption. Commercial CC and ACC systems typically operate in limited speed range and expect drivers to actively monitor the longitudinal performance and the driving environment in order to take over the control whenever necessary (Eskandarian, 2012). Moreover, the ACC systems are inadequate in dealing with hilly and curvy roads with traffic signs information where the driver has to intervene and take back control of the throttle and brake pedals. An enhanced ADAS application with the Eco-driving strategy is considered to be one of the most cost-effective methods in ITS to improve the road safety and environment-friendly driving style. Utilising available technologies to assist drivers by enhancing handling, safety, efficiency, and the comfort of driving with environmentally friendly impacts is the main goal of the intelligent vehicles. Improving the wheels-to-distance efficiency by controlling the driving profile reveals its potential when considering that it does not require structural changes to the system (Sciarretta et al., 2015).

Several concepts attempt to implement the predictive Eco-driving in a more rigorous framework. In these concepts, the Eco-driving is regarded as the OCP where the drive commands minimise the energy consumption for a given trip (Sciarretta et al., 2015). The MPC, also known as receding horizon optimal control, has been an attractive approach in comparison with alternative methods of multivariable control (D. Q. Mayne, 2014). The OCP is solved repeatedly in a receding horizon principle and the first element in a sequence of finite control actions is applied to the system at each sampling time. For instance, several works of literature related to the predictive controller for the Eco-CC,

the Eco-ACC, and the Eco-CACC systems can be found. The introduced MPCs can be categorised into various groups. In linear MPC, system model dynamics and constraints are linear functions. Nonlinear Model Predictive Control (NMPC) is distinguished by the use of non-linear system models in the OCP to improve performance specifications. Parametric uncertainties and exogenous disturbances are pervasive features of complex dynamical systems. For instance, high entropy in traffic system leads to a challenging task to derive a computationally efficient and tractable model to predict the traffic motion flow. If unexpected events in the traffic such as lane change of other vehicles are not considered in the prediction, the efficiency of the MPC might dramatically decrease.

Linear Robust Model Predictive Control (RMPC) has been effectively utilised for systems with uncertainties. In RMPC, the worst-case based design may lead to conservative control actions and low system performance. Stochastic Model Predictive Control (SMPC) has been introduced as a stochastic alternative to address the shortcomings of the RMPC. The SMPC is based on the stochastic uncertainty of a process model and generally formulated as an expectation of the objective function with probabilistic constraints, so-called *chance-constraints*. Even though the Stochastic Nonlinear Model Predictive Control (SNMPC) has been introduced to improve the shortcoming of the SMPC and has shown promise to balance the conservatism in decision making with robustness to uncertainties, it has received relatively little attention in works of literature. There are several limitations, which prevent the application of the SNMPC. For example, computational complexity limit the real-time applicability. Moreover, most of the mentioned SNMPCs are based on risk-neutral performance measures, which may not be a suitable control strategy for the safety-critical ADAS applications. Beside, assumed fix risk allocation leads to the conservative solution for the feedback design. An advanced real-time risk-sensitive optimal control algorithm has high potential to meet the specific requirements of the semi-autonomous Eco-ADAS applications for the BEVs to extend its cruising range, which is the main motivation of this study.

## 1.3   Aim and Scope

The aim of this study is to develop an exhaustive optimal energy management system in order to address the cruising range challenge of the BEV that supports ecological driving. From the control engineering perspective, RSNMPC is the promising approach to realize the semi-autonomous ecological driving in the BEVs. Similar to the conventional ACC systems, the driver pre-sets the desired velocity with preferred safe distance from the preceding vehicle in this system. The semi-autonomous Ecological Adaptive Cruise Control (Eco-ACC) system predictively regulates the velocity with respect to the

longitudinal motion of the BEV dynamics, its energy consumption characteristic map, road geometric navigation and traffic sign information, as well as the plausible motion of the preceding vehicle. While the driver handles the steering control of the vehicle, this system should plan a proper safe and energy-efficient cruising velocity profile autonomously for the entire trip without requiring the driver's interventions. In addition, the proposed Eco-ACC system should be able to operate at full-range speed assistance and handles the cut-in/out scenarios.

In order to reach the objectives of this study, the following research questions will be addressed:

1. What are the most effective factors that influence on the BEV's cruising range?

2. Which ADAS concepts can be utilised to improve the safety and energy efficiency of the BEVs?

3. How to enhance the performance of the ACC systems for the BEVs?

4. How to formulate the controller of the proposed Eco-ACC system in the OCP?

5. How should the control system be modelled?

6. How to deal with uncertainties of the Eco-ACC system in the OCP?

7. How to enhance the tradeoff challenge between the performance and the robustness of the controller?

8. Which approaches have prospects to solve the obtained OCP in a real-time manner?

9. What are the performance indexes to evaluate the Eco-ACC system and its impact on the BEV's cruising range?

10. How does the proposed Eco-ACC system perform on the BEV under various driving and traffic situations?

11. What are the impacts of the Eco-ACC system on safety and cruising range of the BEV?

A three-step is taken to answer the research questions. The first step is to review the works of the literature to identify the state-of-the-art and knowledge gap on the ADAS concepts as well as principle system design and their impact on the safety and energy efficiency of the BEV. This step answers research questions 1-3. In the second step, the overall control system is derived in the domains of SNMPCs and fast optimisation

approaches. A real-time stochastic optimal control framework based on the SMPC theory for the proposed Eco-ACC is developed. This system is based on the ACC system with extended functionalities to deal with the hilly and curvy roads with traffic signs information. The main source of the system uncertainty in this study is the unknown behaviour of the preceding vehicle in traffic network. Different approaches to handle the system uncertainties are reviewed and a real-time RSNMPC with generic numerical solution algorithm is proposed.

The overall route is provided by the navigation system including 3D terrain information. The optimisation algorithm will compute the safe and ecological velocity profile in a way that the overall energy consumption of the BEV is minimised along the route. For that purpose, dynamics of the BEV, as well as its energy consumption model, will be identified. In addition, the road profile is modelled regarding the upcoming route slopes, curves, and traffic sign information. This information will also be used to introduce a physical-statistical model of the preceding vehicle motion. From a control algorithm point of view, it is important to develop an efficient algorithm that delivers robust optimisation results in real-time including a nonlinear dynamics and chance-constraints without demanding too high computational power. This step answers research questions 4-8. In the third step, the proposed Eco-ACC system with RSNMPC is applied and tested on the BEV. The performance and impacts of the Eco-ACC on safety and cruising range of the BEV are evaluated under different scenarios using the numerical simulation tests and field practical experiments. This step answers research questions 9-11.

The target of this study is the ADAS applications for the BEV on motorway traffic due to fewer interruptions caused by e.g., traffic lights. The assumed traffic conditions are motorway with moderate traffic where stop&go phases are also considered. The proposed semi-autonomous ADAS application with limited capability to sense the surrounding environment has low efficiency in urban traffic situations and driver intervention might be required. Moreover, the main focus of the ADAS applications is based on the ACC system with extended functionalities. The automatic steering control manoeuvres such as lane changes as well as overtaking are not considered and the driver has the responsibility for these steering manoeuvres. Moreover, the proposed system depends on the road map information that requires driver's intervention if it is not provided. From a methodological perspective, this study focuses on the real-time RSNMPC for safe and ecological driving in the BEV using the Eco-ACC system to improve the cruising range. In this study, all the driving situations are not covered by the proposed Eco-ACC system and an emergency braking system is developed to overcome its limitations and ensure the safety in critical situations. Furthermore, other aspects of the ITS and the ADAS applications applied to the BEVs are not considered and the SNMPC algorithms that are computationally expensive are not in the main spotlight of this study.

## 1.4   Significance of the Study

The main contributions of this study to the field of the SNMPC and ADAS applications in BEV is highlighted in this section.

1. *Integration and extension of the ACC system with ecological driving strategies for the BEVs.*
   The energy consumption characteristic map of a BEV is identified and the ACC system is extended with ecological driving techniques for the BEV to address the limited cruising range challenge.

2. *Development of a full-range ACC system with enhanced functionalities.*
   An extended ACC system with Stop&Go functionalities that is also able to deal with the hilly and curvy roads as well as taking the traffic signs information into account is introduced.

3. *Road geometries and static traffic information are modelled.*
   Mathematical models which describe the road geometries and traffic sign information are modelled as the differentiable and continuous functions.

4. *Statistically accurate traffic motion estimation.*
   Traffic motion flow especially the preceding vehicle plays a significant role in the energy efficiency of the BEV. A novel physical-statistical motion model for the preceding vehicle is introduced.

5. *Review of stochastic OCPs and different methods to handle the chance-constraints.*
   Various types of the stochastic OCPs with chance-constraints is reviewed. Different methods to handle the chance-constraint and trade-offs of each technique are presented.

6. *Reduced conservativeness for the stochastic OCPs.*
   A method is developed to improve the risk allocation of the chance-constraints based on taking advantage of the feedback design. The presented method enhances the tradeoff challenge between the performance and the robustness.

7. *An economic penalty function for the nonlinear OCPs is presented.*
   In many practical NMPC applications, which consider the energy-efficiency, the presented economic penalty function for the OCPs is a suitable approach.

8. *Extended softening approach for inequality constraints handling methods.*
   A novel efficient computational method handling inequality constraint with a softening approach based on Nonlinear Complementarity Problem (NCP) is presented.

9. *A real-time RSNMPC is introduced.*
   By applying the methods presented in this study, a real-time RSNMPC for the proposed Eco-ACC system is introduced to address the shortcoming of the risk-neutral and computationally expensive SNMPC algorithms.

10. *Practical implementation and real-time field experimental demonstration.*
    The proposed different types of the RSNMPC are applied on the Eco-ACC system and solved in real-time to plan the energy efficient velocity profile of the BEV in various traffic situations. The introduced solution methods improve the energy efficiency of the BEVs and extend their cruising range.

## 1.5 Outline of the Thesis

This thesis consists of six further chapters, which some of these chapters are based on published material.

In Chapter 2 the works of literature review related to the BEVs, the fundamental longitudinal dynamics of the BEVs, and factors that effect on the energy consumption of the BEV are presented. In addition, an energy consumption characteristic map for a commercial BEV as the main contribution of this chapter is introduced with high coefficient of determination.

Chapter 3 presents the works of literature review related to the ADAS, ACC systems, and ecological driving strategies. In this chapter, the proposed Eco-ACC system for optimal energy management of the BEV as well as road geometry models are introduced. In addition, a novel physical-statistical motion model for the preceding vehicle behaviour estimation is proposed as the main contribution of this chapter.

In Chapter 4, the works of literature review related to the MPC, NMPC with the automotive applications are presented. An overview of the OCPs and different types of deterministic as well as stochastic MPCs are provided. In addition, the proposed general RSNMPC framework and its application on the Eco-ACC system for the BEV as the main contribution of this chapter is given.

Chapter 5 demonstrates the numerical simulation results and evaluation of the proposed Eco-ACC system with the introduced RSNMPC. Robustness against model mismatch, capability of the risk-sensitive OCP, and performance of the proposed concept are presented in this chapter.

In Chapter 6, the proposed semi-autonomous Eco-ACC system for the BEV is experimentally implemented to validate the results of this study. The field experimental tests

are carried out on a closed test track to demonstrate the improvement of the energy consumption of the BEV.

The thesis concludes in Chapter 7 with the findings, a discussion of the contributions of this study, and research direction of future outlook.

# Chapter 2

# Electric Vehicle

The technological evolution of vehicles throughout these years turns them into more sophisticated machines. Development of ICE vehicles is one of the considerable achievements of modern technology. Like most of the other technologies, modern technology of the vehicles is also associated with its own challenges in safety, energy requirement, and environmental contamination. A large number of ICE vehicles in use lead to serious problems for the environment and human life around the world. Air pollution and global warming are instances of problems of predominant concern. Today continuous innovation from the automotive industry and researchers aim at finding out new ways to reduce costs, increase transport efficiency, safety, and environmentally friendly technologies. It is now well recognised that EV, Hybrid Electric Vehicle (HEV), Fuel Cell Electric Vehicle (FCEV), and BEV are the most promising vehicle drivetrain technologies for the predictable future.

This chapter is structured as follows. Section 2.1 presents a brief overview of the development history of the BEVs. Section 2.2 introduces the longitudinal dynamics of a series-production BEV, followed by the energy consumption model of the BEV in Section 2.3. Section 2.4 concludes the findings of this chapter.

## 2.1 History of Electric Vehicle

The advent of automobiles revolutionised the human mobility. With the advancement of the technology in automobiles, roads were expanded and allowed people to travel faster and farther, which enlarge their connectivity. Due to the increasing number of automobiles, traffic regulations were developed to control vehicle's movement in a systematic and safe way. The EV is not a new concept in the automotive industry. The

FIGURE 2.1: First electric automobile to reach $100\,km/h$ in 1899 (© Public Domain).

history of EV began in the 19th century. Rechargeable batteries bring an applicable means for accumulating electricity on board of a vehicle. The vehicle with rechargeable battery was not introduced until 1859. Various people are associated with the EV invention. Gustave Trouvé, a French inventor, in 1881 and Thomas Parker, English inventor, in 1884 were the first persons who developed EV. The first practical lead-acid battery, which significantly improved the design of the battery was developed by a Luxembourgish engineer, Henri Owen Tudor, in 1886. The first EV in Germany was built by Andreas Flocken in 1888. William Morrison from Des Moines, Iowa was the first developer of EV in the United States of America (USA) in 1890. For more details about the early EVs follow Guarnieri (2012).

Interests in the EVs expanded largely in the late 1890s and early 1900s since the EVs provide a level of comfort and ease of operation compared to ICEs. The EV taxis were available at the end of the 19th century. Limited range of the EVs demonstrated to be less of a disadvantage among customers who used the EVs as city vehicles. Furthermore, an exchangeable battery supply was proposed in order to tackle the limited cruising range problem of the EVs in 1896. One of the most significant developments of the EV in this decade was the invention of regenerative braking by Alexandre Darracq, French automobile manufacturer in 1897. This braking method could make the electric motor behave as a generator charging the battery that enhances the driving range significantly. The EVs have several notable records like breaking of the $100\,(km/h)$ speed barrier by Camille Jenatzy with *La Jamais Contente* EV in 1899 (Figure 2.1).

At the beginning of the 20th century, discoveries of large oil reserves, improved road infrastructure, and producing cheaper ICE vehicles. Advances in ICE vehicles make

them more flexible, powerful, and easier to handle. The longer range and their quicker refuelling times encouraged a rapid expansion of ICE vehicles and decreased the relative advantages of EVs. Some of the last commercially EVs were released around 1905. During nearly 60 years passed without a considerable renewal in EV technology. In 1947, one of the most important inventions was developed at Bell Laboratories, the transistor. This made possible to efficiently deliver power to an electric motor with variable frequency. In the late 1950s, despite some improvements in performance with respect to the previous EVs, they were found much expensive in compare to equivalent ICE vehicles. In the late 1960s, a new battery based on lithium was developed. During the 1970s, the energy crisis raised and in addition concerns about the environmental contaminations triggered some interest in research on EVs. In 1971, the most significant EV named *moon buggy* collected a unique distinction of becoming the first human driven vehicle on the Moon during the Apollo 15 mission.

Although some technological progress achieved in the EVs, it became clear during the 1980s and early 1990s that EVs could hardly compete with ICE vehicles for range and performance. The reason is a high weight to energy ratio stored in batteries than gasoline for the same energy content. Throughout the 1990s, interest in fuel-efficient, and environmentally friendly vehicles was reduced due to lower oil prices. However, after the global economic recession in the late 2000s, automotive manufacturers abandoned the productions of fuel inefficient vehicles. Some governments initiated the policy of moving toward more fuel efficient, and lower emissions vehicles. In 2008, the first highway capable EV in serial production, which uses lithium-ion battery cells was accessible in the USA and expressed a goal of having one million EVs on the roads by 2015. During the recent years, after several failures in the competitions with ICE vehicles, the EVs started to emerge in the market again with promising features. Many automotive manufacturers have been introducing their own EV models while the global interest in the EV's technology and its markets is growing. For more details about the EVs, see, e.g., Eberle et al. (2010) and Hosseinpour et al. (2015).

## 2.2 Fundamentals of Vehicle Dynamics

Vehicle dynamics mathematically expresses the vehicle's behaviour, based on the general principles of mechanics. An EV is a complex system consisting of several thousands of components. Deep mechanical and mathematical knowledge is required to describe the vehicle's behaviour. A lot of literature related to vehicle dynamics already exists. Since this section relates to the BEV dynamics, the fundamentals discussion of vehicle dynamics will be restricted to the one-dimensional longitudinal motion of a commercial BEV.

The vehicle longitudinal motion control has greatly advanced since decades of research and development. In this study, the relations and models are identified and parameterized based on a Smart Fortwo Electric Drive (Smart-ED) Fortwo series-production model 2013. This model is used for the system design, simulations, and practical experiments in this study. Hence, this section focuses on the performance of the Smart-ED, such as velocity, gradability, acceleration, braking performance, and energy consumption.

### 2.2.1 Smart Fortwo Electric Drive

The Smart Fortwo Electric Drive, is a BEV city car. Production began in 2007 and the second generation was introduced in 2009. A near series-production version was unveiled in Frankfurt Motor Show in 2011. Mass-production of the third generation Smart-ED began in 2013 and delivered in USA, Europe, and 30 markets worldwide. The first generation of the Smart-ED vehicles was powered by a $30\,kW$ electrical machine. A $13.2\,kWh$ of sodium-nickel chloride Zebra battery package was the energy source for the powertrain. The range of a fully charged battery was up to $110\,km$. The second generation Smart-ED has a lithium-ion battery package with a capacity of $14\,kWh$ provided by Tesla Motors. The maximum range of a fully charged battery can be up to $135\,km$. The required charge time for lithium-ion battery package from 20 to 80 percent of its capacity can take roughly three hours with a standard $220\,V$ outlet.

The third generation Smart-ED has a powerful $55\,kW$ electric motor with $130\,Nm$ torque. It has a new $17.6\,kWh$ lithium-ion battery package with a quick-charge capability. The battery pack allows increasing the range up to $145\,km$. The Smart-ED has an electronic accelerator pedal, a friction and regenerative based hybrid brake system. The lithium-ion battery pack is installed under the cabin's floor. The water-cooled three-phase Permanent Magnet Synchronous Machine (PMSM), gearbox, cooling system, brake vacuum pump, power inverter, and onboard charger power electrics is installed in a rear-wheel-drive layout. The main specifications of the Smart-ED are given in Table 2.1.

### 2.2.2 Smart-ED Longitudinal Dynamics

The motion of the Smart-ED in forward direction is defined by the sum of all the forces acting on longitudinal axis. Figure 2.2 shows the forces acting on longitudinal motion of the Smart-ED moving uphill. On the one hand, the traction force ($F_{trac}$), propels the vehicle forward and acts on the contact area between tires of rear driven wheels and road surface. This force is produced by the powertrain system and generated by power flow from the battery pack to the drive wheels through the electrical motor and speed

| Description | Value, Unit |
|---|---|
| Rated power output | 55 $kW$ |
| Continuous power output | 35 $kW$ |
| Maximum torque | 130 $Nm$ |
| Top speed | 125 $km/h$ |
| Range | 145 $km$ |
| Battery capacity | 17.6 $kWh$ |
| Number of battery cells | 93 |
| Vehicle length/width/height | 237.744 $cm$/155.448 $cm$/155.448 $cm$ |
| Wheelbase | 186.69 $cm$ |
| Turning circle | 874.776 $cm$ |
| Track width (front/rear) | 128.2954 $cm$/138.5062 $cm$ |
| Transmission ratio | 1 : 9.922 |
| Front tyre dimensions | 155/60R15 |
| Rear tyre dimensions | 175/55R15 |
| Net weight (kerb weight) | 950 $kg$ |

TABLE 2.1: Main specifications of the Smart Fortwo Electric Drive (Smart Automobile, 2015).
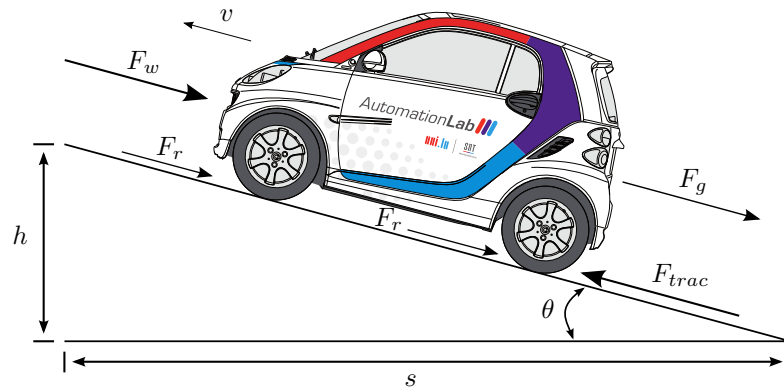


FIGURE 2.2: Forces acting on longitudinal axis of the Smart-ED moving uphill.

gearbox. On the other hand, there are resistive forces acting against the traction force that attempts to stop the forward motion of the vehicle. The most effective resistive forces generally are the aerodynamic drag ($F_w$), grading resistance ($F_g$), and tire rolling resistance ($F_r$). It is clear that in a downhill motion case, the grading force is in the same direction as the traction force and contributes to the vehicle's propulsion.

The forward one-dimensional motion of vehicle at velocity $v$ is assumed as a point mass at the center of gravity. Hence, its acceleration along the longitudinal direction expressed by the Newton's second law of motion as follows:

$$\frac{dv}{dt} = \frac{F_{trac} - \sum F_{res}}{m_{eq}} \tag{2.1}$$

where $F_{res}$ represents the total resistive forces, and $m_{eq}$ is equivalent mass of the Smart-ED.

The equivalent mass includes kerb weight and rotational inertia of rotating components. The calculation of the equivalent mass requires knowing the values of the mass moments of inertia for all the rotating parts. The equivalent mass of the Smart-ED with unknown values for the inertias of rotating parts, can be calculated by an empirical relation as follows:

$$m_{eq} = m(1 + \delta_1 + \delta_2 i_g^2) \tag{2.2}$$

where $m$ is the kerb mass of the Smart-ED, $\delta_1$ represents the total angular inertial moment of the vehicle, $\delta_2$ represents the effect of rotating parts in the powertrain system, and $i_g^2$ is the single transmission ratio (Ehsani et al., 2009).

### 2.2.3   Resistive Forces

As mentioned before, the total resistive forces acting against the vehicle forward motion are the aerodynamic drag ($F_w$), grading resistance ($F_g$), and tire rolling resistance ($F_r$). Hence the $F_{res}$ can be expressed as,

$$\sum F_{res} = F_w + F_g + F_r. \tag{2.3}$$

Detail of these resistive forces will be discussed in following subsections.

#### 2.2.3.1   Aerodynamic Drag Force

Aerodynamic drag is the fluid drag force between the moving vehicle at velocity $v$ in opposite direction to air in the direction of the fluid free stream flow. This force mainly results from shape drag and skin friction. The frontal area of the vehicle during its motion pushes the air. Since the air cannot immediately move away, the air pressure in front is increased and creates a high-pressure area. Similar behaviour happens behind the vehicle that the air cannot immediately fill the space left and creates a low-pressure area. The resulting force on the vehicle is the namely *shape drag* and is the consequence of the vehicle's body shape. In addition, air close to the body moves approximately at the same speed of the vehicle while air away from the body has different speed. This difference in speed between air molecules produces a friction namely *skin friction* (Ehsani et al., 2009).

Aerodynamic drag is a function of vehicle speed $v$ as follows:

$$F_w = \frac{1}{2}\rho_a A_f C_D v^2 \tag{2.4}$$

where $\rho_a$ is air density, $A_f$ is vehicle frontal area, and $C_D$ is the aerodynamic drag coefficient. It is assumed that at sea level and at $20\,^\circ$C, air has a density of approximately $\rho_a = 1.2041\,(kg/m^3)$. The Smart-ED frontal area is $A_f = 2.057\,(m^2)$, and its aerodynamic drag coefficient is $C_D = 0.35$ (Bloch, 2009).

### 2.2.3.2 Grading Resistance Force

When a vehicle goes up or down a slope, its weight drives to either opposite or assisting the forward motion. In vehicle performance analysis, the only uphill operation is considered. This grading force is usually called grading resistance (Ehsani et al., 2009). This force can be expressed as:

$$F_g = m_{eq}g sin(\theta) \tag{2.5}$$

where $g = 9.81\,m/s^2$ is the gravitational constant. In order to simplify the calculation, the road angle, $\theta$, is usually replaced by the grade value, when the road angle is small (Ehsani et al., 2009).

$$sin(\theta) \approx tan(\theta) = \frac{h}{s}. \tag{2.6}$$

### 2.2.3.3 Rolling Resistance Force

The rolling resistance is the force resulting from the motion when the tire rolls on a surface and mainly caused by hysteresis in the tire materials or the surface (e.g. soil). The rolling resistance has a different and broad range of definitions depending on the application point of view. In this study, the rolling resistance can be expressed as:

$$F_r = \mu_{rr}(v)m_{eq}g cos(\theta) \tag{2.7}$$

where $\mu_{rr}$ is rolling resistance coefficient. In vehicle performance calculation, it is sufficient to consider the rolling resistance coefficient as a linear function of speed as follows:

$$\mu_{rr}(v) = 0.01(1 + \frac{v}{576}). \tag{2.8}$$

This equation predicts the values of $\mu_{rr}$ with acceptable accuracy for speeds up to $v \leq 35.55\,(m/s)$ (Ehsani et al., 2009).
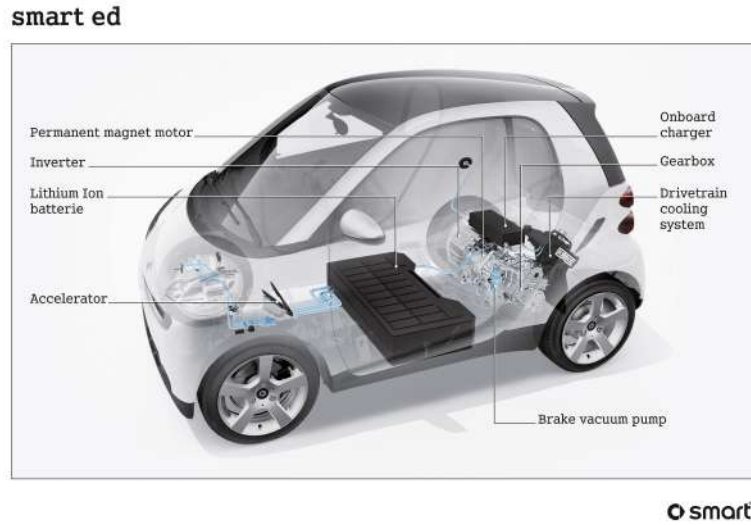
FIGURE 2.3: Smart Fortwo third generation Electric Drive, powertrain components (*Smart Automobile* 2016).

### 2.2.4 Traction Force

The electric propulsion system is the heart of the EVs. The main components of the Smart-ED powertrain are shown in Figure 2.3. The power flow from the battery pack passes throughout the inverter, which inverts the battery DC voltage to a three phase AC voltage applicable to the electrical motor, single gear ratio gearbox, to the rear wheels or vice versa to enable regenerative braking. The regenerative braking can generate electricity in order to charge the onboard battery pack. The traction force on the rear-driven wheels can be expressed as:

$$F_{trac} = \frac{i_g \eta_t \tau_{trac}}{r_d} \tag{2.9}$$

where $r_d$ is the effective radius of the rear wheel, $\tau_{trac}$ is the powertrain torque output, and $\eta_t$ is the total mechanical efficiency of the transmission between the electrical motor output shaft and rear driven wheels. The $\eta_t$ is the product of the efficiencies of all the components in the driveline. The average value of the overall mechanical efficiency of a BEV can be approximated to 90% (Ehsani et al., 2009). The powertrain torque output is the result of power exchange among mainly three components of the electric machine, inverter, and the battery pack. Details of these components will be discussed in following subsections.

### 2.2.4.1 Electrical Machine

For the propulsion of an EV usually the Induction Machine (IM), PMSM, and Switched Reluctance Machine (SRM) can be considered (Schaltz, 2011). As mentioned before, the Smart-ED has a three phase PMSM, which can be divided into an electric part and mechanic part. The electric part of the PMSM can be modelled for instance in a D-Q transformation model as follows:

$$v_q = R_s i_q + L_q \frac{di_q}{dt} + \omega_e (L_d i_d + \lambda_{pm}) \tag{2.10}$$

$$v_d = R_s i_d + L_d \frac{di_d}{dt} - \omega_e L_q i_q \tag{2.11}$$

$$p_{EM} = \frac{3}{2}(v_d i_d + v_q i_q), \tag{2.12}$$

where $v_d$ is D-axis voltage, $v_q$ is Q-axis voltage, $i_d$ is D-axis current, $i_q$ is Q-axis current, $R_s$ is stator phase resistance, $L_d$ is D-axis inductance, and $L_q$ is Q-axis inductance. The mechanical part of the PMSM can be modelled as follows:

$$\tau_s = \tau_e - (J_s \frac{d\omega_e}{2} + \tau_c + B_v \omega_e) \tag{2.13}$$

$$\omega_s = 2\omega_e, \tag{2.14}$$

where $\omega_e$ is rotor rotational speed, $\omega_s$ is shaft angular velocity, $J_s$ is shaft moment of inertia, $\tau_e$ is electrical torque, $\tau_s$ is shaft mechanical torque, and $\tau_c$ is coulomb torque. The electromagnetic torque of the machine is given by

$$\tau_e = \frac{3}{2}\frac{P_n}{2}(\lambda_{pm} - (L_q - L_d)i_d)i_q, \tag{2.15}$$

where $P_n$ is the number of poles. For more information about the fundamentals of electric machines, see (Emadi, 2014).

### 2.2.4.2 Inverter

Power electronics can be described as the technology that combines contributions from electronic, magnetic, and electrochemical components to control and convert electric power (Emadi, 2014). The inverter transmits and manages power flow between the electrical machine and the battery. Three-phase inverter is used to transform a DC-voltage source into a three-phase AC output in the Smart-ED. The output power of the inverter is the motor input power $P_{EM}$. The inverter input power, $P_{Inv}$, is

$$P_{Inv} = v_{bat} i_{Inv} = P_{EM} + P_{Inv.Loss} \tag{2.16}$$

where $v_{bat}$ is the battery pack voltage, $i_{Inv}$ is the inverter input current, and $P_{Inv.Loss}$ is the total power loss of the inverter. For more detailed information, see i.e (Schaltz, 2011), (Emadi, 2014). Note that during the charging from the electrical grid or regenerative braking, a rectifier converts AC-voltage to DC-voltage to charge the onboard battery package. It is an important point that the recovered power should not exceed the maximum power of the battery.

### 2.2.4.3 Battery Package and Models

The battery pack is one of the main components of an EV. Many EVs have been developed and are commercially available with different battery types. The ultimate goal for battery performance would be to offer similar energy and power densities to petroleum fuels used in conventional vehicles, with a comparable cost of an ICE. However, this is not feasible with the current technology and a compromise has to be made (Emadi, 2014). Lithium-ion battery technology as an energy storage system is heavily researched. A high energy density, small memory effect, and low self-discharge are the key features of Lithium-ion cells. For more information, follow Emadi (2014).

Equivalent electric circuit and electrochemical modelling are the two main approaches to mimic and model the experimental responses observed from cell characterization data. The electrochemical modelling is based on electrochemical equations of the battery chemistry. In contrast, equivalent circuit modelling is based on the electrical behaviour of the battery. The simplest circuit model is the resistance model with battery voltage $V_{bat}$, and current $I_{bat}$ that can be described as:

$$V_{bat}(t) = V_{bat.oc} - R_{bat}I_{bat}(t).$$ (2.17)

This is based on an open circuit voltage $V_{bat.oc}$, and a resistor $R_{bat}$ to model the equivalent series internal resistance of the battery. The simplest approach to track the battery's State Of Charge (SOC) that ranges from empty ($SOC = 0$) to full ($SOC = 1$) can be described as follows:

$$SOC(t) = SOC(t_0) + \frac{1}{C_{bat.N}} \int_{t_0}^{t} I_{bat}(t)dt$$ (2.18)

where $C_{bat.N}$ is the battery's charge storage capacity. The energy delivered from the battery ($E_{bat}$) can be expressed as:

$$E_{bat} = \int_{t_0}^{t} V_{bat}I_{bat}dt$$ (2.19)
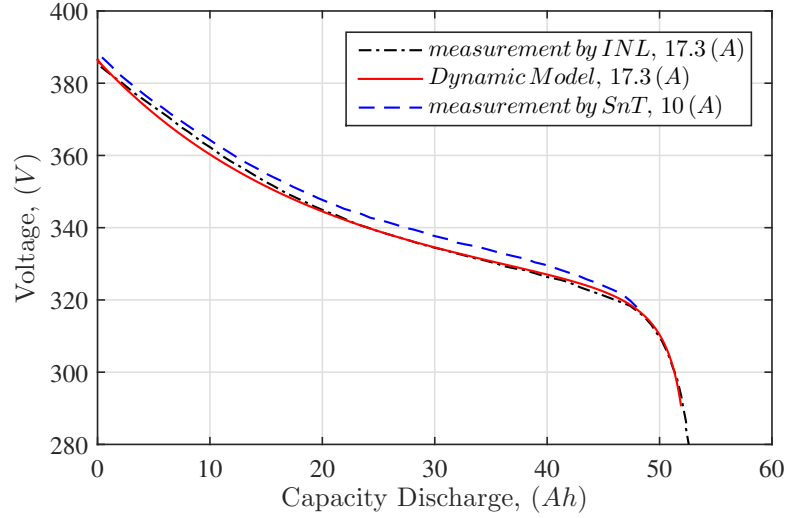
FIGURE 2.4: Voltage-capacity discharged of Smart-ED during the static capacity test.

which is a function of the battery voltage and electric current. For more details about mathematics based equivalent circuit and electrochemical battery models, follow Emadi (2014) and Seaman et al. (2014).

A dynamic battery model for the EV applications is proposed in (Tremblay et al., 2009). In this model, the battery voltage for lithium-ion discharge model is obtained by:

$$V_{bat} = V_{bat.oc} - K_{pol}\frac{C_{bat.N}}{C_{bat.N} - i_t}(i_t - i^*) - R_{bat}I_{bat} - A_{zon.amp}\exp^{(-B_{zon.inv}i_t)}. \quad (2.20)$$

The battery voltage for lithium-ion charge model is obtained by:

$$\begin{aligned} V_{bat} =& V_{bat.oc} - K_{pol}\frac{C_{bat.N}}{i_t - 0.1C_{bat.N}}i^* \\ & - K_{pol}\frac{C_{bat.N}}{C_{bat.N} - i_t}i_t - R_{bat}I_{bat} + A_{zon.amp}\exp^{(-B_{zon.inv}i_t)} \end{aligned} \quad (2.21)$$

where $i_t$ is the battery charge consumption $(Ah)$, equivalent to:

$$i_t = \int i dt. \quad (2.22)$$

The common time-domain tests to characterise the battery pack are used and compared to measurements. These tests generally are performed in a controlled environment such as constant conditions for temperature and pressure in order to produce unbiased information (for more information, follow Emadi (2014)). Figure 2.4 shows a common test result known as a *C-rates* static discharge capacity test for the discharge rate of the Smart-ED battery package with a constant discharge to a minimum cut-off voltage. This test was performed for the USA Department of Energy, which was conducted by the Idaho National Laboratory (INL) and Intertek Testing Services, North America

| Symbol | Description | Value, Unit |
|:---:|:---|:---:|
| $V_{bat.oc}$ | Open circuit battery voltage | 384.1 $V$ |
| $K_{pol}$ | Polarisation constant | 0.017874 $V/Ah$ |
| $C_{bat.N}$ | Battery charge capacity | 52.174 $Ah$ |
| $R_{bat}$ | Battery internal resistance | 0.17507 $\Omega$ |
| $A_{zon.amp}$ | Exponential zone amplitude | 64.9 $V$ |
| $B_{zon.inv}$ | Exponential zone time constant inverse | 0.052043 $Ah^{-1}$ |

TABLE 2.2: Parameters of the Smart-ED battery dynamic model
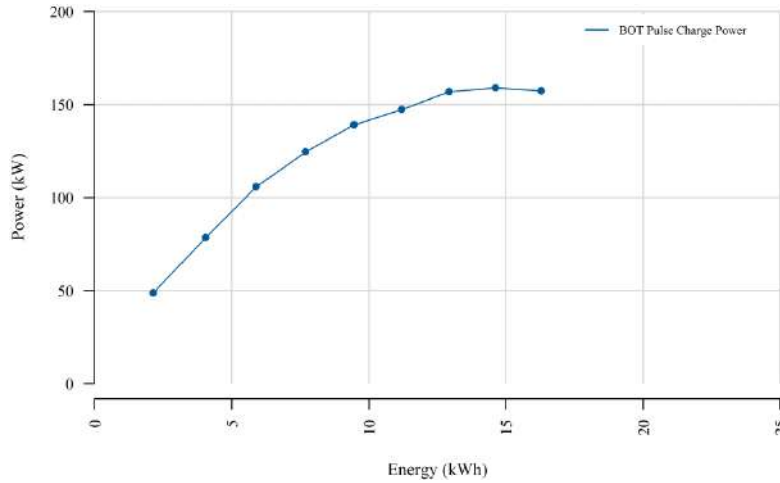


FIGURE 2.5: Charge power capability of Smart-ED versus energy discharged (INL, 2014).

(INL, 2014). In addition, this test is compared with the Smart-ED battery *dynamic model* proposed by (Tremblay et al., 2009), and the experimental tests was performed by the Automation Research Group Laboratory at Interdisciplinary Centre for Security, Reliability and Trust (SnT), at the University of Luxembourg (Tim Schwickart, 2015).

The discharge measurement carried out by the INL, and the simulation with the battery dynamic model is based on a three-hour discharged with a constant current rate at 17.3 $(A)$. The parameters of the dynamic model are given in Table 2.2. The battery discharge measurement performed by SnT is based on approximately constant current at 10 $(A)$ within around five hours. Figure 2.5, and Figure 2.6 show the Smart-ED 10-second charge and 30-second discharge pulse power capabilities of battery as a function of capacity discharge (INL, 2014). These show that the requested power by the powertrain can be supplied by the battery pack over the major SOC range.

The power consumption values for the low-voltage consumer units is shown in Figure 2.7 (Geringer et al., 2012). In addition, the battery pack can be discharged over a large temperature range. Temperature variations can significantly affect the battery performance. The influence of the ambient temperature on battery efficiency is shown in Figure 2.8 (Geringer et al., 2012). Furthermore, Figure 2.9 shows the ranges achievable
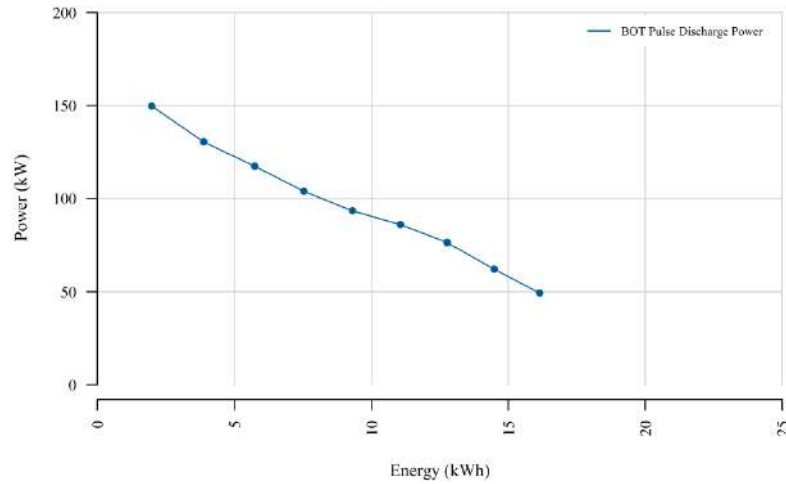
FIGURE 2.6: Discharge power capability of Smart-ED versus energy discharged (INL, 2014).
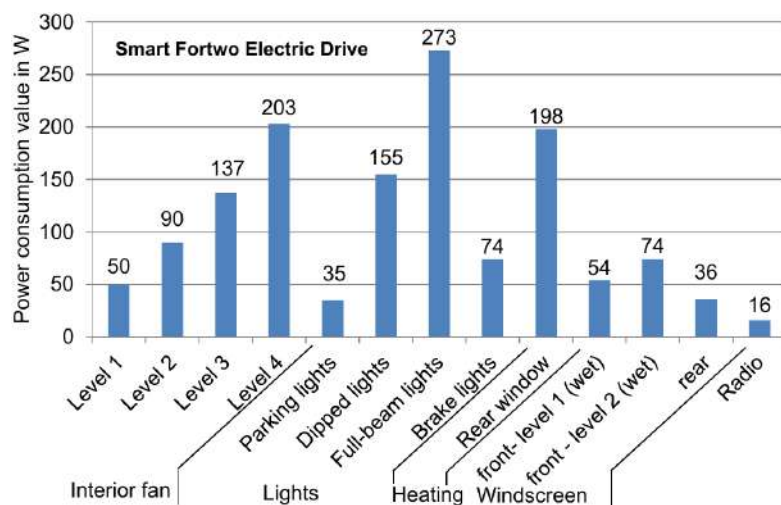


FIGURE 2.7: Smart-ED power consumption of various low-voltage consumer units (Geringer et al., 2012).
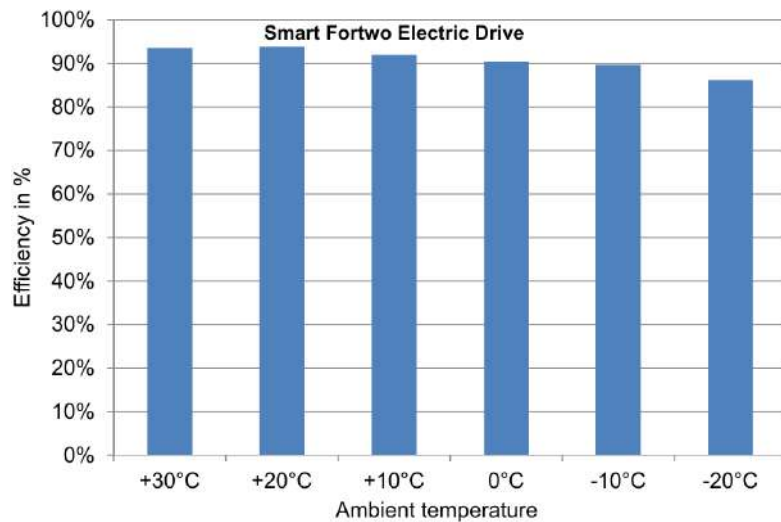


FIGURE 2.8: Efficiency of the Smart-ED battery at different ambient temperature (Geringer et al., 2012).
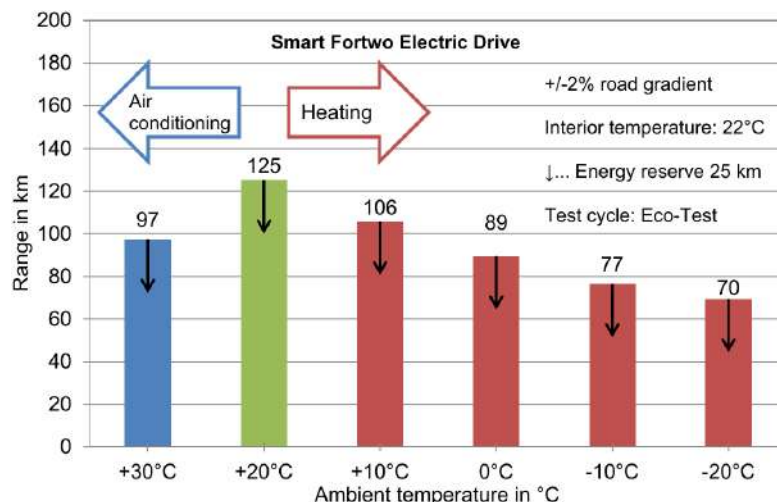
FIGURE 2.9: Range of the Smart-ED at different ambient temperature (Geringer et al., 2012).

in a test with single battery charge on a road gradient of $\pm 2\%$ as a function of the ambient temperature (Geringer et al., 2012). For more detailed information about the Smart-ED battery tests results, see INL (2014) and Geringer et al. (2012).

In concluding of this section, it is clear that a detailed exact analytical model for the electric propulsion system of the Smart-ED including all models and relations of the components with unknown parameters can be complex for the ADAS and ITS applications. Hence, a dynamometer test has been conducted in order to avoid complex models and achieve proper system identifications. The next section will relate to simple models for the propulsion system and energy consumption of the Smart-ED.

## 2.3 Dynamometer Test Bench

The dynamometer is representing the load system in test-beds with high accuracy force, torque, or power measurements. On the one hand, modelling the Smart-ED propulsion system including all the components might be complex for the ADAS and ITS applications. On the other hand, the traction forces of the wheels are measurable at the contact areas with the road. These forces are measurable by a dynamometer test bench which the total traction force applied to the Smart-ED can be calculated. To this end, a professional two-axle dynamometer test has been carried out at Delphi Automotive Systems Luxembourg S.A. in Bascharage, Luxembourg (*Delphi Automotive Systems Luxembourg S.A.* 2016) (Figure 2.10).

FIGURE 2.10: Smart-ED on the two-axle dynamometer test bench.

In order to cover the full-range operating points of the Smart-ED, the dynamometer test bench starts with an initial constant speed at $5\,km/h$. The related battery current and voltage at different throttle and brake positions from released to fully applied $(0 - 100\%)$ are measured by reading Controller Area Network (CAN) bus data through the On-Board Diagnostics (OBD) interface available in the Smart-ED. This procedure is repeated at different constant speed up to $120\,km/h$. The acquired data from the dynamometer and the Smart-ED internal sensor measurements shape the traction force versus velocity characteristic map. Furthermore, the electrical power consumption characteristic map can be achieved based on the related traction force, velocity, battery current, and voltage data. This test helps to achieve the traction force data that is a result of the power flow between the battery and the wheels without the requirement to model internal components of the powertrain with unknown parameters. It is noteworthy that the Smart-ED features a boost switch (kick-down) below the throttle pedal, which can be activated for the maximum acceleration of the vehicle (Tim Schwickart, 2015). Furthermore, the dynamometer test was carried out at normal room temperature with battery SOC between $60 - 80\%$. The auxiliary electrical loads have been disabled and the kick-down feature is ignored in further calculations.

The identified characteristic map helps to introduce a simple model for the Smart-ED performance and energy consumption evaluations. The next subsections are related to the performance of the Smart-ED acceleration and brake as well as the proposed energy consumption model for the BEVs.

### 2.3.1 Acceleration Performance and Model

The sustainable tire–ground contact and the maximum force of the powertrain are mainly the limitation factors of maximum traction capability. During vehicle operation, the
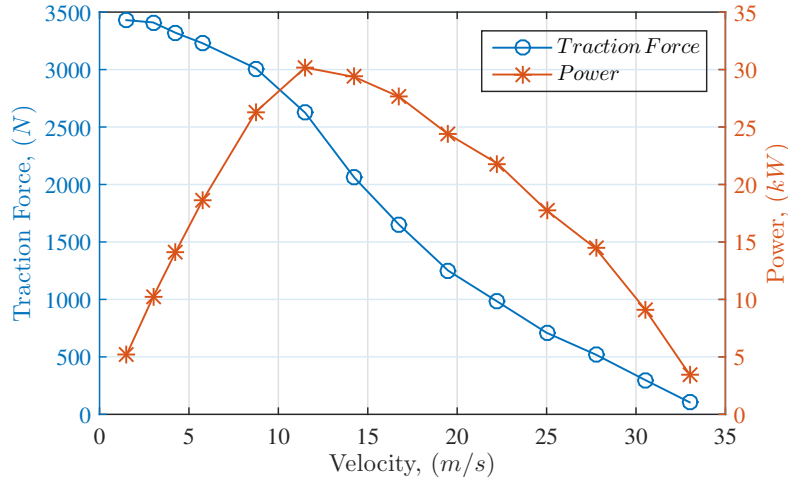
FIGURE 2.11: Dynamometer measurement results of the Smart-ED at 100% throttle pedal position.

maximum traction force on the rear-driving wheels should not exceed the maximum values that are limited by the tire-ground grip, in any other way the driving wheels will spin on the ground which may lead to vehicle instability. It is true especially when the vehicle drives on wet, icy, snow-covered, or soft soil roads. The smaller of these two factors will determine the performance potential of the vehicle (Ehsani et al., 2009).

The performance of the Smart-ED is characterised by its maximum cruising velocity, gradeability, and acceleration. It is assumed that the maximum tractive capability of the Smart-ED is limited by the maximum force of the powertrain, rather than tire-ground adhesion. Figure 2.11 shows the Smart-ED maximum traction force and its powertrain maximum power output at 100% throttle pedal position from the dynamometer test. In addition, the traction force is related with equivalent mass of the vehicle as follows:

$$F_{trac}(t) = m_{eq}u(t) \tag{2.23}$$

where $u(t)$ is traction input of the Smart-ED. Figure 2.12 shows the dynamometer measurement data and their relationship between maximum traction input ($u$) and the velocity at the maximum throttle pedal position (100%). This data can be approximated through a curve-fit process in order to mathematically express the correlation between maximum traction input and velocity as follows:

$$u_{max}(v) = c_1 - c_2 tanh(c_3(v - c_4)) \tag{2.24}$$

where the constants are identified as $c_1 = 1.523$, $c_2 = 1.491$, $c_3 = 0.08751$, and $c_4 = 15.6$ with 99.74% coefficient of determination (R-squared).

The maximum velocity is described as the constant cruising speed that the Smart-ED
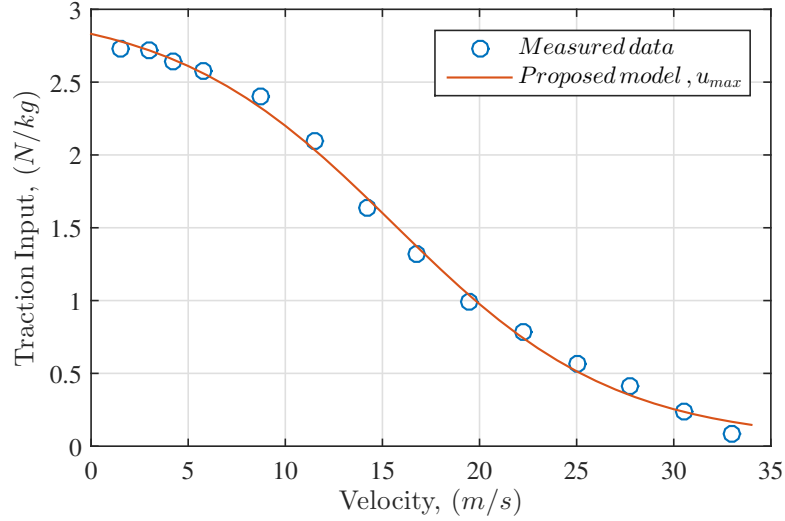
FIGURE 2.12: Smart-ED maximum traction input measured data, and its model at 100% throttle pedal position.
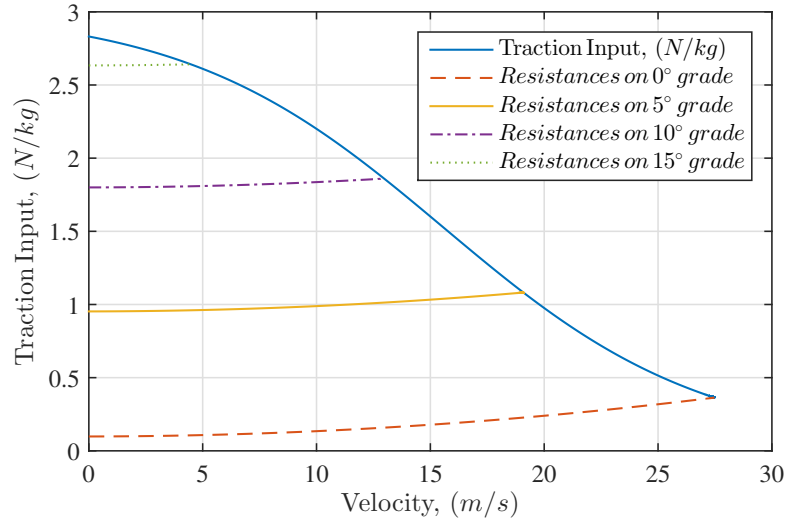


FIGURE 2.13: Smart-ED maximum cruising velocity, gradeability and its resistance effort.

can reach with full throttle (100%) on a flat road. The equilibrium value of the traction and the resistance effort determines the maximum speed of the Smart-ED, which can be expressed as:

$$u_{max}(v) = \frac{\rho_a A_f C_d v^2}{2m_{eq}} + gsin(\theta) + \mu_{rr}gcos(\theta). \tag{2.25}$$

Figure 2.13 shows different maximum speeds of the Smart-ED at different road grades. The junction point of the traction input and the resistances is the maximum speed of the Smart-ED. In addition, gradeability is generally expressed as the maximum grade that the vehicle can overcome in the full speed range. Figure 2.13 shows also the gradeability of the Smart-ED. The acceleration performance of the vehicle is described by its acceleration time and distance covered from the standstill to the maximum speed
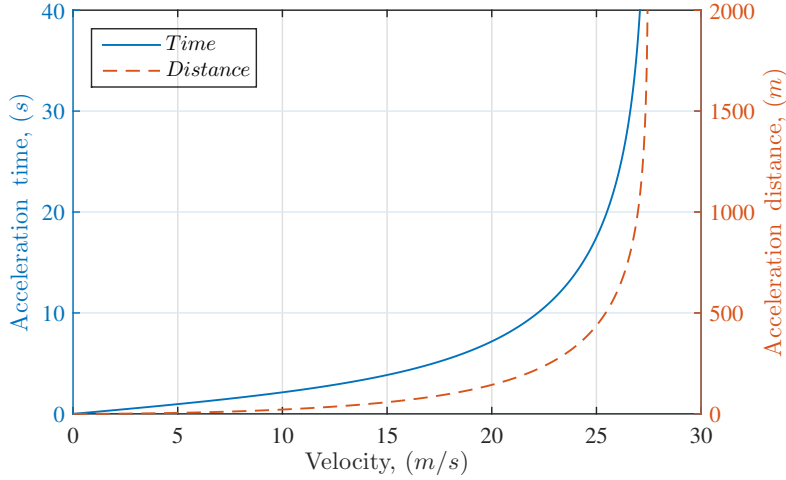
FIGURE 2.14: Smart-ED acceleration time and distance along with velocity.

on a flat road. Figure 2.14 shows the acceleration time, and distance of the Smart-ED along with velocity.

### 2.3.2 Brake Performance and Model

Brake performance of a vehicle is one of the most serious matters for vehicle safety. A considerable amount of energy is consumed during braking in the urban area driving. One of the most important features of the EVs is their ability to recover significant amounts of braking energy (Ehsani et al., 2009). The electric motors in the Smart-ED can operate as a generator to convert the kinetic or potential energy of vehicle mass into electric energy. This recovered energy can be stored in the battery or supercapacitor and then reused. In addition, a mechanical brake system to meet the required brake power is foreseen in the Smart-ED. Hence, a hybrid brake system is working together to provide sufficient braking force to reduce the velocity. In addition, this system balances the braking force distribution on the front and rear wheels, and recovery of braking energy as much as possible.

The driving power ($P_{drv}$ in $kW$) on the Smart-ED wheels can be expressed by:

$$P_{drv} = \frac{v}{1000}(F_{trac} - \frac{1}{2}\rho_a A_f C_D v^2 - m_{eq}gsin(\theta) - \mu_{rr}m_{eq}gcos(\theta)). \qquad (2.26)$$

The propulsion rear-driving wheels accept power from the powertrain and push the vehicle forward while the braking power is zero for $P_{drv} > 0$. However, while braking, the kinetic energy of the Smart-ED is dissipated by the hybrid brake system for $P_{drv} < 0$, the driving power is zero. The Smart-ED is cruising with constant velocity while $P_{drv} = 0$. For more information about fundamentals of vehicle brake performance, follow Ehsani et al. (2009).
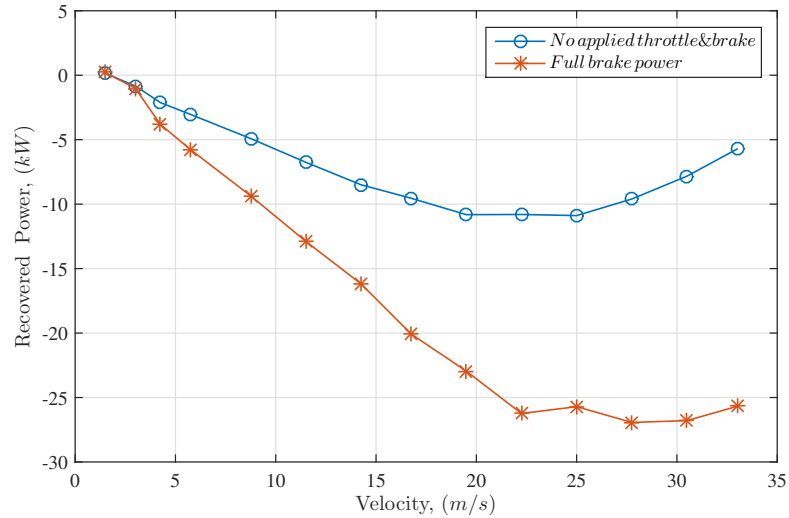
FIGURE 2.15: Dynamometer test results of Smart-ED regenerative power along with full velocity range.

Braking power distribution over the velocity range is useful information for investigating the regenerative brake system. As soon as the throttle pedal released in the Smart-ED, regenerative mode of the powertrain is activated to recover the power without using friction braking. The amount of recovered power is different along with the applied brake force and velocity range. The more brake pedal is pressed, the more power can be recovered. Figure 2.15 shows the dynamometer test result of regenerative power for the released throttle & brake pedals, and applied full brake power without tires being locked (100% brake pedal position) at the different velocity. Note that the negative power is inferred as the power is being recovered by regenerative hybrid brake system.

During braking, the hybrid brake system of the Smart-ED applies distributed and balanced brake forces to the wheels without being locked. The more brake force is applied, the more power is recovered up to the physical limits of the powertrain. This is due to the power capacities of the electric motor and battery pack that are not big enough to handle the immense braking power during the short but strong braking. Note that the regenerative braking may be deactivated with no considerable compromise on power recovered at low velocities. At lower velocities, mechanical braking should be primarily applied to ensure to meet the braking performance. In addition, it is noteworthy that the full applied brake force (minimum traction input) is assumed to be in the stable region of longitudinal tires slip ratio. For more information about longitudinal tires slip ratio, see Ehsani et al. (2009).

In addition, another important factor is regenerative recovered power versus the braking power. At different velocity, the recovered power is related to the applied brake power. Figure 2.16 shows the result of the braking test on the dynamometer for the Smart-ED at constant velocity of 40 (km/h). Note that the brake power (in percentage %) is a
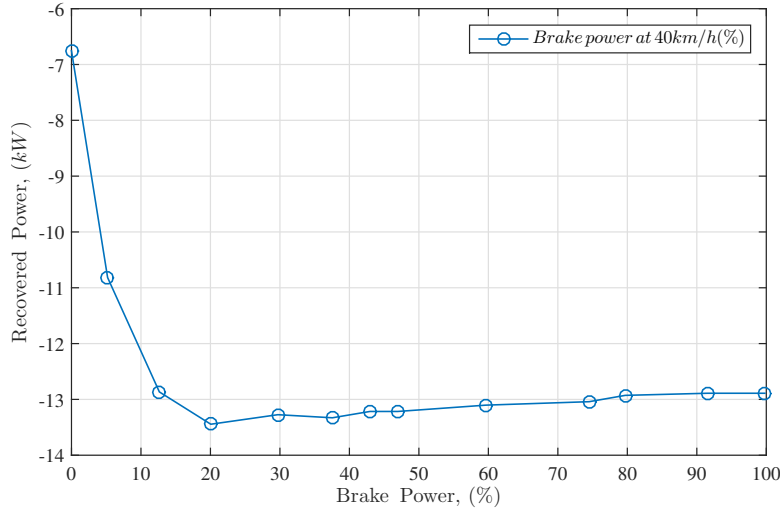
FIGURE 2.16: Dynamometer test result of Smart-ED regenerative power along with brake power at $40\,(km/h)$.

unified definition of the brake pedal positions with the assumption of operating in the stable region of longitudinal slip ratio of tires. It is clear that the recovered power is increased to a stationary value by increasing the applied brake power. The minimum traction input is introduced in order to represent the hybrid brake force (minimum traction force) as follows:

$$u_{min}(v) = -5 + c_5 v, \tag{2.27}$$

where $c_5 = 0$ in this study. This indicates that the maximum hybrid brake force applicable to the Smart-ED is independent of velocity without leading to locked wheels.

### 2.3.3   Energy Consumption Model

Rating the efficiency of a vehicle can be a complex task. Usually, the type approval consumption is used as an indicator (Eskandarian, 2012). The energy consumption of a vehicle is evaluated by the amount of energy per $100\,km$ travelling distance. The energy consumption of an EV depends on a number of factors, such as energy consumption characteristics of the electrical motor, gear ratio, driven speed, vehicle resistance, road and traffic conditions. The motor power output is always equal to the resistance power plus the dynamic power for acceleration of the vehicle as follows (Ehsani et al., 2009):

$$P_{mtr} = \frac{v}{1000}\left(m_{eq}\frac{dv}{dt} + \frac{1}{2}\rho_a A_f C_D v^2 + m_{eq}g\sin(\theta) + \mu_{rr}m_{eq}g\cos(\theta)\right). \tag{2.28}$$

After determination of the motor power by Equation (2.28), the total energy consumption ($E_{cns}$) within the total distance, $s$, at a constant cruising speed, $v$, is obtained

by

$$E_{cns} = \frac{P_{mtr} E_G}{E_M E_E} \frac{s}{v} \tag{2.29}$$

where $E_G$ is equivalent energy content per gallon of gasoline ($kWh$), $E_M$ is electrical energy consumed per kilometre, and $E_E$ is electrical energy in $kWh$.

#### 2.3.3.1   State of the art in Energy Consumption Models

The scientific methodology related to the energy consumption of passenger cars relies on simulation models validated by real-world tank-to-wheel emission and energy measurements performed in urban and motorway areas (Eskandarian, 2012). The term *tank-to-wheel* refers to the energy transfer chain from the on-board energy storage system, typically fuel tank, battery, or compressed hydrogen, to the wheels during vehicle operation (Eskandarian, 2012). A vehicle's tank-to-wheel energy consumption is determined by a defined driving cycle (e.g., New European Driving Cycle (NEDC)), which is carried out on a test bed at stringently monitored conditions (Eskandarian, 2012).

The BEV is able to achieve an efficiency of about 70% in type approval scenarios, a much higher value compared to levels achievable by conventional vehicles in standard driving cycles (Eskandarian, 2012). In the real-world scenario, the tank-to-wheel efficiency drops down to 35% in urban driving and to 60% at higher velocities (Eskandarian, 2012). These values are strongly dependent on the efficiency of the electrical motor and the discharge efficiency of the battery. Additionally, the range of a BEV is very limited due to the battery capacity. In the NEDC, the BEV is able to achieve a range of more than 120 $km$. During real-world driving, the maximum range is reduced to 70 $km$ (Eskandarian, 2012).

Few works of literature about full-range energy consumption models can be found for the EVs especially for the ADAS applications. The energy consumption model based on road topography information and traffic situation was considered by S. Yang et al. (2013), Jiquan Wang et al. (2015), and Graser et al. (2015). A quasi-static drivetrain energy consumption model for the Smart-ED was introduced by Tim Schwickart, Voos, and Darouach (2014). A physical and statistical approach aiming to develop a systematic energy consumption estimation approach suitable for the EV was introduced by R. Zhang et al. (2015). Power-based electric vehicle energy consumption model that computes the instantaneous energy consumption of an EV using second-by-second vehicle speed, acceleration and roadway grade data as input variables was introduced by Y. Li et al. (2015), Xinkai Wu et al. (2015), and Fiori et al. (2016).

**2.3.3.2 Proposed Energy Consumption Model and Validation**

The velocity and traction force have a significant influence on the energy consumption. The energy consumption during cruising at constant velocity is equitable to the resistive powers. This can be approximated through the curve-fit process with measurement data by a polynomial of velocity as:

$$f_{cruise}(v) = b_3 v^3 + b_2 v^2 + b_1 v + b_0 \qquad (2.30)$$

where $b_3 = 0$, $b_2 = 0.02925$, $b_1 = 0.257$, and $b_0 = 1.821$ for the Smart-ED. It is noteworthy that the $f_{cruise}$ formulation is adapted from (M. A S Kamal et al., 2011). The acceleration and deceleration of the Smart-ED considering only the regenerative energy zone in the hybrid brake system can be approximated by a similar curve-fit process with measurement data using a polynomial of the traction input as:

$$f_{acl}(u) = a_2 u^2 + a_1 u + a_0 \qquad (2.31)$$

where $a_2 = 0.01622$, $a_1 = 0.244$, and $a_0 = 1.129$. Power-to-mass ratio is a performance measurement index of a vehicle, with the power of powertrain output being divided by the mass of the vehicle which is independent of the vehicle's size. Therefore, combining the $f_{cruise}(v)$ and the $f_{acl}(u)$, can lead to a model of the power consumption $P_{mtr}$ of the Smart-ED. At any given velocity and control input, a linear relation of the traction power-to-mass ratio $(p_{trac}/m_{eq})$ of the vehicle can be expressed as:

$$\dot{E}_{cns} = P_{mtr} = f_{acl}(u)\frac{p_{trac}}{m_{eq}} + f_{cruise}(v). \qquad (2.32)$$

Figure 2.17 shows power consumption model of the Smart-ED based on traction input and velocity. Each contour line represents the related power consumption (in $kW$). At the higher traction input and velocity, the positive energy with the higher rate is consumed. In contrast, at regenerative braking zone at different velocity, a limited amount of energy can be recovered. This novel model is capable of representing the regenerative braking effect when $u(t) < 0$ for the full-range velocity and traction input. This way, the power consumption of the BEV can be estimated by modelling traction-velocity characteristics map of the electric machine. The proposed model for the energy consumption is approximated through the curve-fit process with 98.46% coefficient of determination (R-squared).
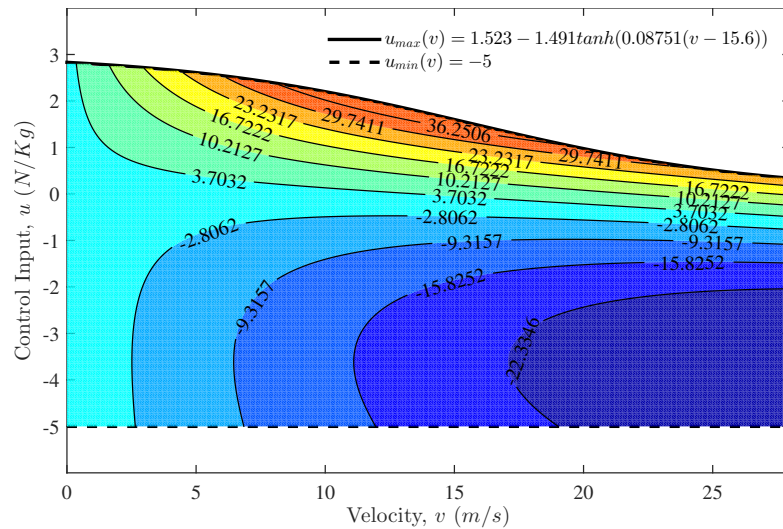
FIGURE 2.17: Power consumption of the Smart-ED

## 2.4 Conclusions

In this chapter, the works of literature reviewed to identify the state-of-the-art and knowledge gap on the BEVs. The historical development of the BEVs during the last centuries surveyed. It discussed not only significance of the BEV in recent years but also as the promising vehicle for the future. The longitudinal dynamics of the Smart-ED as a test case of the BEV introduced. Different components of the BEV reviewed and demonstrated that knowledge about the vehicle longitudinal dynamics plays a fundamental role in the identification of factors affect the motion dynamics and the energy consumption of the BEVs. The challenge of the system identification and modelling the energy consumption of the BEVs reviewed. The proposed system identification for the dynamics of the BEV as well as modelling its energy consumption based on the dynamometer test bench addressed the mentioned challenge as the main contribution of this chapter. Based on these findings in terms of system identification and modelling, the following chapter will review the ADAS concepts that can be utilised to improve the safety and energy efficiency of the BEVs.

# Chapter 3

# Eco-Driving Assistant System

The ADAS refers mainly to the vehicle handling functions that an intelligent vehicle provides either autonomously or supports the driver to execute a trip including planning and reaching from origin to destination safer, more efficient, and with less harmful environmental impacts (Eskandarian, 2012). The term *intelligent* vehicle refers to cover a specific level of machine intelligence in the scope of ADAS applications. Utilising available technologies to assist drivers by enhancing handling, safety, efficiency, and the comfort of driving with environmentally friendly impacts is the main goal of the intelligent vehicles.

This chapter is structured as follows. Section 3.1 provides an overview of the ADAS applications and operational modes. Section 3.2 presents Ecological Driver Assistance System (EDAS) with a specific focus on the ACC systems. Section 3.3 introduces the proposed Eco-ADAS system for the BEV. Section 3.4 presents the aimed road geometry and traffic modellings approach followed by Section 3.5 that introduces a novel motion estimation for the preceding vehicles. Section 3.6 concludes the findings of this chapter.

## 3.1 Advanced Driver Assistance Systems

Most of the road accidents are caused by human errors. Restricted reaction time, perception, and control are the limited capabilities of the human drivers. Passive safety systems such as safety belts, head restraints, or vehicle crush zone are the features that help to mitigate the effects of crashes. In contrast, developing active safety systems with the aim to increase safety, the comfort of driving, and improving energy consumption efficiency has been made a significant progress to either avoid a collision or reduce the severity of collisions as well as economic efficiency. Several systems have been introduced

and developed to strengthen vehicle active safety and handling, while still, the driver has to share a large part of control tasks in driving. Digital electronics and computers advancement have had a huge impact on different vehicle systems and design.

Nowadays, modern vehicles have many sensors and actuators that share the driver's vehicle control tasks as automatic control systems. These systems cover a wide range of functions such as Brake Assist System (BAS), assisting the driver with enough brake force when faced with an emergency situation, or ABS, and ESC maintain traction and stability control of the vehicle. When the driver fails to prevent a threatening crash situation, obstacles ahead can be sensed and automatically braked by the Collision Avoidance System (CAS). Automated driving has been an element in many future visions of mobility, enabling safe, efficient, reliable, and clean transportation. A smart navigation system can optimise the trip planning to improve the energy consumption of the vehicle. In an extreme, driverless vehicles can be driven autonomously to complete an entire trip from origin to the destination while avoiding obstacles and obeying traffic laws. For more detailed information about various aspects of the ADAS applications follow Eskandarian (2012).

### 3.1.1 History of Advanced Driver Assistance Systems

The experiments of automated vehicles, which include the longitudinal control of vehicle have been conducted since the 1920s. In 1925, *Houdina Radio Control* demonstrated a radio-controlled driverless car "linrrican Wonder". This was equipped with a transmitting antenna and was operated by a following second car that sends operating signals to control every movement of the vehicle. During the 1930s, an automated guided car was Norman Bel Geddes's "Futurama" sponsored by General Motors exhibited at the 1939 World's Fair (Eskandarian, 2012). During the 1950s throughout the 1960s, General Motors and RCA lab developed and demonstrated an automatic control of the steering and speed of automobiles. Inspired by the efforts, advertising was posted on many leading newspapers about predicting automated driving (e.g., Figure 3.1). In 1960, a long-term research program on both steering and longitudinal control of the vehicle was conducted at the Ohio State University, USA.

From 1960 to 1980, interest in automated vehicles was revived in the USA and Europe with different driverless vehicles tested such as the automated vehicle interacting with magnetic cables that were buried in the road. In Europe, the Program for European Traffic with Highest Efficiency and Unprecedented Safety (PROMETHEUS) was initiated by the motor vehicle industry, with funding support from the governments of the major western European Countries. A framework for cooperative development
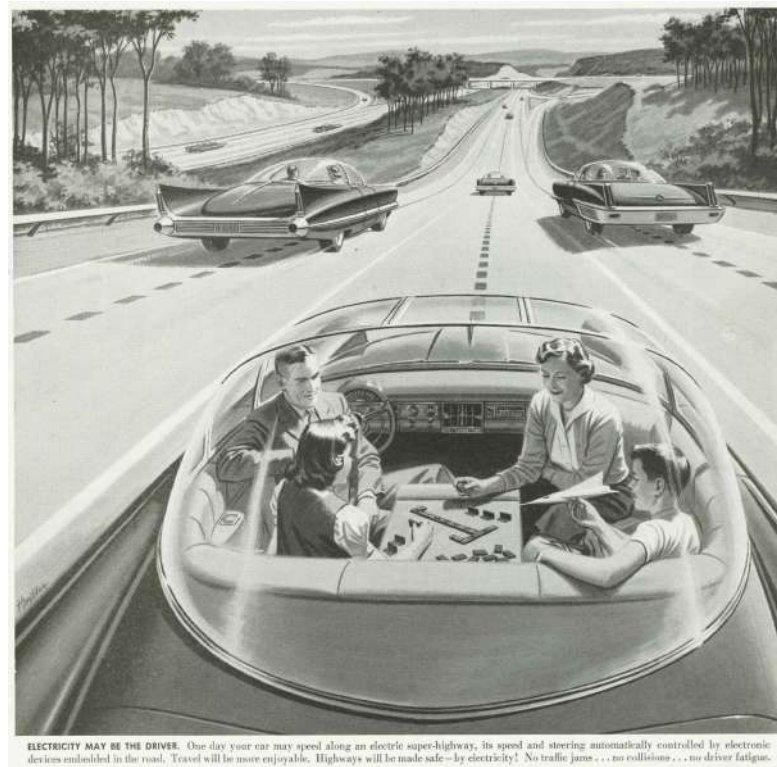
FIGURE 3.1: Predicted automated driving during 1950s (Weber, 2014).

to improve the safety and capacity of road transportation systems was provided. In 1986, the California Department of Transportation (Caltrans) cooperated with the Institute of Transportation Studies of the University of California at Berkeley initiated the Program on Advanced Transit and Highways (PATH). The PATH program includes clean propulsion technologies, highway automation, and road vehicle navigation and guidance (S. Shladover et al., 1991). In 1989, the Carnegie Mellon University made use of new technologies to use Light Detection and Ranging (LIDAR), computer vision and autonomous robotic control to direct a first road-following robotic vehicle (Pomerleau, 1989) in Defense Advanced Research Projects Agency (DARPA) funded autonomous vehicle project. In 1995, an autonomous Mercedes-Benz undertook a journey from Munich in Bavaria, Germany to Copenhagen, Denmark and back, using computer vision and transputers, a pioneering microprocessor architecture of the 1980s, to react in real time. In May 1998, Toyota became the first to introduce an ACC system on a production vehicle when it unveiled a laser-based system for its Progrès compact luxury sedan, which it sold in Japan (Jones, 2001).

In 2004, the first Grand Challenge funded by the DARPA offered a million dollar prize to any team, which could create an autonomous car capable of finishing a 150-mile course in the Mojave Desert. No team was successful in completing the course (Dudley, 2014). In 2005, DARPA Grand Challenge II was again held in a desert environment. This time,
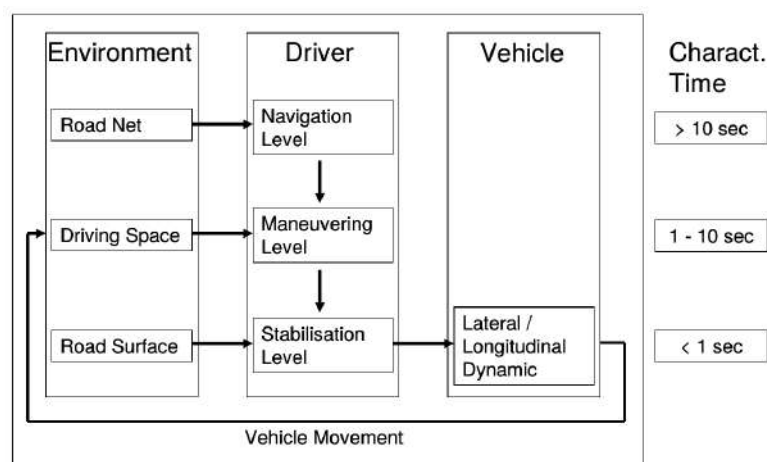
FIGURE 3.2: Driving task levels (Knapp et al., 2009).

five vehicles completed the course (Thrun, 2010). In 2007, the DARPA again sponsored Grand Challenge III, but this time the Challenge was held in an urban environment. An autonomous car from the Carnegie Mellon University earned the 1st place (Thrun, 2010). Google began developing its self-driving cars and they have driven more than one million kilometres since the company started secretly developing them in 2009, but they have been tested only once by a government body on open roads—by Nevada Department of Motor Vehicles (DMV) officials in May 2012 (Harris, 2014).

During the last decade, many major automotive manufacturers are testing their driverless car systems. The *BMW* has been testing driverless systems since around 2005. The Volkswagen began testing a system that will allow a car to drive itself at different speeds on the highway in 2012. The Toyota demonstrated a partially self-driving car with various sensors and communication systems in 2013. The 2014 Mercedes S-Class has options for autonomous steering, lane keeping, acceleration/braking, parking, accident avoidance, and driver fatigue detection, in city traffic and highway. The Tesla had announced their Autopilot technology in mid-2015. In 2016, Google Corporation announced a spin-off company called *Waymo* for the self-driving technology. In 2017, Waymo announced the driverless cars without a safety driver in the driver position (Hawkins, 2017).

### 3.1.2 Strategic Approach

The task of human driving may basically be classified into the Stabilisation, Manoeuvring and Navigation levels. Each level of driving tasks corresponds to the characteristic allocated time period of the respective driving task (Knapp et al., 2009). Figure 3.2 shows the typical three levels of driving task and the related allocated time period. The Society of Automotive Engineers (SAE) summarizes international levels of driving automation

| Level | Name | Narrative definition | Execution of steering and acceleration/ deceleration | Monitoring of driving environment | Fallback performance of *dynamic driving task* | System capability (*driving modes*) | BASt level | NHTSA level |
|---|---|---|---|---|---|---|---|---|
| *Human driver* monitors the driving environment | | | | | | | | |
| 0 | No Automation | the full-time performance by the *human driver* of all aspects of the *dynamic driving task*, even when enhanced by warning or intervention systems | Human driver | Human driver | Human driver | n/a | Driver only | 0 |
| 1 | Driver Assistance | the *driving mode*-specific execution by a driver assistance system of either steering or acceleration/deceleration using information about the driving environment and with the expectation that the *human driver* perform all remaining aspects of the *dynamic driving task* | Human driver and system | Human driver | Human driver | Some driving modes | Assisted | 1 |
| 2 | Partial Automation | the *driving mode*-specific execution by one or more driver assistance systems of both steering and acceleration/deceleration using information about the driving environment and with the expectation that the *human driver* perform all remaining aspects of the *dynamic driving task* | System | Human driver | Human driver | Some driving modes | Partially automated | 2 |
| *Automated driving system* ("system") monitors the driving environment | | | | | | | | |
| 3 | Conditional Automation | the *driving mode*-specific performance by an *automated driving system* of all aspects of the *dynamic driving task* with the expectation that the *human driver* will respond appropriately to a *request to intervene* | System | System | Human driver | Some driving modes | Highly automated | 3 |
| 4 | High Automation | the *driving mode*-specific performance by an *automated driving system* of all aspects of the *dynamic driving task*, even if a *human driver* does not respond appropriately to a *request to intervene* | System | System | System | Some driving modes | Fully automated | 3/4 |
| 5 | Full Automation | the full-time performance by an *automated driving system* of all aspects of the *dynamic driving task* under all roadway and environmental conditions that can be managed by a human driver | System | System | System | All driving modes | | |

FIGURE 3.3: SAE International levels of driving automation (Smith, 2013).

for on-road vehicles (Smith, 2013). Figure 3.3 shows the driving automation in five levels of autonomy. Information Report J3016 provides full definitions for these levels (SAE International, 2013). The levels are descriptive rather than normative and technical rather than legal. Elements indicate minimum rather than maximum capabilities for each level. *System* refers to the driver assistance system, combination of driver assistance systems, or automated driving system, as appropriate (SAE International, 2013). Figure 3.3 shows how SAE's levels definitively correspond to those developed by the Germany Federal Highway Research Institute (BASt) and approximately correspond to those described by the USA National Highway Traffic Safety Administration (NHTSA) in its *Preliminary Statement of Policy Concerning Automated Vehicles* of May 30, 2013 (SAE International, 2013).

The ADAS consists different types of sensors and actuators that are used to estimate the state of the vehicle through a user interface. In addition, vehicular communication systems such as Vehicle-to-Vehicle Communication (V2V), or Vehicle-to-Infrastructure Communication (V2I) can obtain additional data from vehicle's environment in order to enhance functionalities of the ADAS. RADAR systems, vision-based systems, infra-red sensors, laser scanner systems, Global Positioning System (GPS), accelerometer, Inertial Measurement Unit (IMU) are typical sensor systems used for the ADAS applications. The common aspect of the sensor systems despite their specific advantages and disadvantages is that they are aimed to provide a sophisticated surroundings image for the vehicle in terms of situations of other vehicles, road conditions, pedestrians, etc. The ACC, ESC, Lane Keeping Support (LKS), Parking Assistance Systems (PAS), blind
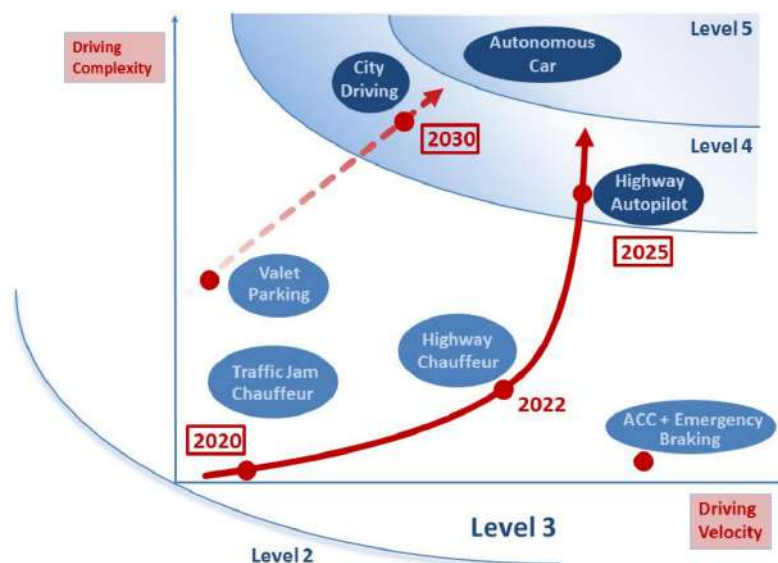
FIGURE 3.4: Development paths and milestones for Levels 3 and 4 of road vehicle automation until 2030 (Dokic et al., 2015).

spot warning, and driver state monitoring are commercial examples of ADAS applications. The V2V, or V2I communication systems have been studied in numerous research projects, but their commercial introduction is expected around 2015-2020 (Eskandarian, 2012).

In the EU project Advanced Driver Assistance Systems in Europe (ADASE2) (Dirk et al., 2004), the future research roadmap and activities of ADAS applications are expressed. It bases on discussions between the experts of the ADASE2 project partners. In 2014, European Road Transport Research Advisory Council (ERTRAC) established a task force with stakeholders and experts from its members associations and individual members to define a joint roadmap for Automated Driving (ERTRAC Task Force, 2015). In addition, the EU funded five Large-Scale Pilots (LSPs) on the Internet of Things. The AUTOPILOT project was selected as Pilot 5: autonomous vehicle in a connected environment in 2016 (European, 2016). Furthermore, there are numerous calls for H2020 projects currently launched for 2018 and 2019 (European, 2018). Figure 3.4 shows development paths and milestones for Levels 3 and 4 of the road vehicle automation until 2030 depending on velocity and complexity of the driving situation (Dokic et al., 2015). The solid path represents the evolutionary scenario and the dashed line the revolutionary one. Both paths may eventually lead to the autonomous car, which is indicated here as Level 5 of automation (Dokic et al., 2015).

Based on the automation level (Figure 3.3), vehicle control functions can be generally categorised into active safety, semi-automated, and fully automated vehicle control functions. In the active safety systems, the driver is in charge of the vehicle control and the systems are automatically activated only in emergency situations. The semi-automated

vehicle can take full control of specific vehicle control functions. For example, the ACC system can take control of the longitudinal motion of the vehicle without driver's interference. These systems generally can be activated manually by the driver, and give back control of the vehicle to the driver at any request. The fully automated vehicle control can completely replace the driver in all vehicle functions and tasks. It not only has the full control of vehicle longitudinal and lateral motions but also has the capability to determine necessary manoeuvres and can even decide which route to take to arrive at its destination (Eskandarian, 2012). The next section reviews the scope of the longitudinal control of automated vehicles and describes functionality.

### 3.1.3   Vehicle Longitudinal Control

Longitudinal control of automated vehicles plays a major role in the automated vehicle functions. The feedback of spacing and relative velocity of the preceding vehicle is a popular controller structure due to its simplicity and its potential for mixed traffic applications. Recently, this feedback control structure has become extremely popular for use in the ACC and the CACC systems (Eskandarian, 2012).

The desired manoeuvres of an automated vehicle are based on longitudinal and lateral motions control through feedback laws. Supporting the drivers to change lanes safely, parking assistance, or tracking vehicle between lanes on highways are the objectives of vehicle lateral control. In addition, longitudinal vehicle motion control in the most fundamental function is to control the speed of the host vehicle and to maintain its distance from the preceding vehicle. The vehicle following control systems provide essentially all of the longitudinal regulation control functionality for the vehicle (Rajesh Rajamani et al., 2000). Due to its potential to significantly increase lane capacity and reduce the costs, vehicle following control has become the mainstream since 1980s (Eskandarian, 2012).

The requirement for the automated vehicle longitudinal control may vary depending on applications and operating conditions. General performance of a longitudinal control should fulfil following requirements (Eskandarian, 2012):

- Accuracy: The achievement of small deviation from a vehicle's desired state.

- Ride comfort: Bounded acceleration/deceleration and jerk for smoothness; no noticeable oscillation and sufficient damping for passenger comfort.

- Consistency: Consistent operation over the range of the expected environmental conditions and for all expected disturbance inputs.

- Efficiency: Effective utilization of the vehicle capabilities and efficient fuel usage.

- Collision detection and avoidance: Automated vehicles require the ability to detect obstacles on the road and to cope with surrounding vehicles in order to avoid collisions.

- Robustness: The vehicle needs to maintain a bottom-line performance even under adverse road and weather conditions.

Typically, tracking accuracy and ride quality are considered as the primary performance requirements for vehicle longitudinal control. Ride quality is important for driver and passenger acceptance but is also closely related to the ability of the control system to save energy consumption (Eskandarian, 2012).

The longitudinal control system can be divided into sensors (and sensor signal processing), control computation, and control actuation of feedback control systems. Sensing vehicle position and its motion play a vital role in the success of a vehicle's longitudinal control system. The sensors can be classified into autonomous sensors and cooperative sensing technologies. The autonomous sensors such as speed sensor, accelerometer, RADAR, LIDAR, or cameras. The cooperative sensing technologies that provide measurements of positions such as GPS in the earth inertial coordinates, or positions of neighbouring vehicles via inter-vehicle communication (Eskandarian, 2012). Control computation (control Algorithm) involve the vehicle longitudinal control command that achieves desired longitudinal motions. Control actuation receives the control command computed by the controllers and *actuate* the corresponding vehicle subsystems so that the desired force can be delivered to the vehicle by utilising the throttle and brake torque actuators (Eskandarian, 2012).

### 3.1.4 Adaptive Cruise Control

During the last decades, technological progress in the field of sensing, communication, and information processing has led to an increasing interest in intelligent functions in vehicles. Driver support systems, such as the ACC, extend a driver's perceptual capabilities since the system accounts for continuous monitoring of headway distance unaffected by fatigue. The ACC system controls the speed and headway of the vehicle, but it can be overruled by the driver, and it even must be overruled by the driver in the case of an imminent collision that is beyond the operational scope of the ACC (Eskandarian, 2012). Future ADAS based on car-to-car communication and car-to-infrastructure systems, so-called *cooperative* systems, will extend the perceptual capabilities of the ADAS applications. The ACC and CACC systems are the extension to the conventional CC.

This section reviews the introduction of various design methodologies for ACC systems, its operation modes, system architecture, and spacing policy are presented in order to illustrate concepts and functions of the ACC. For more details about the ACC systems, follow Eskandarian (2012).

The ACC systems can be categorized into two types: *autonomous* and *non-autonomous*. For an autonomous ACC, the vehicle is controlled based on self-gathered information, whereas communications with adjacent vehicles or transportation infrastructure are required for a non-autonomous system (J. Zhou et al., 2005). The autonomous ACC obtains information about the relative distance and relative speed to the preceding vehicle utilising the forward ranging sensor. This sensor is subject to noise, interference, and inaccuracies, which require that its outputs be filtered heavily before being used for control (Eskandarian, 2012). That introduces response delays and limits the ability of the ACC vehicle to follow other vehicles accurately and respond quickly to changes of traffic flow. For instance, approximately $0.5\,s$ delay in sensing the relative speed by range finder has shown in compared with wireless communication (Fanping Bu et al., 2010). Fusing the forward ranging sensor data with additional information communicated over a wireless data link from the surrounding vehicles and infrastructures makes it possible to extend the ACC to CACC. The CACC compare to ACC vehicles has a high potential to improve traffic flow capacity and smoothness, reducing congestion on highways (Milanes, S. E. Shladover, et al., 2014). In addition, it is found analytically that CACC vehicles enhance the stabilisation of traffic flow with respect to both small and large perturbations compared to the ACC vehicles (Ngoduy, 2013). The impact of different spacing policies for ACC systems on traffic and environment was assessed by Bayar et al. (2016).

The ACC and the CACC systems have been studied extensively from highway speed to stop&go function. With the different point of view, a survey can be found in recent papers (e.g., Vahidi et al. (2003), Khodayari et al. (2010), Bengler et al. (2014), and D. Jia et al. (2016)). In general, these works of literature can be classified into human factor, traffic network operation, and system design. From human factor point of view, the effect of driver behaviour with the ACC were analysed (e.g., see Viti et al. (2008), MarkVollrath et al. (2011), Winter et al. (2014), and Wu et al. (2015)). From traffic network operation point of view, the influence of the ACC on traffic flow characteristics such as capacity, and stability was investigated (e.g., see Junmin Wang et al. (2004), Bianchi Piccinini et al. (2014), and Delis et al. (2015)). Better string stability and tighter following gap of the ACC system compared with manual driving may also provide an improvement in traffic safety and capacity with enough penetration rate of the ACC systems (Marsden et al., 2001; Vahidi et al., 2003). A modelling study shows that if 10% of the vehicles in traffic are equipped with the ACC system, congestion delay can
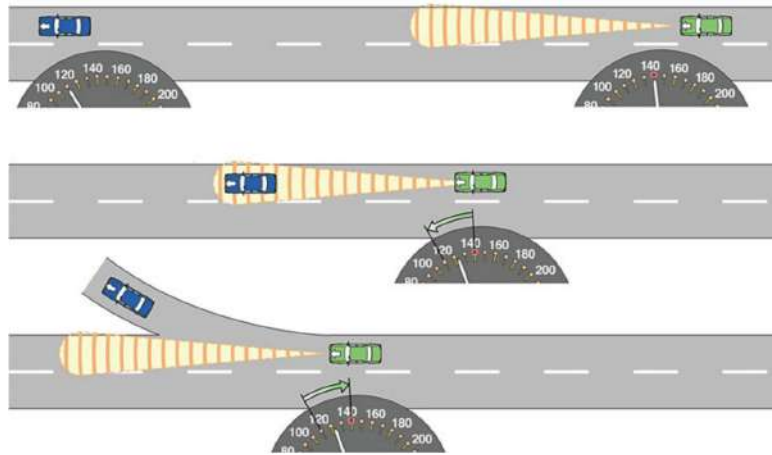
FIGURE 3.5: Adaptive Cruise Control system overview (© Bosch)

decrease by 30% (Driel et al., 2010). From system design point of view, the research and development of the ACC and the CACC system were focused on the two crucial parts which are range sensor (e.g., Tokoro et al. (2003), Miyata et al. (2010), and Dey et al. (2016)) and the controller design which is the main focus of this study.

#### 3.1.4.1 System Overview

A CC system maintains a set fixed speed without further driver intervention. This system enables the vehicle to maintain a fixed velocity whether up or down hill. The ACC system is an enhancement to the conventional CC system (ISO 15622, 2010; ISO 22178, 2009). Compared with the conventional CC systems, which regulate vehicle speed only, an ACC system automatically adjusts the vehicle speed to keep a proper range when a preceding vehicle is detected. When no preceding vehicle is detected, it functions like a conventional CC vehicle (Figure 3.5).

The commercial introduction of the ADAS started in the 1990s with the introduction of CC, while the modern CC systems were offered since 1948. Most early ACC models introduced in the early 1990s and they are equipped with a Laser-based or radar-based sensor used to assess the relative speed and space headway to the preceding vehicle (Eskandarian, 2012). The system automatically adapts the vehicle's speed to maintain a safe distance from vehicles ahead. Sensors of the ACC system extend the possibility to detect lead cars in fog conditions beyond what is possible with the human vision. The driver can switch on/off the system with a preferred cruising speed and space headway setting (within certain boundaries). The ACC system generates appropriate throttle or brake command to maintain a preset cruising speed and preset the following gap to the preceding vehicle. The first-generation ACC systems operated only at speeds above $50\,km/h$ and did not actively brake (Eskandarian, 2012). Although, emergency braking
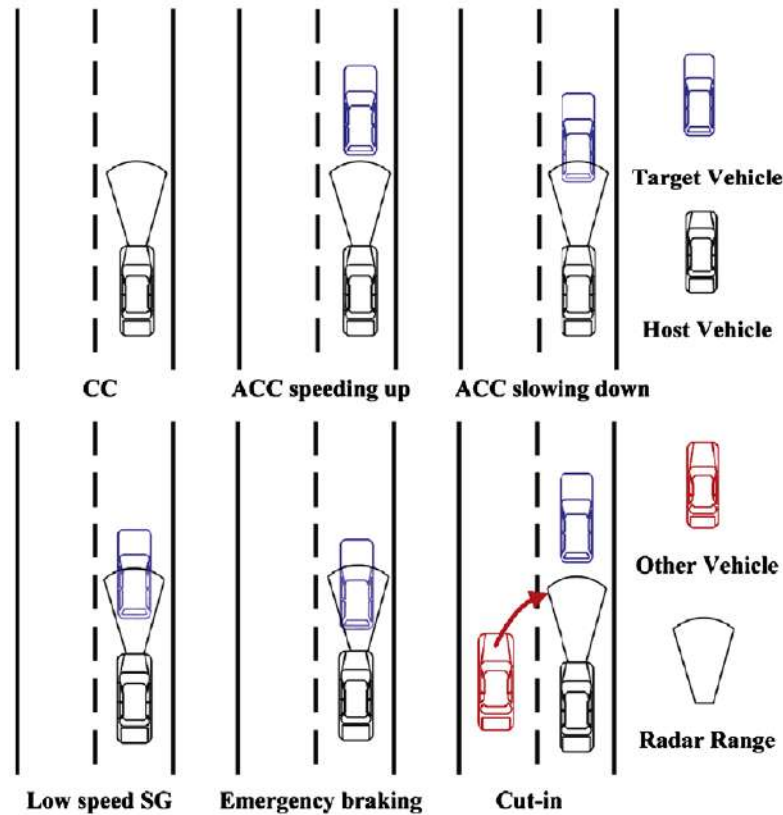
FIGURE 3.6: Full-range ACC system in various driving scenarios (Zhao, Hu, et al., 2014)

is outside of the operational range of the ACC, which in such cases, the driver needs to intervene (Eskandarian, 2012). Nowadays, ACC systems are capable of applying the brake actively (Stop&Go function) and operate at full-range speeds up to stand still. Figure 3.6 shows full-range ACC in various driving situations. The ACC system assists the driver's longitudinal control task with limited acceleration range which reduces workload and stress during daily driving. When the ACC system is turned on, the driver could focus more on other important driving tasks and thus achieve improved comfort and safety.

#### 3.1.4.2 Operation Modes and System Architecture

The typical operation of an ACC system is shown in Figure 3.7. When the ACC system is turned on and no *preceding vehicle* ($v_p$) is present, the vehicle equipped with the ACC system, *host vehicle* ($v_h$), regulates the vehicle speed similar to the conventional CC. Once a preceding vehicle is detected by the range sensor, the ACC system will adjust its velocity to preserve relative distance ($d$), and relative velocity ($v_r$) without driver
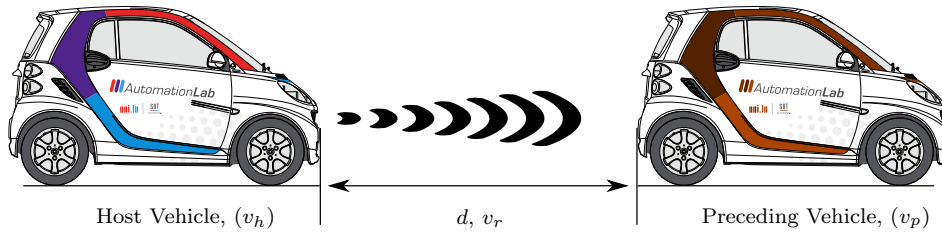
FIGURE 3.7: Typical operation of an Adaptive Cruise Control system
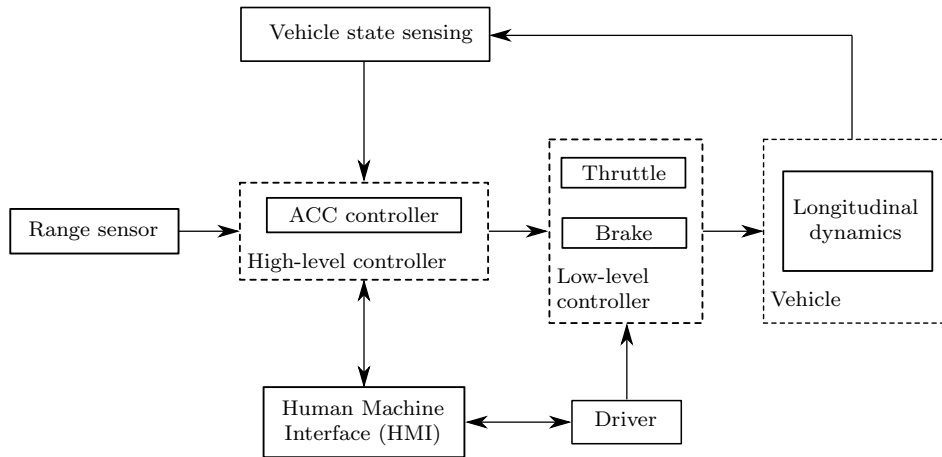


FIGURE 3.8: System architecture of an Adaptive Cruise Control system

intervention requirement. The relative velocity and relative distance are expressed as:

$$v_r := v_p - v_h \tag{3.1}$$

$$d := s_p - s_h. \tag{3.2}$$

The driver can take over longitudinal control by either turning off the ACC system or using brake/throttle pedal to override the ACC system commands (Eskandarian, 2012).

An ACC broad system architecture that fulfils the system operational goals is shown in Figure 3.8. Physically, an ACC system is usually designed as a distributed system comprised of several different Electric Control Unit (ECU)s which are connected by an in-vehicle network such as CAN (Eskandarian, 2012). The range sensor detects preceding vehicles around the host vehicle and measure the relative distance ($d$), and relative velocity ($v_r$) to the preceding vehicles. The long and short range RADAR, LIDAR, wide dynamic range cameras, ultrasonic sensors and laser scanners are commonly used range sensors (Jeong et al., 2012). Robust sense, classify, and assess a large variety of conditions as effectively as conscientious drivers are critical for vehicle applications (Bayless et al., 2014). Vehicle's states sensing provides internal states measurements such as wheel speed, engine speed, gear position, and brake pressure. Most of these measurements already exist and are shared through the in-vehicle network of modern vehicles (Eskandarian, 2012). The ACC systems have several operational modes, and

drivers can be unaware of the mode in which they are operating (Eom et al., 2015). The driver interacts with the ACC system through a Human Machine Interface (HMI). A typical HMI for the ACC system includes displays, switches, and warning devices. The controller is the core of the ACC system. It receives the driver's commands such as turning on or off the system and the following gap setting from the HMI (Eskandarian, 2012). The high level ACC controller maintains the driver's desired velocity and gap setting between the host vehicle and its preceding vehicle based on the detection and measurements results from range sensor, internal states measurements of the vehicle and applies computed control command to throttle or brake actuators through the low level controller.

### 3.1.4.3 Sensing Technology

Detection of the relevant preceding vehicle plays an important role in success or failure of the ACC functionality. The first prerequisite is a set of surrounding sensors which are necessary to detect and then to decide, of the vehicles in the relevant area, whether and which of the detected objects is to be selected as the target object (Eskandarian, 2012). RADAR, LIDAR, and even computer vision are used as surroundings sensor technologies. The background and an overview of the state-of-the-art of millimeter-wave technology for automotive RADAR applications are presented by many research and development centres (see e.g., Hasch et al. (2012), Jeong et al. (2012), Dickmann et al. (2014), and Dudek et al. (2015)). Computer vision-based ADAS applications are designed and implemented in modern vehicles improving the perception performance. A survey of recent works of the literature, placing vision-based vehicle detection in the context of sensor-based on-road surround analysis was reviewed by (Sivaraman et al., 2013). Interest of future ADAS applications including the ACC system lies in principally fusing the RADAR/LIDAR sensors with vision-based sensors (e.g., see Bertozzi et al. (2008) and Widmann et al. (2000)). Fusion with the data from additional sensors will provide a reliable situation assessment which will permit increased performance and functionalities, e.g., vehicle following in traffic queues with automatic longitudinal and lateral guidance (Andrieu et al., 2012).

Millimeter-wave RADARs play an important role for the ADAS applications that require reliable perception in various environmental conditions such as in the rainy, or foggy weather (Stanislas et al., 2015). The Delphi Electronically Scanning Radar (ESR), shown in Figure 3.9, has been designed for the automotive ADAS applications and is aimed at efficient and cost competitive mass production. Unlike classic RADAR system which uses multiple beams with mechanical scanning, this RADAR uses solid state technology with Simultaneous Transmit and Receive Pulse Doppler (STAR PD)

FIGURE 3.9: Delphi Electronically Scanning Radar (*Delphi Automotive Systems Luxembourg S.A.* 2016)
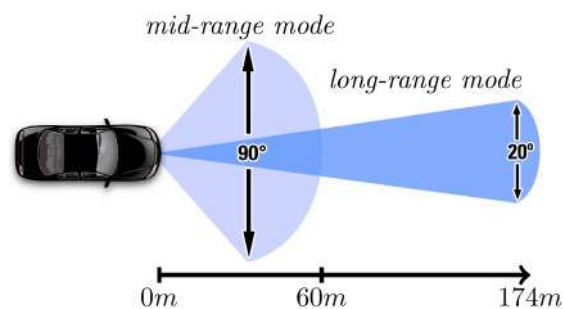


FIGURE 3.10: Delphi Electronically Scanning Radar radar detection zone (Stanislas et al., 2015)

Waveform to electronically perform forward detection (Stanislas et al., 2015). According to the datasheet provided by Delphi, the RADAR operates in two different detection modes simultaneously. As illustrated in Figure. 3.10, the long-range mode should be able to detect targets as far as $174\,m$, within a field of view of $\pm 10°$, whereas the mid-range mode would detect targets at a distance of up to $60\,m$, within a field of view of $\pm 45°$. The range and bearing measurements accuracy of the RADAR are given as a minimum of $\pm 0.25\,m$ and $\pm 0.5°$, respectively. A maximum of 64 targets can be tracked simultaneously by the Delphi ESR (Stanislas et al., 2015). Table 3.1 shows the technical specifications of this RADAR.

The detection process of the RADAR is carried out by an internal high level signal processing unit. For each target detected, the sensor provides information on the estimated centroid of the detected object and its bearing angle. The data are transmitted using a CAN communication protocol, and the minimum measurement rate is $20\,Hz$ (Stanislas et al., 2015). Target detection and tracking play an important role in the quality of the ACC system which in some cases, for instance, false targets may be detected. Determination of the path curvature, path prediction, driver corridor are some of criteria for the target selection (Eskandarian, 2012). In addition, the object speed is one of the most significant criteria for target selection which for instance the oncoming vehicles are

| Parameter | ESR Long-Range Requirement | ESR Mid-Range Requirement |
|---|---|---|
| Minimum Range | < 1m (> 10dB target) < 1m (> 0dB target) | < 1m (> 10dB target) < 1m (> 0dB target) |
| Maximum Range | > 175m (> 10dB target) > 100m (> 0dB target) | > 60m (> 10dB target) > 50m (> 0dB target) |
| Range Accuracy | < +/-0.5m noise component with +/- 5% bias component | < +/-0.25m noise component with +/- 5% bias component |
| Range Discrimination for two targets at same angle & range rate | < 2.5m | < 1.25m |
| Minimum Range Rate | < -100m/s | |
| Maximum Range Rate | > +40m/s | |
| Range Rate Accuracy | < +/- 0.12m/s | |
| Range Rate Discrimination for two targets at same range & angle | < 0.5 m/s | |
| Acceleration | Acceleration to be generated as an output of the Tracker | |
| Minimum Lateral Relative Velocity | < -20 m/s | |
| Maximum Lateral Relative Velocity | > +20m/s | |
| Lateral Relative Velocity Accuracy | Lateral velocity is derived in the tracker based on change in measured angle vs. time. Accuracy in m/sec is a function of range. | |
| Azimuth Field of View | > 20deg | > 90deg |
| Azimuth Angle Centroid Accuracy | < +/- 0.3deg (corner reflector targets) < +/- 0.5deg (other targets) | < +/- 1.0deg |
| Azimuth Angle Resolution of two targets at same range & range rate | < 3.5 deg | < 12 deg |
| Vertical Field of View | 4.2deg – 4.75deg | |
| Minimum Amplitude | < -10dB | |
| Maximum Amplitude | > 40dB | |
| Minimum Update Interval | >= 20Hz | |
| Minimum Target Tracking | 64 fused targets total | |

TABLE 3.1: Delphi Electronically Scanning Radar technical specification (Stanislas et al., 2015)
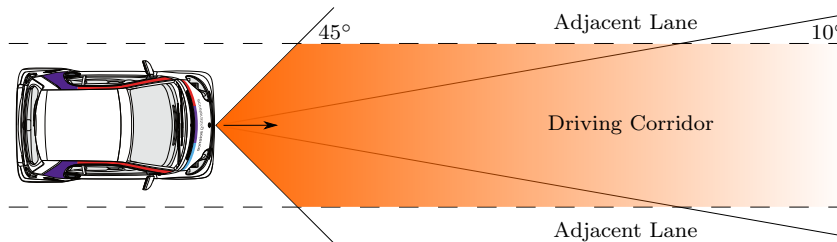


FIGURE 3.11: Driving corridor in order to avoid wrong assignment

completely ignored for control purposes. Another simple but very effective approach is to limit the maximum relative target distance as a function of the travel speed (Equation 3.3). Empirical values suggest a distance value $d_{to.0} = 50\,m$ and an increase of $\tau_{to} = 2\,s$ (Eskandarian, 2012).

$$d_{to.max} := d_{to.0} + v_h \tau_{to} \tag{3.3}$$

Taking the Delphi ESR specification and the Smart-ED maximum speed into account, the $\tau_{to}$ can be also increased to $4.4\,s$. If several objects meet the criteria for a target object, the smallest distance target can be selected. Figure 3.11 shows the Smart-ED with Delphi ESR RADAR driving corridor for target selection and tracking utilised in this study. When negotiating bends, target loss is possible due to the maximum azimuth angle of the ACC sensor is inadequate to detect the target object (Eskandarian, 2012). The reaction to target losses can be improved using a digital filter, or digital map information.

### 3.1.4.4 Spacing Policy

Desired gap determination plays an important role in ACC design. Constant spacing policy ($d_{ref} := d_0$), where $d_0$ is a constant was proposed for the vehicle platoon of Automatic Highway System (AHS). It is shown that string stability can be achieved only if the lead vehicle velocity and acceleration are broadcasted to the other vehicles in the platoon. String stability generally means that gap regulation errors will not be amplified from the lead vehicle to the last vehicle in the platoon (Eskandarian, 2012). A speed-dependent spacing policy also called *time headway* is the most commonly used for the commercial ACC systems (Eskandarian, 2012). The desired spacing can be defined as follows:

$$d_{ref} := d_0 + v_h t_{hw} \tag{3.4}$$

where $d_0$ is the minimum constant safe distance and $t_{hw}$ is the time headway ranging between $0.8\,s$ and $2.2\,s$ (ISO 15622, 2010). The maximum braking deceleration capability, the delay and execution rate of the sensors and actuators are important factors in determination of the minimum time headway of an ACC vehicle. One of the drawbacks of the time headway policy is its poor robustness against traffic flow fluctuation. A nonlinear spacing policy for the stability of traffic flow related with a traffic density parameter was developed by Junmin Wang et al. (2004). In addition, a *quadratic spacing policy* that was optimized for both string stability and traffic flow stability was introduced by J. Zhou et al. (2005) as follows:

$$d_{ref} := 3 + 0.0019v_h + 0.0448v_h^2 \tag{3.5}$$

In order to create a controller that also consider vehicle safety explicitly, Meng Wang, Winnie Daamen, et al. (2014) proposed a variable time gap policy, which tries to keep larger time gaps at lower densities and vice versa. In addition, a field test was conducted to determine whether or not the drivers would be comfortable with the sub-second following time-gaps that could be provided by the ACC and the CACC systems (e.g., Figure 3.12). From the traffic network operation point of view, string stability means smooth traffic flow and less *shock wave*. From the driver's point of view, guaranteed string stability will provide a smooth ride and possible safety benefit (Eskandarian, 2012).

### 3.1.4.5 Control Design Methodologies

Various control methodologies have been proposed in the works of literature for the controller design of the ACC systems. Linear and nonlinear controllers such as Proportional
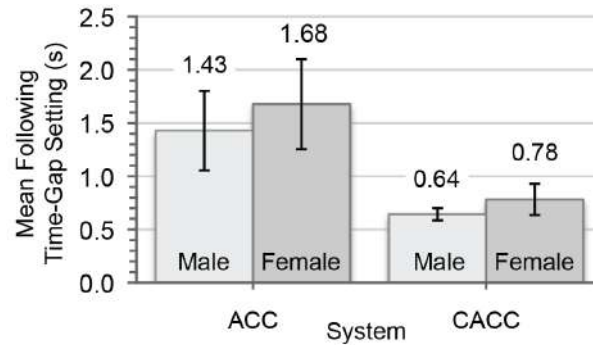
FIGURE 3.12: Mean Following Time-Gap Setting for ACC and CACC (Nowakowski et al., 2010)

Integral Derivative (PID), linear optimal control, gain scheduling, and slide mode control introduced for the ACC (see e.g., R. Rajamani et al. (2002), Moon et al. (2009), and Ganji et al. (2014)). Liner controller alone could not achieve adequate performance for all traffic conditions (Eskandarian, 2012). Soft computing methods such as fuzzy logic controller, neural network, or Adaptive Neuro Fuzzy Inference System (ANFIS) is introduced to mimic human driver behavior for the ACC controller design (see e.g., Naranjo et al. (2006), Milanes, Villagra, et al. (2012), Zhao, B. Wang, et al. (2013), and Khayyam and Bab-Hadiashar (2014)).

To design an ACC controller that has satisfactory performance in real traffic environment, either pure linear controller needs to be complemented by certain nonlinear elements or a nonlinear design needs to be adopted (Eskandarian, 2012). The ACC controller design often needs to meet multiple contradictory design objectives with stringent constraints. MPC is a control framework that could perform constrained multi-objective optimisation. More details about the different MPC controllers for the ACC system as the main focus of this study have been reviewed in Chapter 4.

### 3.1.4.6 Other System Aspects

The ACC and the CACC with various design objectives have been introduced and evaluated from different aspects of the system. Driver acceptance and adaptation for the ACC examined by e.g., Xiong et al. (2012), Hajek et al. (2013), Winter et al. (2014), and Eom et al. (2015). The ACC and the CACC systems extensions and performance improvement explored by e.g., see R. Rajamani et al. (2002), D. K. D. Kim et al. (2009), Miyata et al. (2010), Malakorn et al. (2010), Bifulco et al. (2013), and Montanaro et al. (2014).

## 3.2   Ecological Driver Assistance System

Transportation is the second largest sector after energy production in worldwide energy consumption and greenhouse gas emissions (Sciarretta et al., 2015). Improvement of energy efficiency is a challenging task in the reduction of the contribution of transportation. Generally, three energy conversion steps are investigated for the energy efficiency of the transportation. Impacts of *grid-to-tank*, which convert stationary distribution nodes to an onboard storage have been studied for the EVs (see e.g., Veldman et al. (2015)). Considering the component level or the system control level, *tank-to-wheels* efficiency can improve propelling the vehicle by converting the onboard energy to mechanical energy. This was investigated by several approaches (see e.g., Poullikkas (2015) and Rahman et al. (2015)).

The *wheels-to-distance* efficiency, which is influenced by vehicle parameters and the driving profiles is in support of this study. In the wheels-to-distance conversion step, the energy required by the displacement is achieved by conversion of the mechanical energy into the kinetic and potential energy. The wheels-to-distance efficiency can be achieved by several methods. Reducing the external load of the powertrain, such as the vehicle mass, rolling resistance and aerodynamic drag are the main approaches. In addition driving behaviour, infrastructure and traffic management, law, policy and legislation have significant impacts on the wheels-to-distance efficiency.

The vehicle mass has an important effect on vehicle inertia, road rolling resistance, and road slope resistance. Hence the lightweight vehicles can have a significant improvement in the energy consumption. The energy consumption of the vehicle may also be reduced by utilising the low rolling resistance tires. The aerodynamic drag resistive force can be reduced with an improved aerodynamic design of the vehicle. The energy losses and gains for an EV for combined, city and highway driving is shown in the Table 3.2 (Lohse-Busch et al., 2013). Unlike the ICE vehicles, a loss of 16% energy during the grid-to-tank charging experienced for the EVs. However, the energy delivering from the tank-to-wheels of the EVs are highly efficient even before energy is reclaimed through regenerative braking. When energy gains from regenerative braking are included, the amount of energy used for travelling down the road can rise to more than 80% in the Environmental Protection Agency (EPA)-combined city and highway driving cycle (Lohse-Busch et al., 2013). This section provides an abstract overview of methods to an energy efficient transportation.

| | Types of Driving | | |
|---|---|---|---|
| | **Combined** | **City** | **Highway** |
| **Types of Losses** | Energy Losses | | |
| Energy Lost in Charging Battery | 16% | 16% | 16% |
| Electric Drive System Losses | 16% | 18% | 14% |
| Parasitic Losses | 3% | 4% | 2% |
| **wheels-to-distance, dissipated as:** | | | |
| Wind Resistance | 36% | 29% | 45% |
| Rolling Resistance | 23% | 25% | 22% |
| Braking | 23% | 40% | 7% |
| **Types of Gains** | Energy Gains | | |
| Regenerative Braking | -17% | -32% | -6% |

TABLE 3.2: Energy losses and gains for an Electric Vehicle (Lohse-Busch et al., 2013)

### 3.2.1 Ecological Driving

The effects of decisions a driver make to influence on the vehicle's energy consumption include strategic decisions (vehicle selection and maintenance), tactical decisions (route selection and vehicle load), and operational decisions (driver behaviour) (Sivak et al., 2012). The Eco-driving goal is to adapt the driving profile to an energy-aware driving profile. The Eco-driving is considered to be one of the most cost-effective methods in the ITS to improve the road safety and environment-friendly driving style. The Eco-driving describes the adaptation of driving style to reduce energy consumption in an efficient and cost-effective manner. Many investigations of the Eco-driving policy have reported potential reductions in the fuel consumption and $CO_2$ emissions ranging from 5 % to 40 % across various jurisdictions and initiatives (M. S. Alam et al., 2014). The Eco-driving is of high importance when driving the BEVs in terms of prolonging the vehicle's limited range (Franke et al., 2015). The Eco-driving strategies for the BEVs are as follows (for more details see Franke et al. (2015)):

- Avoid high speeds

- Accelerate moderately

- Drive evenly (speed and acceleration)

- Use regenerative braking/avoid braking

- Choose anticipatory driving style

- Avoid auxiliary features

- Drive in a way that the instantaneous power meter indicates low energy consumption

- Let the car cruise (sailing)

- Choose the most energy-efficient route to destination

- Choose optimal tires/tire pressure

- Minimise load

Improving the wheels-to-distance efficiency by controlling the driving profile reveals its potential when considering that it does not require structural changes to the system (Sciarretta et al., 2015).

### 3.2.2 Ecological Advanced Driver Assistance Systems

There is a variety of EDASs proposed to support the driver in more energy efficient driving. Software tools and systems that assist the driver (or replace the driver) in performing Eco-driving have also emerged and are divided into three main categories as follows (Sciarretta et al., 2015):

- *Pre-trip* systems: support the driver in the planning phase before the trip is started. These systems are integrated within navigation systems providing the most energy-efficient route to the driver.

- *In-trip* systems: support the driver during the trip by providing relative information on Eco-driving. These systems under the ADAS are categories as follows:

  - Online assessment systems: provide feedback advice based on current performance by visual displays, audible or haptics.

  - Online advice systems: give a predictive, feedforward advice, based on upcoming events

  - Predictive CC and ACC: automatic driving is performed.

- *Post-trip* systems: support the driver by providing summaries and statistics of the travelled trip and recommendations for the next trip.

The pre-trip systems such as navigation system balance distance and time by providing a route based on various methods. The shortest route that is generally slow routes, with many starts and stops that may lead to high energy consumption. The fastest route provides fewer intersections and less start and stops, but longer distances and high energy consumption (Eskandarian, 2012). A third option so-called Ecological Routing (Eco-routing) provides the most energy-efficient route based on energy consumption information. The Eco-routing for the BEVs that suffer from the *range anxiety* have
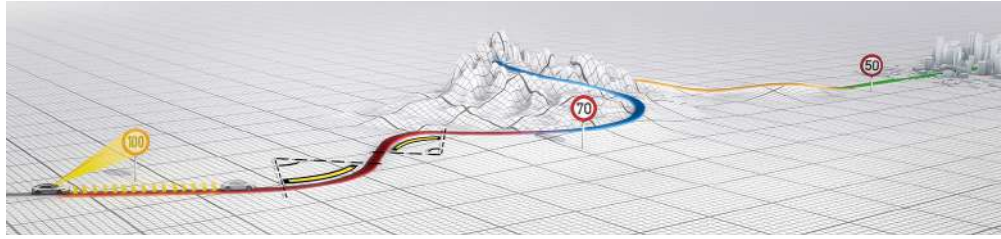
FIGURE 3.13: Porsche InnoDrive, the extended ACC system (Porsche, 2016)

investigated in works of literature e.g., by Moran et al. (2010), M. Richter et al. (2012), and Ondruska et al. (2014).

The in-trip systems are offered by the vehicle manufacturers and third parties such as the Scania CC with Active Prediction, Porsche Innodrive ACC system, Honda EDAS, Nissan Eco Pedal, TomTom ecoPlus, and European Research Project ecoMove (for more detail review see Hof et al. (2014)). For instance, the Porsche InnoDrive is an extended version of the ACC system that utilise digital map to adapt the vehicle velocity to the upcoming road (Roth et al., 2011). With an extended preview horizon based on a precise digital map, the driving strategy can be optimised according to efficiency criteria (Roth et al., 2011). An electronic horizon provides road slope, road curvature, speed limit zones and the position of intersections are taken into account to provide an optimal velocity profile (for more details see (Maurer et al., 2013)).

An example for a post-trip system is Fiat's *eco:Drive*. This system supports the driver in saving fuel by analysing the recorded driving behaviour. The driver receives a score as well as advice to improve their driving style. Smooth acceleration and early gear changes have the most influence on fuel consumption whereas moderate braking is easier to realise (Hof et al., 2014).

Encouraging drivers towards the Eco-driving can reduce the energy consumption (see e.g., Andrieu et al. (2012) and Dib et al. (2014)). They do not provide concrete information such as the level of velocity or acceleration required for long-term fuel-efficient driving by analysing current vehicle-road-traffic situation and its trend (M A S Kamal et al., 2011). Most of the current approaches are based on heuristic rules of thumb associated with the Eco-driving. Moreover, drivers do not always and under all circumstances drive ecologically. Besides, driver's Eco-driving mental workload is still high, which may lead to distraction (see e.g., Rouzikhah et al. (2013)). On the other hand, utilising automatic ADAS systems can support drivers in an ecological way. A few approaches are based on anticipatory driving ADAS to reduce the energy consumption by anticipating earlier the future situations (Rommerskirchen et al., 2014). Several concepts attempt to implement the Eco-driving in a more rigorous framework (Sciarretta et al., 2015). In these concepts, the Eco-driving controller is regarded as an OCP, where the drive

commands minimise the energy consumption for a given trip (Sciarretta et al., 2015). More details about the Eco-driving ACC design assumptions and system objectives is reviewed in next section while control objectives will be reviewed in Chapter 4.

### 3.2.3 Ecological Adaptive Cruise Control

The EDAS anticipates the future states of vehicles and calculates the optimum vehicle control input required for ecological driving using current road-traffic information, dynamic models, anticipate future states and the energy consumption model of the engine (M A S Kamal et al., 2011). The vehicle under control of Eco-ACC systems minimise energy consumption in addition to other control objectives of the conventional ACC systems. Compared to the ACC systems, the Eco-ACC systems lead to a smoother vehicle following behaviour and a substantial reduction of consumed energy (Meng Wang, Winnie Daamen, et al., 2014). In addition, the impacts of the Eco-ACC systems for the ICE vehicles on traffic and environment investigated in the works of literature (see e.g., (Meng Wang, S. Hoogendoorn, et al., 2014)).

There are several key factors that affect the energy consumption of the BEV. Road slope is one of the main factors that affect significantly on the vehicle energy consumption rate. The conventional CC and ACC systems have to spend more energy to maintain a preset speed during uphill driving, while they have to waste the kinetic energy of the vehicle by applying the brake in downhills to preserve the desired speed. The Eco-driving strategies, on the other hand, could take the advantages of gravity force of the road during the up/down hills to improve the energy consumption level. The velocity of the vehicle can be decreased from a specific percent of the preset value during uphills and increased in downhills to improve the tradeoff between travel time and energy consumption. For instance, Figure 3.14 shows the *Scania Active Prediction System* utilising the road slopes to improve the fuel-efficiency and travel time.

An ecological predictive CC system that utilises topographical data to develop proactive CC to minimise the ICE vehicles fuel consumption investigated in works of literature. An Eco-ACC with driver behaviour learning capability for improving the performance of powertrain was designed by Bichi et al., 2010. A development of an ecological CC system for running a vehicle on roads with up–down slopes introduced by M A S Kamal et al. (2011). The system requires a GPS-based navigation system with the digital road map to obtain the position of the car and road gradient (M A S Kamal et al., 2011). Utilising of the upcoming traffic signal information within the vehicle's ACC system to reduce idle time at stop lights and fuel consumption introduced by Asadi et al. (2011). A control policy that prescribes vehicle speed to minimise on average a weighted sum
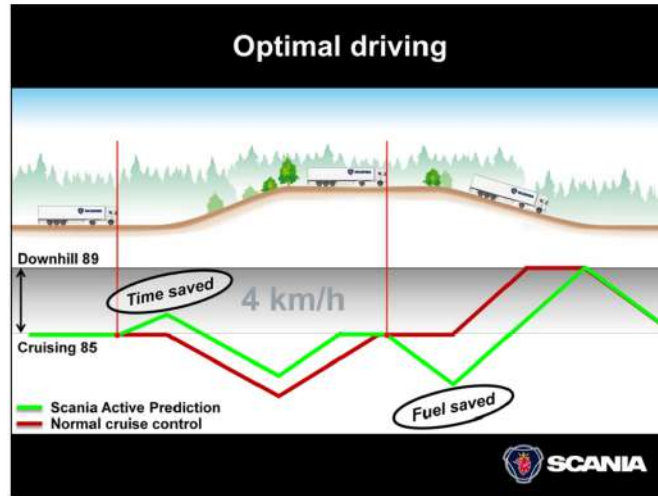
FIGURE 3.14: Scania Active Prediction Advanced Cruise Control System (Scania, 2011)

of fuel consumption and travel time, while travelling along the same route or a set of routes in a given geographic area presented by McDonough et al. (2012). An ACC system based on ANFIS that reduce the energy consumption of the vehicle and improves its efficiency introduced by Khayyam, Nahavandi, et al. (2012). In addition, an Eco-ACC system to drive a vehicle efficiently on roads containing varying traffic and signals at intersections for improved fuel economy introduced by Md Abdus Samad Kamal et al. (2013). An optimisation of a conventional ACC for the specific use of the EVs with regenerative capacity, namely the Smart and Green ACC introduced by Glaser et al. (2013). An approach for the analysis of potential fuel efficiency for the HEV is proposed by Heppeler et al. (2014), where torque split, gear shift and velocity trajectory are optimised. An energy-efficient CC for the BEVs as well as a simulation model of the longitudinal vehicle dynamics and its energy consumption presented by Tim Schwickart (2015) and Tim Schwickart, Voos, Hadji-Minaglou, et al. (2016). Last but not least, an Eco-ACC to improve both fuel economy and safety of HEV introduced by Vajedi et al. (2016).

## 3.3 Proposed Eco-Driving Assistant System Concept

Albeit operational and fundamental principle in the BEVs and ICE vehicles are similar, there are some differences between them Ehsani et al. (2009). For instance, the BEVs in contrast to the ICE vehicles have a lower centre of gravity due to heavy battery package versus gasoline tank. In addition, unlike the ICE vehicles, the BEVs generally have single-speed transmission system and capabilities to obtain regenerative energy. Therefore, any EDAS system for the BEVs should account the properties of them.
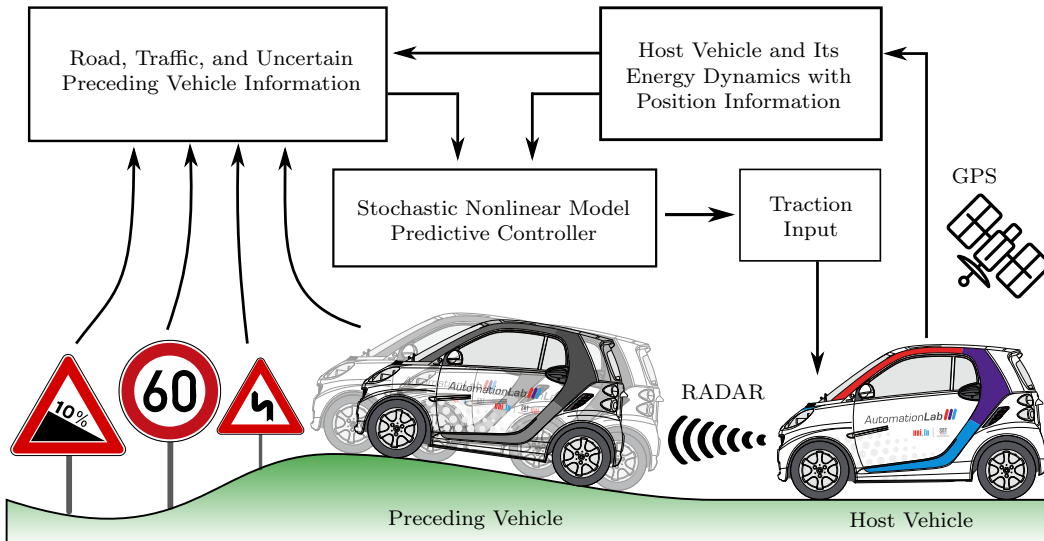
FIGURE 3.15: Semi-autonomous Eco-ACC system with extended functionalities (SEDAS)

This study extends the functionalities of the conventional Eco-ACC system in a various manner which specialised for the BEVs. In addition to the standard CC and ACC operations, the proposed Stochastic Model Predictive Control for Eco-Driving Assistance System (SEDAS) concept takes the road curves, traffic speed limit zones, and the preceding vehicle statistical motion information into account to improve the ecological driving.

The main idea of the proposed Eco-driving concept is to minimise the improper acceleration and deceleration of the BEV based on various road and traffic conditions. The SEDAS allows the vehicle to adjust the desired reference velocity and to hold a desired lateral acceleration during curves without any input from the driver. This could be an energy efficient technique since the more optimal speed carried into a corner, the less energy it takes to compensate afterwards. This technique is helpful also for the velocity profile planning in traffic speed limit zones and the preceding vehicle following scenarios. In addition, this system includes Stop&Go function that automatically regulates the velocity of the vehicle while maintaining a safe distance from the preceding vehicle. In addition, the proposed concept is to follow the preceding vehicle close enough to take advantage of the aerodynamic drag force reduction. The energy consumption revenue arising from the close spacing with the preceding vehicle by reduction of the aerodynamic drag force.

The SEDAS concept is presented in Figure. 3.15. Similar to the typical CC and ACC system, the driver pre-sets the desired velocity with preferred safe distance from the preceding vehicle. The semi-autonomous SEDAS regulates the traction input with respect to the longitudinal motion, energy consumption dynamics of the BEV (host vehicle), as

well as the road geometry, traffic sign, and motion of the preceding vehicle information. While the driver simply focuses on the steering control of the vehicle, this system should plan for a safe and energy-efficient cruising velocity profile autonomously on the entire trip without requiring driver interventions. The GPS based navigation system is used with a proposed digital road map model to obtain the position of the BEV, road slope, road curvatures, and speed limit zones. The states of the BEV such as velocity, battery voltage, battery current, etc can be sensed by utilising the CAN network.

An energy efficient driving has to be based on the predicted future states of the vehicle, road and traffic situations. Thus, the SEDAS could have promising potentials for ride quality, vehicular performance, road safety, and energy efficiency for the BEVs. The optimal traction input is calculated by the mathematical optimisation method based on SNMPC. The control input is generated by anticipating future situations of the BEV dynamics, its energy consumption, road geometries and traffic situations such as the preceding vehicle motion. In addition, the road map model is also utilised to estimate predictively the uncertain plausible preceding vehicle motion and its position in order to regulate a safe distance with efficient planning. Thus, the result of the mathematical optimisation is provided as a reference tracking value for the low-level controllers to apply proper actuation on the accelerator and brake pedals. The longitudinal dynamics, energy consumption of the BEV, road geometry, as well as traffic sign information, are modelled as deterministic components. The preceding vehicle's motion and its position are considered as the stochastic part of the system that imposes uncertainty during the decision-making process. Details of the problem OCP formulation including the performance index, and the control method are described in Chapter 4.

### 3.3.1 Aerodynamic Drag Reduction

Vehicle drag reductions arising from close spacing discussed in works of literature (see e.g., Liang et al. (2013) and A. Alam et al. (2015)). Drag and lift data from wind-tunnel tests on two co-linear Ahmed bodies presented by Watkins et al. (2008). The Ahmed body is the representative vehicle shapes able to replicate typical car airflow, configured with 30° slant back angles. Figure 3.16 shows the aerodynamic drag and lift variations in close spacing.

The aerodynamic drag coefficient of the Smart-ED depends also on the relative space to the preceding vehicle which it is proposed to be modelled as follows:

$$C_D(d) = C_{D0}(a_1 + a_2 tanh(a_3(d - d_0)^2)), \qquad (3.6)$$
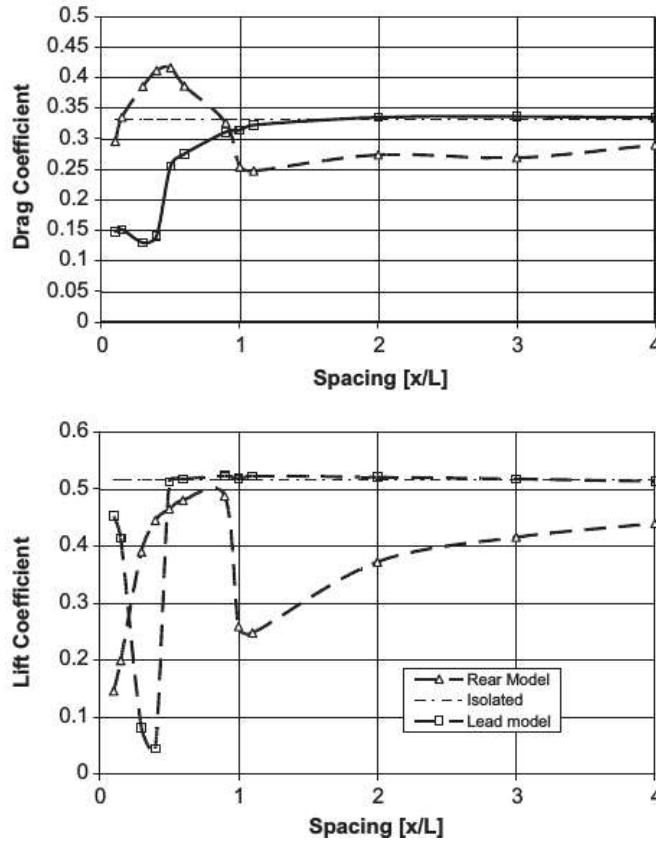
FIGURE 3.16: Aerodynamic drag and lift variations in close spacing (Watkins et al., 2008)

where $C_{D0}$ is the nominal aerodynamic drag coefficient in isolated mode and coefficients of the model $(a_1, a_2, a_3)$ are estimated by the curve-fit process from the data points presented by Watkins et al. (2008). Thus, the aerodynamic drag force 2.4 can be rewritten as follows:

$$F_w = \frac{1}{2} \rho_a A_f C_D(d) v^2, \tag{3.7}$$

where the aerodynamic drag of the Smart-ED is a function of relative distance to the preceding vehicle.

## 3.4 Road Geometry and Static Traffic Model

In order to have proper functionality for the proposed SEDAS concept, the surrounding world such as the road infrastructure, or the surrounding vehicles including the preceding vehicle should be modelled and interpreted as accurately as possible. The term *virtual* sensor is used for an information source, which is not an actual sensor, but comprises an important input for the intelligent vehicle's applications (Eskandarian, 2012). One of the most important representatives of this category is the digital road map. A standard

digital map used in automotive applications mainly contains geometric information and other relevant attributes about the road (Eskandarian, 2012). The digital map data can be extracted and used by a vehicle when positioning information is available. Standard map positioning techniques are based on the GPS technology combined also with inertial sensors such as gyroscopes and odometers in case the satellite connection with the GPS is unavailable (Eskandarian, 2012).

A compact, informative road map and traffic conditions ahead are beneficial for the Eco-driving safety and energy management ADAS applications. This allows the ADAS to be informed of static and dynamic situations, and take effective actions based on this information. Generally, the road mainly depends on static parameters such as road slope, road curvature, speed limits, pedestrian crossings, and the number of lanes as well as dynamic parameters such as real-time traffic data, weather, and road conditions (Eskandarian, 2012). Continuity of the road slopes, road curvatures, and traffic speed limit zones are an important criterion that a road model should fulfil in order to ensure that the SEDAS controller system can deal with.

One of the most typical ways of representing the road geometric data is to define data points of interest along the road centreline with specified intervals corresponding to the desired road profile accuracy level. Curvatures are represented as piecewise linear lines for a gentle curve (see e.g., (Yu et al., 2014)) or as a polyline for a sharp curve Eskandarian (2012). There are several interpolation methods to construct new data points of interest and road model estimation (see, e.g, Daniel et al. (2009), Yan et al. (2013), B. Kim et al. (2014), Thomas et al. (2015), X. Li et al. (2016)). The commonly preferred method is the clothoid spirals curves that are used as a smooth transition curve for connecting and transiting the geometry between points of interests. However, most of these methods are applicable for two coordinate system dynamics and are less flexible to be directly applied in a single coordinated ADAS applications. Moreover, the interval determination of data points of interest can lead to either overestimated or underestimated accuracy levels for different road segments. Those approaches impose a tradeoff challenge between accuracy level and fidelity levels of the models which may not be desirable for the real-time SEDAS concept.

### 3.4.1 Proposed Road Geometry Model

A new way of defining accurately the road geometry and traffic data in four dimensions is proposed in this study to support the SEDAS. Topological road data are expressed as a series of connected data points of interest (segments) in four dimensions. The digital map database provides carefully measured data points which represent the centre line position
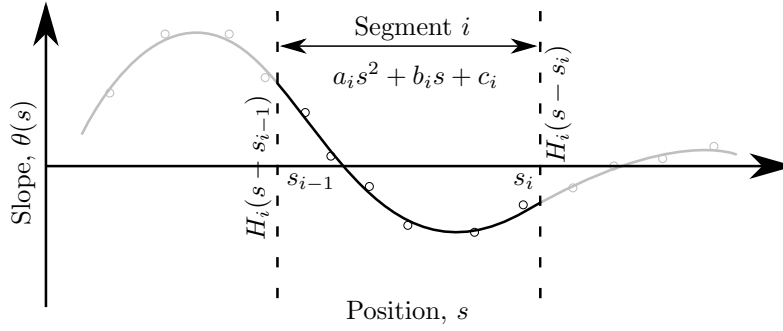
FIGURE 3.17: Proposed road slope model at segment $i$

of the road. In this study, the road slopes, road curvatures, and traffic speed limit zones data are modelled as continuous and differentiable functions of the vehicle's position. These functions represent the data points of interest in each segment of the road. The hyperfunction concept as a kind of generalised functions is used to interconnect the estimated segments of the road to each other at the boundaries. These models use the vehicle's position to provide the upcoming road geometries and traffic information to the system controller.

### 3.4.1.1 Road Slopes Model

The road slope data allows the vehicle to be informed of static road slope conditions, and take efficient actions based on that information. This is an effective Eco-driving strategy that takes advantage of the gravity to improve the travel time and energy consumption efficiency. The road altitude $R_{alt}$ information from the digital road map (in meters) is used to calculate the gradient angle $\theta(s_h)$ at location $s_h$ as follows (M. A S Kamal et al., 2011):

$$\theta(s_h) = tan^{-1}\left(\frac{R_{alt}(s_h + \Delta s_h) - R_{alt}(s_h - \Delta s_h)}{2\Delta s_h}\right) \tag{3.8}$$

where $\Delta s_h$ is a relatively small value (in meters). The interval determination of data points of interest can lead to a tradeoff challenge between the accuracy level and size of data points. In this study, the road slope profile is proposed to be the sum of quadratic functions of the position representing each road segments slope data. The modelling concept is shown in Figure 3.17. Based on the stated context, the road slope profile can be defined as:

$$f_{slope}(\theta(s)) := \sum_{i=1}^{N_{sgm}} H_i(s - s_{i-1})(a_i s^2 + b_i s + c_i)H_i(s - s_i), \tag{3.9}$$

where $N_{sgm}$ is the number of road segments, the $H_i(s - s_{i-1})$ and $H_i(s - s_i)$ are the hyperfunctions of the *ith* road segment. These hyperfunctions may be represented by

the approximate Heaviside's functions at the boundary position values, $s_{i-1}$ and $s_i$, as follows:

$$H_i(s - s_{i-1}) = \frac{1}{2}(1 + tanh(k_{i+}(s - s_{i-1}))), \qquad (3.10)$$

$$H_i(s - s_i) = \frac{1}{2}(1 - tanh(k_{i-}(s - s_i))) \qquad (3.11)$$

where a large $k_{i\pm}$ corresponds to a more sharp transition at the boundary positions. The $k_{i\pm}$ and coefficient of the quadratic functions are estimated by the curve-fit process from the data points, which provides a smooth transition from one road segment to another. The vehicle position based function (3.9) is a continuous and differentiable function that represents the data points of interest in each segment of the road. In this approach, the tradeoff challenge between the high and low-fidelity models for SEDAS is avoided. The proposed model can now be efficiently integrated into the BEV dynamics (2.1) to form a unified system model.

### 3.4.1.2 Road Curves Model

A horizontal curve provides the directional transition on the horizontal plane, between two straight sections of the roadway running in different directions. Horizontal curves are expressed as circular curves with constant radii, or successive curves with different radii (for more details see Fwa (2006)). The road curves alignments can also be modelled in a similar concept with the proposed road slope model. The horizontal road curves may be parabolic or circular, which can be classified as simple, compound, reverse, and deviation curves. A simple road curve has the same radii (in meters) around a single arc of the circle ($R_{crv}$). Since the road curve is defined as $R_{crv}^{-1}$, similar to the geometry of the Euler spiral, the simple circular curve is used to express the total absolute curvature alignment in this study, which is defined as:

$$f_{curve}(\delta(s)) := \sum_{i=1}^{N_{crv}} H_i(s - s_{ent}) \left| \frac{1}{R_{crv_i}(s)} \right| H_i(s - s_{ext}), \qquad (3.12)$$

where $N_{crv}$ is the number of roadway curves, and $R_{crv_i}$ is the radii of a circle valid for the curve's constant radii with two position points, $s_{ent}$ and $s_{ext}$, at the respective entrance and exit position of the curve $i$ independent of the bend direction. The $R_{crv_i}$ for a straight road segment can be considered as a large numerical number. It is noteworthy, the related $k_{i\pm}$ in the approximate hyperfunctions (3.10) can determine the transition between the straightforward segment of the roadway, known as tangents and the circular curve.

FIGURE 3.18: Centre de Formation pour Conducteurs S.A., Colmar-Berg, Luxembourg (Schroeder, 2016)

#### 3.4.1.3 Road Traffic Speed Limit Zones Model

The road sign information that have influence on the cruising velocity play an important role in the Eco-driving strategy. In this study, the traffic speed limit zones as one of the most effective item is considered to be modelled similarly to the previous road geometry methodology as follows:

$$f_{lmt}(s) := \sum_{i=1}^{N_{lmt}} H_i(s - s_{str})(v_{lmt} - v_{max})H_i(s - s_{end}) + v_{max}, \tag{3.13}$$

where $N_{lmt}$ is the number of speed limit zones along the roadway, and $v_{lmt}$ is the specified speed limit value at positions starts from $s_{str}$ upto the end of the zone position $s_{end}$. The $v_{max}$ is the maximum speed value of the vehicle. Note that, the associated $k_{i\pm}$ in the approximate hyperfunctions can regulate the transition policy between the speed free and limit zones. The proposed model for the road curves and traffic speed limit zones can now be efficiently utilised in the SEDAS concept.

### 3.4.2 Road Geometry and Static Traffic Models Validation

The proposed road geometry and traffic speed limit zone models are evaluated on a closed test track located at Centre de Formation pour Conducteurs S.A. Colmar-Berg, Luxembourg (CFC, 2015). The test track's geometry with assumed traffic information is modelled and validated. Figure 3.18 shows the aerial view of the test track (Schroeder, 2016). The test track has a total length of 1.255 *km* which has curves, speed limit zone,
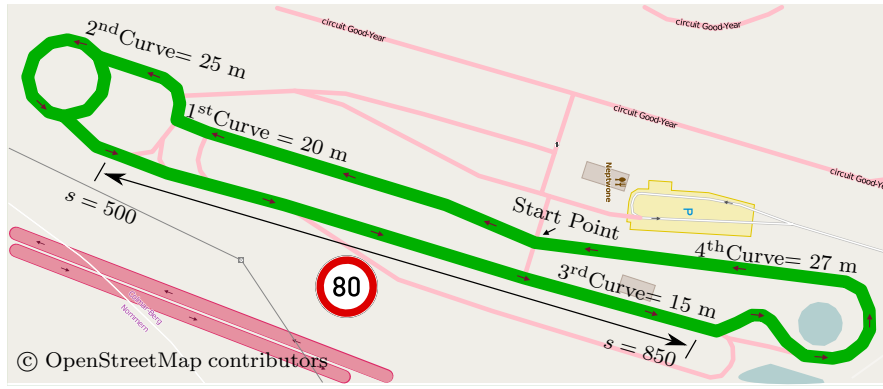
FIGURE 3.19: Test track, Centre de Formation pour Conducteurs S.A.



(A)

(B)
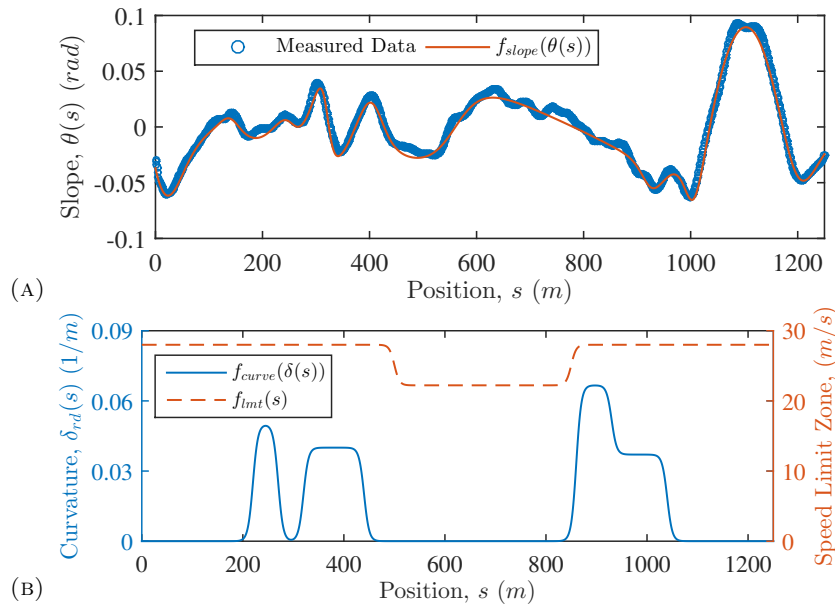
FIGURE 3.20: Test track slope, curves, and speed limit zone profile

and relative slope profile. This track has four main curves with first curve radii equal to 20 $m$, second curve radii equal to 25 $m$, third curve radii equal to 15 $m$, and the fourth curve radii equal to 27 $m$. A speed limit zone ($v_{lmt} = 22.22\ m/s$) is between the positions $500 \le s \le 850$. Figure 3.19 shows the top view of the test track with the start point, the main road curves, and speed limit zone.

The slope profile, $f_{slope}(\theta(s_h))$, is fitted within nine segments with 98.93% coefficient of determination. The road geometry model accuracy has favourable potential of utilising the road information in term of the safety, and energy efficiency improvements. Figure 3.20. shows the measured data with the proposed road slope model, roadway curves, and speed limit zone profile formulated using the (3.9), (3.12), and (3.13). The introduced road geometry models and assumed traffic speed limit zone model is utilised in the SEDAS concept.

## 3.5 Preceding Vehicle Motion Model

The goals of the EDAS applications are to improve road safety, performance, and energy efficiency. However, the anticipated driving consequences are not generally fulfilled as aimed for. Part of this is due to behavioural changes of other drivers following a change to the roadway and traffic situation (Eskandarian, 2012). Therefore, drivers behaviour may have direct or indirect effects on the EDAS efficiency.

Knowledge representation of traffic including a prediction model of the plausible future motion of vehicles can improve the performance of the ADAS and the EDAS applications. However, high entropy in traffic system leads to a challenging task to derive a computationally efficient and tractable model to predict the motion flow. A wide range of both mathematical identification methods and modelling methods of driver behaviour are presented (W. Wang et al., 2014). The core of the mathematical identification methods is the specification of the intelligent function and the human driver model. The driver model usually consists of a longitudinal and lateral model. The longitudinal driver model results in the longitudinal acceleration of a vehicle. For an extensive review of the human driver models see e.g., Ossen (2008), Eskandarian (2012), and W. Wang et al. (2014).

The ACC systems are not capable of properly predicting the future behaviour of the other vehicles in traffic, while experienced drivers usually predict the plausible behaviours of several vehicles ahead. The anticipation of the velocity profile of the preceding vehicle is an effective ecological driving technique for the Eco-ACC systems. Research related to anticipating the possible trajectory of the preceding vehicle into the near/far-term future has a long track in the ADAS and the EDAS applications. A simple choice to consider the preceding vehicle motion is to assumed either its acceleration remains constant during the prediction horizon or to be a bounded external disturbance (G.J.L. Naus et al., 2010) and (Shakouri and Ordys, 2014). However, such a choice is not realistic since it may lead to a very high or a negatively predicted velocity of the preceding vehicle at the end of a long prediction horizon (Md Abdus Samad Kamal et al., 2013). A stochastic process by a set of Markov chains model to anticipate the driver behaviour presented by Bichi et al. (2010). In addition, the presented stochastic driver model can be updated online by different learning algorithms, in order to adapt to different driver behaviours (Bichi et al., 2010). A sigmoid-based function to an approximate range of velocities defined by (Md Abdus Samad Kamal et al., 2013). Generalized exponentially varying predictor, Markov-chain based predictor and artificial neural network based velocity predictor reviewed by Chao Sun et al. (2015). A stochastic prediction strategy using Bayesian networks is presented by (Moser, 2015; Schmied et al., 2015; Moser, Schmied, et al., 2018).
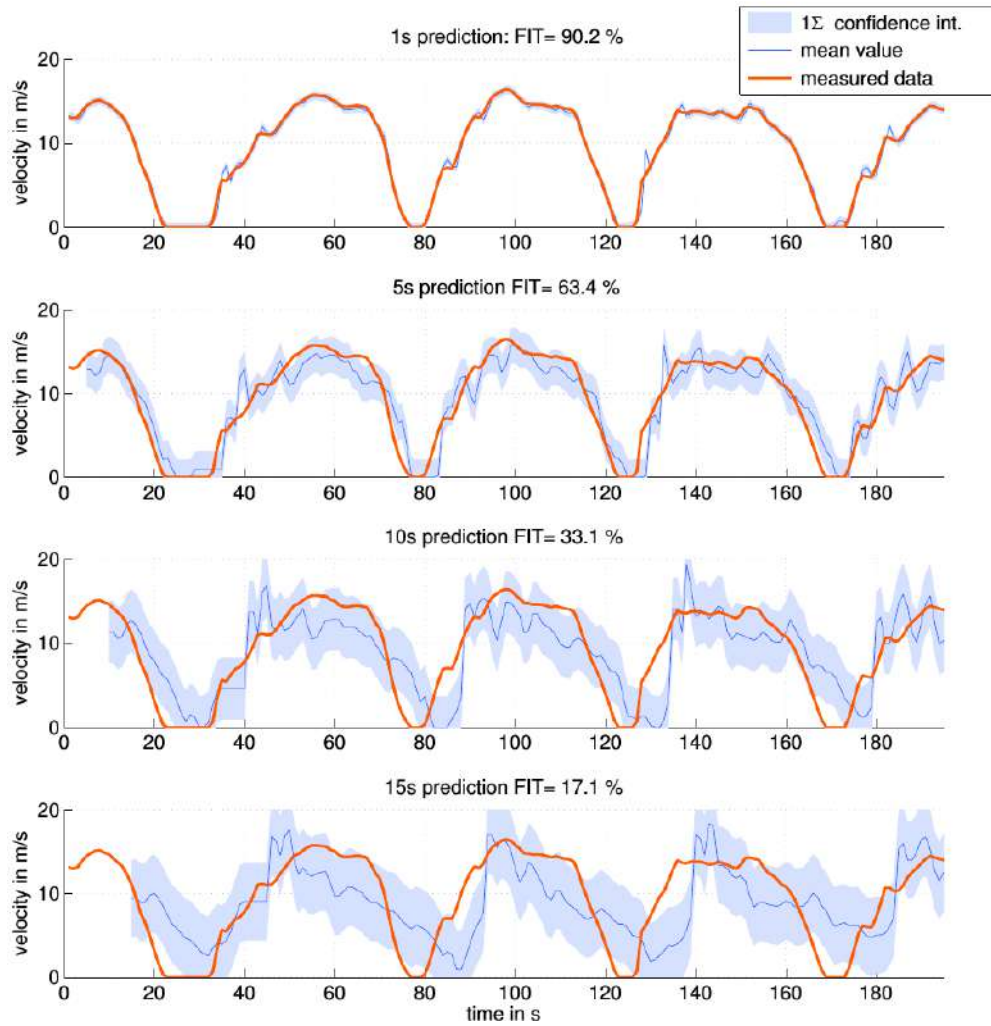
FIGURE 3.21: Performance of predicting the velocity of the preceding vehicle in ACC (Moser, 2015)

Although the methods mentioned in literature are effective for near-term prediction, most of the works of literature are considered to be insufficient for the far-term future prediction, while the accuracy of prediction may decline drastically for the far-term prediction horizon. For instance, Figure 3.21 shows the predicted velocity of the preceding vehicle for 1, 5, 10 and 15 $s$ ahead in ACC system obtained by (Moser, 2015). The performance of predicting velocity of the preceding vehicle is decreasing significantly the longer the prediction horizon is considered. This is mainly due to the insufficient knowledge of the future traffic situation (for more details see Moser (2015) and Moser, Schmied, et al. (2018)).

### 3.5.1 Proposed Preceding Vehicle Motion Model

A physical-statistical preceding vehicle motion model robust to far-term future prediction is introduced in this study. Since the preceding vehicle covers the path that the
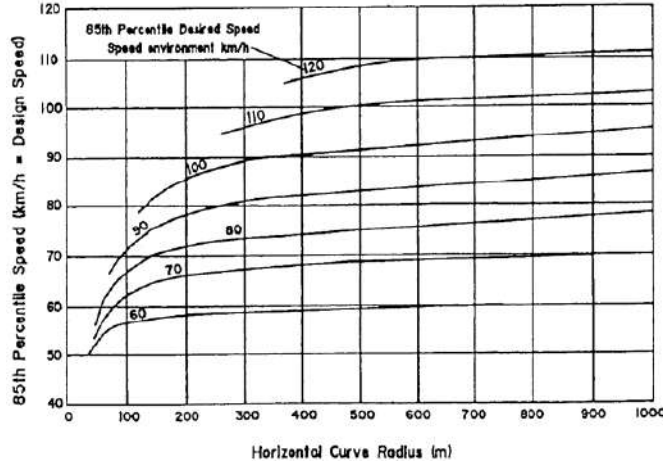
FIGURE 3.22: Velocity prediction on horizontal curves (Turne et al., 2011)

host vehicle will also cover, it is reasonable to estimate the preceding vehicle velocity profile based on the available road geometry information. The main idea is to introduce a mathematical dynamic model that propagate plausible velocity profile of the preceding vehicle. This model is based on approximate continuous $85^{th}$ percentile speed concept. The $85^{th}$ percentile speed is referred to as *spot speed study*, defined as the speed at or below which $85^{th}$ percent of vehicles travel a given location based on free-flowing conditions over a time period. Note that, the free-flowing conditions refer to the motion of the preceding vehicle that has at least three seconds time headway (for more details, see e.g. Turne et al. (2011), and references therein).

Curve parameters have significant influence on the vehicle's operating velocity on roadway curves. Figure 3.22 shows the velocity prediction on horizontal curves (Turne et al., 2011). In addition to the $85^{th}$ percentile speed at road curvatures, factors such as road slope profile, and traffic speed limit zones information can be considered to estimate more appropriate and realistic velocity profile. Therefore, the proposed dynamic model to propagate the velocity of the preceding vehicle, $v_p$, at time $t$ can be estimated as follows:

$$dv_p(t)/dt := X_{85^{th}}(1 - (\frac{v_p}{f_{85^{th}}})^4 - \frac{sin(f_{slp}(\theta(s_p)))}{sin(\frac{\pi}{4})}), \tag{3.14}$$

$$f_{85^{th}} := min(\omega_{85^{th}} v_{85^{th}}(f_{crv}(\delta(s_p))), f_{lmt}(s_p)), \tag{3.15}$$

$$v_{85^{th}}(f_{crv}(\delta(s_p))) := m_1 \exp(-m_2 f_{crv}(\delta(s_p)))$$
$$+ m_3 \exp(-m_4 f_{crv}(\delta(s_p))), \tag{3.16}$$

where $X_{85^{th}}$ is the $85^{th}$ percentile acceleration of the preceding vehicle assumed to lie in a normal distribution i.i.d. $X \sim \mathcal{N}(\mu_p, \sigma_p^2)$ with the mean, $\mu_p$, and variance $\sigma_p$. The $\omega_{85^{th}}$ is a tunable constant, and the position based function $v_{85^{th}}(f_{crv}(\delta(s))$, represents
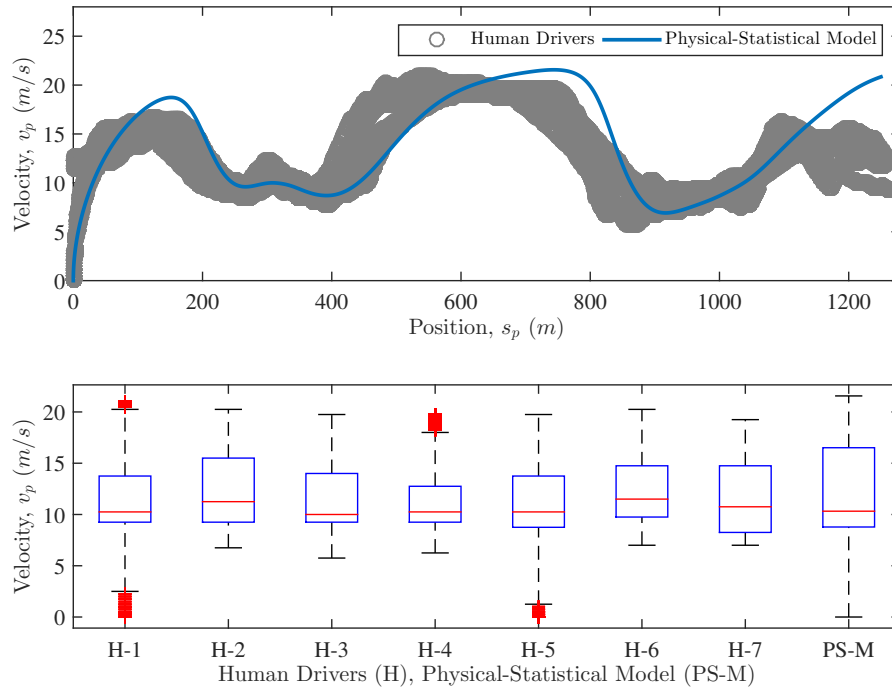
FIGURE 3.23: Far-term future prediction without feedback update, and relative statistics of the experiments vs. proposed model

the $85^{th}$ percentile curve speed of the vehicles along the roadway curves. The curve speed data that is adapted from Turne et al. (2011), can be approximated through the curve-fit process by (3.16) (for more details, see e.g. Turne et al. (2011)). To conclude, the proposed model is a continuous and differentiable model, which is capable of propagating a probabilistic optimistic trajectory for the preceding vehicle motion based on approximate $85^{th}$ percentile speed concept associated by the road geometry, and traffic information.

### 3.5.2 Preceding Vehicle Motion Model Validation

The proposed preceding vehicle motion model has been evaluated and validated with practical experiments on the test track with its geometry and speed limit zone information. Figure 3.23 shows far-term future prediction $(105\,s)$ without feedback update with the relative statistics of the experimental results compared to the proposed preceding vehicle motion model. The measured data include seven different rounds of human drivers velocity profiles on the test track. It can be shown that the physical-statistical motion model is capable of foreseeing an expected velocity profile based on road and traffic information. The average velocity of all human drivers is 11.68 $m/s$, and the average predicted velocity of physical-statistical motion model is 12.26 $m/s$. It is noteworthy that the prediction of the preceding vehicle in the Figure 3.23 is capable of performing

far-term future prediction (105 seconds) of the plausible velocity without feedback measurement updates. Significant statistical accuracy can be shown in term of the median and the related variations from the practical experiments obtained by the human drivers (H-#), and the proposed physical-statistical motion model (PS-M) on the test track.

## 3.6 Conclusions

In this chapter, the works of literature reviewed to identify the state-of-the-art and knowledge gap on the ADAS and the EDAS applications. The historical development of the ADAS during the last centuries surveyed. It discussed not only the strategic approach but also the ACC system overview as the fundamental ADAS application for the vehicle longitudinal control. Different Eco-driving techniques reviewed and a semi-autonomous Eco-ACC system with extended functionalities proposed to improve the limitations of the conventional ACC system. This system was based on the digital road map which the challenge of the road identification and modelling reviewed. A new method introduced to model the road geometry and static traffic data compatible with the ADAS and EDAS applications. In addition, the uncertain preceding vehicle motion model based on the spot speed study and the road geometry and traffic information introduced. The proposed models evaluated and validated on a test track as the main contribution of this chapter. Based on these findings, the following chapter will review the SMPC algorithms that are the main unit in the ADAS and the EDAS applications.

# Chapter 4

# Stochastic Model Predictive Control

As mentioned in the previous chapter, there are multiple design objectives in the proposed semi-autonomous Eco-ACC system design such as minimising gap error, preserving string stability, increasing driving comfort and minimising the energy consumption of the BEV which some of these objectives are contradictory. In addition, the Eco-ACC controller has many hard constraints such as actuators limit (throttle and brake) and soft constraints such as safety limits. The MPC is a control framework that usually results in an OCP to optimise multiple performance criteria under different design constraints (Eskandarian, 2012). This chapter focuses on the introduction of various predictive control methodologies for the proposed SEDAS concept.

This chapter is structured as follows. Section 4.1 provides the works of literature review related to MPC and its applications for automotive industry. Section 4.2 presents an overview of the constrained OCP with various solution approaches. Section 4.3 investigates on different predictive controller designs such as linear MPC, NMPC, and Economic Model Predictive Control (EMPC) with an overview on the stability analysis and real-time methods. In Section 4.4, robust and stochastic predictive control design are reviewed. The stochastic OCP formulation and multiple design objectives are described and a novel real-time RSNMPC framework is designed, followed by its application for the proposed semi-autonomous Eco-ACC system in Section 4.5. Section 4.6 concludes the findings of this chapter.
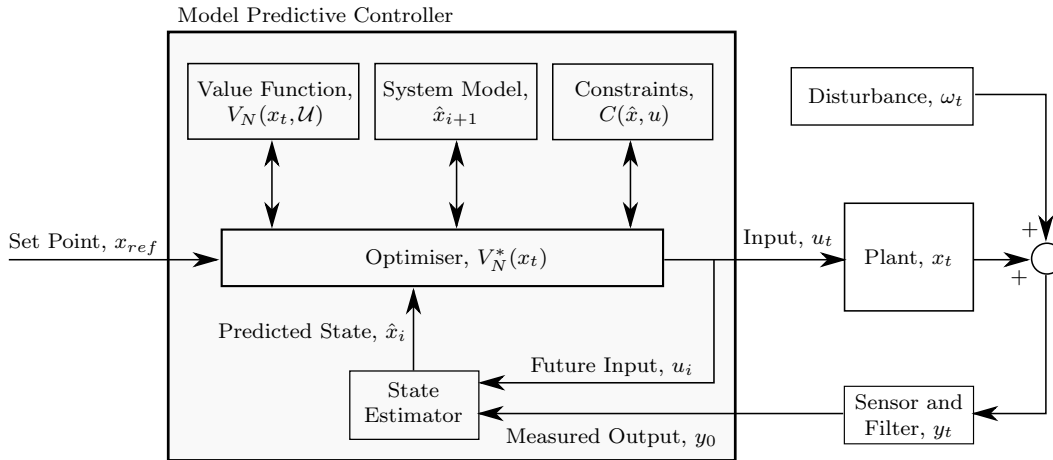
FIGURE 4.1: Block diagram of a conventional Model Predictive Control

## 4.1 History of Model Predictive Control

The only advanced control methodology which has made a significant impact on industrial control engineering is predictive control (Maciejowski, 2002). Predictive control appears to have been proposed in the late 1970s which pioneers were mostly industrial practitioners. The main reasons for its success are handling multivariable control problem, taking account of actuator limitations, and operating the system close to constraints. Block diagram of a conventional MPC is shown in Figure 4.1. The main components in a conventional MPC are the system model dynamics, a value function, the system constraints, a state estimator, and an algorithm to solve the OCP.

The main idea of predictive control is based on the *receding horizon* strategy. Figure 4.2 shows an example of the receding horizon principle for a Single-Input, Single-Output (SISO) plant. In the discrete-time setting with $\Delta t$ sample time, the current time is labelled as the time step $t_k$. Figure 4.2 shows the previous history of plant measured state, $x(t_{k-2,...,k})$, and closed-loop input trajectory, $u(t_{k-2,...,k})$. The desired *set-point*, $x_{ref}(t_k)$, is the trajectory that the measured state should follow. The MPC has an internal *system model* which is used to predict the behaviour of the plant within $N$ steps, starting at the current time, over a future prediction horizon. This predicted trajectory depends on the input trajectory $u(\tau_{0,...,N-1})$ with $\Delta\tau$ steps that are to be applied over the prediction horizon. In the simplest case, one may choose the input trajectory such as to bring the plant output at the end of the prediction horizon. There are several input trajectories that achieve this, and one may choose one of them, for instance, the one which requires the smallest input energy (Maciejowski, 2002).

Once a future input trajectory has been chosen, only the *first element* of the trajectory is applied as the input signal to the plant. Then, the whole cycle of state measurement, prediction, and input trajectory determination is repeated. One sampling interval later:
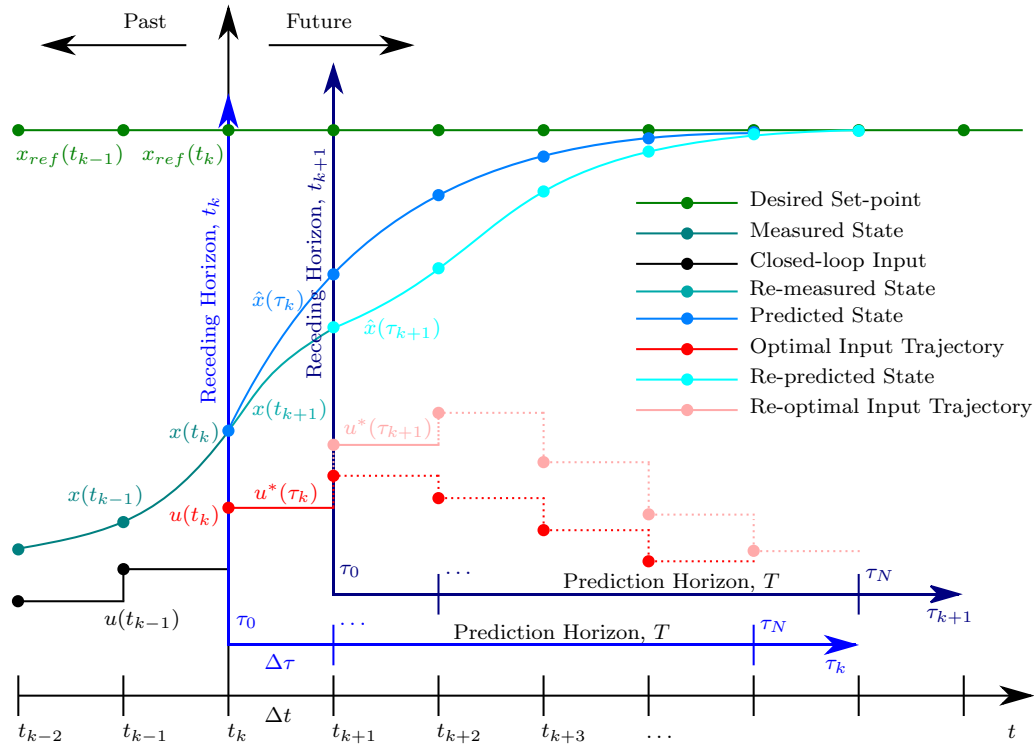
FIGURE 4.2: Receding Horizon principle

a new state measurement is obtained; a new state prediction is made over the prediction horizon; a new input trajectory is chosen; finally the next input is applied to the plant. It is noteworthy that the new state measurement might not be the same as the predicted state due to various reasons such as disturbance occurrence. Since the prediction horizon remains of the same length as before but slides along by one sampling interval at each step, this way of controlling a plant is often called a *receding horizon* strategy. For more details about the predictive control and the MPC follow Maciejowski (2002).

### 4.1.1 Model Predictive Control for Automotive Applications

Due to the computational complexity of the OCP, the MPC has been applied mainly for *slow* dynamic systems, such as the chemical and process industry. During the last decades, however, several developments including modern computing hardware have allowed using these methods also for *fast* dynamic systems with a growing interest for automotive applications (Re et al., 2010). One of the earliest MPC design to improve fuel economy of the CC was introduced by Gilbert (1976), while one of the earliest MPC designs for the ACC was presented by Goodrich et al. (1998) and Seki et al. (1999).

Spacing-control laws were computed by formulating the objective of a transitional maneuvers as an OCP by Bageshwar et al. (2004). A linear MPC for the ACC system was designed by Corona et al. (2007), and implemented on a *SMART* vehicle. An explicit

MPC was designed and implemented for the ACC with Stop&Go function by Gerrit Naus et al. (2008) and G.J.L. Naus et al. (2010). Vehicular following MPC considering fuel economy and tracking capability was introduced by Shengbo Li et al. (2008).

SMPC for improving the performance of powertrain control algorithms such as the ACC was introduced by Bichi et al. (2010). Challenges of tracking capability, fuel economy and driver desired response for the ACC was addressed utilising a linear MPC approach by S. Li et al. (2011). A single NMPC was designed by Shakouri, Ordys, and Askari (2012) for the ACC with the objective of the distance tracking. This approach was demonstrated to be more effective in tracking the speed and distance by eliminating the necessity of switching between the two controllers. An ACC was introduced on a HEV platform by K. Li et al. (2012). An OCP framework for the ACC with the assumption of stationary conditions for the dynamics of other vehicles was introduced by M. Wang, W. Daamen, et al. (2012). A linear MPC approach for the CACC that directly minimizing the fuel consumption rather than the acceleration of the vehicle presented by Stanger et al. (2013). A real-time novel control system to drive a vehicle efficiently on roads containing varying traffic and signals at intersections for improved fuel economy was presented by Md Abdus Samad Kamal et al. (2013). In this system, the relevant information of the current road and traffic, simplified prediction of the future states of the preceding vehicle were taken into account. An NMPC was introduced by Shakouri and Ordys (2014) for the ACC and the CC systems which carry out automatic switching between ACC and CC, depending on the situation in front of the vehicle. A novel rolling horizon control framework for non/cooperative driver assistance systems was introduced by Meng Wang, S. Hoogendoorn, et al. (2014) and W. Wang et al. (2014). A terrain-information, actuator-efficiency-incorporated energy management and driving strategy for maximizing the travel distance of in-wheel motor BEV was introduced by Chen et al. (2014). A control methodology that unifies control barrier functions and control Lyapunov functions through quadratic programs was developed by Ames et al. (2014).

A CACC system using stochastic, linear MPC strategies with the goal of minimisation of fuel consumption in a car-following scenario was presented by Moser, Waschl, et al. (2015). A real-time algorithm to reduce the online computational burden of the MPC by combining an *move blocking* strategy with a *constraint-set compression* strategy was introduced by S. E. Li, Z. Jia, et al. (2015). A NMPC scheme with the target of emission and fuel-efficient driving for the CACC system introduced by Schmied et al. (2015). A novel energy-efficient MPC was designed for the BEVs Eco-CC system by T. Schwickart et al. (2015) and Tim Schwickart, Voos, Hadji-Minaglou, et al. (2016). Another NMPC was introduced by Vajedi et al. (2016) to optimally control the velocity profile for the HEV using the Eco-ACC system. Considering CACC system, a comprehensive review

with main focus on communications, driver characteristics, and controls was presented by Dey et al. (2016). A novel strategy to enhance string stability of autonomous vehicles with sensor delay and actuator lag based on a MPC framework was proposed by M. Wang, S. P. Hoogendoorn, et al. (2016). A self-tuning control algorithm for an ACC system that can adapt its behaviour to variations of vehicle dynamics and uncertain road grade was proposed by Marzbanrad et al. (2016). A comprehensive review of power management strategy in HEVs with an emphasis on MPC based strategies and the factors that affect the performance of the MPC was presented by Y. Huang et al. (2017). A RMPC approach that regulates a minimum safety distance between vehicles taking into account the overall system delays and braking capacity of each vehicle proposed by Filho et al. (2017). The introduced RMPC was developed to guarantee the minimum safety distance should not be violated due to uncertainties in the lead vehicle behaviour. An enhanced MPC for the ACC system considering road elevation information was presented by S. E. Li, Guo, et al. (2017). A real-time NMPC for the ecological CC of a HEV was presented by Tajeddin et al. (2017). Another real-time RMPC for the Eco-CACC system with the consideration of gear shift was presented by Shao et al. (2017). A SMPC for the ACC and CACC systems under uncertainty based on the constant time gap policy was presented by Y. Zhou et al. (2017). A four-component analysis framework for platoon CACC systems from a networked control perspective, including a literature review by network awareness, unified models of key components, and two application cases for controller synthesis was reviews by S. E. Li, Zheng, et al. (2017). A safe- and eco-driving control system that enables the connected and automated EV to accelerate or to decelerate optimally while preventing both collision with preceding vehicle and violation of speed limitations was proposed by Ojeda et al. (2017). Last but not least, flexible spacing ACC system using SMPC was introduced by Moser, Schmied, et al. (2018). In this paper, a conditional linear Gauss model is developed and trained with real measurements to estimate the probability distribution of the future velocity of the preceding vehicle (Moser, Schmied, et al., 2018).

To conclude, the optimal control methods have made a considerable impact on ADAS and especially the ACC systems. The next sections review more details of the general MPC design methods for a class of dynamic system. Throughout this study, $\mathbb{R}^n$ denotes the n-dimensional Euclidean space. $\mathbb{R}_+ := [0, \infty)$. $\mathbb{N} = \{1, 2, \ldots\}$ is set of natural numbers. $\mathbb{N}_+ := \mathbb{N} \cup \{0\}$. $\mathbb{Z}_{[a,b]} := \{a, a+1, \ldots, b\}$ is set of integers from $a$ to $b$. $\mathbf{E}$ denotes expectation and $\mathbf{E}_x[\cdot] := \mathbf{E}[\cdot|x(0) = x]$ is the conditional expectation. $\mathbf{Pr}$ denotes probability, and $\mathbf{Pr}_x[\cdot|x(0) = x]$ is the conditional probability distribution of random variable(s) $x$.

## 4.2   Overview of Optimal Control Problem

Let us consider the class of dynamic systems which we are interested in this study. Suppose the longitudinal dynamics of the BEV being controlled has a state vector and input vector which has full state measurement and nonlinear deterministic behaviour governed by Ordinary Differential Equation (ODE) as follows:

$$\dot{x}(t) = f(x(t), u(t)), \tag{4.1}$$

where $t$ is time; $x(t) \in \mathbb{R}^{n_x}$ is the system time-dependent states vector; and $u(t) \in \mathbb{R}^{n_u}$ is time-dependent input vector. The notation $\dot{x}(t) = \frac{dx(t)}{dt}$ is used for differential state derivatives and the Jacobian matrix $\frac{\partial f}{\partial x}(\cdot)$ is assumed to be invertible for $\forall t$. Consider the (4.1) with initial condition $x(t) = \hat{x}(\tau_k)$ which form the Initial Value Problem (IVP). Assume the corresponding Jacobian matrix is invertible and the continuous-time system dynamics $f(\cdot)$ is Lipschitz continuous in $x(t)$ and continuous in the control input $u(t)$. Thus, for some value $\epsilon > 0$, there exists a unique solution $x(t)$ to the IVP on the interval $[\tau_k - \epsilon, \tau_k + \epsilon]$ (Picard–Lindelöf Theorem).

Suppose at time $t_k$, the actual system state is $x(t_k)$. The OCP for the system at time $t_k$ is to find optimal control action sequence $u(t_k) = u_{opt}(t_k, x(t_k))$, which is a state feedback control law. The receding horizon control problem is essentially a family of finite horizon OCPs along a fictitious time $\tau$ (Ohtsuka, 2004). The control objective is to minimise a *cost function* (or *value function*) which has the form over the prediction horizon, $T$, as follows:

$$V(x, u, t_k) := \int_0^T J_c(\hat{x}(\tau, t_k), u(\tau, t_k)) d\tau + J_f(\hat{x}(T, t_k)), \tag{4.2}$$

where $J_c : \mathbb{R}^{n_x} \times \mathbb{U} \to \mathbb{R}_+$ and $J_f : \mathbb{R}^{n_x} \to \mathbb{R}_+$ are the none-negative *cost-per-stage function* and the *final cost function*, respectively. The $\hat{x}(\tau, t_k)$ denotes the predicted states at time $t_k$ along the prediction $\tau$ axis given by the actual states as the initial states, $\hat{x}(0, t_k) = x(t_k)$, over the prediction horizon.

Using the cost function (4.2), the OCP for the system (4.1) is formulated as follows:

$$V_T^*(x(t_k)) := \underset{u^*}{\text{minimise}} \quad V(x, u^*, t_k) \tag{4.3a}$$

subject to:

$$\hat{x}_\tau(\tau, t_k) = f(\hat{x}(\tau, t_k), u^*(\tau, t_k)), \tag{4.3b}$$

$$\hat{x}(0, t_k) = x(t_k), \tag{4.3c}$$

where $V_T^*(x(t_k))$ denotes the optimal value function under the optimal control law vector $\boldsymbol{u}^*$. The optimal control input $u^*(\tau, t_k)$ is determined on the $\tau$ axis as the solution of the finite horizon OCP for each $t_k$, and the actual control input is given by $u(t_k) = u^*(0, t_k)$ (Ohtsuka, 2004).

### 4.2.1 Discrete-time Optimal Control Problem

Consider a discrete-time system as follows:

$$x_{t+1} = f(x_t, u_t), \tag{4.4}$$

where $t \in \mathbb{N}_+$; $x_t \in \mathbb{R}^{n_x}$ is the system states vector; $u_t \in \mathbb{R}^{n_u}$ is the control input; and the $f(\cdot)$ is nonlinear vector of functions that describes the system dynamics. Let $N \in \mathbb{N}$ be the both state and control prediction horizon. Define an *N-stage feedback control law* as:

$$\boldsymbol{u} := \{u_0, u_1, \ldots, u_{N-1}\}, \tag{4.5}$$

where the $u_i$, for all $i = 0, \ldots, N-1$ is a general state feedback control law. The prediction horizon can be divided into $N$ steps and discretise the cost function on $\tau$-axis as follows:

$$V(x(t_k), \boldsymbol{u}) := \sum_{i=0}^{N-1} J_c(\hat{x}_i, u_i)\Delta\tau + J_f(\hat{x}_N), \tag{4.6}$$

where $\Delta\tau(t_k) := T(t_k)/N$. Thus, the OCP in discrete form on $\tau$-axis with forward difference can be defined as follows:

$$V_N^*(x(t_k)) := \underset{u}{\text{minimise}} \quad V(x(t_k), \boldsymbol{u}) \tag{4.7a}$$

subject to:

$$\hat{x}_{i+1} = f(\hat{x}_i, u_i), \tag{4.7b}$$

$$\hat{x}_0 = x(t_k), \tag{4.7c}$$

where the predicted state trajectory $\hat{x}_i$ along the $\tau$-axis starts from $x(t_k)$ at $\tau = 0$ with the optimal control input sequence vector $\{u_i^*\}_{i=0}^{N-1}$. The optimal control input to the system is given by $u(t_k) = u_0^*$ (Ohtsuka, 2004).

### 4.2.2 Solution Approaches

General methods to solve the OCPs are classified into three main categories:

- *Dynamic Programming (DP)* breaks the problem into smaller sub-problems. It is based on Bellman's principle of optimality to propagate the cost-per-stage function. This approach generally lead to the Hamilton–Jacobi–Bellman (HJB) equation where it is mainly solved backwards in time, from the end of prediction horizon $t = T$ to the beginning $t = 0$.

- *Direct Methods*, which also known as *first-discretise-then-optimise* approach is based on numerical solution of a finite dimensional optimisation problem corresponding to a discrete approximation of the original OCP.

- *Indirect Methods*, which also known as *first-optimise-then-discretise* approach is based on Pontryagin's Minimum Principle (PMP) to formulate the infinite dimensional first-order necessary optimality conditions. The achieved nonlinear Two-Point Boundary-Value Problem (TP-BVP) can be solved numerically.

In general, the direct optimisation of a control law requires a solution of the HJB equation as follows:

$$\frac{\partial V^0(x, t_k)}{\partial t_k} = \min_u H(x, u, \frac{\partial V^0(x, t_k)}{\partial x}), \tag{4.8}$$

where $H(x, u, \lambda) = J_c(x, u) + \lambda f(x, u)$, with boundary condition $V^0(x, T) = J_f(x)$ (Maciejowski, 2002). The control input can be achieved by minimising $H$ as follows:

$$u^0(x, t_k) = \arg \min_u H(x, u, \frac{\partial V^0(x, t_k)}{\partial x}). \tag{4.9}$$

The main advantage of DP is that the globally optimal solution can be found and provides a necessary and sufficient condition for an optimum solution, but this condition should be satisfied over the entire dimension of state space. Unfortunately, it is virtually impossible to solve the achieved partial differential equation in most cases (Maciejowski, 2002). Moreover, due to the *curse of dimensionality*, it is in general computationally expensive and is only applicable to systems with low dimensions. Indirect methods based on PMP relate closely to the DP scheme, but they are more efficient in solving the OCP which satisfy the necessary conditions for optimality. The globally optimal solution can be achieved if the OCP is convex (for more detail see e.g, Boyd et al. (2004)). Instead of indirectly determining the optimal control input by solving the necessary conditions as in the indirect methods, direct methods involve the generation of a sequence of control functions with the property that each successive control functions directly results in a lower value of the cost function. The open-loop OCP for Mechatronic systems controlled with a sampling period in the order of milliseconds, which leads to a TP-BVP in receding horizon control principle need to be solved in real-time. Indirect methods are known to show fast numerical convergence in the neighbourhood of the optimal solution. Therefore, this study focuses on the indirect methods based on PMP

for the real-time OCP. For an overall overview see e.g., Rao (2009) and James B. Rawlings and D. Q. Mayne (2009).

### 4.2.3 Pontryagin's Minimum Principle

Let's consider the dynamic of system (4.1) with initial states, $x(0, t_k) = x(t_k)$. The control input $u$ should be chosen for all $\tau \in [0, T]$ to minimise the cost function (4.2). The constraints on the system dynamics can be adjoined to the Lagrangian $J_c(\cdot)$ by introducing time-varying Lagrange multiplier vector $\lambda \in \mathbb{R}^{n_x}$, where its elements are also known as the *co-states* of the system. This motivates the construction of the Hamiltonian ($H$) defined as Lagrangian duality as follows:

$$H(x, u, \lambda) := J_c(x, u) + \lambda^{\mathrm{T}} f(x, u), \tag{4.10}$$

where $\lambda^T$ denotes the transpose of $\lambda$. Reformulating the Lagrangian as a Hamiltonian, in which case the solutions are local minima for the Hamiltonian is known as Pontryagin's Minimum Principle (PMP). The PMP states that the optimal state trajectory $x^*$, optimal control input $u^*$, and corresponding co-state multiplier vector $\lambda^*$ should satisfy:

$$H(x^*, u^*, \lambda^*) \leq H(x^*, u, \lambda^*), \forall u \in \Upsilon. \tag{4.11}$$

The first-order necessary conditions for the sequences of the optimal control input $u^*$ and co-state $\lambda^*$ are obtained as follows:

$$u^* = \arg \min_{u^*} H(x^*, u^*, \lambda^*) = H_u(x^*, u^*, \lambda^*) = J_{c_u}(x^*, u^*) + \lambda^{\mathrm{T}} f_u(x^*, u^*) = 0, \tag{4.12}$$

where $H_u$ is the Jacobian matrix of Hamiltonian with respect to the control input. In addition,

$$\dot{\lambda}^* = -H_x(x^*, u^*, \lambda^*) = -J_{c_x}(x^*, u^*) - \lambda^{*\mathrm{T}} f_x(x^*, u^*), \tag{4.13}$$

where $H_x$ is the Jacobian matrix of Hamiltonian with respect to the system states. If the final state, $x(T)$, is not constant then the terminal co-states should satisfy (*Transversality Condition*):

$$\lambda^*(T) = J_{f_x}(x^*(T)). \tag{4.14}$$

These four conditions in (4.11)-(4.14) are known as the necessary conditions for the OCP. The co-state variables represent the *marginal cost* of violating system dynamic constraints.

### 4.2.4 Constrained Optimal Control Problem

Let's consider the OCP for the dynamic system (4.1). The system state vector might subject to the constraint set as follows:

$$x(t) \in \Xi, \ \forall t \geq 0. \tag{4.15}$$

In addition, the system input vector might subject to the constraint set as follows:

$$u(t) \in \Upsilon, \ \forall t \geq 0. \tag{4.16}$$

The OCP with equality constraints is generally formulated as follows:

$$V_T^*(x(t_k)) := \underset{u^*}{\text{minimise}} \quad V(x, u^*, t_k) \tag{4.17a}$$

subject to:

$$\hat{x}_\tau(\tau, t_k) = f(\hat{x}(\tau, t_k), u^*(\tau, t_k)), \tag{4.17b}$$

$$g_j(\hat{x}(\tau, t_k), u^*(\tau, t_k)) = 0, \quad \text{for all } j \in \mathbb{Z}_{[1, n_g]}, \tag{4.17c}$$

$$\hat{x}(0, t_k) = x(t_k), \tag{4.17d}$$

where $g_j(\cdot) \in \mathbb{R}^{n_g}$ is the vector of equality constraints. Let's define the Hamiltonian for the (4.17) as follows:

$$H(x, u, \lambda, \mu) := J_c(x, u) + \lambda^{\mathrm{T}} f(x, u) + \mu^{\mathrm{T}} g(x, u), \tag{4.18}$$

where $\mu \in \mathbb{R}^{n_g}$ denotes the Lagrange multiplier associated with the equality constraint (Ohtsuka, 2004). Similar to the OCP (4.3), the necessary conditions for the OCP (4.17) are obtained by the calculus of variation based on the four conditions (4.11)-(4.14).

A large variety of constraints may be imposed in an OCP. The OCP based on Nonlinear Programming (NLP) with inequality constraints is the main concern of in this study. The NLP is generally defined as follows:

$$V_T^*(x(t_k)) := \underset{u^*}{\text{minimise}} \quad V(x, u^*, t_k) \tag{4.19a}$$

subject to:

$$\hat{x}_\tau(\tau, t_k) = f(\hat{x}(\tau, t_k), u^*(\tau, t_k)), \tag{4.19b}$$

$$g_j(\hat{x}(\tau, t_k), u^*(\tau, t_k)) = 0, \qquad \text{for all } j \in \mathbb{Z}_{[1, n_g]}, \tag{4.19c}$$

$$h_j(\hat{x}(\tau, t_k), u^*(\tau, t_k)) \leq 0, \qquad \text{for all } j \in \mathbb{Z}_{[1, n_h]}, \tag{4.19d}$$

$$\hat{x}(0, t_k) = x(t_k), \tag{4.19e}$$

where $h_j(\cdot) \in \mathbb{R}^{n_h}$ is the vector of inequality constraints. The original OCP (4.19) is called the primal problem while the Lagrange dual function for (4.19) is called dual problem as follows:

$$\mathcal{L}(x, u, \lambda, \mu, \nu) := J_c(x, u) + \lambda^{\mathrm{T}} f(x, u) + \mu^{\mathrm{T}} g(x, u) + \nu^{\mathrm{T}} h(x, u), \qquad (4.20)$$

where $\nu \in \mathbb{R}^{n_h}$. Solution to:

$$\inf_u \mathcal{L}(x, u, \lambda, \mu, \nu), \qquad (4.21)$$

provides a lower bound to the original problem (Borrelli et al., 2014). The $n_h^{\mathrm{th}}$ inequality constraint $h_j(x, u) \leq 0$ is known as *active* at feasible pair $(x^*, u^*)$ if $h(x^*, u^*) = 0$. On the other hand, if $h_j(x^*, u^*) \leq 0$, the constraint is known as *inactive* at pair $(x^*, u^*)$. A constraint is *redundant* if removing it from the list of constraints in the OCP (4.19) does not change its solution (Borrelli et al., 2014). The equality constraints are always active for feasible points.

The first-order necessary conditions for a solution in the NLP (4.19) to be optimal are based on Karush–Kuhn–Tucker (KKT) conditions as follows:

$$\nabla J_c(x^*, u^*) + \nabla \lambda^* f(x^*, u^*) + \nabla \mu^* g(x^*, u^*) + \nabla \nu^* h(x^*, u^*) = 0, \qquad (4.22\mathrm{a})$$

$$f(x^*, u^*) = 0, \qquad (4.22\mathrm{b})$$

$$g(x^*, u^*) = 0, \qquad (4.22\mathrm{c})$$

$$h(x^*, u^*) \leq 0, \qquad (4.22\mathrm{d})$$

$$\nu^* \geq 0, \qquad (4.22\mathrm{e})$$

$$\nu_j^* h_j(x^*, u^*) = 0, \text{ for all } j \in \mathbb{Z}_{[1, n_h]}, \qquad (4.22\mathrm{f})$$

where the gradient symbol $\nabla$ is the transpose of the Jacobian i.e. $\nabla g(x) := \frac{\partial g(x)^T}{\partial x}$. Conditions (4.22f) are also called *complementary slackness* conditions. It can be interpreted as if the $n_h^{\mathrm{th}}$ inequality constraint of the primal problem is inactive at the optimum $h_j(x^*, u^*) \leq 0$, then the $j^{\mathrm{th}}$ dual variable has to be zero ($\nu_j^* = 0$). The KKT approach to the NLP generalises the method of Lagrange multipliers, which allows only equality constraints. For more details see e.g., Borrelli et al. (2014).

### 4.2.5 Numerical Methods for Optimal Control Problem

There is a great variety of algorithms for the solution of unconstrained and constrained optimization problems (Borrelli et al., 2014). Suppose we are looking to find a minimiser

$z^*$ to a general OCP as follows:

$$\underset{z}{\text{minimise}} \quad f(z) \tag{4.23a}$$

subject to:

$$z \in \mathcal{S}, \tag{4.23b}$$

where both the objective function $f : \mathbb{R}^s \to \mathbb{R}$ and feasible set $\mathcal{S}$ are convex. Assuming that the problem is feasible, an optimiser $z^* \in \mathcal{S}$ is achieved $f(z^*) = f^*$. Despite some of the simplest OCPs, finding an analytical solution is not possible where one has to utilise numerical methods to compute an approximate optimal solution. An iterative method start from an initial guess $z^0$, computes a sequence $\{z^k\}_{k=1}^{k=k_{max}}$, where:

$$z^{k+1} = \Psi(z^k, f, \mathcal{S}), \tag{4.24}$$

which $\Psi$ is a method dependent update rule (Borrelli et al., 2014). The numerical method should be terminated after maximum $k_{max}$ iterations and return an approximate minimiser $z^{k_{max}}$ which satisfies:

$$|f(z^{k_{max}}) - f(z^*)| \leq \epsilon, \text{ and } \quad \text{dist}(z^{k_{max}}, \mathcal{S}) \leq \delta, \tag{4.25}$$

where:

$$\text{dist}(z^{k_{max}}, \mathcal{S}) = \min_{y \in \mathcal{S}} \|y - z\|, \tag{4.26}$$

is the shortest distance between a point and a set in $\mathbb{R}^s$ measured by the norm $\|\cdot\|$. The parameters $\epsilon$ and $\delta \geq 0$ define the required accuracy of the approximate minimiser (Borrelli et al., 2014). In general there exist two classes of numerical optimisation methods as *first-order* methods utilise the gradients information of the cost function and *second-order* methods which require additional *Hessians* of the cost function. For more details about important key aspect of any optimisation method including the *Convergence*, *Convergence rate*, *Feasibility*, *Numerical robustness*, *Warm-starting*, *Preconditioning*, *Computational complexity* see e.g., Borrelli et al. (2014).

For the purpose of this section, we focus on *descent* methods for the unconstrained OCP. One of the most well-known methods is *Newton* method which is based on a quadratic approximation of $f$ at the current point $z$. In the Newton method, the iterative become insensitive toward the scaling of the problem. In the remainder of this section, we will only consider iterative numerical methods that solve equality constrained OCP. The equality constrained OCP can be solved by utilising Newton-type methods to the nonlinear KKT conditions. Applying Newton's method on the KKT conditions is also known as Sequential Quadratic Programming (SQP). Inequality constrained OCP can
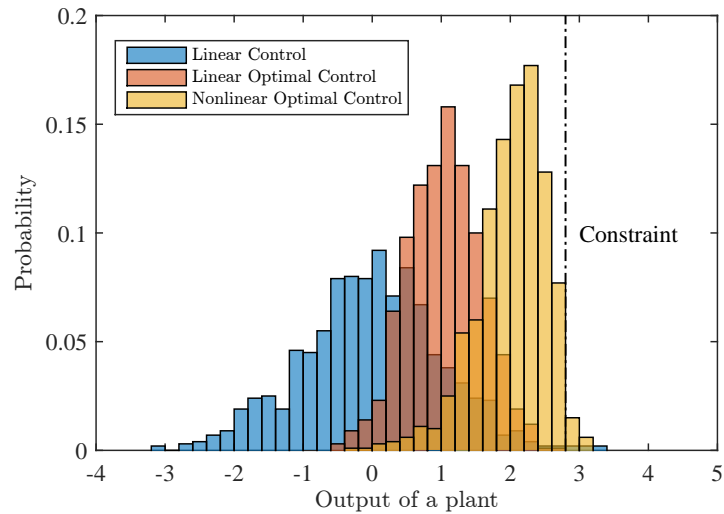
FIGURE 4.3: Qualitative performance of constrained output of a plant

be reformulated to equality constrained OCP, afterwards, iterative methods can be utilised. An overview of algorithms for NLP and more details about iterative methods can be found in e.g., Kelley (1995), Luenberger et al. (2008), Izmailov et al. (2014), and Asprion et al. (2014).

### 4.2.6   Inequality Constraints Handling

Compare to traditional control methods, the operating points in the predictive control could be chosen close enough to the constraints boundaries with a reasonable likelihood of the violation. On the other hand, one may not prefer to operate the plant at the limits of its capabilities where has to have power in the reservation to deal with unexpected disturbances from various sources. A classical argument in favour of linear OCP is that if the disturbances are random, and if one can reduce the variance of the controlled outputs as far as possible, then one can operate as near as possible to the constraints, hence operate the plant as near as possible to its optimal performance (Maciejowski, 2002).

Figure 4.3 illustrates the three hypothetical probability distributions of some controlled output of a plant and an inequality constraint which the output should not remain in the region beyond. The Figure 4.3 is supposed to demonstrate the qualitative performance of a plant output using predictive control. The Gaussian shape distribution for the controlled output of a plant with relatively large variance results from a poorly tuned linear controller (*Linear Control*). An acceptable low probability of violating the constraint could be achieved only if the output set-point tuned relatively far away from the constraint boundary. Therefore, the plant operates far away from the optimal point during

run-time of the system. A tighter Gaussian shape distribution could be achieved by the use of linear OCP (*Linear Optimal Control*) since the control law is linear (Maciejowski, 2002). The distribution of *Nonlinear Optimal Control* shows the performance obtained by utilising the nonlinear constrained aware OCP. The distribution of the plant's output was pushed toward the inequality constraint boundary while retaining an acceptably low probability of violation.

As mentioned before, the indirect methods are known to show fast numerical convergence in the neighbourhood of the optimal solution. However, handling of inequality constraints via PMP is in general non-trivial, since the overall structure of the TP-BVP depends on the sequence between singular/nonsingular and unconstrained/constrained arcs (if the respective constraint is active or not) and require a prior knowledge of the OCP structure (Graichen et al., 2010). There are several works of literature to systematically transform a general inequality constrained OCP into a surrogate OCP by various methods. Two mainstream inequality constraints handling approaches for the NLP are *Active Set* methods and *Interior-Point (IP)* methods. In addition, we review complementarity functions for NCP (also called as C-function) as the *Semi-smooth* transformation to include the complementarity conditions in the necessary conditions.

The Active Set method assumes that a feasible solution is available. An active set method uses a combinatorial approach to iteratively determine the set of constraints active at the optimum. Consider the NLP (4.19), whenever the inequality constraint is $h_j(\cdot) > 0$, it is treated as active equality constraint. The inactive inequality constraint $h_j(\cdot) \leq 0$ has no effect on the solution of the OCP, which can be neglected. The inequality constrained OCP with the Active Set method is approximated by replacing the original OCP with an equality constrained OCP where PMP and the first-order necessary conditions can be applied. For more details about the Active Set method see e.g., Maciejowski (2002) and Borrelli et al. (2014).

### 4.2.6.1   Interior-Point Methods

In the last twenty years or so, a rival family of algorithms so-called IP methods for solving convex optimization problems have emerged. Today interior point methods are among the most widely used numerical methods for solving convex OCPs. *Primal Barrier* methods were the first polynomial-time algorithms. Modern *Primal-Dual* methods are powerful class of the IP methods which forms the basis of almost all OCP implementations (Borrelli et al., 2014). The attraction of IP methods is that their computational complexity (number of iterations) is not worse than some polynomial function of parameters such as the number of constraints or the number of variables, whereas the

complexity of other known approaches, including the Active Set methods, can be exponential in these parameters in the worst case (Maciejowski, 2002).

The main idea of the barrier methods is to convert the inequality constrained OCPs (4.19) into equality constrained OCPs by utilising a *barrier* function $\Phi_h(\cdot) : \mathbb{R}^{n_h} \to \mathbb{R}$ as follows:

$$V_T^*(x(t_k), \gamma) := \underset{u^*}{\text{minimise}} \quad V(x, u^*, t_k) + \gamma \Phi_h(\hat{x}(\tau, t_k), u^*(\tau, t_k)) \tag{4.27a}$$

subject to:

$$\hat{x}_\tau(\tau, t_k) = f(\hat{x}(\tau, t_k), u^*(\tau, t_k)), \tag{4.27b}$$

$$g_j(\hat{x}(\tau, t_k), u^*(\tau, t_k)) = 0, \quad \text{for all } j \in \mathbb{Z}_{[1, n_g]}, \tag{4.27c}$$

$$\hat{x}(0, t_k) = x(t_k), \tag{4.27d}$$

where $\gamma$ is *barrier parameter*. The $\Phi_h(\cdot)$ must take on the value $+\infty$ whenever $h_j(\cdot) > 0$ for some $j$ and a finite value otherwise. The indicator function:

$$I_h(\hat{x}, u) := \begin{cases} 0 & \text{if } h_j(\hat{x}, u) \leq 0, \\ +\infty & \text{otherwise,} \end{cases} \tag{4.28}$$

trivially achieves the purpose of a barrier. However, the barrier function is required to be convex and continuously differentiable (Borrelli et al., 2014). One of the most well-known continuous and twice differentiable function that approximates (4.28) is *logarithmic barrier* function as follows:

$$\Phi_h(\hat{x}, u) := - \sum_{j=1}^{n_h} \ln(-h_j(\hat{x}, u)), \tag{4.29}$$

with domain $\{\hat{x} \in \mathbb{R}^{n_x} \,|\, h_j(\hat{x}, u) \leq 0, \, \forall j = 1, \ldots, n_h\}$.

Let $u_\gamma^*$ be the minimiser of $V_T^*(x(t_k), \gamma)$, and let $u^*$ be the solution of the original OCP. After $u_{\gamma^0}^*$ has been computed, the barrier parameter is decreased by a constant factor. This procedure is repeated until $\gamma$ has been sufficiently decreased (Borrelli et al., 2014). $u_0^*$ is known as the *analytic center* of the constraint; if the feasible region is not empty then $u_0^*$ lies in its interior and does not depend on the objective function $V(x, u)$ at all. On the other hand, $u_\gamma^* \to u^*$ as $\gamma \to 0$ under mild conditions. The path traced out by $u_\gamma^*$ is known as *central path* (Maciejowski, 2002).

A modified type of barrier method is *Exterior Penalty* method. In this method, an exterior penalty function is included in the cost function on the constraint violations.

The Exterior penalty function is defined as:

$$\Phi_e(\hat{x}, u) := \begin{cases} 0 & \text{if} \quad h_j(\hat{x}, u) \leq 0, \\ w_j h_j(\hat{x}, u)^2 & h_j(\hat{x}, u) \geq 0, \end{cases} \tag{4.30}$$

where $w_j > 0$ is the penalty weight of the $j^{\text{th}}$ constraint (M. Huang et al., 2015).

*Auxiliary Variable* method is an alternative type of inequality constraints handling introduced with an additional optimisation variable to transform the inequality constraints into equality constraints. Let $\eta \in \mathbb{R}^{n_h}$ be a vector of the auxiliary variables, the inequality constraint $h_j(\cdot)$ can be transformed into equality constraint as follows:

$$h_j(\hat{x}, u) + \eta_j^2 = 0. \tag{4.31}$$

A penalty term $-w_j \eta_j$ is included in the cost function to avoid singularity (Ohtsuka, 2004).

If the solution of the OCP (4.27) is very close to the constraint boundary, where the logarithmic barrier function is increasing extremely quickly, and as a result the optimisation problem becomes very *ill-conditioned*. One of the most effective IP methods capable of dealing with ill-conditioning is so-called *primal-dual* methods. These algorithms operate in both the primal and dual space and find solutions to the primal OCPs and their duals simultaneously.

Most barrier methods track the central path to the solution set. These methods are also called *path-following* methods. In the primal-dual space, the central path for the NLP (4.19) is defined as the set of points $(x^*, u^*, \lambda^*, \mu^*, \nu^*)$, for which the following *relaxed* KKT conditions hold:

$$\nabla J_c(x^*, u^*) + \nabla \lambda^* f(x^*, u^*) + \nabla \mu^* g(x^*, u^*) + \nabla \nu^* h(x^*, u^*) = 0, \tag{4.32a}$$

$$f(x^*, u^*) = 0, \tag{4.32b}$$

$$g(x^*, u^*) = 0, \tag{4.32c}$$

$$h(x^*, u^*) < 0, \tag{4.32d}$$

$$\nu^* > 0, \tag{4.32e}$$

$$\nu_j^* h_j(x^*, u^*) = \epsilon, \text{ for all } j \in \mathbb{Z}_{[1, n_h]}, \tag{4.32f}$$

where the KKT condition (4.22) is relaxed by a scaler $\epsilon > 0$ in (4.32), and multipliers $\nu$ are required to be positive instead of nonnegative (here is where interior property comes into play). The main idea of primal-dual methods is to solve (4.32) for successively decreasing values of $\epsilon$, and thereby to generate iterates $(x^k, u^k, \lambda^k, \mu^k, \nu^k)$ that approach

$(x^*, u^*, \lambda^*, \mu^*, \nu^*)$ as $\epsilon \to 0$. Primal-dual methods are in practice more efficient than primal barrier methods, since they generate different search directions using also information from the dual space, and therefore iterates generated by the two algorithms do not coincide in general (Borrelli et al., 2014). For further details about the central path and its interpretation via KKT conditions see e.g., Maciejowski (2002) and Boyd et al. (2004).

### 4.2.6.2 Complementarity Functions

Let's consider the OCP (4.19) and its first-order necessary conditions (4.22), in order to account complementarity conditions in the necessary conditions and avoid the ill-conditioning, a *semi-smooth* transformation can be utilised. Two important and most widely used examples of complementarity functions are *natural residual* function and a semi-smooth Fischer-Burmeister (FB) function introduced by Fischer (1992). The *natural residual* function ($\Phi_{NR}(\cdot)$) given by:

$$\Phi_{NR}(\mu_j^*, h_j(\hat{x}, u)) = \max\{\mu_j^*, h_j(\hat{x}, u)\}, \tag{4.33}$$

and the FB function ($\Phi_{FB}(\cdot)$), which is used in this study given as follows:

$$\Phi_{FB}(\mu_j, h_j(\hat{x}, u)) = \sqrt{\mu_j^2 + h_j(\hat{x}, u)^2} - (\mu_j - h_j(\hat{x}, u)). \tag{4.34}$$

Complementarity functions provide a convenient tool for converting problems that involve complementarity conditions into equations (Izmailov et al., 2014). The KKT conditions of an OCP with inequality constraints are transformed equivalently into a special nonlinear system of equations $\Phi_{FB}(\mu_j, h_j(\hat{x}, u) = 0$ where $\Phi_{FB}$ is applied element-wise (Fischer, 1992). The FB transformation provides an equivalent OCP while the exterior penalty and auxiliary variable methods do not (M. Huang et al., 2015). A geometric property of surfaces of the generalized FB function with the convergent behaviour and its induced merit function was studied by Tsai et al. (2014). The natural residual or the FB function, can have appropriate regularity properties without strict complementarity and are thus generally preferred for constructing Newton-type methods for the NCP. For more details related to the state-of-the-art theoretical analysis of the fundamental Newtonian and Newtonian-related approaches to solving optimization and variational problems see e.g., (Izmailov et al., 2014).

The FB function is differentiable everywhere except at the $(\mu_j, h_j(\hat{x}, u)) = (0, 0)$. Several works of literature were proposed to construct smoothing functions of the natural residual or FB functions. For instance, the Kanzow smooth FB function is proposed by

Kanzow et al. (1999) as follows:

$$\Phi_{SFB}(\mu_j, h_j(\hat{x}, u)) = \sqrt{\mu_j^2 + h_j(\hat{x}, u)^2 + 2\epsilon} - (\mu_j - h_j(\hat{x}, u)), \qquad (4.35)$$

where the (4.35) was replaced by $\epsilon$ or $\epsilon^2$ proposed by Fukushima et al. (1998) and Jiang et al. (2000). In addition, a smoothing inexact Newton method was presented for solving nonlinear complementarity problems by Tang et al. (2013). The smoothed FB function is continuously differentiable and if $\epsilon \to 0$, then the smooth FB function (4.35) coincides with the FB function (4.34).

### 4.2.6.3 Constraint Softening

The optimiser may face an infeasible problem that can lead to a serious problem with the predictive control problem. This might happen due to an unexpectedly large disturbance or the real plant behaves differently from the internal model. There are many ways in which the predictive control problem can become infeasible, and most of them are difficult to anticipate (Maciejowski, 2002).

An effective strategy is required to handle the infeasibility. For instance, standard algorithms for solving Quadratic Programming (QP) problems just gave up with a message such as "`Infeasible Problem!`". One systematic strategy for dealing with infeasibility is to "*soften*" the constraints. That is, rather than regard the constraints as "*hard*" boundaries, which can never be crossed, to allow them to be crossed occasionally, but only if really necessary (Maciejowski, 2002).

It is noteworthy to distinguish between the control inputs and states constraints. Generally, the control inputs constraints are hard constraints, which there is no possibility to soften. Actuators have limited ranges of action which reaching on the limited range cannot be exceeded. Thus, the control inputs are generally defined as the hard constraint in the OCP. On the other hand, states constraints can be violated if needed which lead to soft constraints definition in the OCP.

One of the most well-known continuous and twice differentiable function to soften the logarithmic barrier (4.29) is the exponential function defined as follows:

$$\hat{\Phi}_h(\hat{x}, u) := \sum_{j=1}^{n_h} \exp(h(\hat{x}, u)), \qquad (4.36)$$

with domain $\{\hat{x} \in \mathbb{R}^{n_x} | h_j(\hat{x}, u) \leq 0, \forall j = 1, \ldots, n_h\}$. A straightforward way of softening states constraints is to add new variables, so-called "*slack variables*", which are defined in such a way that they are non-zero only if the constraints are violated. Then their

non-zero values are very heavily penalised in the cost function so that the optimiser has a strong incentive to keep them at zero if possible (Maciejowski, 2002). Later on in this chapter, we will introduce a FB based constraints softening method, which does not require slack variables in the OCP (see subsection 4.4.3.7).

## 4.3 Deterministic Predictive Control

In order to carry out the desired control task, the MPC can be designed by formulating and solving a corresponding OCP such as (4.19). The first elements in the computed trajectory of the control inputs are applied in *open-loop* to the system. One sample interval later, based on the receding horizon strategy, the predictive controller computes the next control inputs by recalculating the corresponding OCP with updated plant information. A nominal open-loop plant model is mainly considered in the deterministic MPC. In other words, if there are no disturbances or model error, the problem is deterministic. The deterministic MPC is also known as closed-loop OCP or open-loop MPC. This section focuses on the brief review of deterministic linear, nonlinear, and economic MPCs with overview on the stability analysis and real-time algorithms. For more details see e.g., D.Q. Mayne et al. (2000) and James B. Rawlings, D. Q. Mayne, and M. M. Diehl (2015).

### 4.3.1 Model Predictive Control

The linear MPC is generally referred to QP based OCP, where the cost function is quadratic and the constraint set is polyhedral, i.e., defined by linear inequalities. The ease of solution and analysis of linear models is the main motivation to approximate the plant with linear models. A typical nominal MPC for a linear state-space model can be defined as follows:

$$V_N^*(x) := \underset{u^*}{\text{minimise}} \quad V_N(x, u) := \sum_{i=0}^{N-1} J_c(x_i, u_i) + J_f(x_N) \tag{4.37a}$$

subject to:

$$x_{i+1} = Ax_i + Bu_i, \qquad \text{for all } i \in \mathbb{Z}_{[0,N-1]}, \tag{4.37b}$$

$$(x_i, u_i) \in X \times U, \qquad \text{for all } i \in \mathbb{Z}_{[0,N-1]}, \tag{4.37c}$$

$$x_N \in X_f, \qquad x_0 = x, \tag{4.37d}$$

where $X$ and $X_f$ are invariant compact convex sets and $U$ is set of feasible control sequences. It is assumed that $J_c(\cdot, \cdot)$ is a convex function and there exist $\kappa$-class function

$\alpha_{J_c}(\cdot)$ such that $J_c(x, u) \geq \alpha(\|x\|)$. The objective function depends on the input sequence and state sequence. The initial state is available from the measurement. The stage cost and terminal cost are given by quadratic functions as follows:

$$J_c(x_i, u_i) := x^T Q x + u^T R u, \quad \text{for all } i \in \mathbb{Z}_{[0,N-1]}, \tag{4.38}$$

$$J_f(x_N) := x_N^T P x_N, \tag{4.39}$$

where we assume the $Q$, $P$, and $R$ are real and symmetric; $Q$ and $P$ are positive semidefinite, and $R$ is positive definite. These assumptions guarantee that the solution to the OCP exists and is unique (James B. Rawlings, D. Q. Mayne, and M. M. Diehl, 2015). For more recent achievements about the MPC follow e.g., D. Q. Mayne (2014).

### 4.3.2   Nonlinear Model Predictive Control

The MPC is considered to be a mature technique for linear and rather slow systems like the ones usually encountered in the process industry. More complex systems, such as nonlinear, hybrid, or very fast processes, were considered beyond the realm of the linear MPC. Consequently, the application of linear control methods does not always lead to satisfactory performance, and here nonlinear methods must be employed (Raff et al., 2007). Nonlinear Model Predictive Control (NMPC) is an optimisation based method for the feedback control of nonlinear systems (Grüne and Pannek, 2011). The NMPC is able to directly handle nonlinear system models, nonlinear constraints and nonlinear objectives in the OCP to improve performance specifications. Additionally, the widespread availability and steadily increasing power of modern computers, as well as the development of specially tailored numerical solution methods for NMPC, bring the practical applicability of NMPC within each even for fast systems (Raff et al., 2007).

The NMPC is generally defined as an NLP based on (4.19) as follows:

$$V_N^*(x_t) := \underset{u^*}{\text{minimise}} \quad V(x_t, \boldsymbol{u}) \tag{4.40a}$$

subject to:

$$x_{i+1} = f(x_i, u_i), \qquad \text{for all } i \in \mathbb{Z}_{[0,N-1]}, \tag{4.40b}$$

$$g_j(x_i, u_i) = 0, \qquad \text{for all } j \in \mathbb{Z}_{[1,n_g]}, i \in \mathbb{Z}_{[0,N-1]}, \tag{4.40c}$$

$$h_j(x_i, u_i) \leq 0, \qquad \text{for all } j \in \mathbb{Z}_{[1,n_h]}, i \in \mathbb{Z}_{[0,N-1]}, \tag{4.40d}$$

$$x_0 = x_t, \tag{4.40e}$$

where the $\boldsymbol{u}$ is the N-stage feedback control law and $V(x_t, U)$ is the quadratic function as follows:

$$V(x_t, \boldsymbol{u}) := \sum_{i=0}^{N-1} J_c(x_i, u_i) + J_f(x_N), \tag{4.41}$$

$$J_c(x_i, u_i) := \|x_i\|_Q^2 + \|u_i\|_R^2, \quad \text{for all } i \in \mathbb{Z}_{[0,N-1]}, \tag{4.42}$$

$$J_f(x_N) := \|x_N\|_P^2. \tag{4.43}$$

In case of using the NMPC for set-point tracking problem, the cost function $J_c(\cdot, \cdot)$ and $J_f(\cdot)$ vanish if and only if the states are exactly on the reference. For $x \in \Xi$ and $u \in \Upsilon$ with Euclidean norms, a quadratic distance function is now of the form:

$$J_c(x_i, u_i) := \|x_i - x_{i_{ref}}\|_Q^2 + \|u_i - u_{i_{ref}}\|_R^2, \quad \text{for all } i \in \mathbb{Z}_{[0,N-1]}, \tag{4.44}$$

$$J_f(x_N) := \|x_N - x_{N_{ref}}\|_P^2, \tag{4.45}$$

where $x_{ref}$ and $u_{ref}$ are the references (Grüne and Pannek, 2011). In linear MPC, the optimisation at each sampling time is occasionally performed over control sequence with predefined values $u(K), \cdots, u(N-1)$ for some $K \in \{1, \cdots, N-1\}$, i.e. only $u(0), \cdots, u(K-1)$ are used as optimisation variable in the OCP. In this setting, $K$ is referred to as the optimisation horizon or the control horizon (Grüne and Pannek, 2011). Regarding the NMPC, this variant is less common which is also not considered in this study.

### 4.3.3 Economic Model Predictive Control

During the last couple of years, EMPC has attracted significant attention. Due to the availability of fast and reliable solution algorithms for the underlying optimal control problems and an increasing demand for efficiency, e.g., in terms of consumptions of resources and energy or regarding a reduction of the environmental impact, the idea to use more sophisticated "economic" objectives directly in an (nonlinear) MPC formulation is both natural and appealing (Grüne and Stieler, 2014).

The main difference between tracking NMPC and EMPC is that tracking NMPC uses a positive definite stage cost with respect to a set-point or reference trajectory (typically, a quadratic stage cost is used that is zero at the economically optimal steady state), while EMPC uses a general stage cost that does not need to be positive definite with respect to a set-point, steady state, or reference trajectory (Ellis and Christofides, 2015). Additionally, EMPC is generally more computationally intensive compared to tracking

NMPC given the additional possible nonlinearities in the stage cost of EMPC (Ellis and Christofides, 2015).

The cost function may be a direct or indirect reflection of the process economics. However, the EMPC may operate a system in a possibly time-varying fashion to optimise the process economics. For instance, one may not operate the system at a specified steady-state or reference (Ellis, Durand, et al., 2014). In addition, there are several works of literature had integrated economic optimisation of process operations and MPC into the same algorithm. The main idea is focused on combining steady-state economic optimisation and MPC into one optimisation problem. For instance, MPC schemes that integrate steady-state optimisation use a cost function of the form:

$$J_c(x_i, u_i) := x^T Q x + u^T R u, \quad \text{for all } i \in \mathbb{Z}_{[0,N-1]}, \tag{4.46}$$

$$J_f(x_N, u_s) := l_e(x_N, u_s) \tag{4.47}$$

which has both a quadratic (tracking) component at cost-per-stage and an economic final cost component in the terminal cost function with steady-state input $u_s$ (Ellis, Durand, et al., 2014).

It is important to point out that the use of OCPs with an economic cost function is not a new concept. In fact, MPC with an economic cost is not new either. However, closed-loop stability and performance under EMPC has only recently been considered and proved for various EMPC formulations (Ellis, Durand, et al., 2014). A strong duality condition is shown to be a sufficient condition for asymptotic stability of EMPC with nonlinear models (James B. Rawlings, D. Q. Mayne, and M. M. Diehl, 2015). Fundamentals and details of the EMPC design were given by James B. Rawlings, Angeli, et al. (2012) for more information.

### 4.3.4   Stability and Feasibility in Model Predictive Control

Predictive control, using the receding horizon idea, is a feedback control policy. There is, therefore, a risk that the resulting closed-loop might be unstable. Even though the performance of the plant is being optimised over the prediction horizon, and even though the optimisation keeps being repeated, each optimisation 'does not care' about what happens beyond the prediction horizon, and so could be putting the plant into such a state that it will eventually be impossible to stabilise. One might guess that the short prediction horizon ('short-sighted') can lead to instability. It turns out that stability can usually be ensured by making the prediction horizon long enough, or even infinite (Maciejowski, 2002).

In addition, there are generally two principal methods of guaranteeing nominal stability. *Terminal constraints* at the end of the prediction horizon and *Infinite Horizon*. For the purpose of proving stability, it is enough to consider the case when the state is to be driven to the origin, from some initial condition (Maciejowski, 2002). All the 'nominal stability' analysis of the closed-loop is under the assumption that an exact model of the plant is available. In most of the control algorithms presented in this chapter, the decrease in the optimal cost, on which the proof of stability is founded, is based on the assumption that the next state is exactly as predicted and that the global solution to the optimal control problem can be computed (James B. Rawlings and D. Q. Mayne, 2009). The use of terminal penalties and/or constraints, Lyapunov functions or invariant sets has given rise to a wide family of techniques that guarantee the stability of the controlled system. *Terminal constraint* considering a finite horizon and ensuring stability by adding a state terminal constraint of the form $x_N = x_s$. With this constraint, the state is zero at the end of the finite horizon and therefore the control action is also zero. *Infinite horizon* consists of increasing the control and prediction horizons to infinity. In this case, the objective function can be considered a Lyapunov function, providing nominal stability (Raff et al., 2007).

In order to state the sharpest results on stabilization, we require the concepts of controllability, stabilisability, observability, and detectability (James B. Rawlings, D. Q. Mayne, and M. M. Diehl, 2015). A system is controllable if, for any pair of states $(x, z)$ in the state space, $z$ can be reached in finite time from $x$ (or $x$ controlled to $z$). A linear discrete-time system $x_{i+1} = Ax_i + Bu_i$ is therefore controllable if there exists a finite time $N$ and a sequence of inputs that can transfer the system from any $x$ to any $z$. The basic idea of observability is that any two distinct states can be distinguished by applying some input and observing the two system outputs over some finite time interval (James B. Rawlings and D. Q. Mayne, 2009).

Because of the finite horizon in the OCP, the predicted state can differ considerably from the actual state. Ideally, the horizon $N$ in the OCP solved online should be infinite in which case the predicted state would equal the actual state. A relaxed version of the dynamic programming principle, which allows proving stability and suboptimality results for nonoptimal feedback laws without using the optimal value function is the infinite horizon OCP. For practical reasons, $N$ is usually finite with the result that the controlled system is not necessarily stable or optimal nor is recursively feasible (D. Q. Mayne, 2014). The performance below is the infinite horizon cost of the controlled system:

$$V_\infty^*(x) := J_c(x_i, u_i) := \sum_{i=0}^\infty x_i^T Q x_i + u_i^T R u_i. \tag{4.48}$$

The OCP with infinite horizon when $N \to \infty$ provides a control law that is guaranteed to asymptotically stabilise system and is recursively feasible (J. B. Rawlings et al., 1993). A control law $\kappa(x) := u_0^*(x)$ is called recursively feasible for $x(0)$ if $\kappa(x_i) \in U$ and $x_i \in X$ along the closed-loop trajectory $x_{i+1} = Ax_i + B\kappa(x_i)$ for all $i \in \mathbb{Z}_{[0,N-1]}$. In order to recover feasibility and stability in the finite horizon MPC there are rules to setup the problem, which are provided by D.Q. Mayne et al. (2000). However, it was also shown that near optimal infinite horizon performance is not needed for ensuring stability and admissibility (Grüne and Pannek, 2011). Moreover, it is shown that the stability properties of the infinite horizon OCPs are, in general, not preserved in MPC as long as purely quadratic costs are employed. This indicates the necessity of using the stage cost as a design parameter to achieve asymptotic stability (Müller et al., 2017). For the purpose of proving stability e.g., Maciejowski (2002), Worthmann et al. (2017) provides the related theorems for more information.

General constrained optimisation problems can be extremely difficult to solve, and just adding a terminal constraint may not be feasible (Maciejowski, 2002). In addition, there are several works of literature present stability analysis for various types of MPC. For instance, a novel NMPC scheme, which is based on the concept of passivity, was presented by Raff et al. (2007). A passivity-based constraint is used to obtain a NMPC scheme with guaranteed closed-loop stability for any, possible arbitrarily small, prediction horizon. Since passivity and stability are closely related, the proposed approach by Raff et al. (2007) can be seen as an alternative to NMPC schemes, which are based on the concept of control Lyapunov functions.

The fact that predictive control is usually implemented on top of traditional local controllers had important implications for its acceptance and development. The great majority of the process plant is stable in this condition, so although this may not be the most profitable condition, it is at least a safe one. This is one of the reasons why there were many predictive controllers installed even before there was a satisfactory stability theory for predictive control, and indeed why many current installations take no account of that stability theory. In addition, the commercial predictive controllers being developed almost exclusively for the stable plant. The plant 'seen' by the predictive controller is one which is already running under closed-loop control and is almost invariably stable (Maciejowski, 2002).

### 4.3.5 Real-time Nonlinear Model Predictive Control

During the past years, different algorithms and tools have been introduced that can be used to implement the various type of NMPCs. Due to the computational delay of the

NMPCs, having a real-time online algorithm that is capable of dealing with the OCP is a challenging task. However, there are some algorithms, which can be utilised in real-time systems. Some of these algorithms classified and reviewed by M. Diehl, Ferreau, et al. (2009). The main focus of this study is to implement a real-time NMPC. Many software packages are currently available for real-time NMPCs on embedded hardware. For example, ACADO Toolkit is a software environment and algorithm collection for automatic control and dynamic optimization. In this tool, several open-source convex solvers such as qpOASES (Ferreau et al., 2014) and FORCES (Domahidi et al., 2012) have been interfaced for direct optimal control.

Considering the indirect method based NMPC solvers, Continuation/Generalized Minimal RESidual (C/GMRES) as a fast numerical algorithm for nonlinear receding horizon control is proposed by Ohtsuka (2004). Similar to the Newton-Type controller, the C/GMRES method performs only one Newton type iteration in each sampling time and is based on a sequential formulation. It is based on an IP treatment of the inequalities with fixed path parameter and it uses the iterative GMRES method as a Krylov subspace method for linear system solution in each Newton step. For more information about GMRES method see e.g., Kelley (1995). Most important, it makes no use of a shift, but instead, use of the tangential predictor. This feature seems to allow it to follow the nonlinear IP solution manifold well which is strongly curved at active set changes (M. Diehl, Ferreau, et al., 2009). The closed-loop stability of the method is in principle covered by the stability analysis for the real-time iterations without shift given by M. Diehl, Findeisen, et al. (2007). A variant of the method is given by Shimizu et al. (2009), which uses a simultaneous approach and condensing and leads to improved accuracy and lower computational cost in each Newton type iteration. Recent NMPC research along similar ideas has benefited considerably from progress in numerical optimization, being able to take advantage of structural properties on the NMPC problem and general efficiency improvements and important issues such as robustness (Grancharova et al., 2012). For instance, there are several automotive application of NMPC that were introduced by Md Abdus Samad Kamal et al. (2013), Gagliardi et al. (2014), and M. Huang et al. (2015). In addition, the C/GMRES have been implemented in various applications such as the Large Hadron Collider (LHC) at the European Organization for Nuclear Research (CERN), the world's highest energy particle accelerator and collider, which was presented by Noga et al. (2011). Thus, the real-time C/GMRES algorithm is the main numerical method applied in this study. The next subsection presents the detailed solution approach of the NMPC based on the C/GMRES.

### 4.3.5.1 Problem Formulation

Let's consider a continuous-time system and assume that every function is differentiable as many times as necessary. The state equation and an $n_c$-dimensional equality constraint are given as:

$$\dot{x} = f(x(t), u(t)), \quad C(x(t), u(t)) = 0. \tag{4.49}$$

An inequality constraint can be converted into equality constraint by introducing a dummy input based on auxiliary variable method (Ohtsuka, 2004). The following performance index with the initial state given by the actual state $x(t)$ is minimised:

$$V_T(x(t), u(t)) = \int_t^{t+T} J_c(x(t'), u(t'))dt' + J_f(x(t+T)). \tag{4.50}$$

The optimal control $u^*(t'; t, x(t))$ minimising $V_T(x(t), u(t))$ is computed over prediction horizon $t' \in [t, t+T]$. The NMPC problem is essentially a family of finite-horizon optimal control problems along a fictitious time $\tau$ as follows:

$$V_T^*(x(t)) := \underset{u^*}{\text{minimise}} \quad \int_0^T J_c(x^*(\tau, t), u^*(\tau, t))d\tau + J_f(x^*(T, t)) \tag{4.51a}$$

subject to:

$$x_\tau^*(\tau, t) = f(x^*(\tau, t), u^*(\tau, t)), \tag{4.51b}$$

$$C(x^*(\tau, t), u^*(\tau, t)) = 0, \tag{4.51c}$$

$$x(0, t) = x(t), \tag{4.51d}$$

where subscript $\tau$ denotes partial differentiation with respect to $\tau$ (M. Diehl, Ferreau, et al., 2009). The new state vector $x^*(\tau, t)$ represents a trajectory along the $\tau$ axis starting from $x(t)$ at $\tau = 0$ and the prediction horizon $T$ is a function of time, $T = T(t)$ in general (Ohtsuka and Ozaki, 2009).

Let $H$ denotes the Hamiltonian defined by:

$$H(x, \lambda, u, \mu) = J_c(x, u) + \lambda^{\mathrm{T}} f(x, u) + \mu^{\mathrm{T}} C(x, u), \tag{4.52}$$

where $\lambda \in \mathbb{R}^{n_x}$ denotes the costate, and $\mu \in \mathbb{R}^{n_c}$ denotes the Lagrange multipliers associated with equality constraints.

The first-order conditions necessary for the OCP are obtained by the calculus of variation as the Euler-Lagrange equations (Ohtsuka and Ozaki, 2009):

$$x^*_\tau = f(x^*, u^*), \qquad\qquad x^*(0, t) = x(t), \qquad\qquad (4.53\text{a})$$

$$\lambda^*_\tau = -H^\mathrm{T}_x(x^*, \lambda^*, u^*, \mu^*), \qquad \lambda^*(T, t) = J^\mathrm{T}_f(x^*(T)), \qquad (4.53\text{b})$$

$$H^\mathrm{T}_u(x^*, \lambda^*, u^*, \mu^*) = 0, \qquad\qquad\qquad\qquad\qquad (4.53\text{c})$$

$$C(x^*, u^*) = 0. \qquad\qquad\qquad\qquad\qquad\qquad (4.53\text{d})$$

The control input $u^*$ and the Lagrange multiplier $\mu^*$ at each time $\tau$ on the prediction horizon are determined from $x^*$ and $\lambda^*$ by algebraic equations $H_u(\cdot) = 0$ and $C(\cdot) = 0$. The nonlinear TP-BVP has to be solved within the sampling period for the measured state $x(t)$ at each sampling time, which is one of the major difficulties in NMPC (Ohtsuka and Ozaki, 2009).

In real-time NMPC algorithm using the C/GMRES, the update of the optimal solution (more precisely, a stationary solution) is regarded as a continuous-time dynamic process described as a differential equation (Ohtsuka, 2004). This algorithm can be viewed as a type of continuation method (S. Richter et al., 1983). In order to find the initial costate $\lambda^*(0, t)$ without an iterative search, its differential equation along real time $t$ is derived. Note that $\dot\lambda = \lambda^*(0, t)$ holds and $\lambda^*_t$ is unknown while $\lambda^*_\tau$ is given as $\lambda^*_\tau = -H^T_x$. In practice, the initial value $\lambda(0) = \lambda^*(0, 0)$ is given by the trivial solution to the TP-BVP for $T = 0$, and the horizon length $T$ is smoothly increased to some constant value. More details of real-time costate equation computation was presented by Ohtsuka and Ozaki (2009).

The control input function over the prediction horizon is regarded as the unknown quantity in the TP-BVP. In order to represent the unknown control input function with a finite number of parameters, the prediction horizon of the OCP is discretised into $N$ steps. Then, the discretised conditions for optimality are given as follows:

$$x^*_{i+1}(t) = x^*_i(t) + f(x^*_i(t), u^*_i(t))\Delta\tau, \qquad x^*_0(t) = x(t), \qquad (4.54\text{a})$$

$$\lambda^*_i = \lambda^*_{i+1} - H^\mathrm{T}_x(x^*_i(t), \lambda^*_{i+1}(t), u^*_i(t), \mu^*_i(t))\Delta\tau, \quad \lambda^*_N(t) = J^\mathrm{T}_f(x^*_N(t)), \quad (4.54\text{b})$$

$$H^\mathrm{T}_u(x^*_i(t), \lambda^*_{i+1}(t), u^*_i(t), \mu^*_i(t)) = 0, \qquad\qquad\qquad (4.54\text{c})$$

$$C(x^*_i(t), u^*_i(t)) = 0, \qquad\qquad\qquad\qquad\qquad\qquad (4.54\text{d})$$

where $\Delta\tau := T/N$. On the discretised horizon, sequences of the state, costate, input, and Lagrange multiplier associated with the equality constraint are denoted by $\{x^*_i(t)\}^N_{i=0}$, $\{\lambda^*_i(t)\}^N_{i=0}$, $\{u^*_i(t)\}^{N-1}_{i=0}$, $\{\mu^*_i(t)\}^N_{i=0}$, respectively. As a result, NMPC is formulated as a

discrete-time TP-BVP (4.54) for a measured state $x(t)$ at time $t$ (Ohtsuka and Ozaki, 2009).

Let us define vector $U(t) \in \mathbb{R}^{nN}$ ($n := n_u + n_c$) composed of the sequences of the input vectors and multipliers as follows:

$$U(t) := [u_0^{*\mathrm{T}}(t), \mu_0^{*\mathrm{T}}(t) \cdots u_{N-1}^{*\mathrm{T}}(t), \mu_{N-1}^{*\mathrm{T}}(t)]^{\mathrm{T}}. \tag{4.55}$$

The sequences of $\{x_i^*(t)\}_{i=0}^N$ and $\{\lambda_i^*(t)\}_{i=0}^N$ can be regarded as functions of $U(t)$ and $x(t)$. Then, the optimality conditions (4.54) can be regarded as an $nN$-dimensional equation system given by:

$$F(U(t), x(t), t) := \begin{bmatrix} H_u^{\mathrm{T}}(x_0^*, \lambda_1^*, u_0^*, \mu_0^*) \\ C(x_0^*, u_0^*) \\ \vdots \\ H_u^{\mathrm{T}}(x_{N-1}^*, \lambda_N^*, u_{N-1}^*, \mu_{N-1}^*) \\ C(x_{N-1}^*, u_{N-1}^*) \end{bmatrix} = 0, \tag{4.56}$$

where $F$ depends on $t$ when the horizon length $T$ is time dependent (Ohtsuka and Ozaki, 2009).

Solving (4.56) at each time by the iterative methods such as Newton's method is computationally expensive and thus inefficient. Instead, the continuation method is applied (S. Richter et al., 1983), considering the real time $t$ as the continuation parameter. That is, the time derivative of $U$ obtained so that (4.56) is satisfied identically. If the initial solution $U(0)$ of the problem is determined so as to satisfy $F(U(0), x(0), 0) = 0$, then we can trace $U(t)$ by integrating $\dot{U}(t)$ fulfilling the condition:

$$\dot{F}(U(t), x(t), t) = A_s F(U(t), x(t), t), \tag{4.57}$$

where $A_s$ is a positive real number. The right-hand side of (4.57) stabilizes $F = 0$. Equation (4.57) is equivalent to a linear equation with respect to $\dot{U}(t)$ given by:

$$\dot{U} = F_U^{-1}(-A_s F - F_x \dot{x} - F_t). \tag{4.58}$$

If the matrix $F_U$ is nonsingular, (4.58) is solved efficiently by the GMRES (Kelley, 1995), one of the Krylov subspace methods for linear equations. We can update the unknown quantity $U$ by integrating the obtained $\dot{U}(t)$ by, for example, the Euler method in real-time. In the case of the explicit Euler method, the computational cost for updating $U$ corresponds to only one iteration in Newton's method but achieves higher accuracy by taking the time dependency of the equation into account (Ohtsuka and Ozaki, 2009).

For more details about the C/GMRES see e.g., Ohtsuka (2004), Ohtsuka and Ozaki (2009), Shimizu et al. (2009), and Knyazev et al. (2017).

## 4.4 Stochastic Predictive Control

Parametric uncertainties and exogenous disturbances are the pervasive features of complex dynamical systems. Real systems and their mathematical models do not exactly coincide with each other. This means that in practice the behaviour of the real system will deviate from the mathematically idealised model (Grüne and Pannek, 2011). For instance, modelling errors, uncertain parameters, external disturbances acting on the system, numerical errors, and measurement errors are sources for falsities.

The MPC controller inherently has some degree of robustness to the system uncertainties due to its receding horizon implementation. In fact, repeated solution of the OCP confers an "implicit" feedback action to MPC to cope with system uncertainties and disturbances (Mesbah, 2016). However, uncertainties in the process model can reduce the MPC performance and destabilise the system. In order to achieve robustness, the controller must stabilise the system for all possible realisations of the uncertainty (Shuyou Yu et al., 2010). RMPC and SMPC have been effectively utilised to systematically handle uncertainties of the system. In this section, we review RMPC, SMPC formulations, and propose a risk-sensitive SNMPC with its application for optimal energy management in the BEVs.

### 4.4.1 Robust Model Predictive Control

The past two decades have witnessed significant developments in the area of RMPC with the aim to devise computationally affordable OCP approaches (Mesbah, 2016). The RMPC approaches consider set-membership-type uncertainties that modelling errors and disturbances are assumed to be unknown-but-bounded quantities. Early work on RMPC was primarily based on min-max OCP formulations. In case of min-max approach, the performance index is minimised with respect to the worst-case realisation of the uncertainty (Herceg et al., 2017).

In order to formulate the RMPC, consider a general system with disturbance:

$$x_{t+1} = f(x_t, u_t, \omega_t), \tag{4.59}$$

where $\omega \in \mathbb{R}^{n_w}$ is disturbances vector. It is assumed that $\mathbf{E}[\omega] = 0$ and model uncertainty is described as follows:

$$x_{t+1} = f(x_t, u_t, \omega_t), \tag{4.60}$$

$$y = h(x_t), \tag{4.61}$$

$$\omega = \Delta(y_t(\cdot)), \tag{4.62}$$

where $\Delta(\cdot)$ is a causal input-output operator representing the unmodelled dynamics with input $y(\cdot)$ and output $\omega$; $\Delta$ does not necessarily have a finite-dimensional state representation (David Mayne, 2016).

The $\Delta$ is an operator representing the unmodelled dynamics that, at time $t$, maps the output sequence $y_t := \{\cdots, y(-2), y(-1), y(0), y(1), \cdots\}$ into $\omega_t$. In RMPC it is assumed that the disturbance $\omega$ takes values in the compact set $\mathbb{W} \subset \mathbb{R}^{n_w}$ that contains the origin in its interior. For RMPC, in which the system is assumed to satisfy (4.59), $x^\pi(t; x, \omega)$ denotes the solution of:

$$x_{i+1} = f(x_i, \mu_i(x_i), \omega_i), \quad \text{for all } i \in \mathbb{Z}_{[0,N-1]}, \tag{4.63}$$

at time $t$ given the initial state $x_0 = x_t$. The control policy is:

$$\pi = \{\mu_0(\cdot), \mu_1(\cdot), \cdots, \mu_{N-1}(\cdot)\}, \tag{4.64}$$

where $\pi \in \Pi$. The decision variable $u$ may be regarded as a degenerate policy in which $\mu_i(x) = \theta(x, v_i) = v_i = u_i$ for all $i$, all $x$. The definition of cost depends on the type of the RMPC: Nominal cost and Worst Case cost. The Nominal cost is defined as follows:

$$V_N(x, \pi) := \sum_{i=0}^{N-1} J_c(x^\pi(i; x, 0), \mu_i(x^\pi(i; x, 0))) + J_f(x^\pi(N; x, 0)). \tag{4.65}$$

The Worst Case cost for the RMPC is defined as follows:

$$V_N(x, \pi) := \underset{\omega \in \mathbb{W}}{\text{maximise}} \sum_{i=0}^{N-1} J_c(x^\pi(i; x, \omega), \mu_i(x^\pi(i; x, \omega))) + J_f(x^\pi(N; x, \omega)). \tag{4.66}$$

For RMPC, the OCP is defined as follows:

$$V_N^*(x_t) := \underset{\pi^*}{\text{minimise}} \quad V_N(x, \pi) \tag{4.67a}$$

subject to:

$$x_{i+1} = f(x_i, \mu_i(x_i)), \qquad \text{for all } i \in \mathbb{Z}_{[0,N-1]}, \tag{4.67b}$$

$$g_j(x_i, \mu_i(x_i)) = 0, \qquad \text{for all } j \in \mathbb{Z}_{[1,n_g]}, i \in \mathbb{Z}_{[0,N-1]}, \tag{4.67c}$$

$$h_j(x_i, \mu_i(x_i)) \leq 0, \qquad \text{for all } j \in \mathbb{Z}_{[1,n_h]}, i \in \mathbb{Z}_{[0,N-1]}, \tag{4.67d}$$

$$x_0 = x_t, \tag{4.67e}$$

where the $\pi$ is the N-stage feedback control policy. For more detail about the RMPC see e.g., David Mayne (2016).

The min-max MPC approaches could not, however, contain the "spread" of state trajectories, rendering the OCP actions overly conservative or, possibly, infeasible (Mesbah, 2016). To address the shortcomings of min-max OCPs, tube-based MPC has been developed by Langson et al. (2004). Tube-based MPC approaches use a partially separable feedback control law parametrisation to allow for direct handling of uncertainties and their interactions with the system dynamics, constraints, and performance criteria (Mesbah, 2016). For more detail information about the Tube-based MPC follow e.g., D. Q. Mayne and Kerrigan (2007).

### 4.4.2 Stochastic Model Predictive Control

The RMPC approaches rely on bounded, deterministic descriptions of system uncertainties. In practice, however, uncertainties are often considered to be of probabilistic nature. It is more rational to explicitly account for the probabilistic occurrence of uncertainties in a control design method whenever the stochastic system uncertainties can be adequately characterised. Hence, SMPC has recently emerged with the aim of systematically incorporating the probabilistic descriptions of uncertainties into a stochastic OCP (David Mayne, 2016).

In the SMPC, the uncertainty is the random process, a sequence of independent, identically distributed random variables. In particular, SMPC exploits the probabilistic uncertainty descriptions to define chance-constraints, which require the state/output constraints to be satisfied with at least a priori specified probability level or, alternatively, be satisfied in expectation. Chance-constraints enable the systematic use of the stochastic characterisation of uncertainties to allow for an admissible level of closed-loop constraint violation in a probabilistic sense. In addition, SMPC allows for systematically seeking the tradeoff between fulfilling the control objectives and guaranteeing a

probabilistic constraint satisfaction due to uncertainty (Mesbah, 2016). Furthermore, the probabilistic framework of SMPC enables shaping the probability distribution of system states/outputs. The ability to regulate the probability distribution of system states/outputs is important for the safe and economic operation of complex systems (Buehler et al., 2016).

The $\omega(t)$ is a random process, a sequence of independent, identically distributed random variables taking values in a set $\omega \subset \mathbb{R}^P$ that is not necessarily compact in SMPC. In the stochastic case, it is assumed that there is an underlying probability space with probability measure $P$ (David Mayne, 2016). Similar to the RMPC, the cost function of the SMPC for the Nominal case is defined as follows:

$$V_N(x, \pi) := \sum_{i=0}^{N-1} J_c(x^\pi(i; x, 0), \mu_i(x^\pi(i; x, 0))) + J_f(x^\pi(N; x, 0)). \qquad (4.68)$$

The Expected cost for the SMPC is defined as follows:

$$V_N(x, \pi) := \mathbf{E}_x[\sum_{i=0}^{N-1} J_c(x^\pi(i; x, \omega), \mu_i(x^\pi(i; x, \omega)))] + J_f(x^\pi(N; x, \omega)), \qquad (4.69)$$

in which $\mathbf{E} \mid x(\cdot) := \mathbf{E}(\cdot \mid x)$ and $\mathbf{E}$ is expectation under $P$, the probability measure of the underlying probability space (David Mayne, 2016).

Because the probability density of the disturbance $\omega$ does not have finite support, it is impossible to satisfy the state and terminal constraints almost surely (probability one). To obtain a meaningful OCP, it is necessary to soften the state and terminal constraints. Two methods for softening the constraint have been used in the literature. The first approach is the replacement of the hard constraints of the form $x(\omega) \in \mathbb{X}$ for all $\omega \in \mathbb{W}$ are replaced by the average constraint:

$$\mathbf{E}(x(\omega)) \in \mathbb{X}. \qquad (4.70)$$

The second approach is the constraint $x(\omega) \in \mathbb{X}$ for all $\omega \in \mathbb{W}$ is replaced by the chance-constraint:

$$\mathbf{Pr}_x[x(\omega) \in \mathbb{X}] \geq 1 - \alpha, \qquad (4.71)$$

for some $\alpha \in (0, 1)$ (David Mayne, 2016).

Due to the probability density of the disturbance, $\omega$ does not necessarily have finite support, the problem of finding a terminal cost and constraint that ensure closed-loop stability (in the stochastic sense) has not yet been satisfactorily resolved although efforts in this direction have been made. For instance, Lorenzen et al. (2017) assumed that the disturbance $\omega$ is bounded and the deterministic optimal control problem, with tightened

constraints, that is solved online at state $x$ has an extra constraint on $x_{t+1}$ to ensure recursive feasibility. One concludes that there is not yet a fully satisfactory treatment of stabilizing terminal conditions for the SMPC if the disturbance is not bounded (David Mayne, 2016). For more details see e.g., Mesbah (2016), David Mayne (2016), and Lorenzen et al. (2017).

The stochastic OCP for (4.59) is generally formulated as follows. Given the current system states $x_t$, the centrepiece of an SMPC algorithm with hard input constraint and individual chance-constraint is the stochastic OCP (Mesbah, 2016):

$$V_N^*(x_t) := \underset{\pi^*}{\text{minimise}} \quad V_N(x, \pi) \tag{4.72a}$$

subject to:

$$\hat{x}_{i+1} = f(\hat{x}_i, \pi_i, \omega_i), \qquad \text{for all } i \in \mathbb{Z}_{[0,N-1]}, \tag{4.72b}$$

$$\pi_i(\cdot) \in \mathbb{U}, \qquad \text{for all } i \in \mathbb{Z}_{[0,N-1]}, \tag{4.72c}$$

$$\mathbf{Pr}_{x_t}[h_j(\hat{x}_i) \leq 0] \geq \beta_j, \qquad \text{for all } j \in \mathbb{Z}_{[1,n_h]}, i \in \mathbb{Z}_{[1,N]}, \tag{4.72d}$$

$$\omega_i \sim P_\omega, \qquad \text{for all } i \in \mathbb{Z}_{[1,N-1]}, \tag{4.72e}$$

$$\hat{x}_0 = x_t, \tag{4.72f}$$

where different $\beta_j = 1 - \alpha_j$ known as *confidence level* are assigned for the inequality constraints. The $\hat{x}_i$ denotes the predicted states at time $i$ given the initial states $\hat{x}_0 = x_t$, control law $\{\pi_i(\cdot)\}_{i=0}^{i-1}$, and disturbance realizations $\{\omega_i\}_{i=0}^{i-1}$ (Mesbah, 2016). The $\omega_t \in \mathbb{R}^{n_\omega}$ is disturbances vector that is unknown at the current and future time instants. The $\omega_t$ is composed of i.i.d. random variables within the known sample space $\Omega$, the set of events ($\sigma$-algebra) $\mathcal{F}$, and the allocations of probabilities, $\mathcal{P}$ to events (exogenous information). The $f(\cdot)$ is a nonlinear Borel-measurable [1] vector of functions that describes the system dynamics (Mesbah, 2016).

The key challenges in solving the stochastic OCP (4.72) include:

 i) the arbitrary form of the feedback control laws;

 ii) the nonconvexity and general intractability of chance-constraints;

 iii) the computational complexity associated with uncertainty propagation through complex system dynamics;

 iv) establishing theoretical properties (see Mesbah (2016), and the references therein),

---

[1] Borel measure $\chi$ defined on the $\sigma$-algebra of Borel set. The $\chi$ is locally compact if $\chi(C) \leq \infty$ for every compact $C$.

v) and moreover, the risk-neutral expectation assessment of future random outcomes for safety-critical systems where one desires to regulate the control actions so that they are robust enough to uncertainties (X. Yang et al., 2015).

Evaluating and satisfying the chance-constraints are the main challenging aspect of the SMPC. There are two general approaches known as analytical methods and sampling methods. In the analytical methods the chance-constraints are generally converted into a deterministic set or the probability of violation is evaluated. Ellipsoidal Relaxation e.g.Hessem et al. (2003), and Boole's Inequality e.g., Blackmore et al. (2009) are the methods assume a specific analytical form to evaluate the chance-constraints. On the other hand, the probability distribution of the system states can be approximated by utilising the sampling based methods such as Monte Carlo (MC), Markov Chain Monte Carlo (MCMC), or convex bounding methods. For more information about the chance-constraint evaluation see e.g., Ohsumi et al. (2011) and Vitus et al. (2012).

### 4.4.2.1 Risk-sensitive Control

The chance-constraints lead to a notion of risk. Due to the future uncertainty in the system, the controller has to make a decision with only partial information associated with risk. The made decision might cause the violation of constraints in the system. The risk quantification and measurement method should be introduced to determine the cost of violating the system constraints. For instance, the expected constraint (4.70) is a risk-neutral criterion. In fact, risk-neutral control policies may lead optimisers to a large amount of risk exposure. An alternative objective is to minimise the *risk* associated with or to find a tradeoff between the expected total reward and risk (Gonzalez and Moriarty, 2014). Considering the risk in the OCP is referred as *risk-sensitive* OCP.

The Risk-sensitive Model Predictive Control (RSMPC) has been introduced for more effective control policy in the sense that for a reduced level of expected performance willing to scarify an increased level of robustness based on level of the risk can be obtained. In RSMPC, the risk-sensitive of (4.69) can be defined as follows:

$$\underset{\pi^*}{\text{minimise}} \quad \kappa(V_N(x, \pi)), \tag{4.73}$$

where $\kappa$ defines the measure of risk. Furthermore, we are interested in a nonlinear measure of risk of the form:

$$\kappa(X) = \frac{1}{\rho_e} \log \mathbf{E}(\exp^{\rho_e X}) \tag{4.74}$$

where $\rho_e \in \mathbb{R} \setminus \{0\}$ is risk-sensitive parameter determining the controller's attitude towards uncertainty: $\rho_e < 0$ corresponds to an 'uncertainty-seeking' attitude, while $\rho_e > 0$ implies an 'uncertainty-avoiding' one (X. Yang et al., 2015). The risk-sensitive cost that was proposed by Jacobson (1973) and later by Whittle et al. (1986) is also known as a stochastic risk-sensitive OCP. Using a risk-sensitive optimisation objective, aim to find suitable control policies to manage the downside risk faced by the high-impact low-probability events, which although with a small probability can impose disastrous results.

The intuition behind the optimisation criterion (4.74) is seen by finding its Taylor series expansion around the point $\rho_e = 0$ as follows:

$$\frac{1}{\rho_e} \log \mathbf{E}(\exp^{\rho_e X}) = \mathbf{E}(X) + \frac{\rho_e}{2} \mathbf{Var}(X) + O(\rho_e^2). \tag{4.75}$$

where $\mathbf{Var}(X)$ denotes the variance of random variable $X$. In addition, $\kappa(X) \to V_N(X)$ when $\rho_e \to 0$ which corresponds to the risk neutrality, and therefore risk-sensitive control can be seen as a generalisation of risk-neutral control (Gonzalez and Moriarty, 2014). The (4.75) is related to mean-variance framework. The mean-variance developed within modern portfolio was very popular in economics. The variance, as a measure of risk, however, does not account for the asymmetry proper of financial variables, where one is mainly interested in downside risk (Gonzalez, 2015).

The importance of risk in RSMPC presents a challenge in quantifying attitudes to risk and developing appropriate risk-sensitive OCP. In general, a risk measure is a mapping that assigns a real number to a random outcome or risk position. Let $L(\Omega, \mathcal{F}, \mathcal{P})$ the set of Borel measurable function. The mapping $\kappa : L(\Omega, \mathcal{F}, \mathcal{P}) \to \mathbb{R} \cup \{-\infty, +\infty\}$ is a convex risk measure, if for every $X_1, X_2 \in L$ and $c \in \mathbb{R}$, $m \in [0,1]$ it satisfies the following properties:

- *Monotonicity*: if $X_1 \leq X_2$, then $\kappa(X_1) \leq \kappa(X_2)$.

- *Translation invariance*: $\kappa(X + c) = \kappa(X) + c$.

- *Convexity*: $\kappa(mX_1 + (1 - m)X_2) \leq m\kappa(X_1) + (1 - m)\kappa(X_2)$.

A convex risk measure is called a coherent risk measure if it also satisfies *Positive homogeneity*: if $c \geq 0$, then $\kappa(cX) = c\kappa(X)$. Note that under the assumption of positive homogeneity, convexity is equivalent to the *subadditivity* property: for every $X_1, X_2 \in L$, $\kappa(X_1 + X_2) \leq \kappa(X_1) + \kappa(X_2)$ (Gonzalez, 2015). Some of the elementary examples of risk measures are given as:

- the expectation operator defines a coherent risk measure

$$\kappa_E(X) := \mathbf{E}(X), \tag{4.76}$$

- the essential supremum of random variables,

$$\kappa_{MAX}(X) := \operatorname{ess\,sup}(X), \tag{4.77}$$

while this risk measure can be interpreted as the worst-case scenario implied by the realisations of $X$.

- Markowitz mean-variance risk measure

$$\kappa_{MS}(X) := \mathbf{E}(X) + \gamma\sqrt{\mathbf{Var}(X)}, \quad \gamma > 0. \tag{4.78}$$

while this risk measure does not satisfy the monotonicity property, and therefore it is neither convex nor coherent (Gonzalez, 2015).

### 4.4.2.2 Value at Risk

One of the most popular and widely used risk measures is Value at Risk (VaR) measure. For a confidence level $\beta = 1 - \alpha$, the VaR of $X$ is defined as the $\beta$-percentile of the distribution of $X$,

$$\mathrm{VaR}_{1-\alpha}(X) := \inf_z\{z : \mathcal{P}(X \leq z) \geq 1 - \alpha\}, \tag{4.79}$$

where typical values of $\alpha$ are in the range $[0.01, 0.1]$. The VaR provides an intuitive interpretation of the risk position $X$. However, VaR does not give any indications about the potential losses in the case that the VaR is exceeded. The VaR satisfies monotonicity, convexity, and positive homogeneity properties; however, it does not satisfy the subadditivity property in general (Gonzalez, 2015).

The Conditional Value at Risk (CVaR) is a coherent risk measure that has been proposed as a suitable alternative to overcome the weaknesses of VaR. For a confidence level $1 - \alpha$, the CVaR is related to the VaR by:

$$\mathrm{CVaR}_{1-\alpha}(X) := \frac{1}{\alpha}\int_0^\alpha \mathrm{VaR}_{1-t}(X)dt. \tag{4.80}$$

The CVaR may be interpreted as the average loss that can be incurred provided the VaR has been exceeded. The VaR measure is less conservative or risk-averse than CVaR measure, in the sense that for a given random outcome CVaR is in general larger than the VaR at the same confidence level (Gonzalez, 2015).

The Entropic Value at Risk (EVaR) has been recently introduced and studied by Ahmadi Javid (2012). The EVaR measure provides the tightest upper bound for both VaR and CVaR that can be obtained from the Chernoff inequality. The EVaR of $X \in L$ at the confidence level $1 - \alpha$ is defined by the quantity:

$$\text{EVaR}_{1-\alpha}(X) := \inf_{z>0}\{z^{-1}\log(\alpha^{-1}M_X(z))\}, \tag{4.81}$$

where $M_X$ is the moment-generating function of $X$ (Gonzalez, 2015). The EVaR is a coherent risk measure for every $\alpha \in (0,1]$. There are important connections between EVaR and some of the previous risk measures. The EVaR is a more conservative risk measure than CVaR. More specifically, it can be shown that:

$$\mathbf{E}(X) \leq \text{VaR}_{1-\alpha}(X) \leq \text{CVaR}_{1-\alpha}(X) \leq \text{EVaR}_{1-\alpha}(X) \leq \text{ess sup}(X). \tag{4.82}$$

In addition,

$$\mathbf{E}(X) = \text{VaR}_{0.5}(X) = \text{EVaR}_0(X), \quad \lim_{\alpha \to 0}\text{EVaR}_{1-\alpha}(X) = \text{ess sup}(X). \tag{4.83}$$

For more details about the EVaR see Ahmadi Javid (2012).

Another risk measure is the Entropic Risk (ER), which is one of the most important examples of a convex risk measure that is not coherent. The ER measure with risk parameter $\theta \in \mathbb{R}$ is:

$$\kappa_{ER}^{\theta}(X) = \begin{cases} \frac{1}{\theta}\log\mathbf{E}(\exp^{\theta X}), & \text{if } \theta \in \mathbb{R} \setminus \{0\} \\ \mathbf{E}(X), & \text{if } \theta = 0 \end{cases} \tag{4.84}$$

where $X \in L$. The connection between the risk-sensitive criterion in (4.74) and convex measures of risk is clear (Gonzalez, 2015).

One may optimise a risk-sensitive criterion, or equivalently the ER measure. From a practitioner point of view, however, whether minimising the convex entropic risk measure is not equivalent to minimising coherent risk measures such as CVaR and EVaR, or even the risk measure VaR. Nevertheless, it is possible to obtain the equivalence by carefully choosing the risk-sensitivity parameter $\rho_e$. For more details about the modelling and controlling risk follow e.g., Gonzalez (2015).

### 4.4.3 Proposed Stochastic Nonlinear Model Predictive Control

The majority of reported SMPC have been developed for linear systems based on stochastic programming approaches and MC sampling techniques. Moreover, most of the current methods are risk-neutral for safety-critical systems and depend on computationally expensive algorithms. The SNMPC has received relatively little attention, with only a few applications reported mainly in the area of process control (Mesbah, 2016). One of the essential goals of this study is to generalise a real-time stochastic risk-sensitive optimal control applied to the ecological ADAS for optimal energy management in BEV.

The main contribution in this area is the design of a real-time RSNMPC with the aim of performance improvement in dynamical systems that involve uncertainties. The basic idea is to use the system states information and propagate the system uncertainties along the prediction horizon to determine a plausible scenario of the system states and control input trajectories. In this method, we interpret $\omega_i$ as the prediction of expected disturbance values aimed to propagate the uncertainties. Hence, the proposed RSNMPC emphasize the early reduction of large recourse, rather than the compensation of non-optimal decisions. The risk-sensitive evaluation of the trajectories using various methods specifies the approximate optimal solution of the OCP.

In order to achieve a computationally tractable design and integrate knowledge about the uncertainties, bounded trajectories generated to quantify the uncertainties. Scenarios are based on pessimistic, neutral, or optimistic realisations of the uncertainties. The proposed optimal controller considers these scenarios in a risk-sensitive manner. A certainty equivalent NMPC based on PMP is reformulated to optimise nominal cost and the expected value of future recourse actions. Different efficient methods for the numerical solution of the risk-sensitive OCP is proposed. In addition, an economic penalty function is suggested for the deterministic NMPC and the RSNMPC to improve the system economic objectives.

#### 4.4.3.1 Stochastic Optimal Control Problem

Let's consider a general discrete-time system:

$$x_{t+1} = f(x_t, u_t, \omega_t), \tag{4.85}$$

where $t \in \mathbb{N}_+$; $x_t \in \mathbb{R}^{n_x}$ is the system states vector and $u_t \in \mathbb{U} \subset \mathbb{R}^{n_u}$ is a non-empty measurable set for the inputs. $\omega_t \in \mathbb{R}^{n_\omega}$ is a disturbances vector that is unknown at the current and future time instants. The $\omega_t$ is composed of i.i.d. random variables within the known sample space $\Omega$, the set of events ($\sigma$-algebra) $\mathcal{F}$, and the allocations

of probabilities, $\mathcal{P}$ to events (exogenous information). The $f(\cdot)$ is a nonlinear Borel-measurable vector of functions that describes the system dynamics (Mesbah, 2016).

Let $N \in \mathbb{N}$ be the both state and control prediction horizon. Define an *N-stage feedback control policy* as:

$$\boldsymbol{\pi} := \{\pi_0(\cdot), \pi_1(\cdot), \ldots, \pi_{N-1}(\cdot)\}, \tag{4.86}$$

where the Borel-measurable function $\pi_i(\cdot) : \mathbb{R}^{(i+1)n_x} \to \mathbb{U}$, for all $i = 0, \ldots, N-1$ is a general state feedback control law (Mesbah, 2016). The control input $u_i$ is selected as the feedback control law $u_i = \pi_i(\cdot)$ at the $i^{th}$ stage of the control policy. As mentioned before, in receding horizon optimal control, the cost function of the OCP is commonly defined as:

$$V_N(x_t, \boldsymbol{\pi}) := \mathbf{E}_{x_t}[\sum_{i=0}^{N-1} J_c(\hat{x}_i, u_i) + J_f(\hat{x}_N)], \tag{4.87}$$

where $J_c : \mathbb{R}^{n_x} \times \mathbb{U} \to \mathbb{R}_+$ and $J_f : \mathbb{R}^{n_x} \to \mathbb{R}_+$ are the *cost-per-stage function* and the *final cost function*, respectively. The $\hat{x}_i$ denotes the predicted states at time $i$ given the initial states $\hat{x}_0 = x_t$, control law $\{\pi_i(\cdot)\}_{i=0}^{i-1}$, and disturbance realizations $\{\omega_i\}_{i=0}^{i-1}$ (Mesbah, 2016).

A general form of chance-constraints is defined by:

$$\mathbf{Pr}_{x_t}[h_j(\hat{x}_i) \leq 0] \geq \beta_j, \quad \text{for all } j \in \mathbb{Z}_{[1,n_h]}, \, i \in \mathbb{Z}_{[1,N]}, \tag{4.88}$$

where $h_j : \mathbb{R}^{n_x} \to \mathbb{R}$ is a Borel-measurable function, $n_h$ is the total number of inequality constraints, and $\beta_j \in (0,1)$ denotes the lower bound for the probability $h_j(\hat{x}_i) \leq 0$ that needs to be satisfied. Different probability levels $\beta_j$ are assigned for different inequality constraints. The conditional probability $\mathbf{Pr}_{x_t}$ indicates the probability of $h_j(\hat{x}_i) \leq 0$ holds based on initial states $\hat{x}_0 = x_t$; please note that the predicted states $\hat{x}_i$ depend on disturbances $\{\omega_i\}_{i=0}^{i-1}$ (Mesbah, 2016).

Using the cost function (4.87) and the individual chance-constraint (4.88), the stochastic OCP for (4.85) is formulated as follows:

$$V_N^*(x_t) := \underset{\pi^*}{\text{minimise}} \quad V_N(x, \pi) \tag{4.89a}$$

subject to:

$$\hat{x}_{i+1} = f(\hat{x}_i, \pi_i, \omega_i), \qquad \text{for all } i \in \mathbb{Z}_{[0,N-1]}, \tag{4.89b}$$

$$\pi_i(\cdot) \in \mathbb{U}, \qquad \text{for all } i \in \mathbb{Z}_{[0,N-1]}, \tag{4.89c}$$

$$\mathbf{Pr}_{x_t}[h_j(\hat{x}_i) \leq 0] \geq \beta_j, \qquad \text{for all } j \in \mathbb{Z}_{[1,n_h]}, i \in \mathbb{Z}_{[1,N]}, \tag{4.89d}$$

$$\omega_i \sim P_\omega, \qquad \text{for all } i \in \mathbb{Z}_{[1,N-1]}, \tag{4.89e}$$

$$\hat{x}_0 = x_t, \tag{4.89f}$$

where $V_N^*(x_t)$ denotes the optimal value function under the optimal control policy $\boldsymbol{\pi}^*$. The OCP in receding horizon principle involves applying the first element of the control action sequence $u_t = \boldsymbol{\pi}_0^*(\cdot)$ repeatedly to the system at each sampling time.

Generally there is no exact solution to the stochastic OCP (4.89). Several approximations have been developed to obtain a feasible solution rather than an exact solution (see e.g., Kantas et al. (2009) and Ohsumi et al. (2011)). The main drawback of the SMPC is the risk-neutral expectation assessment of future random outcomes. This may not be a proper control policy for safety-critical systems where one desires to regulate the control actions robust enough to uncertainties (X. Yang et al., 2015). Risk-sensitive control law of finite time for linear systems have been formulated (see e.g., Ito et al. (2015) and X. Yang et al. (2015)). On the other hand, most of the SNMPCs depend on computationally expensive algorithms and few approaches have been developed about risk-averse SNMPC (see e.g., Ma et al. (2012)), as well as real-time capable SNMPC (see e.g., Ohsumi et al. (2011)).

In this study, the cost for the RSNMPC is defined as follows:

$$V_N(x, \pi) := \sum_{i=0}^{N-1} J_c(x^\pi(i; x, \mathbf{E}(\omega)), \mu_i(x^\pi(i; x, \mathbf{E}(\omega))))] + J_f(x^\pi(N; x, \mathbf{E}(\omega))), \quad (4.90)$$

where $\mathbf{E}(\omega) \in \mathbb{R}^{n_w}$ is an optimistic scenario to forward propagating the random variables along the prediction horizon, which is known as rolling disturbance estimation. The OCP with expected values that represent only one scenario may be regarded as a poor representation of risk-aversion. However, the uncertain dynamic model captures one essential feature of the problem in the evolution of the scenario, which even simple models can lead to significant savings from non-optimal decisions (Birge et al., 2011). In other words, one may expect that the value of the objective of the stochastic model will closely match the realised total optimistic expected values, and regulate system states in a risk-averse manner. Thus, the system function (4.85) can be rewritten as deterministic surrogate form as:

$$\bar{x}_{t+1} = \bar{f}(\bar{x}_t, u_t), \quad (4.91)$$

where $\hat{\bar{x}}_t \in \mathbb{R}^{n_x + n_\omega}$ denotes the predicted nominal states including auxiliary states $\hat{\omega}_i$. The i.i.d random variables assumption of the $\omega_i$ is no longer required. Therefore, the stochastic OCP cost function defined by (4.87) is reduced to a certainty equivalent form. The next subsections present variously proposed extensions for the SNMPC formulation.

### 4.4.3.2 Current-value Hamiltonian

The stochastic OCP cost function defined by (4.87) is reduced to a certainty equivalent form (4.90). However, it is reasonable to assume that the predicted cost for long-term or infinite-time prediction horizon is less costly in comparison to near-term future prediction horizon. Thus, the deterministic certainty equivalent cost function can be accomplished through the parameter $\rho$ known as *discount factor*, which reduces the future cost to the present cost value. In this study a certainty equivalent cost function with a continuous discount factor on a long $T$ or infinite horizon cost for the OCP is investigated as follows:

$$V_T(x(t), \boldsymbol{\pi}) := \int_t^\infty \exp^{-\rho t} J_c(\bar{x}(t), u(t))dt, \tag{4.92}$$

where $\rho \in [0, 1)$ is a discount factor and the cost-per-stage is $J_c : \mathbb{R}^{n_x + n_\omega} \times \mathbb{U} \to \mathbb{R}_+$. This also is referred as *current-value Hamiltonian*, which mainly arises in economic growth theory. More importantly the prefix "current-value" is used to distinguish it from the so-called *present-value* Hamiltonian. It is common to use indirect methods of optimal control to derive the first-order necessary condition of optimality and a TP-BVP has to be solved. It is noteworthy that $J_f(\hat{x}(t_f)) = 0$, which is known as standard *transversality* conditions. The first-order necessary optimal condition is the same as (4.53) except the update condition for the costate multipliers is modified as follows:

$$\lambda_\tau^* = -H_x^{\mathrm{T}}(x^*, \lambda^*, u^*, \mu^*) + \rho\lambda^{\mathrm{T}}. \tag{4.93}$$

The costate variable, $\lambda(t)$, which is also known as a *shadow price* of the state variable in the financial industry, becomes a current price in this case. The infinite horizon current-value Hamiltonian for discrete time cost of the OCP is stated as:

$$V_N(x(t), \boldsymbol{\pi}) := \sum_{i=0}^\infty (1 - \varrho)^i J_c(\bar{x}_i, u_i), \tag{4.94}$$

where $\varrho \in [0, 1)$ is a discount factor. In practical application, the discrete time finite horizon current-value Hamiltonian is stated as:

$$V_N(x(t), \boldsymbol{\pi}) := \sum_{i=0}^{N-1} (1 - \varrho)^i J_c(\bar{x}_i, u_i) + (1 - \varrho)^N J_f(\bar{x}_N), \tag{4.95}$$

where the discount factor $\varrho$ imposed on the final cost function. It is noteworthy that one may also have OCPs with no discount factor $\rho = 0$, $\varrho = 0$. For more information see e.g., Würth et al. (2009), Dahl et al. (2016), and Naz (2018).

### 4.4.3.3 Expected Quadratic Cost

One of the interesting methods to include risk during a decision-making process was proposed by Whittle et al. (1986). In this method, the expected quadratic-cost replaced by a risk-sensitive benchmark of exponential-quadratic form (X. Yang et al., 2015). A typical quadratic cost over the state is as follows:

$$J_Q = \|\hat{x}_i - x_{i_{ref}}\|_Q^2, \tag{4.96}$$

where $Q$ is a weighting matrix. This can be minimised based on the extremal principle prescribed by the Risk-Sensitive Certainty Equivalence Principle (RSCEP) with the modified benchmark as follows (Whittle et al., 1986):

$$J_\mu(\rho_e) = -\frac{2}{\rho_e} \log(\mathbf{E}_\mu[\exp(-\frac{1}{2}\rho_e J_Q)]), \tag{4.97}$$

where $\rho_e$ is a real scalar risk-sensitivity parameter. This parameter determines the control behaviour towards uncertainty. Therefore, the uncertain expected posterior values of uncertainties treated with the risk-sensitive cost (4.97) can be approximated as:

$$J_\mu(\rho_e) \approx \|\hat{x}_i - x_{i_{ref}}\|_{(Q^{-1}+\rho_e\Sigma_{x_i})^{-1}}^2 + \frac{1}{\rho_e} \log \det(I + Q\rho_e\Sigma_{x_i}), \tag{4.98}$$

where $\Sigma_{x_i}$ is the covariance matrix of a random variable $x_i$ and $\det(I + Q\rho_e\Sigma_{x_i})$ is the volume ellipsoid to the size of the uncertainty (X. Yang et al., 2015).

One of the effective methods to solve the resulting OCP in the receding horizon manner is based on PMP. Appeal to the extremal principle prescribed by the RSCEP yields a symmetric equation system, indicating that the extended Hamiltonian formulation is naturally generalised to the risk-sensitive case. The conjugate variable or auxiliary variables of the Hamiltonian formulation has an interpretation in terms of the predicted course of process and observation noise. The RSCEP, in fact, provides a stochastic minimum principle, which all variables have a clear interpretation and the desired measurable properties (see Whittle et al. (1986)). For more details about expected quadratic cost applied to the proposed Eco-ACC system follow Seyed Amin Sajadi-Alamdari et al. (2017b).

### 4.4.3.4 Distributionally Robust Chance-constraint

A wide class of probability distributions on the data, the chance-constraints can be converted explicitly into convex second-order cone constraints. Thus, the chance constrained OCP can be solved exactly with great efficiency (Calafiore et al., 2006). Consider a single

generic chance-constraint of the form:

$$\mathbf{Pr}[\ell^T \nu \leq 0] \geq 1 - \epsilon, \quad \epsilon \in (0, 1), \tag{4.99}$$

where $\ell \in \mathbb{R}^{n_l}$ denotes some random quantities and $\nu \in \mathbb{R}^{n_l}$ denotes some variables (Mesbah et al., 2014).

For any $\epsilon \in (0, 1)$, a distributionally robust chance-constraint for a wide class of probability distribution is certainty equivalent to the convex second-order cone constraint as follows:

$$\kappa_\beta \mathbf{Var}[\ell^T \nu] + \mathbf{E}[\ell^T \nu] \leq 0, \quad \kappa_\beta := \sqrt{\frac{1 - \epsilon}{\epsilon}}. \tag{4.100}$$

where $\mathbf{E}[\ell^T \nu] = \bar{\ell}\nu$ and $\mathbf{Var}[\ell^T \nu] = \nu\Gamma\nu$. Denote with $\mathcal{L}$ the family of all distributions with known mean $\bar{\ell}$ and covariance $\Gamma$. For more details and related proofs, see Calafiore et al. (2006) and Mesbah et al. (2014).

The chance-constraint (4.88) on the states can be converted into deterministic equivalent constraint as follows:

$$\kappa_{1-\beta} \mathbf{Var}[h(\hat{x}_i)] + \mathbf{E}[h(\hat{x}_i)] \leq 0, \tag{4.101}$$

where $\mathbf{E}[\cdot]$ and $\mathbf{Var}[\cdot]$ are closely related moment concept in physics. The $\mathbf{E}[\cdot]$ is the *first-order moment* of the random variable on a Probability Density Function (PDF) $f_\omega$, which can be computed by its expected value. The $\mathrm{Var}[\cdot]$ is variance, so-called *second-order moment* of the random variable, which can be approximated by using second-order Taylor expansions:

$$\mathbf{Var}[h(\hat{x}_i)] \approx (\dot{h}(\mathbf{E}[\hat{x}_i]))^2 \mathbf{Var}[\hat{x}_i], \tag{4.102}$$

where $h(\cdot)$ is twice differentiable and the mean ($\mathbf{E}[\hat{x}_i]$) as well as the variance ($\mathbf{Var}[\hat{x}_i]$) of $\hat{x}_i$ are finite. For more details about distributionally robust chance-constraint applied to the proposed Eco-ACC system follow (Seyed Amin Sajadi-Alamdari et al., 2017a).

### 4.4.3.5 Closed-loop Entropic Value at Risk

Current chance-constrained SMPC methods based on analytic reformulations or on sampling approaches tend to be partly conservative because they fail to exploit the predefined violation level in closed-loop (Oldewurtel et al., 2013). Using Boole's inequality to upper bound the probability of constraint violation introduces conservatism into the solution (Vitus et al., 2012). For many practical applications, this conservatism can lead to a loss in performance.

The open-loop EVaR evaluation of the chance-constraint (4.81) with the fixed risk allocation is proposed for the RSNMPC; however, the open-loop EVaR can also lead to a conservative behaviour. Inspired by the closed-loop chance-constraint based SMPC proposed by Ono (2012), Oldewurtel et al. (2013), X. Zhang et al. (2014), we introduce a RSNMPC based on closed-loop EVaR evaluation. The motivation for the risk-sensitive optimal controller is to find a tradeoff between the expected profit (desired pre-set velocity tracking) and the risk. One may minimise the stochastic OCP based on approximate coherent risk measure EVaR or minimise the OCP with the risk-sensitive cost function. Although the solution of both approaches is not necessarily equivalent, it is possible to obtain similar results by properly tuning the risk-sensitivity parameter (Gonzalez and Moriarty, 2014). In the case of the risk-averse control policy, the proposed closed-loop confidence level $\{\beta_i(t)\}_{m-1}^0$ is estimated based on a *Two-pass* algorithm to compute the standard deviation using the *Exponential Moving Average* over the past $M$-measurement vector. In this method, the samples moving average is calculated by:

$$\bar{p} = \frac{\sum_{j=0}^{m-1} x_j}{M}. \tag{4.103}$$

Afterwards, the unbiased estimation of the variance can be computed based on the Bessel's correction given by:

$$\text{Var}(P) := \sigma^2 = \frac{\sum_{i=0}^{m-1}(p_i - \bar{p})^2}{M-1}, \tag{4.104}$$

where $\sigma$ is the corrected sample standard deviation ($\sigma = \sqrt{\text{Var}(P)}$). This algorithm is numerically stable if $M$ is small (for more details see Einarsson (2005)). A larger standard deviation estimation results in conservative but robust behaviour while a small standard deviation estimation could lead to high performance.

The properties of coherence in the risk measurement have intuitive interpretations in the financial industry, which can be extended to energy management systems (Gonzalez and Moriarty, 2014). In the case of the Eco-ACC system, for instance, the relative distance can be interpreted as a portfolio of energy consumption and travel time. The higher risk of rear-ends collision cause closer car following situations with shorter travel time (higher probability of constraint violation). The lower risk, on the other hand, leads to a longer travel time (lower expected reward) with a lower risk of rear-end collision or constraint violation. The proposed method to estimate the standard deviation utilises the advantages of feedback to reduce the conservative behaviours of the risk-averse chance-constraints with the predefined fix confidence level and improves the tradeoff between the performance and robustness.

### 4.4.3.6 Deadzone Penalty Functions

In many practical NMPC applications considering the economic objectives are desirable to reach a region of reference set-points with relatively low-cost value rather than costly but accurate and agile set-point tracking. This could be accomplished using a nonnegative and symmetric deadzone-quadratic penalty function such as:

$$\phi_q(x) := \begin{cases} 0 & : |x| \leq z, \\ x^2 - z^2 & : |x| > z, \end{cases} \tag{4.105}$$

where $z$ is the edge of *free* zone that no penalty is assessed if $|x| \leq z$. The $\phi_q(\cdot)$ function agrees with least-square for any residual outside of the zone width. In other words, the residuals smaller than the zone width are ignored that leads to a low-cost function value.

In a case of energy-efficient robust regulations, deadzone-linear penalty function agrees with absolute value for the residual outside of the zone width as follows:

$$\phi_l(x) := \begin{cases} 0 & : |x| \leq z, \\ |x| - z & : |x| > z. \end{cases} \tag{4.106}$$

Unfortunately, these deadzone penalty functions are not convex that leads to a challenging OCPs. However, a smooth approximation of deadzone penalty function addresses the challenge.

In this study, a deadzone penalty function based on *softplus* rectifier is proposed. The softplus is an approximation to the activation function so-called Rectified Linear Unit (ReLU), which is mostly utilised in the deep neural networks (LeCun et al., 2015). The proposed deadzone-linear penalty function is a combination of the two softplus rectifier as follows:

$$\psi_l(x) := \ln(1 + \exp(x - z)) + \ln(1 + \exp(-x - z)). \tag{4.107}$$

The $\psi_l(x)$ have advantages such as being a convex function with efficient computation and gradient propagation (Dugas et al., 2000). The gradient of the deadzone-linear penalty function is a combination of two sigmoid functions as follows:

$$\frac{d\psi_l(x)}{dx} = \frac{\exp(x - z)}{1 + \exp(x - z)} - \frac{\exp(-x - z)}{1 + \exp(-x - z)}. \tag{4.108}$$

Similar to $\psi_l(x)$, the deadzone-quadratic penalty function can be formulated as follows:

$$\psi_q(x) := (\ln(1 + \exp(x - z)) + \ln(1 + \exp(-x - z)))^2. \tag{4.109}$$

The gradient of the deadzone-linear penalty function is a linear continuous function with a deadzone area, $[-z, z]$, as follows:

$$\frac{d\psi_q(x)}{dx} = 2\psi_l(x)\frac{d\psi_l(x)}{dx}. \tag{4.110}$$

For sake of simplicity, Figure 4.4 shows the proposed $\psi_q(x)$ and $\psi_l(x)$ penalty functions for a scalar residual with $z = 5$ in comparison with $\phi_q(x)$, $\phi_l(x)$, $\ell_2$, and $\ell_1$-norms. Note that when the state residual is within the zone, the gradient is non-zero and the
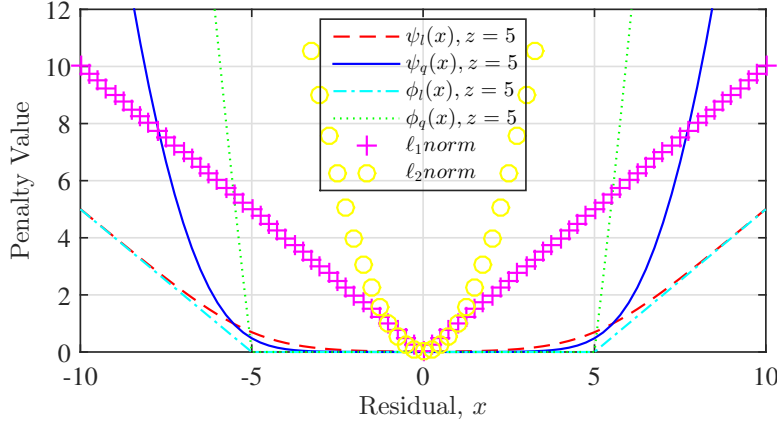


FIGURE 4.4: Deadzone Penalty Functions with Relative Comparisons

optimality conditions are satisfied as $\ell_1$ and $\ell_2$-norms do. In other words, the states will converge to final reference set-point values but slower than conventional norms, what leads to the energy-efficient behaviour. For more details about deadzone penalty functions applied to the proposed Eco-ACC system follow Seyed Amin Sajadi-Alamdari et al., 2018.

#### 4.4.3.7 Soft Complementarity Functions

Complementarity functions provided in (4.34) is the hard constraint implementation. The relaxed KKT conditions of an OCP (4.32) with inequality constraints are transformed equivalently into a special nonlinear system of equations $\hat{\Phi}_{SFB}(\mu_j, h_j(\hat{x}, u)) = \epsilon$ where $\hat{\Phi}_{SFB}$ is applied element-wise. A soft constraint implementation based on FB function is proposed as follows:

$$\hat{\Phi}_{SFB}(\mu_j, h_j(\hat{x}, u)) = \sqrt{(1-\epsilon)\mu_j^2 + h_j(\hat{x}, u)^2 + 2\epsilon} - ((1+\epsilon)\mu_j - h_j(\hat{x}, u)). \tag{4.111}$$

The introduction of the $\epsilon$ as a smoothing parameter transforms the nonsmooth problems into a smooth problem. The orthogonality of the vectors $\mu_j$ and $h_j(\hat{x}, u)$ is relaxed by $(1 \pm \epsilon)$ to prevent the Lagrange multipliers from approaching to infinity in dual space due to constraint violation. Therefore, this opens the way to use the hard and soft

constraints in the OCP with the complementary conditions to address the short coming of the PMP method.

## 4.5 Risk-sensitive Optimal Energy Management for Electric Vehicles

This section presents the RSNMPC applied on the proposed semi-autonomous Eco-ACC system for the Smart-ED. Following, the presented system models in Chapter 2 and Chapter 3 are reviewed.

The position ($s_h$) and velocity ($v_h$) along the longitudinal motion of the BEV can be expressed by Newton's second law of motion, which is assumed to be a point mass at the centre of gravity as follows:

$$\dot{s}_h = v_h, \tag{4.112}$$

$$\dot{v}_h = (F_{trac} - F_{res})/M, \tag{4.113}$$

where $M$, $F_{trac}(t)$, and $F_{res}(t)$ are equivalent mass of the vehicle, traction force, and total motion resistive forces, respectively. Energy consumption of the BEV is described as follows:

$$\dot{e}_h = f_a \ (p_{trac}/M) + f_{cruise}, \tag{4.114}$$

where $p_{trac}$ denotes the traction power.

The state vector for the proposed Eco-ACC concept is defined as $x_t = [s_h, v_h, e_h]^T \in \mathbb{R}^3$; the control input is the traction input with the modelled delay of the power plant applied on the host vehicle as $u_t = u \in \mathbb{U} \subset \mathbb{R}$. The volatility of the preceding vehicle velocity and its position can be unbounded and extremely wide, therefore regulating relative safe distance in an energy efficient method is of fundamental importance to the semi-autonomous Eco-ACC system. The measurable disturbance (e.g., RADAR based system) is defined as position ($s_p$) and velocity ($v_p$) of the preceding vehicles. The introduced dynamic model to propagate the uncertain preceding vehicle position and its velocity at time $t$ can be determined as follows:

$$\dot{s}_p := v_p, \tag{4.115}$$

$$\dot{v}_p := X_{85^{th}}(1 - (\frac{v_p}{f_{85^{th}}})^4 - \frac{\sin(f_{slp}(\theta(s_p)))}{\sin(\frac{\pi}{4})}), \tag{4.116}$$

$$f_{85^{th}} := \min\{\omega_{85^{th}} v_{85^{th}}(f_{crv}(\delta(s_p))), f_{lmt}(s_p)\}, \tag{4.117}$$

$$v_{85^{th}}(\delta(s_p)) := m_1 \exp^{(-m_2\delta(s_p))} + m_3 \exp^{(-m_4\delta(s_p))}, \tag{4.118}$$

where $X_{85^{th}}$ is the acceleration of the preceding vehicle at $85^{th}$ percentile assumed to lie in a normal distribution i.i.d. $X \sim \mathcal{N}(\mu_p, \sigma_p)$ with the mean $\mu_p$ and variance $\sigma_p^2$. Note that we refer the risk as the uncertainty related to the future values of relative distance $\bar{d} := \bar{s}_p - \bar{s}_h$ and all states are measurable in which the measurement noise is negligible. The disturbances as auxiliary states are concatenated with the system state vector to form the nominal state vector. From (4.112), (4.113), (4.114), (4.115), and (4.116), the extended state vector is: $\bar{x}_t = [\dot{s}_h, \dot{v}_h, \dot{e}_h, \dot{\bar{s}}_p, \dot{\bar{v}}_p]^T \in \mathbb{R}^5$.

The cost-per-stage function for the Extended Eco-ACC system is defined as:

$$V_N(x_t, \boldsymbol{\pi}) := \sum_{i=0}^{N-1} \parallel \hat{x}_i - x_{ref} \parallel_Q^2 + \parallel u_i - u_{ref} \parallel_R^2 + C\hat{x}_i^T, \qquad (4.119)$$

with corresponding weights $(Q, R, C)$. The control input is limited by:

$$u_{min}(v) \leq u \leq u_{max}(v) \qquad (4.120)$$

where $u_{min}(v)$ and $u_{max}(v)$ can be identified based on the traction-velocity map of the BEV. The limit $u_{max}(v)$ is identified as:

$$u_{max}(v) = c_1 - c_2 tanh(c_3(v - c_4)), \qquad (4.121)$$

where the constants are identified as $c_1 = 1.523$, $c_2 = 1.491$, $c_3 = 0.08751$, and $c_4 = 15.6$ with 99.74% coefficient of determination. The maximum hybrid brake system control input is chosen to be constant, $u_{min}(v) = -5 + c_5 v$ $(N/Kg)$ $(c_5 = 0)$, which is limited to a stable slip ratio region to avoid the wheels from locking up.

The state inequality constraints are lateral acceleration constraint as comfort level, speed limit constraint respecting the traffic regulation, relative distance constraint as safety constraint. In addition, a *funnel* constraint is introduced for the velocity of the host BEV as well as the energy consumption of the BEV that should be limited to a certain level. The lateral acceleration of the host vehicle should be lower than the comfort level ($\Psi_{ref}$) almost surely ($\beta_1 = 1$) as follows:

$$\mathbf{Pr}_{\Psi_t}[g_1(\hat{s}_{h_i}, \hat{v}_{h_i}) := \hat{v}_{h_i}^2 / f_{crv}(\delta(\hat{s}_{h_i})) \leq \Psi_{ref}] \geq \beta_1. \qquad (4.122)$$

The velocity of the host vehicle almost surely ($\beta_2 = 1$) should also be lower than the speed limit as:

$$\mathbf{Pr}_{s_t}[g_2(\hat{s}_{h_i}, \hat{v}_{h_i}) := \hat{v}_{h_i} \leq f_{lmt}(\hat{s}_{h_i})] \geq \beta_2. \qquad (4.123)$$

The spacing policy to define the safe strategy in following the preceding vehicle is based on *Time-Headway* (for more detail see e.g., Eskandarian (2012)). The relative distance

should be larger than the reference space ($d_{ref} := d_0 + v_h t_{hw}$) with closed-loop $\beta_3$ confident level as follows:

$$\mathbf{Pr}_{d_t}[g_3(\hat{d}_i) := d_{ref} \leq \hat{d}_i] \geq \beta_3. \tag{4.124}$$

Furthermore, the velocity should be within the standstill and the reference set-point almost surely ($\beta_4 = 1$) given by:

$$\mathbf{Pr}_{v_{h_t}}[g_4(\hat{v}_{h_i}) := 0 \leq \hat{v}_{h_i} \leq (v_{h_{ref}} + v_{h_{rlx}})] \geq \beta_4, \tag{4.125}$$

where $v_{h_{ref}}$ is the reference set-point. The $v_{h_{rlx}}$ is the relaxed amount of velocity for the host vehicle to overspeed whenever it is required such as cruising the downhill situations to take advantage of the gravity. The energy consumption of the BEV should be less than the permitted maximum amount almost surely ($\beta_5 = 1$) as follows:

$$\mathbf{Pr}_{e_{h_t}}[g_5(\hat{e}_{h_i}) := \hat{e}_{h_i} \leq (e_{h_{ref}} + e_{h_{rlx}})] \geq \beta_5, \tag{4.126}$$

where $e_{h_{ref}}$ and $e_{h_{rlx}}$ are the reference energy consumption and its relaxed value, respectively. In conclusions, the stochastic OCP for the proposed Eco-ACC system is rewritten as follows:

$$V_N^*(x_t) := \underset{\pi^*}{\text{minimise}} \quad V_N(x_t, \boldsymbol{\pi}) \tag{4.127a}$$

subject to:

$$\hat{x}_{i+1} = f(\hat{x}_i, \pi_i, \omega_i), \qquad \text{for all } i \in \mathbb{Z}_{[0,N-1]}, \tag{4.127b}$$

$$\pi_i(\cdot) \in \mathbb{U}, \qquad \text{for all } i \in \mathbb{Z}_{[0,N-1]}, \tag{4.127c}$$

$$\mathbf{Pr}_{x_t}[h_j(\hat{x}_i) \leq 0] \geq \beta_j, \qquad \text{for all } j \in \mathbb{Z}_{[1,n_h]}, i \in \mathbb{Z}_{[1,N]}, \tag{4.127d}$$

$$\omega_i \sim P_\omega, \qquad \text{for all } i \in \mathbb{Z}_{[1,N-1]}, \tag{4.127e}$$

$$\hat{x}_0 = x_t, \tag{4.127f}$$

where $n_h = 6$. It is noteworthy that the system function rewritten as the deterministic surrogate form by replacing the $\omega$ with its related expected values for the position and velocity of the preceding vehicle along the prediction horizon. Thus, the i.i.d random variables assumption of the $\omega_i$ is no longer required and the stochastic OCP cost function reduces to its certainty equivalent form. The obtained certainty equivalent policy is a quite computationally efficient strategy, while accounts the effects of system uncertainty or risk association with the planning of future control actions. The numerical method to solve the certainty equivalent OCP is based on the PMP utilising the real-time C/GMRES algorithm.

## 4.6 Conclusions

In this chapter, the works of literature are reviewed to identify the state-of-the-art and knowledge gap on the MPCs and its applications for automotive industry. The historical development of the MPCs with various methodologies during the last several decades are surveyed. An overview of OCPs and different solution methods are discussed. Predictive controller designs with a survey of the stability analysis and real-time algorithms reviewed. The C/GMRES based on the PMP was found a real-time numerical method for the solution of the NMPCs. In addition, robust and stochastic OCP formulations reviewed to demonstrate the SNMPC provides the proper control framework for the systems with uncertainties including the proposed semi-autonomous Eco-ACC system. A novel real-time risk-sensitive SNMPC framework developed with various extensions in the OCP formulations. The current-value Hamiltonian and the expected quadratic cost proposed to include the risk during the decision-making process aimed to enhance the PMP performance of the stochastic systems. The distributionally robust chance-constraint adapted to convert the chance-constraints into convex second-order cone constraints. In addition, the open-loop and closed-loop EVaR evaluation of the chance-constraint proposed to account the risk in the OCP formulation with the enhancement in tradeoff challenge between the performance and robustness of the system. The proposed RSNMPC addressed the mentioned challenges for the SNMPCs as the main contribution of this chapter. Furthermore, the convex and continuous deadzone penalty function and soft complementary based on the FB function proposed for the energy efficient NMPC applications with an effective constraint softening method. Based on these findings, the following chapter will evaluate the proposed RSNMPC applied on the semi-autonomous Eco-ACC system based on numerical simulation results.

# Chapter 5

# Simulation Evaluation

This chapter presents the simulation evaluation of the proposed Eco-ACC system with the introduced RSNMPC in the previous chapters. The proposed SEDAS concept is simulated in MATLAB/Simulink environment and evaluated from various points of view. First, the robustness of the BEV dynamics, its energy consumption, and road geometry against the parameters mismatch are analysed. Second, the performance of the various type of the RSNMPC is simulated and examined with different tuning parameters such as the influence of the prediction horizon, confidence level of the chance-constraint, and discount factor in the infinite horizon RSNMPC. Then, the overall performance of the SEDAS concept in terms of the safety and energy efficiency in various predictive control configurations and driving situations are assessed. Finally, the performance of the RSNMPC is compared with state-of-the-art methods that were presented in works of literature.

This chapter is structured as follows. Section 5.1 evaluates the robustness and performance of the proposed RSNMPC based on the system model mismatches. Section 5.2 investigates the capability of the RSNMPC in the set-point (reference) tracking and constraints fulfilment with different design parameters. Section 5.3 presents the overall performance of the SEDAS concept in terms of the safety and energy efficiency for the BEV. Section 5.4 concludes the findings of this chapter.

## 5.1 Robustness Against Model Mismatch

The BEV model is based on accurate knowledge of the parameters. However, only a few of these parameters are known in practice. For example, in Equation (2.4), the air density, $\rho_a$, changes with variation in altitude, temperature, or humidity. The aerodynamic drag coefficient, $C_D$, vary with the air density or relative distance to a preceding

vehicle in a car-following case. In Equation (2.7), the rolling resistance coefficient, $\mu_{rr}$, is a function of tire material, tire structure, tire temperature, tire inflation pressure, tread geometry, road roughness, road material, and presence or absence of liquids on the road (Ehsani et al., 2009). The wheel radius varies based on the air pressure and the rolling resistance between the tire and road surface. In addition, many parameters of the powertrain components and their relations are unknown. In Equation (2.1), the equivalent mass roughly has higher magnitude effects than the other parameters.

In addition, the battery pack performance and introduced energy consumption model vary with many factors such as internal chemical reactions, drain current, battery age, and temperature. However, due to the approximate linear variation of battery voltage within the 20% to 80% SOC, the introduced model might be reliable for mentioned range of SOC that can be validated with the measurement data. Note that the age of the battery and temperature effect is neglected in the model, which could be considered in an updated version of the consumption model later on.

The robustness and performance of the proposed RSNMPC are evaluated based on the system model mismatches. In this setup parameters of the Smart-ED and its energy consumption model is modified by $\pm10\%$. The prediction horizon of the RSNMPC is chosen as $T = 10\,s$ to cover the upcoming road variations. This prediction horizon is discretised into $N = 20$ steps. The reference velocity is chosen as ($v_{ref} = 20\,m/s$).

### 5.1.1 BEV Dynamic Model Mismatch

Figure 5.1. shows the closed-loop step response of the Smart-ED with the proposed RSNMPC in a CC scenario while taking the energy consumption model into account during the velocity profile planning. The nominal response of the Smart-ED and $\pm10\%$ error of the equivalent mass is analysed. The deviation of the velocity response due to the error is shown in Figure 5.1a. A $+10\%$ indicates the equivalent mass is 110% times of the actual nominal value and $-10\%$ indicates 90% of its actual value. Similar results is shown in Figure 5.1b and Figure 5.1c regarding the air density ($\rho_a$) and the aerodynamic drag coefficient ($C_D$). The proposed RSNMPC is found to be robust against the Smart-ED model parameters error. The proposed system is capable to track the desired reference without significant deviation subject to a reasonable sensing error.

### 5.1.2 BEV Energy Consumption Model Mismatch

Figure 5.2. shows the closed-loop step response of the Smart-ED with the proposed RSNMPC in a CC scenario accounting the energy consumption model of the BEV. The
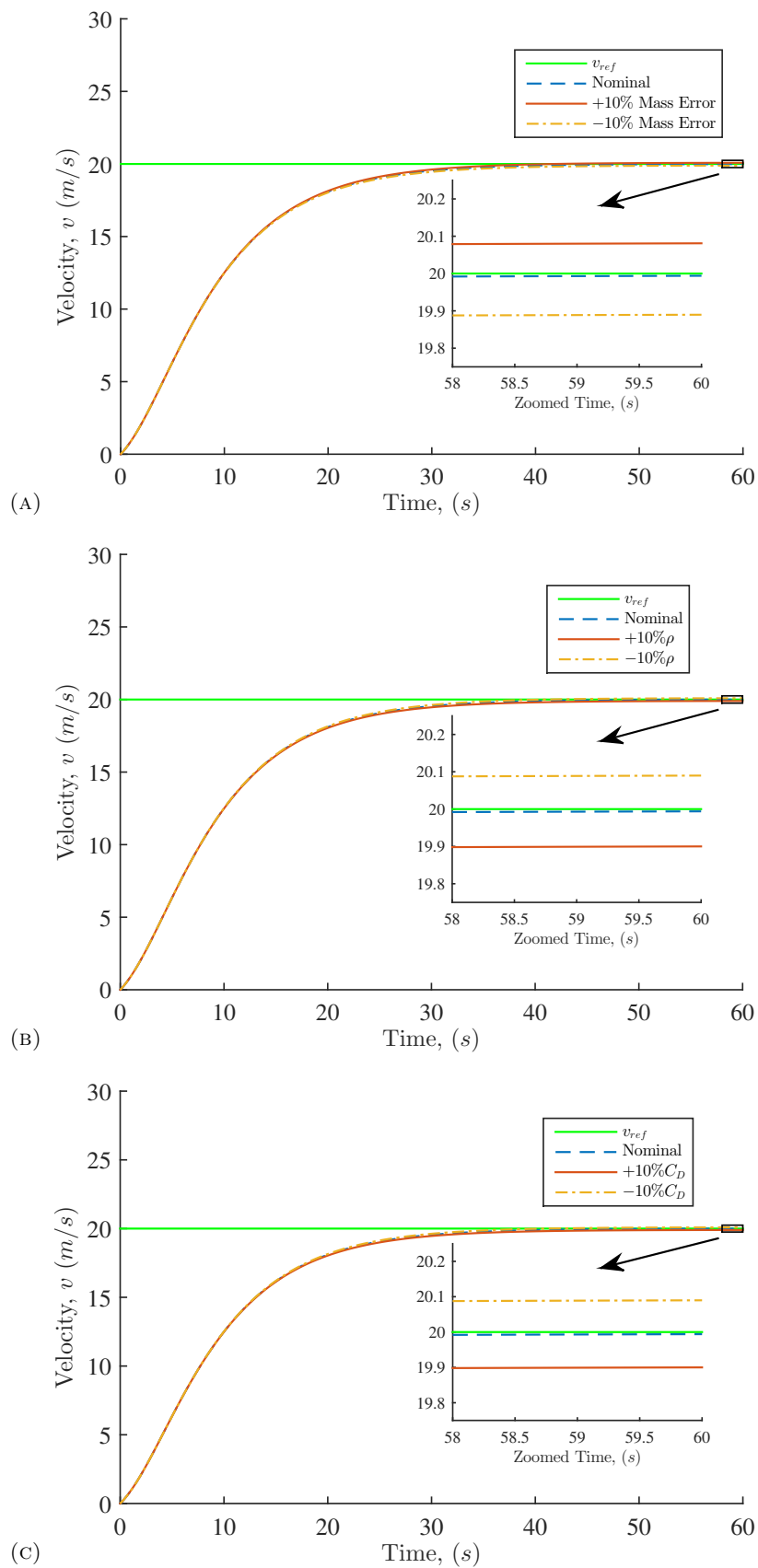
FIGURE 5.1: Performance of the closed-loop step response of the RSNMPC (A) equivalent mass error ($m_{eq}$), (B) air density ($\rho_a$), (C) aerodynamic drag coefficient ($C_D$).
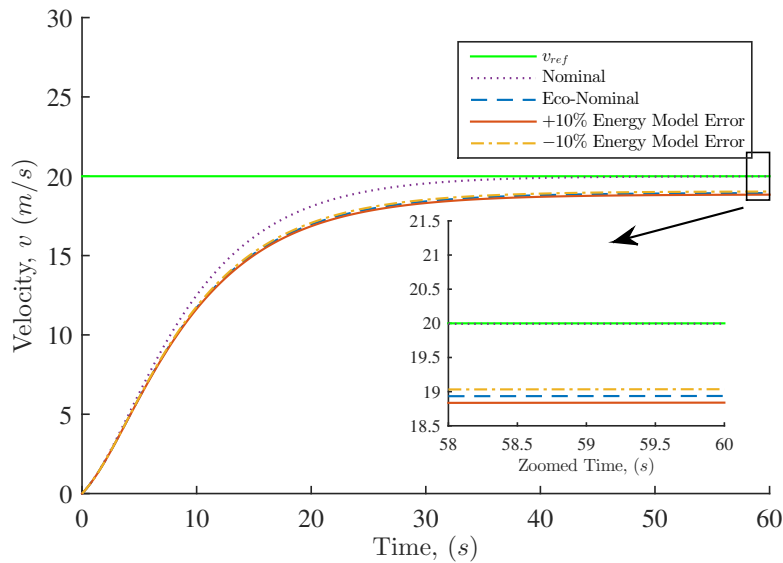
FIGURE 5.2: Performance of the closed-loop step response of the RSNMPC with energy consumption model error.

*Nominal* reference tracking indicates the RSNMPC without taking the energy consumption model in velocity profile planning. The *Eco-Nominal* reference tracking indicates the RSNMPC with the nominal energy consumption model. The $+10\%$ indicates the $110\%$ times of the actual nominal energy consumption value and $-10\%$ indicates $90\%$ of its actual nominal energy consumption model. The deviation from the desired reference value is due to saving the energy consumption which the road is assumed to be flat and straight. Therefore, there are few potentials to save energy, which are achieved by accounting the energy consumption dynamics and compromised from the offset-free reference tracking.

## 5.2 Capability of Risk-sensitive Optimal Controller

The simulation results related to the capability of the proposed RSNMPC set-point (reference) tracking and constraints fulfilment with different design parameters are investigated. First, the reference tracking and constraint satisfaction of the RSNMPC for the CC function in a simple scenario is simulated and evaluated. Second, the impact of the prediction horizon of the RSNMPC for the ACC system is analysed. Then, the proposed chance-constraint with various confidence level is assessed. Finally, the impact of the discount factor parameter for the proposed RSNMPC is examined.

### 5.2.1 Reference Tracking and Constraints Satisfaction

In this subsection, the performance of the proposed RSNMPC for the Extended Eco-CC system is evaluated. The reaction of the predictive controller for the road slope, the road curve, and the speed limit zone is investigated separately. The prediction horizon of the RSNMPC is chosen as $T = 10\,s$ to cover the upcoming road variations. This prediction horizon is discretised into $N = 20$ steps. The reference velocity is chosen as $(v_{ref} = 20\,m/s)$.

#### 5.2.1.1 Road Slope

Figure 5.3 shows the performance of the RSNMPC on the straight hilly road with positive slope. The road has a slope profile shown in Figure 5.3a indicating an up hill step in road elevation. Figure 5.3b shows the velocity profiles of the RSNMPC with and without considering energy consumption (RSNMPC vs Eco-RSNMPC). The BEV speed up from the standstill to reach the reference velocity. The BEV speeds up before the uphill to use the kinetic energy of the vehicle to overcome the up-slope. The BEV slows down during the climbing the hill in an energy efficient manner. Afterwards, the BEV tracks the velocity reference on a straight flat road. Figure 5.3c show the smooth control input of the RSNMPC in the two various modes. The control input of the RSNMPC without ecological driving constraint is more agile and shows an earlier reaction to the road slope variation in comparison to the Eco-RSNMPC, which shows a delayed but more energy efficient behaviour. The effect of the predictive controllers on the energy consumption of the BEV is shown in Figure 5.3d. In total, the Eco-RSNMPC is approximately $+10\%$ more energy efficient in comparison to the RSNMPC.

Figure 5.4a shows the velocity profile distribution of the RSNMPC in comparison with the Eco-RSNMPC. It is shown that the RSNMPC is closer to the desired reference velocity $(v_{ref} = 20\,m/s)$ than the Eco-RSNMPC. However, the slower velocity profile of the Eco-RSNMPC improves the energy consumption distribution of the BEV that is shown in Figure 5.4b.

Figure 5.5 shows the performance of the RSNMPC on the straight hilly road with negative slope. The road has a slope profile shown in Figure 5.5a indicating a down hill step in road elevation. Figure 5.5b shows the velocity profiles of the RSNMPC with and without considering energy consumption (RSNMPC vs Eco-RSNMPC). The BEV speeds up from the standstill to reach the reference velocity. The BEV slows down in advance before the downhill to take advantage of the gravity and uses the kinetic energy of the vehicle to speed up after the down-slope. The BEV speeds up during the declining
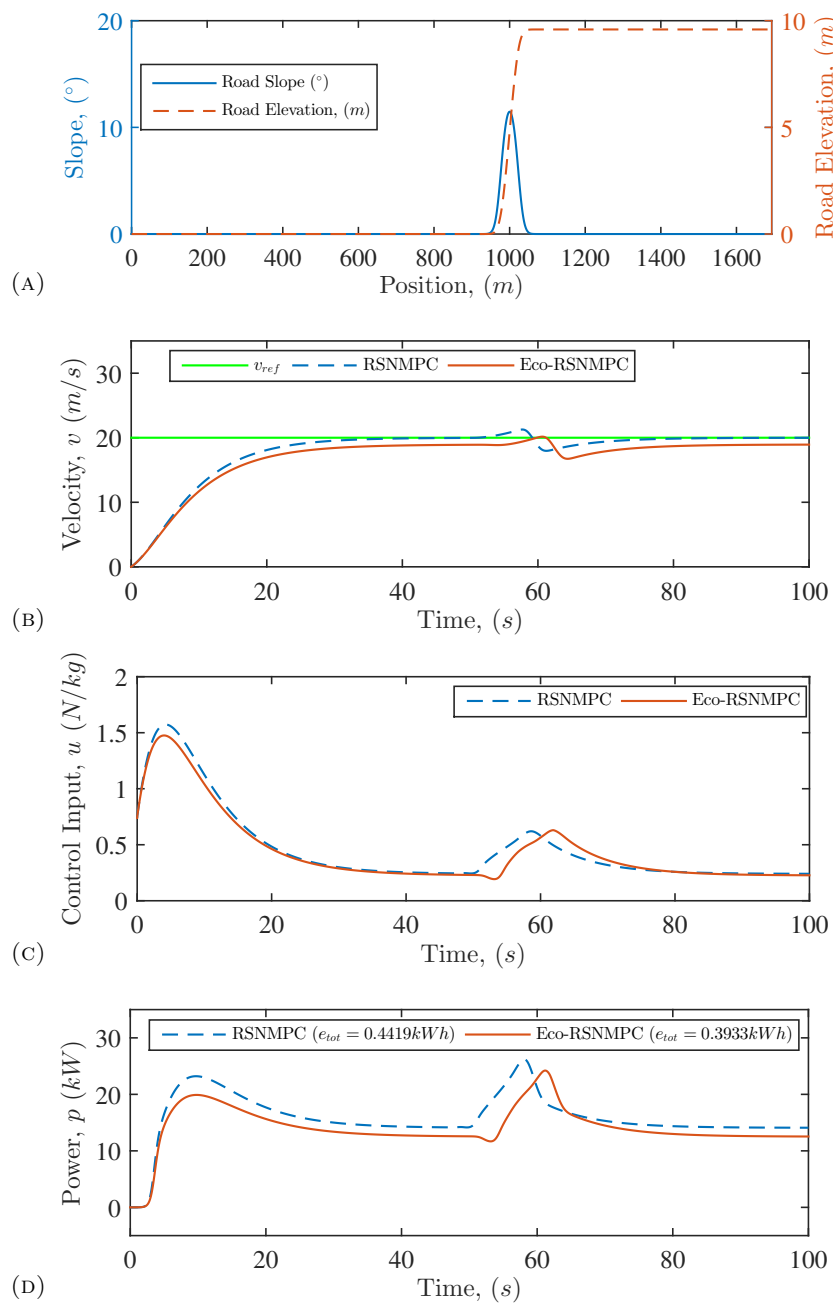
FIGURE 5.3: Performance of the RSNMPC on the straight hilly road with positive slope; (A) road slope profile, (B) velocity profile, (C) control input, (D) energy consumption profile.
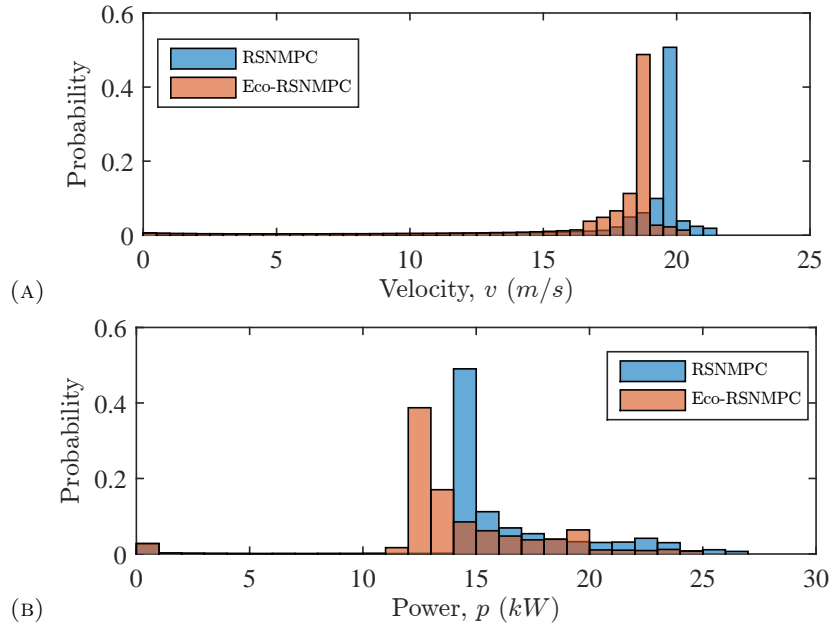
FIGURE 5.4: Statistical performance of the RSNMPC on the straight hilly road with positive slope; (A) velocity distribution, (B) power consumption distribution.

of the downhill in an energy efficient manner. Afterwards, the BEV tracks the velocity reference on a straight flat road. Figure 5.5c shows the smooth control input of the RSNMPC in the two various modes. The control input of the RSNMPC without eco-logical driving constraint is more agile and shows an earlier reaction to the road slope variation in comparison to the Eco-RSNMPC, which shows delayed but more energy efficient behaviour. The effect of the predictive controllers on the energy consumption of the BEV is shown in Figure 5.5d. In total, the Eco-RSNMPC is approximately $+11\%$ more energy efficient in comparison to the RSNMPC during the down hill situation.

Figure 5.6a shows the velocity profile distribution of the RSNMPC in comparison with the Eco-RSNMPC. It is shown that the RSNMPC is closer to the desired reference velocity ($v_{ref} = 20\,m/s$) than the Eco-RSNMPC. However, the slower velocity profile of the Eco-RSNMPC improves the energy consumption distribution of the BEV that is shown in Figure 5.6b.

### 5.2.1.2 Road Curve

The performance of the proposed RSNMPC in both ecological modes dealing with a $25\,m$ radius curvy road is shown in Figure 5.7. Figure 5.7a shows the BEV speeds up from the standstill to reach the reference velocity. The BEV slows down in advance to enter the curve ($s_h = 900\,m$) below the maximum allowed lateral acceleration. The BEV tracks the safe velocity during the curve and speeds up after the curve at the exit
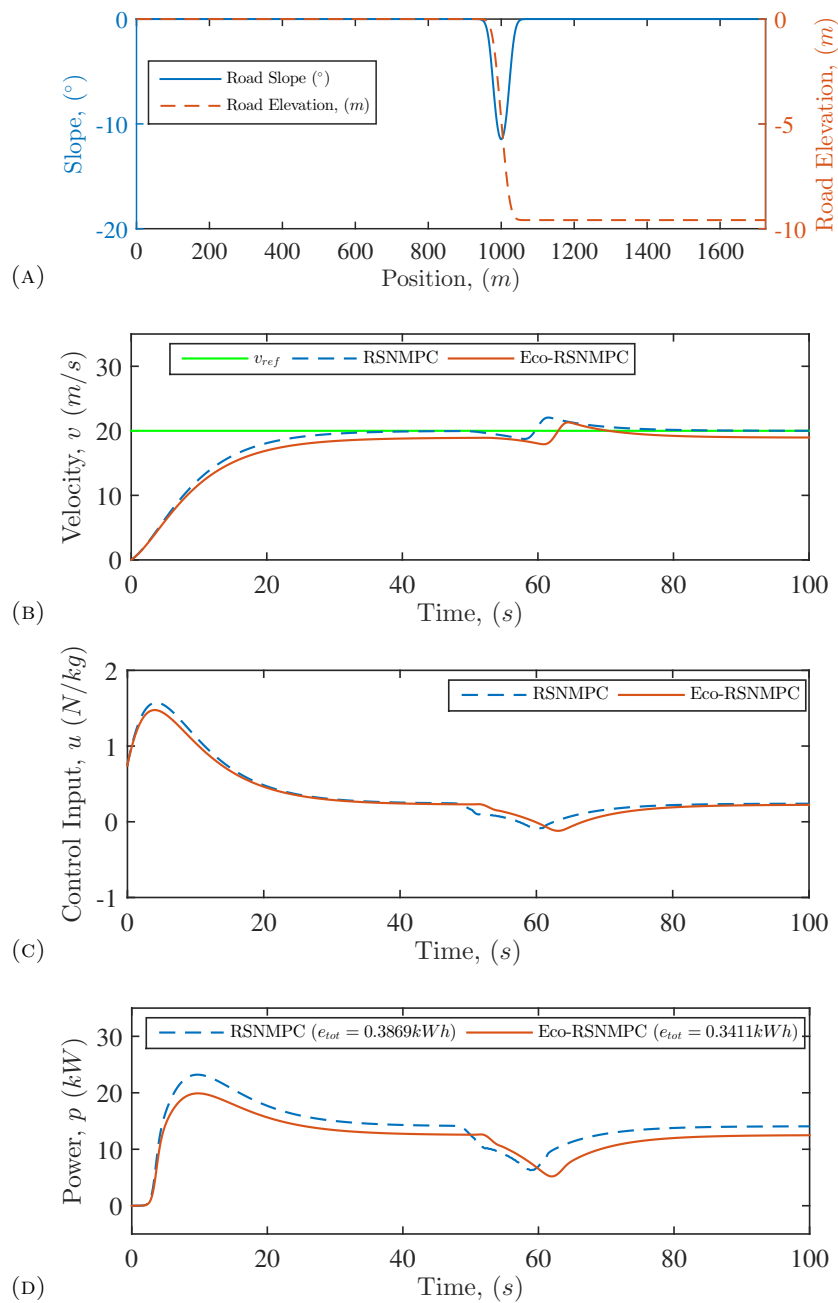
FIGURE 5.5: Performance of the RSNMPC on the straight hilly road with negative slope; (A) road slope profile, (B) velocity profile, (C) control input, (D) energy consumption profile.
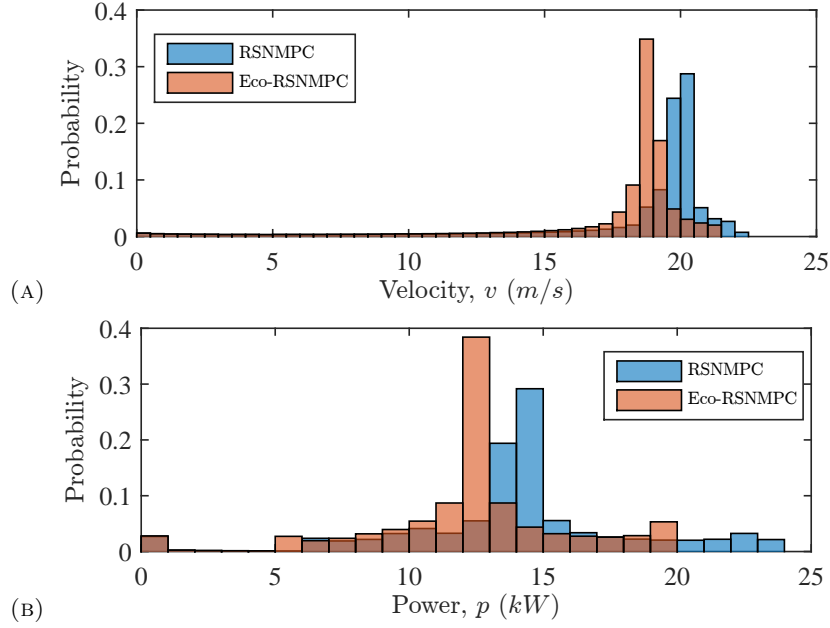
FIGURE 5.6: Statistical performance of the RSNMPC on the straight hilly road with negative slope; (A) velocity distribution, (B) power consumption distribution.

position ($s_h = 1100\,m$). It is shown that the Eco-RSNMPC has the tendency to keep the velocity as fast as the RSNMPC due to energy efficient driving technique during the curve. The lateral acceleration profile for the both RSNMPC and Eco-RSNMPC are shown in Figure 5.7d with a similar reaction to the curvy road. Figure 5.7c shows the control input and Figure 5.7c shows the power consumption of the RSNMPC in the two different modes. In total, the Eco-RSNMPC is approximately $+10.5\%$ more energy efficient in comparison to the RSNMPC.

The probability distribution of the RSNMPC and Eco-RSNMPC are shown in Figure 5.8. It is shown that the RSNMPC is more closer to the desired reference velocity ($v_{ref} = 20\,m/s$) than the Eco-RSNMPC (Figure 5.8a). However, the slower velocity profile of the Eco-RSNMPC improves the energy consumption distribution of the BEV that is shown in Figure 5.8b.

### 5.2.1.3 Speed Limit Zone

Figure 5.9 shows the performance of the RSNMPC on the straight road with a speed limit zone ($v_{lmt} \leq 10\,m/s$). The velocity profile generated by the RSNMPC and Eco-RSNMPC are converging to the reference velocity ($v_{ref} = 20\,m/s$) outside the speed limit zone as shown in Figure 5.9a. Both RSNMPC satisfy the speed limit zone constraint. Figure 5.9b and Figure 5.9c show the control input and the power consumption of both
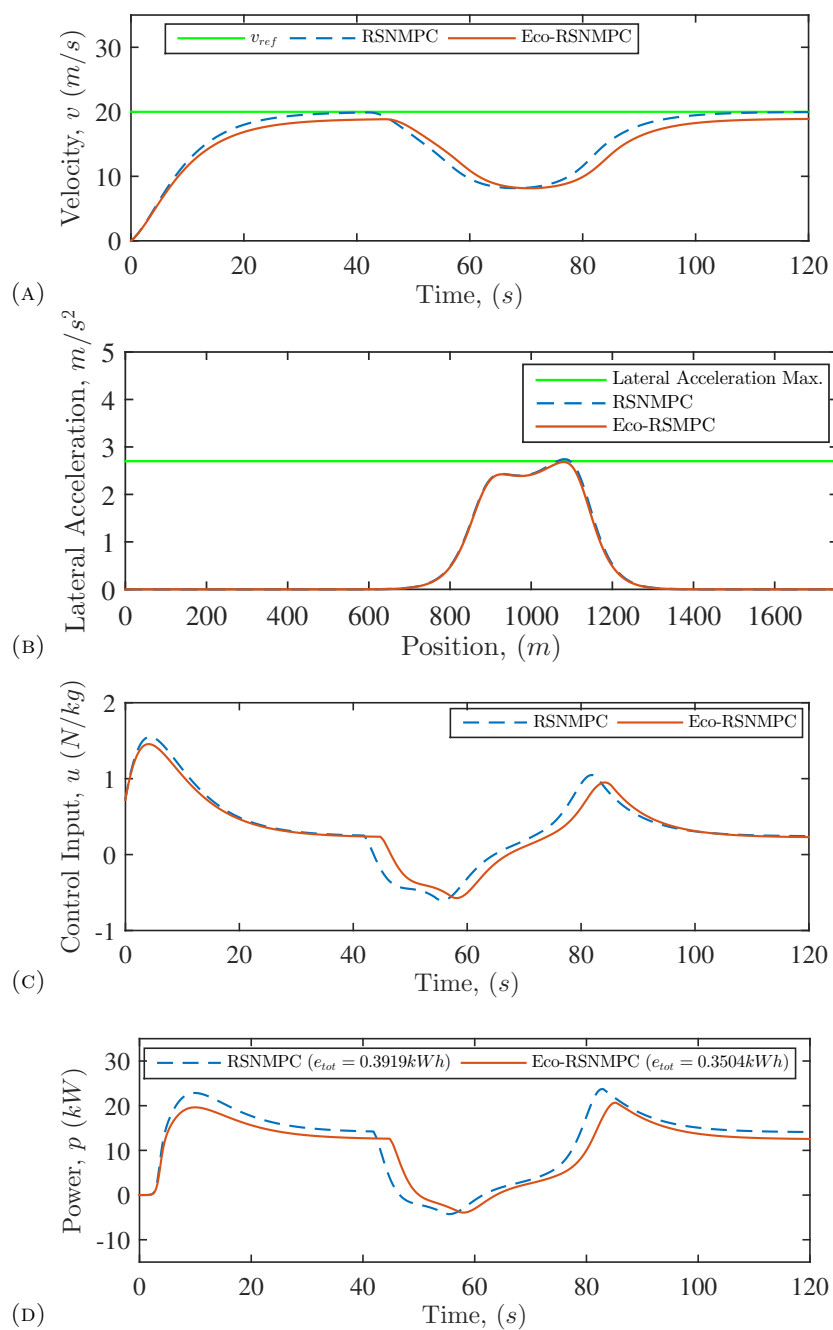
FIGURE 5.7: Performance of the RSNMPC on the curvy road; (A) velocity profile, (B) lateral acceleration profile, (C) control input, (D) energy consumption profile.
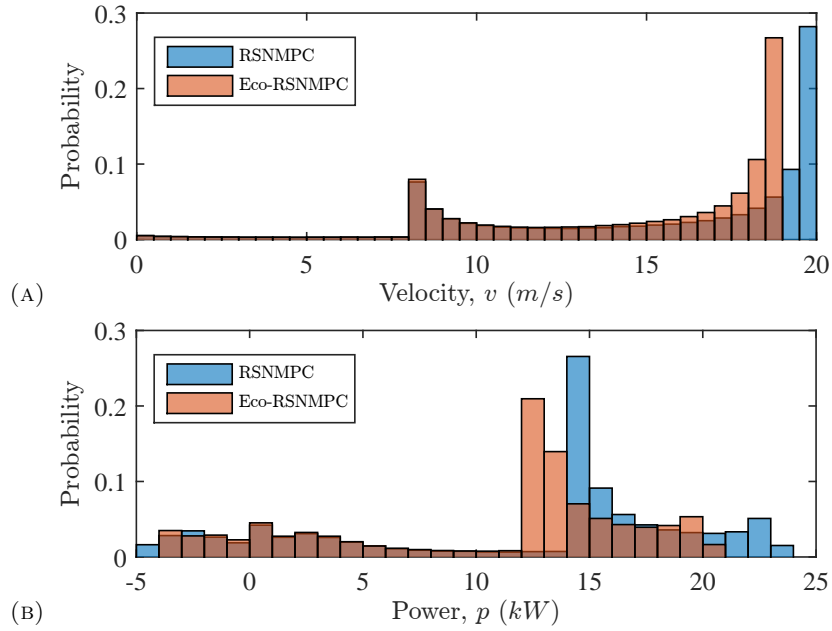
FIGURE 5.8: Statistical performance of the RSNMPC on the curvy road; (A) velocity distribution, (B) power consumption distribution.

RSNMPCs. In total, the Eco-RSNMPC is approximately $+9\%$ more energy efficient in comparison to the RSNMPC in this simulation scenario.

The probability distribution of the RSNMPC and Eco-RSNMPC for the speed limit zone are shown in Figure 5.10. It is shown that the RSNMPC is more closer to the desired reference velocity ($v_{ref} = 20\,m/s$) than the Eco-RSNMPC (Figure 5.10a) outside the speed limit value. The slower velocity profile of the Eco-RSNMPC improves the energy consumption distribution of the BEV that is shown in Figure 5.10b.

### 5.2.2 Prediction Horizon Effects

The effect of prediction horizon on the reaction of the proposed RSNMPC is investigated for the ACC system in a simplified car following scenario. In this setup, the road geometry is assumed to be flat and straight without curves and speed limit zones. The preceding vehicle is moving with a constant velocity at ($v_p = 10\,m/s$). The reaction of the predictive controllers with various prediction horizon for the step response of a reference velocity ($v_{ref} = 25\,m/s$) and relative distance regulation with $d_0 = 6\,m$ and $t_{hw} = 1.5\,s$ is analysed. Figure 5.11 shows the performance of the RSNMPC with various prediction horizons such as $T = 5\,s$, $T = 10\,s$, and $T = 15\,s$. The effect of the evaluated prediction horizon determines a proper prediction horizon length as a tradeoff challenge between the controller performance and computational cost.
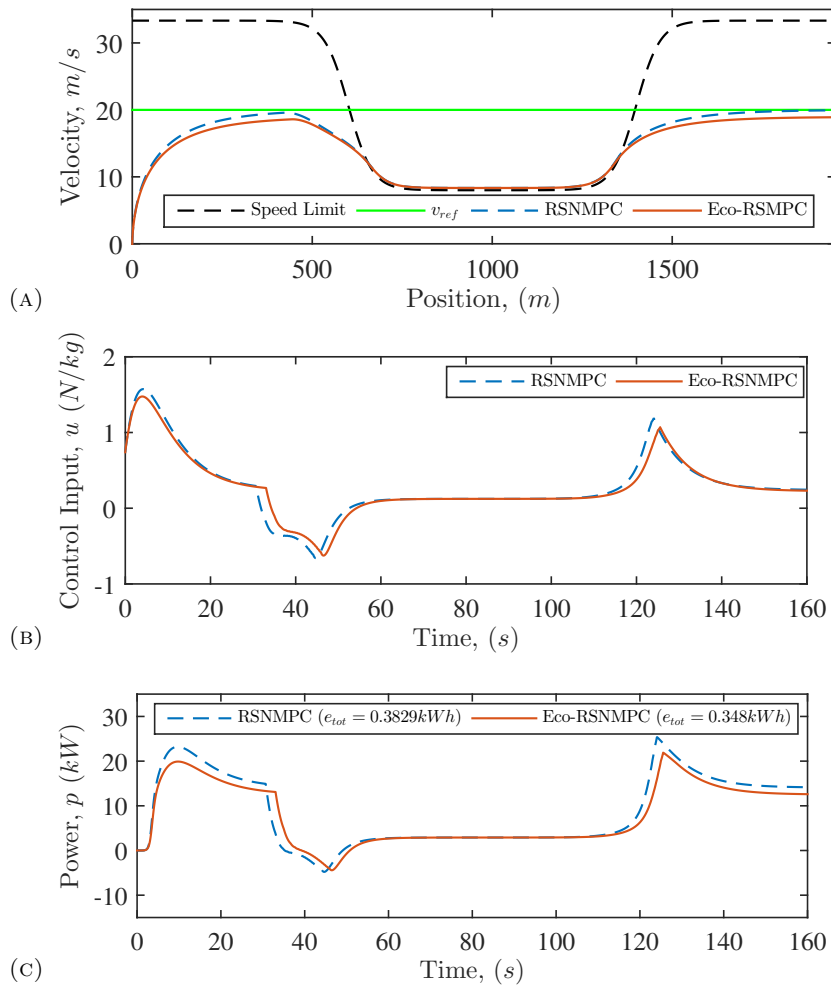
FIGURE 5.9: Performance of the RSNMPC on the straight road with speed limit zone; (A) velocity profile, (B) control input, (C) energy consumption profile.



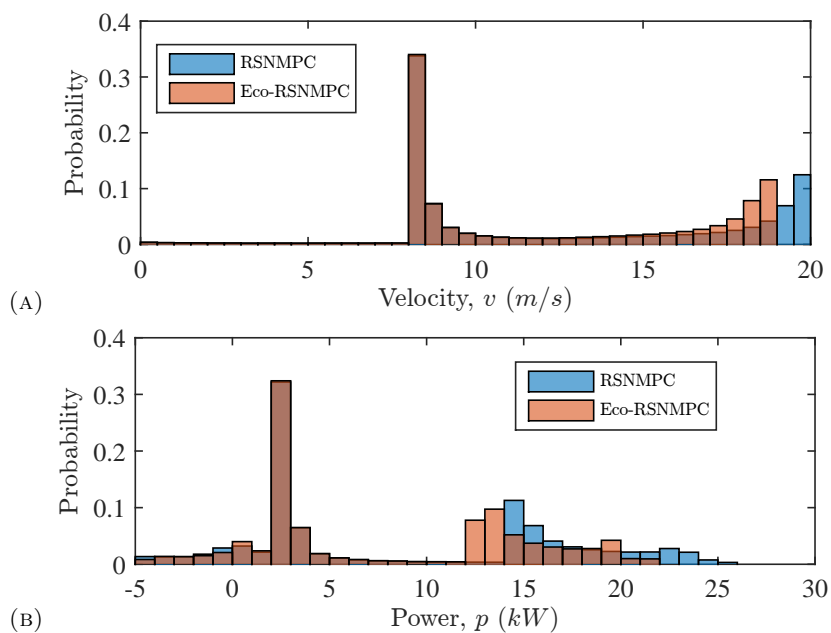FIGURE 5.10: Statistical performance of the RSNMPC on the straight road with speed limit zone; (A) velocity distribution, (B) power consumption distribution.
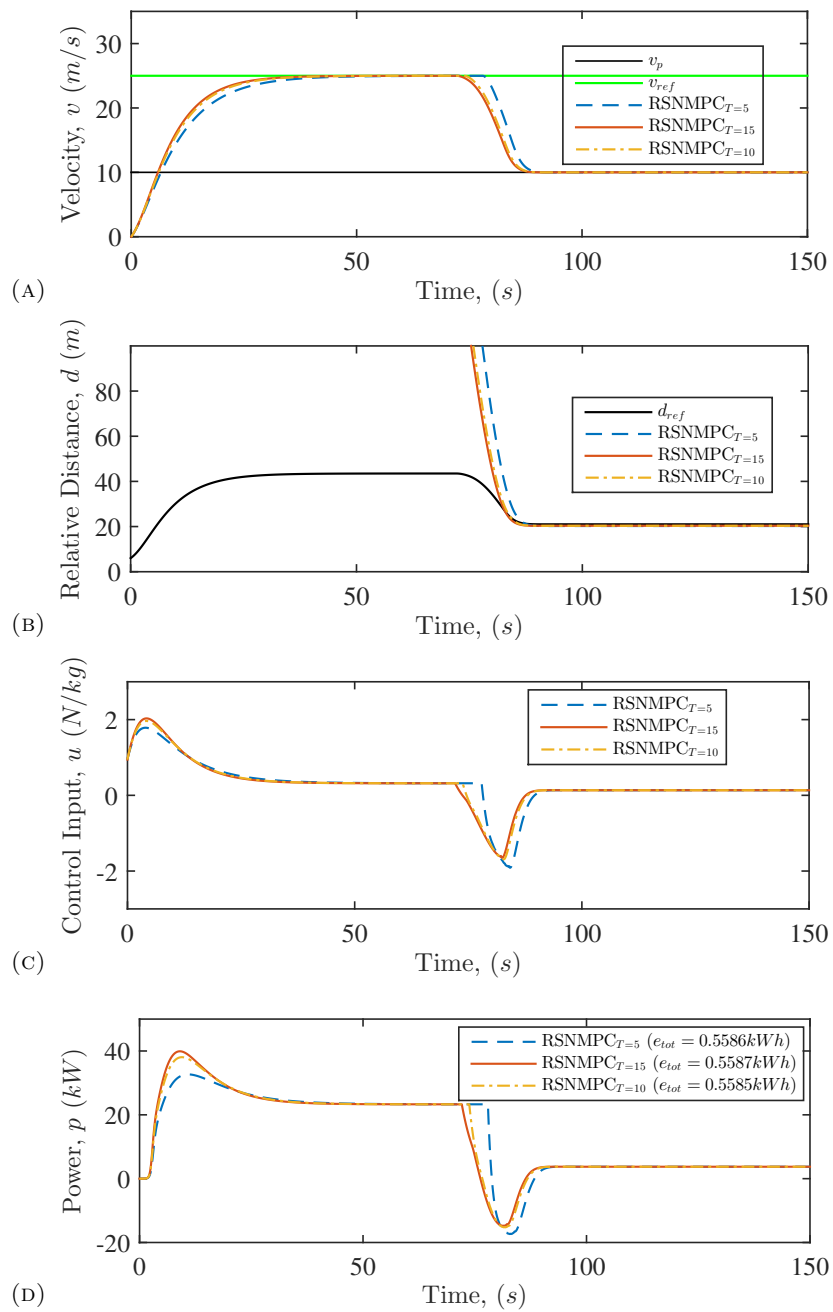
FIGURE 5.11: Performance of the RSNMPC with various prediction horizons; (A) velocity profile, (B) relative distance regulation, (C) control input, (D) energy consumption profile.

Figure 5.11a show the velocity profile of the RSNMPC with $T = 5\,s$, $T = 10\,s$, and $T = 15\,s$. The BEV under control of the various predictive controllers starts from a standstill and converges to the desired reference velocity value. Approaching the preceding vehicle moving with $v_p = 10\,m/s$ causes slowing down the BEV to regulate the related distance safety constraints. Figure 5.11b shows the relative distance constraint satisfaction by the RSNMPCs with different prediction horizon. The RSNMPC$_{T=5}$ shows late reaction during the changing from CC to the car following situation due to short prediction horizon. On the other hand, the RSNMPCs with the $T = 10\,s$ and $T = 15\,s$ improve the reaction of the BEV when approaching the preceding vehicle in earlier time. Figure 5.11c shows the control input profile generated by the predictive controllers. It is shown that the RSNMPC$_{T=5}$ shows late but heavier brake reaction to the preceding vehicle while RSNMPC$_{T=10}$ and RSNMPC$_{T=15}$ shows less aggressive but smoother reaction in advance to the same situation. Although increasing the prediction horizon length may improve the performance of the controller, the gain may be negligible. This can be shown in Figure 5.11d, which the power and total energy consumption of the RSNMPCs are presented. The lower energy consumption is achieved when the prediction horizon is $T = 10$. It is noteworthy that the achieved result in this study verifies the results presented by M. A S Kamal et al. (2011). It is shown that the prediction horizon of $10\,s$ ensures satisfactory performance of the Eco-driving system while keeping the computational burden manageable.

The probability distribution of the RSNMPCs with various prediction horizons is presented in Figure 5.12. Figure 5.12a and Figure 5.12b show the velocity and relative distance distributions of the RSNMPCs. It is shown that the RSNMPC$_{T=10}$ and RSNMPC$_{T=15}$ are closer to the desired reference velocity ($v_{ref} = 20\,m/s$) and reference relative distance at steady state ($d_{ref} = 21\,m$) in comparison to the RSNMPC$_{T=5}$. This indicates the significant effect of a proper prediction horizon on the predictive controllers and its impact on the energy consumption of the BEV as shown in Figure 5.12c.

### 5.2.3 Confidence Level

The effect of the chance-constraint confidence level parameter $\beta$ that is proposed in the RSNMPC is evaluated in this subsection. The open-loop EVaR quantification of the chance-constraint with the confidence level parameter $\beta$ is analysed for the ACC system in a simplified car following scenario with the $\beta = 0.95$, $\beta = 0.50$, and $\beta = 0.05$. In this setup, the road geometry is assumed to be flat and straight without curves and speed limit zones. The preceding vehicle is moving with a constant velocity at ($v_p = 10\,m/s$). The prediction of the RSNMPC is carried out with the introduced physical-statistical motion model of the preceding vehicle. In this case, the predicted motion behaviour
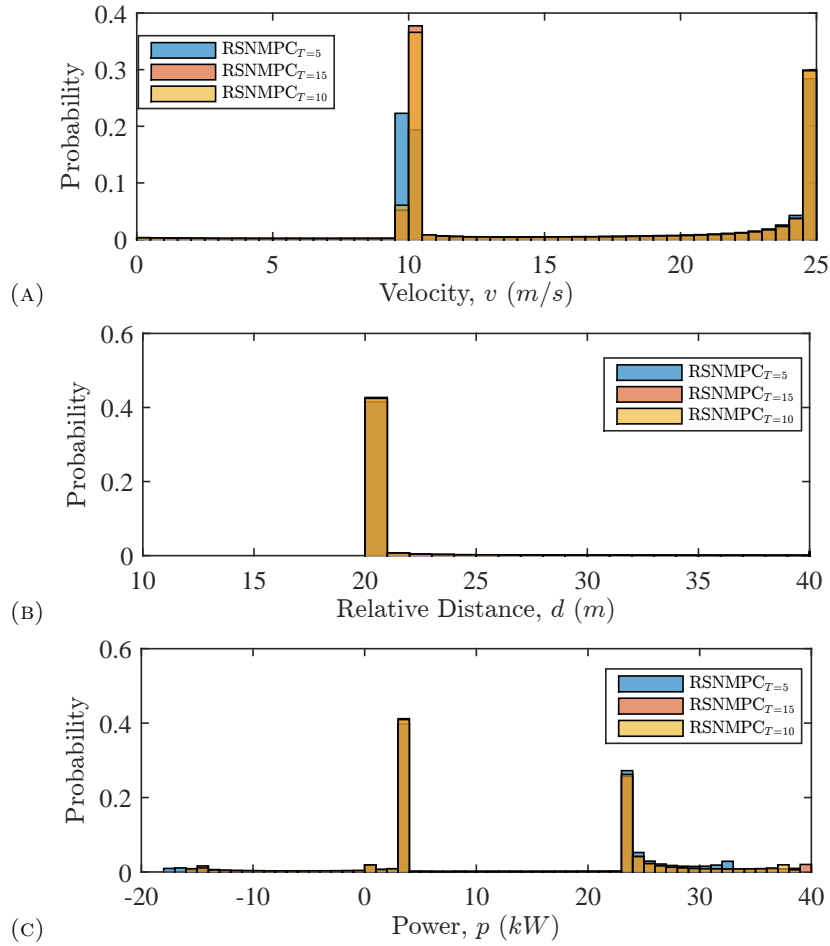
FIGURE 5.12: Statistical performance of the RSNMPC with various prediction horizons; (A) velocity distribution, (B) relative distance distribution, (C) power consumption distribution.

of the preceding vehicle is different than the actual preceding vehicle behaviour with constant cruising velocity. Figure 5.13 shows the performance of the RSNMPC with various confidence levels ($\beta$). The effect of the confidence level determines a proper constraints satisfaction with the tradeoff challenge between the controller performance and constraint robustness.

Figure 5.13a shows the velocity profile of the RSNMPC with $\beta = 0.50$, $\beta = 0.95$, and $\beta = 0.05$, respectively. The BEV under control of the predictive controllers with different confidence levels starts from the standstill and converges to the desired reference velocity value in a similar velocity profile. Approaching the preceding vehicle moving with $v_p = 10\,m/s$ cause slowing down the BEV to regulate the related distance safety constraints. Figure 5.13b shows the relative distance constraint satisfaction by the RSNMPCs with different confidence levels. The RSNMPC$_{\beta=0.50}$ shows closer approach to the reference relative distance than the RSNMPC$_{\beta=0.95}$ while satisfying the relative distance inequality chance-constraint. On the other hand, the RSNMPC$_{\beta=0.05}$ shows
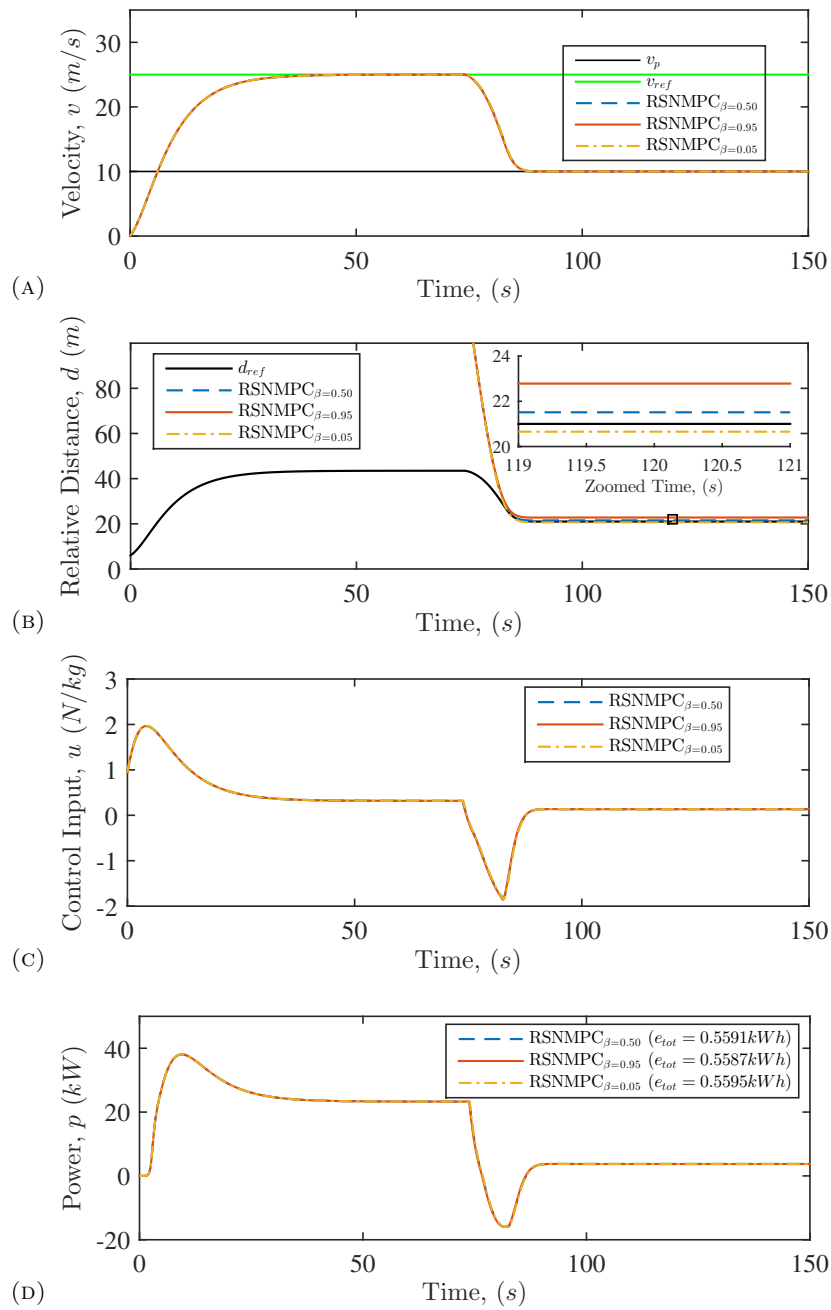
FIGURE 5.13: Performance of the RSNMPC with various confidence level; (A) velocity profile, (B) relative distance regulation, (C) control input, (D) energy consumption profile.

constraint violation due to the low confidence level. Figure 5.13c shows the control input profile generated by the predictive controllers. It is shown that the generated control command is almost identical. However, even the small difference in the confidence level could improve the energy consumption of the BEV as shown in Figure 5.13d. It is shown that the RSNMPC$_{\beta=0.95}$ could achieve the minimum energy consumption in comparison to the RSNMPC$_{\beta=0.50}$ and RSNMPC$_{\beta=0.05}$.

The probability distribution of the RSNMPC with various prediction horizons is presented in Figure 5.14. Figure 5.14a shows the velocity profile distribution of RSNMPC with $\beta = 0.50$, $\beta = 0.95$, and $\beta = 0.05$, respectively. It is shown that the reaction of the RSNMPC are almost identical. Figure 5.14b shows the related distance probability distribution of the RSNMPC with different confidence level. The RSNMPC$_{\beta=0.05}$ violates the relative distance constraint approximately by a meter while the RSNMPC$_{\beta=0.50}$ shows the constraint satisfaction with low robustness. The RSNMPC$_{\beta=0.95}$ shows a proper reaction to the inequality constraint which preserves approximately one meter margin as a degree of robustness from the reference relative distance. Figure 5.14c shows the power consumption probability distribution of the BEV with various confidence levels, which are almost identical.

### 5.2.4 Discount Factor

In this subsection, the performance of the RSNMPC based on the infinite horizon OCP is evaluated for the conventional ACC system on the road geometry, which is assumed to be flat and straight without curves and speed limit zones. The preceding vehicle is moving with a constant velocity at $(v_p = 10\,m/s)$. The prediction of the RSNMPC is carried out with the introduced physical-statistical motion model of the preceding vehicle. The predicted motion behaviour of the preceding vehicle is different than the actual preceding vehicle constant cruising velocity. In this setup, the impact of the discount factor $\rho$ with different values in the infinite horizon OCP based on current-value-Hamiltonian is analysed. Figure 5.15 shows the performance of the RSNMPC with different discount factors. The RSNMPC$_{\rho=0}$ indicates that the discount factor $\rho = 0$, which is equivalent to the deterministic NMPC. It is shown that by increasing the value of discount factor, the predictive controller shows more reaction to near-term future rather than the far-term future.

Figure 5.15a shows the velocity profile of the RSNMPC with $\rho = 0$, $\rho = 0.2$, and $\rho = 0.1$, respectively. The BEV under control of the predictive controllers with different discount factor starts from the standstill and converges to the desired reference velocity value. The RSNMPC$_{\rho=0}$ shows shorter rise time to reach the reference velocity value
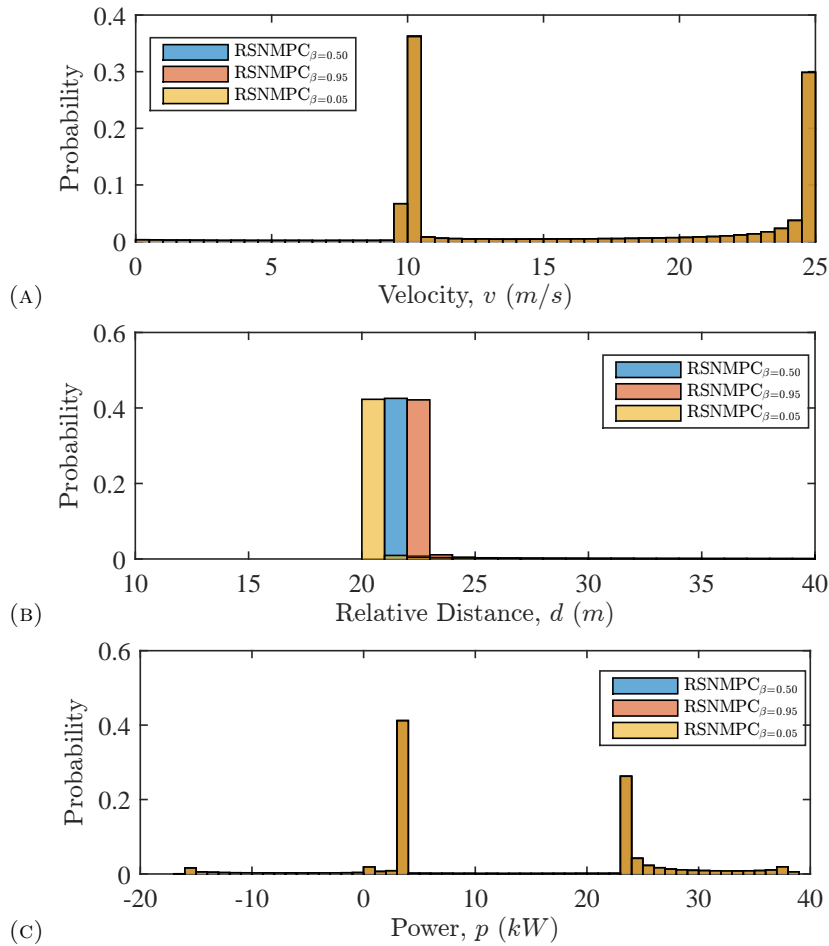
FIGURE 5.14: Statistical performance of the RSNMPC with various confidence levels; (A) velocity distribution, (B) relative distance distribution, (C) power consumption distribution.

($v_{ref} = 25\,m/s$) in comparison to the RSNMPC$_{\rho=0.2}$ and RSNMPC$_{\rho=0.1}$. Approaching the preceding vehicle moving with $v_p = 10\,m/s$ causes slowing down the BEV to regulated the related distance safety constraints. Figure 5.15b shows the relative distance constraint satisfaction by the RSNMPCs with different discount factors. The generated control input profile is shown in Figure 5.15c. It is shown that the control command in RSNMPC$_{\rho=0}$ is more aggressive during the speed up in comparison to the RSNMPC$_{\rho=0.2}$ and RSNMPC$_{\rho=0.1}$. However, the control command in RSNMPC$_{\rho=0}$ shows smoother behaviour during slowing down in comparison to the RSNMPC$_{\rho=0.2}$ and RSNMPC$_{\rho=0.1}$. The different discount factor could impose efficient energy consumption of the BEV as shown in Figure 5.15d. It is shown that the RSNMPC$_{\rho=0.02}$ could achieve the minimum energy consumption in comparison to the RSNMPC$_{\rho=0.1}$ and RSNMPC$_{\rho=0}$.

The probability distribution of the RSNMPC with various discount factors is presented in Figure 5.16. Figure 5.16a shows the velocity profile distribution of the RSNMPC with $\rho = 0$, $\rho = 0.2$, and $\rho = 0.1$, respectively. The relative distance probability distribution of
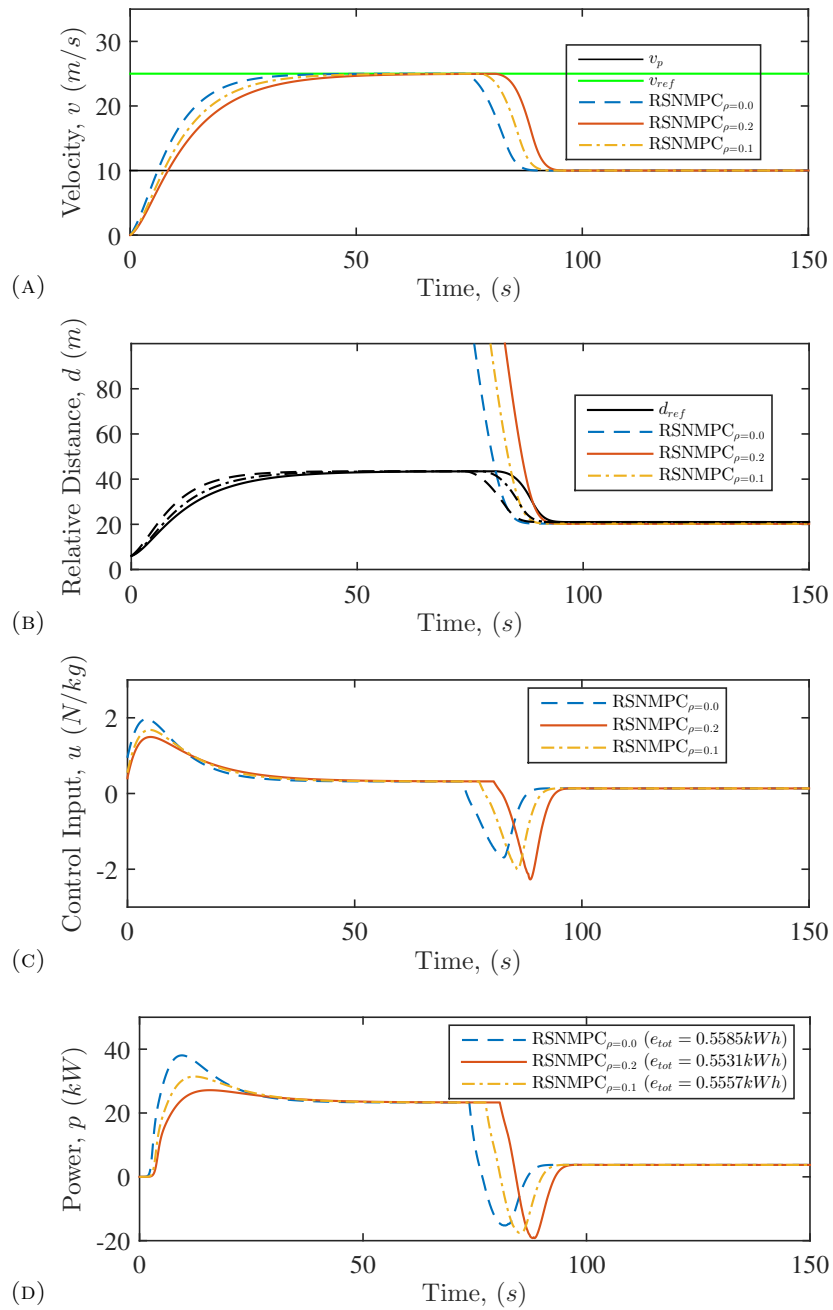
FIGURE 5.15: Performance of the RSNMPC with various discount factors; (A) velocity profile, (B) relative distance regulation, (C) control input, (D) energy consumption profile.

FIGURE 5.16: Statistical performance of the RSNMPC with various discount factors; (A) velocity distribution, (B) relative distance distribution, (C) power consumption distribution.

the RSNMPC with different discount factors is presented in Figure 5.16b. The RSNMPC performance in relative distance constraint satisfaction is almost identical. Figure 5.16c shows the power consumption probability distribution of the BEV with various discount factors.

### 5.2.5 Energy Consumption Constraint Effect

In this subsection, the performance of the RSNMPC based on the open-loop EVaR is evaluated for the conventional ACC system on the road geometry which is assumed to be flat and straight without curves and speed limit zones. The preceding vehicle is moving with a constant velocity at $(v_p = 10\,m/s)$. The prediction of the RSNMPC is carried out with the introduced physical-statistical motion model of the preceding vehicle. The predicted motion behaviour of the preceding vehicle is different than the actual preceding vehicle constant cruising velocity. In this setup, the *Nominal* reference tracking

indicates the RSNMPC without taking the energy consumption model in velocity profile planning. The *Eco-RSNMPC* reference tracking indicates the RSNMPC with the nominal energy consumption model and its inequality constraint (4.126). In addition, the *Eco-RSNMPC*$^+$ reference tracking indicates the RSNMPC with the nominal energy consumption model and its inequality constraint as well as penalty function in the cost function ($C = [0, 0, 0.8, 0, 0]$).

Figure 5.17 shows the performance of the RSNMPC with various energy consumption constraint levels. Figure 5.17a shows the velocity profile of the RSNMPC, Eco-RSNMPC, and Eco-RSNMPC$^+$, respectively. The BEV under control of the predictive controllers with different ecological configuration level starts from the standstill and converge to the desired reference velocity value in a similar velocity profile. It is shown that only the Eco-RSNMPC$^+$ has the off-set tracking performance due to extra penalty term in the cost function. Approaching the preceding vehicle moving with $v_p = 10\,m/s$ cause slowing down the BEV to regulated the related distance safety constraints. Figure 5.17b shows the relative distance constraint satisfaction by the RSNMPCs with different energy consumption configurations. The RSNMPC shows closer earlier arrival to the reference relative distance than the Eco-RSNMPC and Eco-RSNMPC$^+$ while satisfying the relative distance inequality chance-constraint. Figure 5.17c shows the control input profile generated by the predictive controllers. It is shown that the generated control commands are different during the acceleration phase but they are almost identical during the declaration and cruising. The control input and velocity profiles determine the power consumption profile of the BEV as presented in Figure 5.17d. It is shown that the Eco-RSNMPC$^+$ could achieve the minimum energy consumption with the compromise on velocity in comparison to the RSNMPC and Eco-RSNMPC. On the other hand, the Eco-RSNMPC could achieve lower energy consumption in comparison to the nominal RSNMPC with compromise only on the acceleration.

Figure 5.18 shows the power consumption profile of the different controllers with the probability distribution of the RSNMPC with various energy consumption configurations. Figure 5.19 shows the operating points trajectory of the nominal RSNMPC on the Smart-ED energy consumption characteristic map. Figure 5.20 shows the operating points trajectory of the Eco-RSNMPC on the Smart-ED energy consumption characteristic map. Figure 5.21 shows the operating points trajectory of the Eco-RSNMPC$^+$ on the Smart-ED energy consumption characteristic map. It is shown that the operating points of the Eco-RSNMPC and Eco-RSNMPC$^+$ are constrained to reach higher values of power consumption in comparison to the nominal RSNMPC.
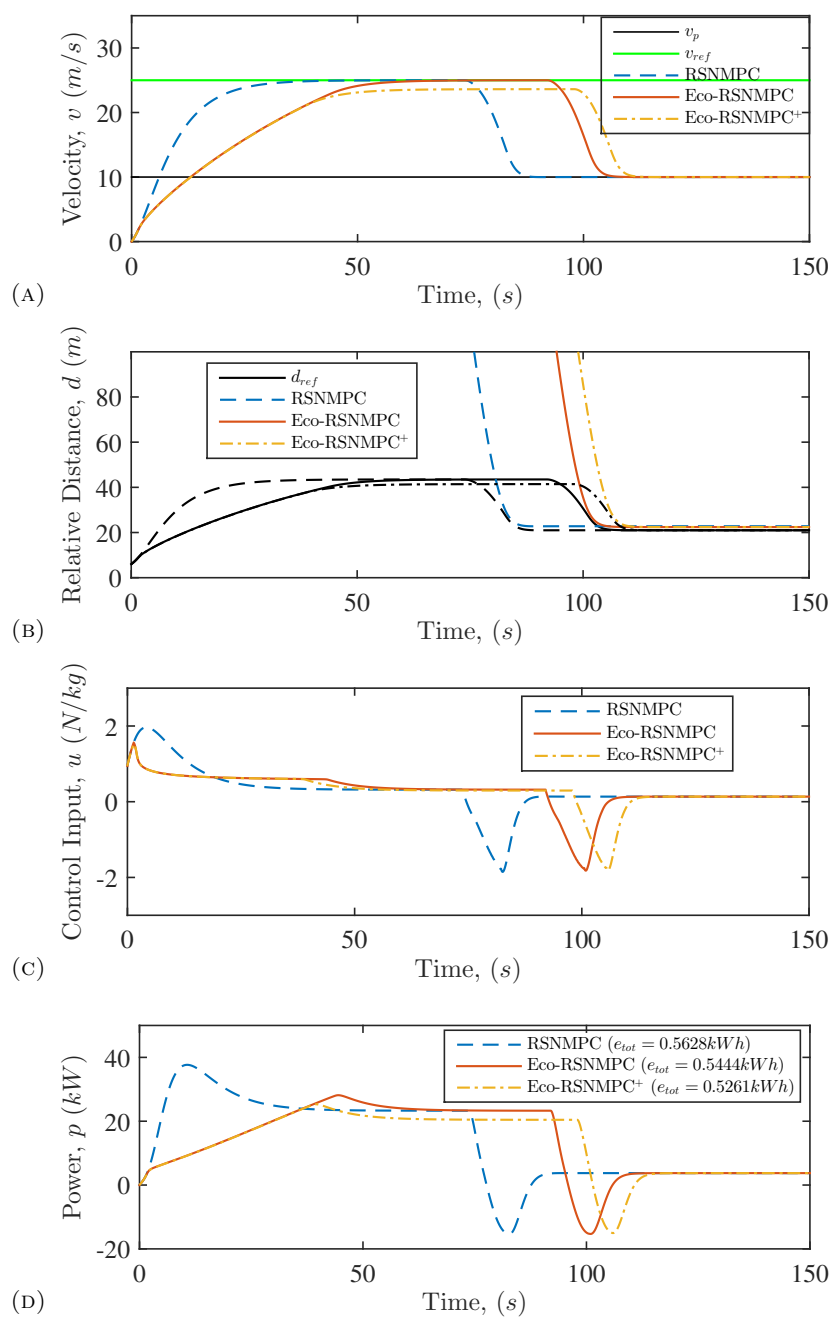
FIGURE 5.17: Performance of the RSNMPC with different energy consumption configurations; (A) velocity profile, (B) relative distance regulation, (C) control input, (D) energy consumption profile.

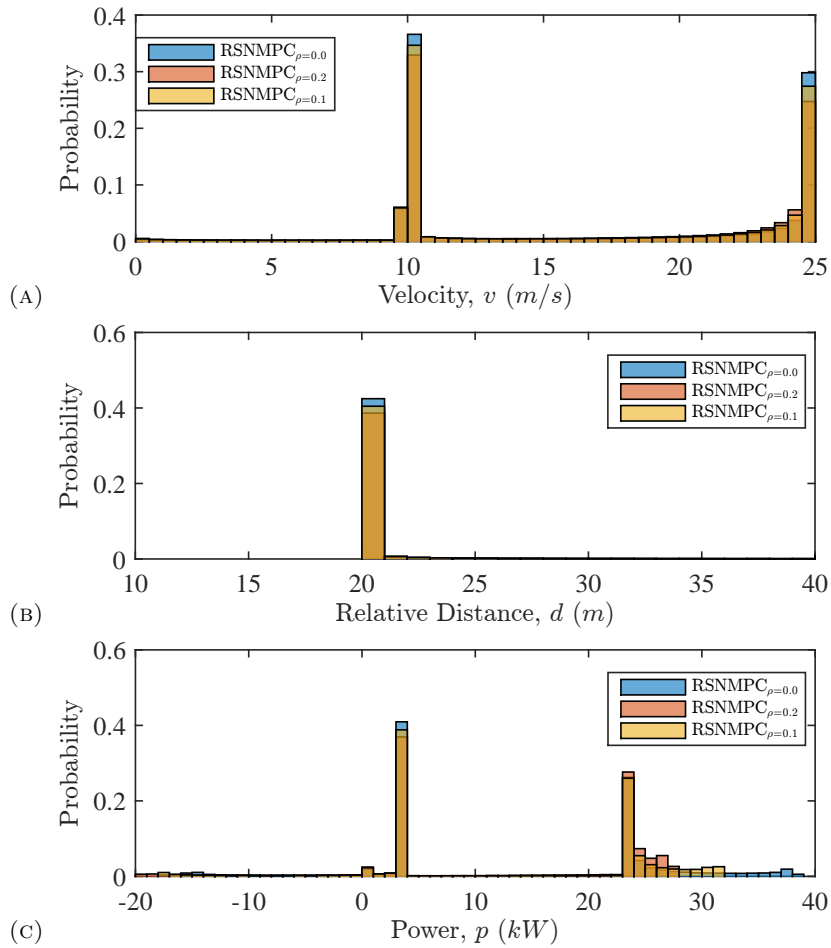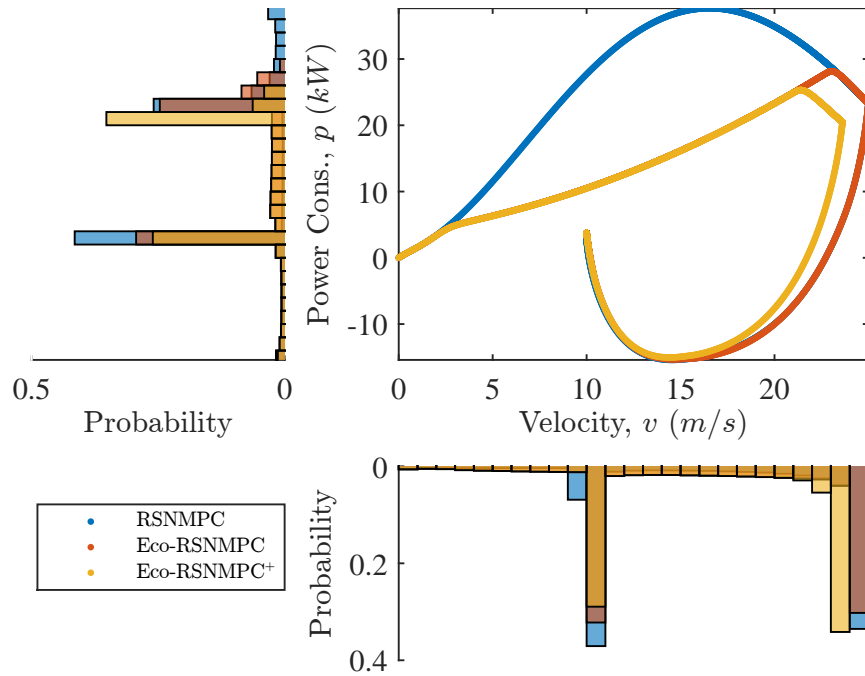FIGURE 5.18: Energy consumption performance of the Nominal, Eco-RSNMPC, and Eco-RSNMPC$^+$ controllers
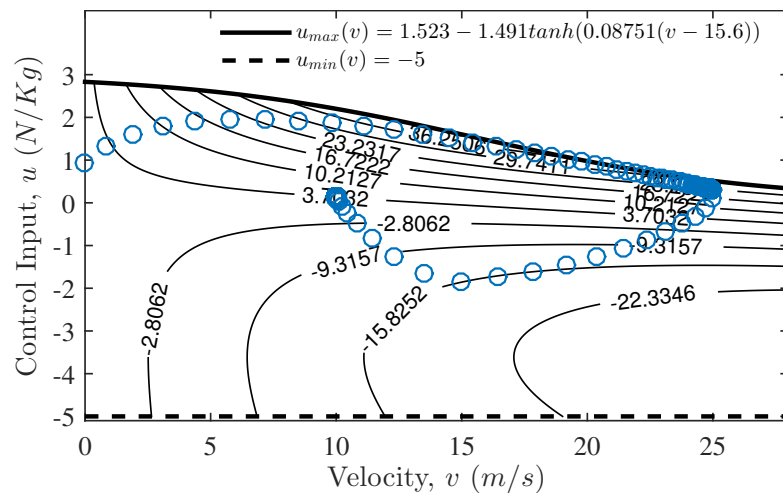


FIGURE 5.19: Projection of the nominal RSNMPC operating points on the energy consumption map

## 5.3 Performance of the Proposed Concept

This section presents the overall performance of the SEDAS concept in terms of the safety and energy efficiency in various predictive control configurations and driving situations. The simulation results for the deterministic NMPC for the Extended Eco-CC, the robust SNMPC, the Risk-averse SNMPC, the current-value Hamiltonian SNMPC, and RSNMPC with open-loop and closed-loop EVaR for the Extended Eco-ACC are presented.
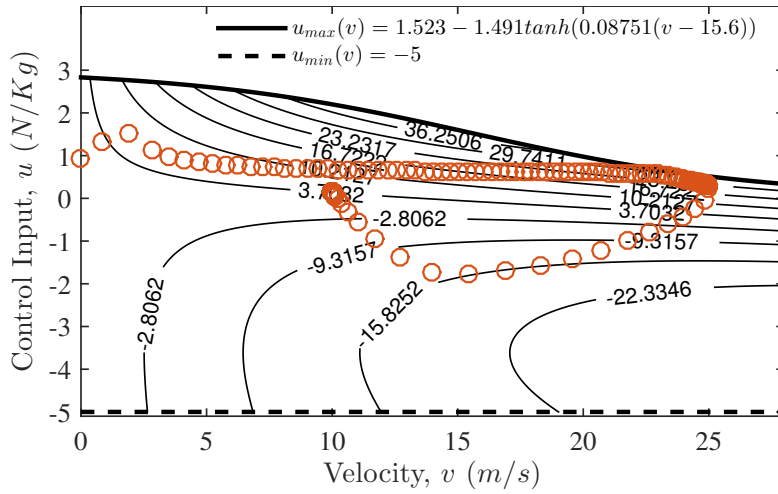
FIGURE 5.20: Projection of the Eco-RSNMPC operating points on the energy consumption map
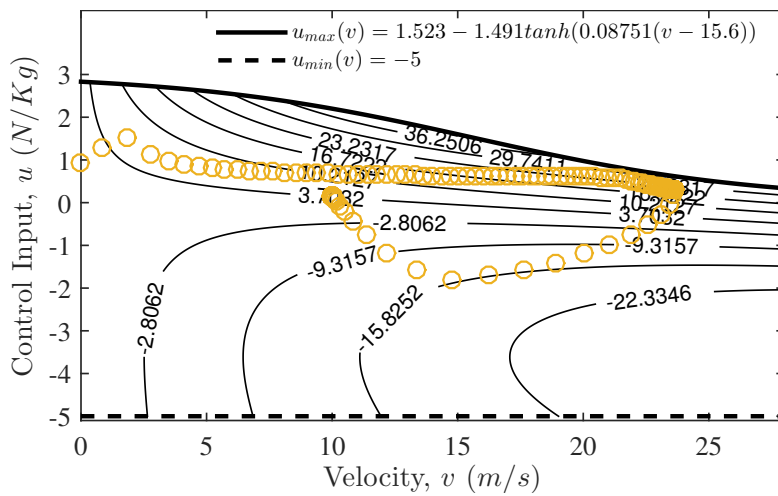


FIGURE 5.21: Projection of the Eco-RSNMPC$^+$ operating points on the energy consumption map

### 5.3.1 NMPC for Extended Eco-CC

The concept of the proposed Extended Eco-CC system (Ext-Eco-CC) based on the NMPC for the BEV on a hilly road with road curves and traffic speed limits are shown in Figure 5.22.

In this study, the final cost function of the NMPC, $J_f$ is chosen as:

$$J_f(x_N) = \frac{1}{2}q_f(e_h - e_{h_{ref}})^2 \tag{5.1}$$

where $e_{h_{ref}}$ is reference energy consumption and $q_f$ is the corresponding weight. The energy consumption, $e_h$, is only evaluated at the end of the prediction horizon in order to benefit from the regenerative energy as much as possible. This helps to choose more
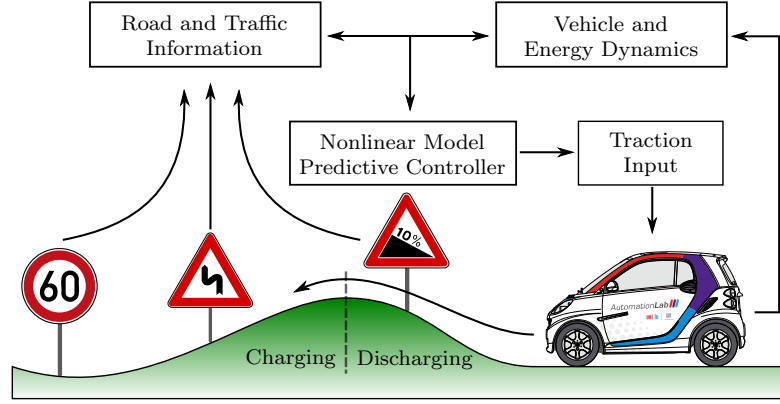
FIGURE 5.22: Extended Ecological Cruise Control concept

flexible control actions independent of the cost-per-stage function, $J_c$, which can be defined as:

$$
\begin{aligned}
J_c(x_i, u_i) =& \frac{1}{2} q_v (v_h - v_{h_{ref}})^2 + \frac{1}{2}(r_u(u - u_{ref})^2 - q_{slk} u_{slk}) \\
& + \exp^{(q_{crv}(a_{lat} - a_{lat.max}))} v^2 + \exp^{(q_{lmt}(v - f_{lmt}(s)))} v,
\end{aligned}
\tag{5.2}
$$

where $u_{ref}$ is the reference input, and $q_v$, $r_u$ are relative weightings. A small slack penalty, $q_{slk}$, is added to avoid the singularity at $s_{slk} = 0$ and keep the control input away from the boundary of the feasible set. The lateral acceleration inequality constraint is $a_{lat} = v^2 f_{crv}(\delta(s))$ and implemented as a soft constraint based on penalty method in the cost function. An exponential function of the maximum allowable lateral acceleration, $a_{lat.max}$, with the related weight, $q_{crv}$ is used. In addition, if the reference speed fixed by the driver is above the speed limit value, the velocity is penalised exponentially with the weight $q_{lmt}$.

The performance of the NMPC applied on the Smart-ED is evaluated on the test track located at Centre de Formation pour Conducteurs S.A. Colmar-Berg, Luxembourg with its road geometry model (CFC, 2015). The prediction horizon $T = 15\,s$ is chosen to cover upcoming road and traffic events. This prediction horizon is discretised into $N = 30$ steps of size $\Delta t = 0.5\,s$ based on the approximate vehicle's actuators maximum delay time. The total-cost function is set as $e_{ref} = 0$, $q_f = 0.25$, $v_{ref} = 25\ m/s$, $q_v = 1$, $u_{ref} = F_{res} - Mgsin(f_{slp}(s))$, $r_u = 20$, $q_{slk} = 20$, $q_{crv} = 1.2$, $a_{lat.max} = 3.7\ m/s^2$, and $q_{lmt} = 0.1$. The maximum speed of the Smart-ED is about $v_{max} = 28\ m/s$ without activating the boost switch available in the vehicle. The weighting parameters are tuned manually by observing the performance in tracking the reference states considering the road and traffic information, safety and energy consumption.

For the sake of a fair comparison, the proposed "Ext-Eco-CC" system with the same initial conditions is compared to the "Ext-CC" system without energy consumption
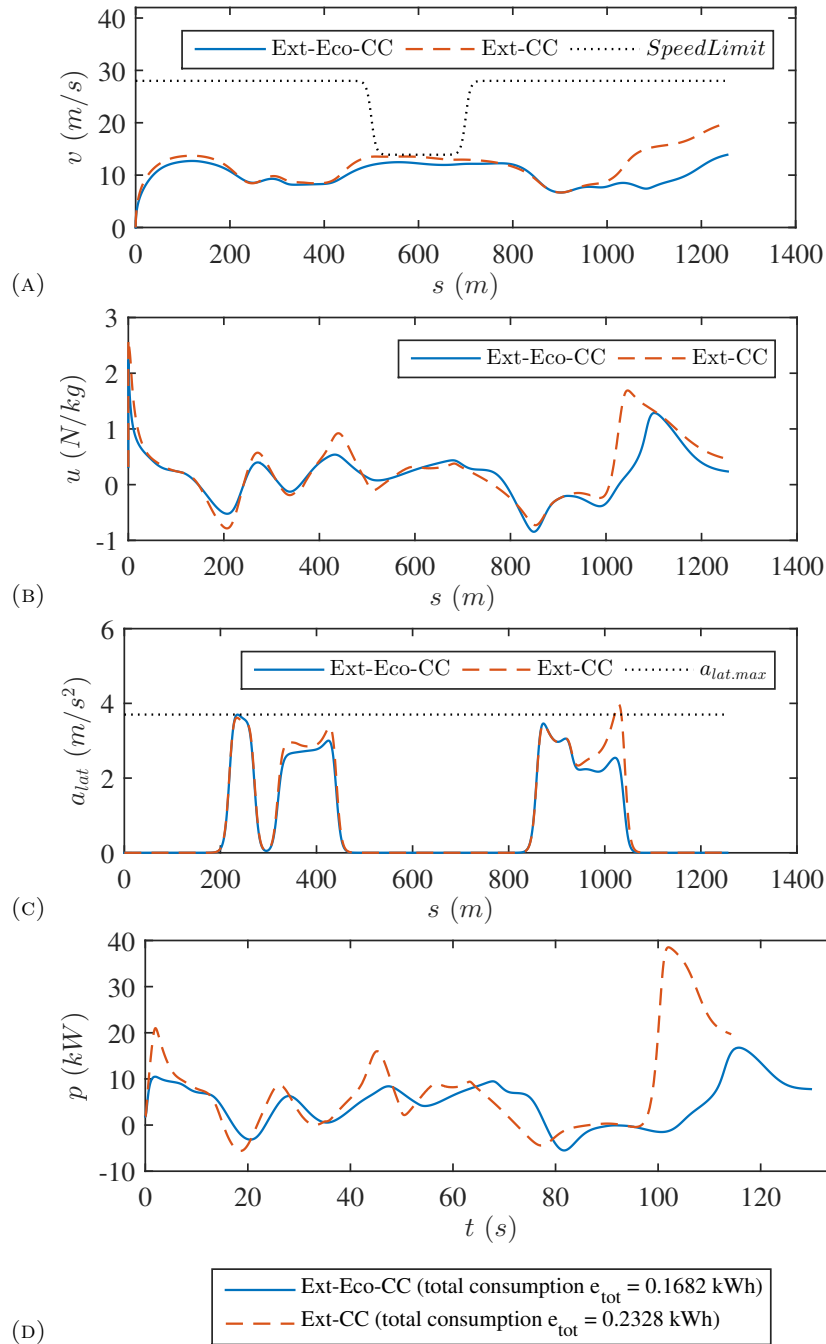
FIGURE 5.23: Performance of the NMPC with the Smart-ED on the test track in terms of (A) velocity, (B) control input, (C) lateral acceleration, and (D) related power consumption with total energy consumption.

model ($q_f = 0$). The conventional Eco-CC and CC systems are not considering road curvature variations and speed limit zones and therefore, these conventional systems may not be comparable with the proposed system. Figure 5.23. shows the optimal driving profile generated by the controller of the Ext-Eco-CC and Ext-CC system.

Figure 5.23a. shows the velocity profile at start point with initial standstill state. The controllers increase the velocity of the vehicle during straight downhill road segment

and later reduce the velocity optimally as the vehicle approaches the first and second curves. Next, the vehicle has to stay below the speed limit zone and afterwards does not speed up to reach the reference velocity due to the upcoming sharp third and fourth curves. Comparing to the Ext-CC system, the Ext-Eco-CC system drives the vehicle much slower in the last segment of the road due to the upcoming hilly road and thus saves a considerable amount of energy. Figure 5.23b. shows the related control input derived from the NMPC. The Ext-Eco-CC controller tries to avoid unnecessary aggressive control inputs namely strong braking and accelerations. Figure 5.23c. shows the lateral acceleration of the vehicle in each curve remains below the reference maximum lateral acceleration value. Note that since the driver controls the steering, the actual lateral acceleration of the vehicle in the real driving test might be different. Figure 5.23d. shows the related power consumptions profile on the test track and the final overall energy consumption, $e_{tot}$, for the whole track. The Ext-Eco-CC takes any advantages of the road profile and traffic information to save as much energy as possible.

The overall direction of the obtained simulation results showed that the proposed Ext-Eco-CC could be helpful to extend the limited cruising range of the BEV. This was achieved by reducing the driver interventions in velocity control and extending the autonomy of the vehicle with respect to road geometric and traffic information. It should be emphasized that with an increase of only 13% of travel time, the Ext-Eco-CC can save 27% of energy compared to the Ext-CC system at the test track. A balanced tradeoff between the energy consumption and travel time can be achieved based on the driver's preference. It is found that the driver's high reference velocity was not possible to be achieved with ecological driving style on the test track. However, the lower reference velocity could be tracked by the controller with mentioned assumptions. During simulation, it is found that the control input can be updated approximately every 1 $ms$ on an Intel® Core™ i7 with memory of 7.7 GiB. Hence, this way of the formulation should be a real-time capable controller for the proposed system. For more details about the proposed NMPC for the extended Eco-CC system, follow S. Amin Sajadi-Alamdari et al. (2016).

### 5.3.1.1 Localisation Error

The concept of the proposed Extended Eco-CC system based on the RSNMPC for the BEV is simulated on a hilly road with road curves without speed limit zone assumption. The localisation of the Smart-ED is based on the GPS signals with a certain degree of accuracy. For instance, the commercial GPS-enable embedded systems are typically accurate to within a 5 $m$ radius approximately. Moreover, if a low-cost GPS receiver is used, the radius of the circle might be as much as 10 $m$ to capture 95% of the points.
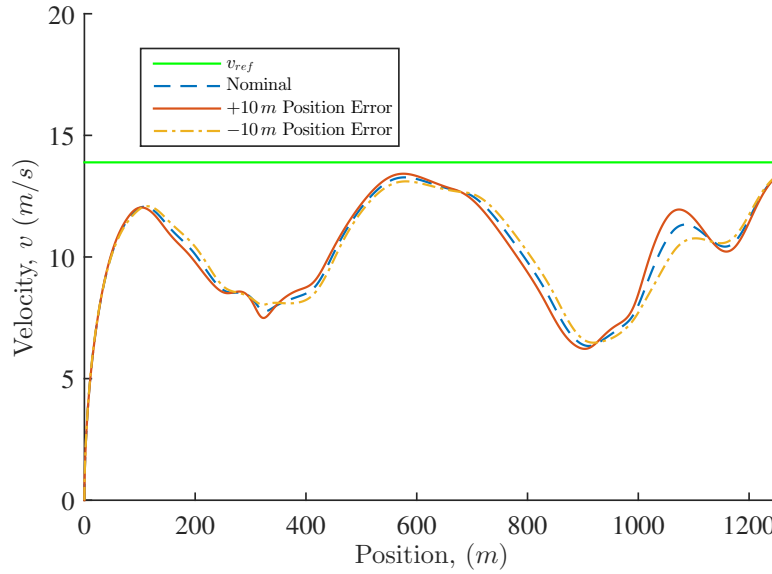
FIGURE 5.24: Performance of the closed-loop step response of the RSNMPC with localisation error on a test track.

Performance of the proposed RSNMPC on the test track is shown in Figure 5.24 including the $\pm 10\%$ localisation errors. The $10\,m$ indicates the ten meters more in the actual nominal position and $-10\,m$ indicates the ten meters less in the actual nominal position value on the test track.

The Figure 5.24 shows the velocity profile at start point with initial standstill state. The controllers increase the velocity of the vehicle during straight downhill road segment and later reduce the velocity optimally as the vehicle approaches the first and second curves. Next, the vehicle has to speed up to reach the reference velocity. Afterwards, the velocity of the BEV has to slow down due to the upcoming sharp third and fourth curves. Finally, the BEV speeds up to hit the desired velocity. Comparing to the *Nominal* case, the RSNMPC shows robust state regulation with various constraint and location errors.

### 5.3.2 Distributionally Robust SNMPC for Extended Eco-ACC

The ecological driving based ADAS concept proposed for a semi-autonomous BEV that extends the functionalities of the Eco-ACC system is presented in Figure 5.25.

In this setup, the spacing policy for regulation of the safe reference relative distance to the preceding vehicle is based on the *time headway* defined as follows:

$$d_{ref} := d_0 + t_{hw} v_h, \tag{5.3}$$
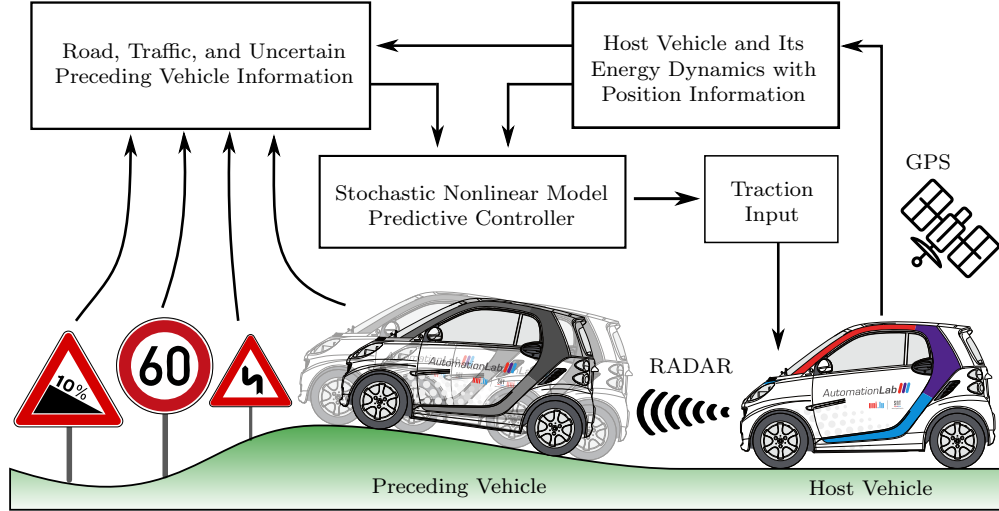
FIGURE 5.25: Extended Eco-ACC Concept for the semi-autonomous BEV

where $d_0$ is a constant minimum safe distance, and $t_{hw}$ is the desired time headway. The statistics of the stochastic position of the preceding vehicle is estimated by:

$$\mathbf{E}[d] := \hat{s}_p - s_h, \tag{5.4}$$

$$\mathbf{Var}(d) := \mathbf{E}[(d - \mathbf{E}[d])^2] \approx \dot{d}^2 \sigma_{\hat{s}_p}^2, \tag{5.5}$$

where the $\mathbf{Var}[\cdot]$ is the variance of the preceding vehicle's position. The deviation from the desired relative distance is formulated in a chance-constraint of the form:

$$\Pr\{d_{ref} \leq d\} \geq 1 - \epsilon, \tag{5.6}$$

where $d$ is a random quantity and $\epsilon := 1 - \beta$ is the risk allocation parameter. A distributionally robust chance-constraint for a wide class of probability distributions is reformulated to a certainty equivalent second-order cone constraint as follows (for more details, see Calafiore et al. (2006) and Mesbah et al. (2014)):

$$\kappa_\beta \mathbf{Var}[d_{ref} - d] + \mathbf{E}[d_{ref} - d] \leq 0, \quad \kappa_\beta := \sqrt{\frac{1 - \epsilon}{\epsilon}}. \tag{5.7}$$

The performance index in order to achieve the ecological driving can be formulated by linearly penalising the energy consumption of the host vehicle at the end of prediction horizon as follows:

$$J_f(\bar{x}_N) := q_f e_h, \tag{5.8}$$

where $q_f$ is the corresponding weight. This definition provides a flexible velocity profile planning in the integral performance index that can be formulated as follows:

$$
\begin{aligned}
J_c(\bar{x}_i, \mu_i) :=& \frac{1}{2} q_c (v_h - v_{h_{ref}})^2 + \frac{1}{2} (r_u (u - u_{ref})^2) \\
&+ q_{crv,lmt}(v_h, f_{crv}(\delta(s_h)), f_{lmt}(s_h)) v_h^2 \\
&+ q_a c(v_h, v_p, d)((\mathbf{E}[d] - d_{ref})^2 + ln(1 + \kappa_\beta \mathbf{Var}(d))),
\end{aligned} \tag{5.9}
$$

where $v_{h_{ref}}$, $u_{ref}$ are desired cruising velocity, and reference input, respectively. The $q_c$, and $r_u$ are corresponding weights.

A safe and comfortable ride can be achieved during the road curve and traffic speed limit zone variations by penalising the host vehicle velocity with relative adaptive weight (similar to the barrier methods) based on the lateral acceleration ($a_{lat} = v_h^2 f_{crv}(\delta(s_h))$) and maximum allowed lateral acceleration ($a_{lat.max}$) as follows:

$$
\begin{aligned}
q_{crv,lmt}(v_h, f_{crv}(\delta(s_h)), f_{lmt}(s_h)) :=& \exp^{(q_{crv}(a_{lat} - a_{lat.max}))} \\
&+ \exp^{(q_{lmt}(v_h - f_{lmt}(s_h)))},
\end{aligned} \tag{5.10}
$$

where $q_{crv}$, and $q_{lmt}$ are relative weights. The $q_{ac}(v_h, v_p, d)$ is an equivalent to a soft barrier function that supplies enough weight to dominate the other objectives during close approaching to the boundary value of reference relative distance defined as follows:

$$
q_{ac}(v_h, v_p, d) := q_{acc}(q_{rv} exp(\frac{-(v_p - v_h)}{q_{rv}}) + q_{rd} \exp(\frac{\mathbf{E}[d]}{q_{rd}})) H(d_{ref} - \mathbf{E}[d]), \tag{5.11}
$$

where $q_{acc}$, $q_{rv}$, and $q_{rd}$ are constants, while the $H(d_{ref} - d)$ is a Heaviside's sigmoid function. Comparable to Shakouri and Ordys (2014), the (5.11) can behave similar to vanishing constraint, which slides continuously between two modes of car following, and cruising automatically depends on the presence of the preceding vehicle. In this subsection, each soft constraint is implemented based on implicit constraint method in the integral performance index. Note that the uncertain variation position of the preceding vehicle is taken into account during decision making that allows allocation of the tradeoff between risk and return of reference relative distance tracking. The robust SNMPC with the probabilistic constraint is reformulated in a computationally efficient certainty equivalent OCP.

The proposed Extended Eco-ACC system has been evaluated on the Colmar-berg test track, and numerical simulations are carried out using realistic values of the parameters. The prediction horizon $T = 15\,s$ is chosen to cover upcoming road geometry, traffic speed limit zone and the preceding vehicle motion prediction. This prediction horizon is discretised into $N = 30$ steps of size $\Delta t = 0.5\,s$.

For the sake of comparison, the proposed robust SNMPC with chance-constraint for the Extended Eco-ACC system is compared with a conventional Deterministic NMPC (DNMPC), where the velocity of the preceding vehicle is assumed to be constant during prediction. Furthermore, these two approaches are compared with the case that the motion of the preceding vehicle is known in advance namely Perfect NMPC (PNMPC). A sinusoid speed profile is considered as the simulation scenario to demonstrate the capabilities of the controllers for the unexpected behaviour of the preceding vehicle and their treatments to the state regulations, constraint fulfilment, and energy efficiency. Figure 5.26. shows the obtained results by the DNMPC, SNMPC, and PNMPC for the Eco-ACC system.

Figure5.26a shows the velocity profile of the host and preceding vehicle with DNMPC, SNMPC, and PNMPC. It can be observed that the velocity profile generated by the SN-MPC is closer to the PNMPC rather than the DNMPC. Figure 5.26b shows the relative distance regulations between the host and the preceding vehicles. Particularly, the SN-MPC fulfils the relative distance constraint with less violation rather than conventional DNMPC with relatively large deviation from reference relative distance. Moreover, an accident can be observed at time $116\,s$, while the SNMPC managing the situation properly. Figure 5.26c shows the control input profile. The DNMPC can be sensitive to unpredicted events that lead to non-smooth control behaviour with input constraint violation. On the other hand, the SNMPC not only demonstrates a robust behaviour against the uncertainties but also is capable of capturing similar behaviour to the PN-MPC. It is shown that the SNMPC generates better velocity profile and reference relative distance tracking than the DNMPC, which leads to a proper energy consumption profile. This can also be observed in Figure 5.26d that demonstrates the power and energy consumption of the DNMPC, SNMPC, and PNMPC with the maximum available power of the host vehicle.

The DNMPC can lead to a violation of maximum power constraint, and higher energy consumption than the SNMPC with relatively close to the PNMPC performance. Figure 5.27a demonstrates the velocity distribution of various controllers. While PNMPC has tight variation around the average velocity of the preceding vehicle $(10\,m/s)$, the SNMPC could regulate the velocity distribution with lower variation compared to DNMPC. The SNMPC enables forming the distribution of performance in terms of the first-moment and the second-moment. Figure 5.27b shows the probability of relative distance chance-constraint around the boundary region. The DNMPC failed to regulate relative safe distance, while the SNMPC could fulfil the chance-constraint lower bound requirement.
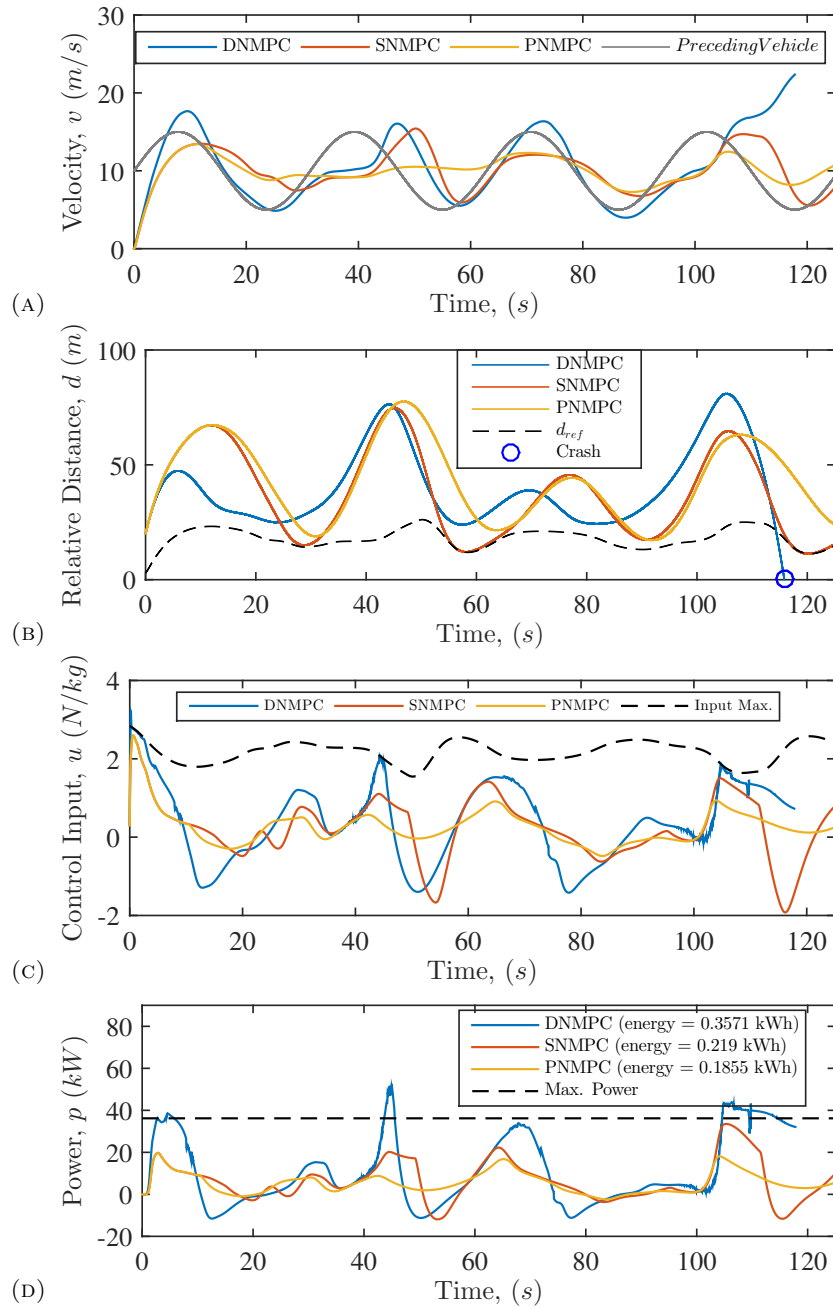
FIGURE 5.26: Performance of the DNMPC, SNMPC, and PNMPC with Smart-ED on the test track in terms of (A) velocity, (B) relative safe distance, (C) control input, and (D) power, with total energy consumption.
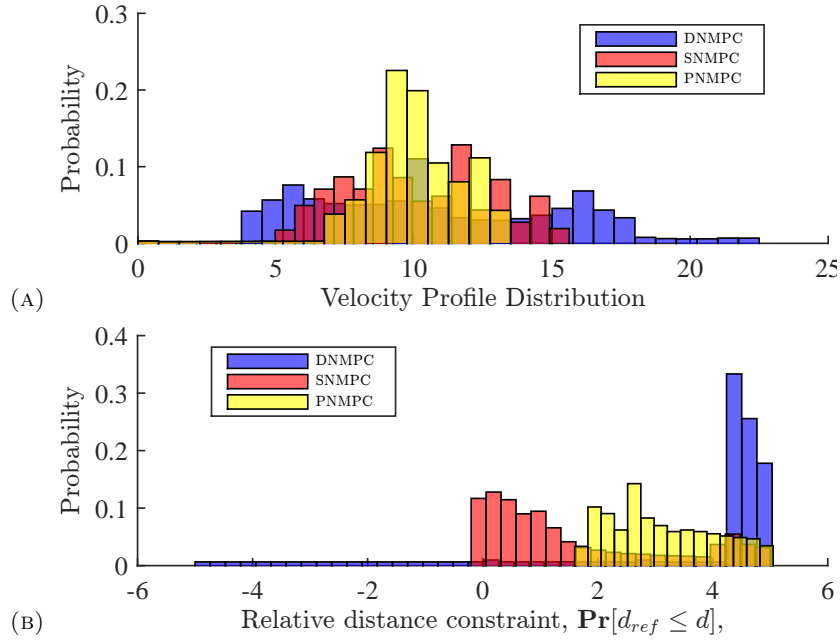
FIGURE 5.27: Performance of the DNMPC, SNMPC, and PNMPC in terms of (A) velocity distribution, (B) probability of chance-constraint around boundary region.

The OCP calculation time for the DNMPC is $2.9ms$, and the SNMPC is $3.2ms$ in average on an Intel® Core™ i7 with memory of 7.7 GiB. The computation time of the OCP might be compared with similar nonlinear and linear controllers proposed by Bichi et al. (2010) with $1s$, Md Abdus Samad Kamal et al. (2013) with $6.43ms$, and the Schmied et al. (2015) with $23.47ms$. In conclude, the proposed SNMPC could be considered a real-time capable optimal predictive controller for the proposed Eco-ACC system. For more details about the proposed fast SNMPC for the ADAS application, follow Seyed Amin Sajadi-Alamdari et al. (2017a).

### 5.3.3 Risk-averse SNMPC for Extended Eco-ACC

The Eco-ADAS concept proposed in Figure 5.25 is equipped with risk-averse SNMPC in this subsection. In the risk-averse SNMPC, the following performance index is formulated to achieve the ecological driving by linearly penalising the energy consumption of the host vehicle similar to the robust SNMPC as follows:

$$J_f(x_N) := q_f e_h, \tag{5.12}$$

where $q_f$ is the corresponding weight. This definition provides a flexible velocity profile planning in the integral performance index that can be formulated as follows:

$$J_c(x_i, u_i) := \frac{1}{2}(q_c(v_h - v_{h_{ref}})^2 + r_u(u - u_{ref})^2)$$
$$- q_{slk}u_{slk} + q_{crv,lmt}(v_h, f_{crv}(\delta(s_h)), f_{lmt}(s_h))v_h^2 + \mathcal{L}_\pi(\gamma), \quad (5.13)$$

where $v_{ref}$, $u_{ref}$ are desired cruising velocity. The lateral acceleration inequality constraint ($a_{lat.max}$) is defined as follows:

$$q_{crv,lmt}(v_h, f_{crv}(\delta(s_h)), f_{lmt}(s_h)) := \exp^{(q_{crv}(a_{lat} - a_{lat.max}))} + \exp^{(q_{lmt}(v_h - f_{lmt}(s_h)))}, \quad (5.14)$$

where $q_{crv}$, and $q_{lmt}$ are relative weights.

The risk-averse cost for the relative distance implicit inequality constraint ($d_{ref} \leq d$) can be formulated as follows:

$$\mathcal{L}_\mu(\gamma) := Q_w(v_h, \bar{v}_p, d)((\mathbf{E}[d] - d_{ref})^2 - \frac{2}{\gamma}\log(1 + \frac{\gamma^2}{2}\mathbf{Var}(d))). \quad (5.15)$$

The $Q_w(v_h, \bar{v}_p, d)$ is an equivalent to a soft barrier function that supplies enough weight to dominate the other objectives during the closing approach to the boundary value of reference relative distance defined as follows:

$$Q_w(v_h, \bar{v}_p, d) := q_{acc}(q_{rv}\exp(\frac{-(\bar{v}_p - v_h)}{q_{rv}}) + q_{rd}\exp(\frac{\mathbf{E}[d]}{q_{rd}}))H(d_{ref} - \mathbf{E}[d]), \quad (5.16)$$

where $q_{acc}$, $q_{rv}$, and $q_{rd}$ are constants. Note that the uncertain variation position of the preceding vehicle is taken into account during decision making that allows enhancement of the tradeoff between risk and return of reference relative distance tracking. In other words, the presence of variance of the random variable and adaptive weights enables the controller to show the proper control actions for the large system uncertainty.

The prediction horizon for the risk-averse SNMPC, $T = 15\,s$, is chosen to cover upcoming road geometry, traffic speed limit zone and the preceding vehicle motion prediction with $N = 30$ discretised steps. The constants in performance index function are set as $q_f = 2$, $v_{ref} = 20\,m/s$, $q_c = 2$, $q_{slk} = 1$, $q_{crv,lmt} = 1$, $a_{lat.max} = 3.7\,m/s^2$, $d_0 = 3\,m$, $t_{hw} = 1.5\,s$, $\gamma = -1$. The parameters for the physical-statistical model are set as $\mu_p = 0\,m/s^2$, $\delta_p = 1.5$, $\omega_{85th} = 0.67$, $m_1 = 20.41$, $m_2 = 13.68$, $m_3 = 13.23$, $m_4 = 151.2$.

The proposed risk-averse SNMPC for the Eco-ACC system is compared with a conventional nominal Deterministic NMPC (DNMPC). Furthermore, these two approaches are compared with the case that the motion of the preceding vehicle is known in advance
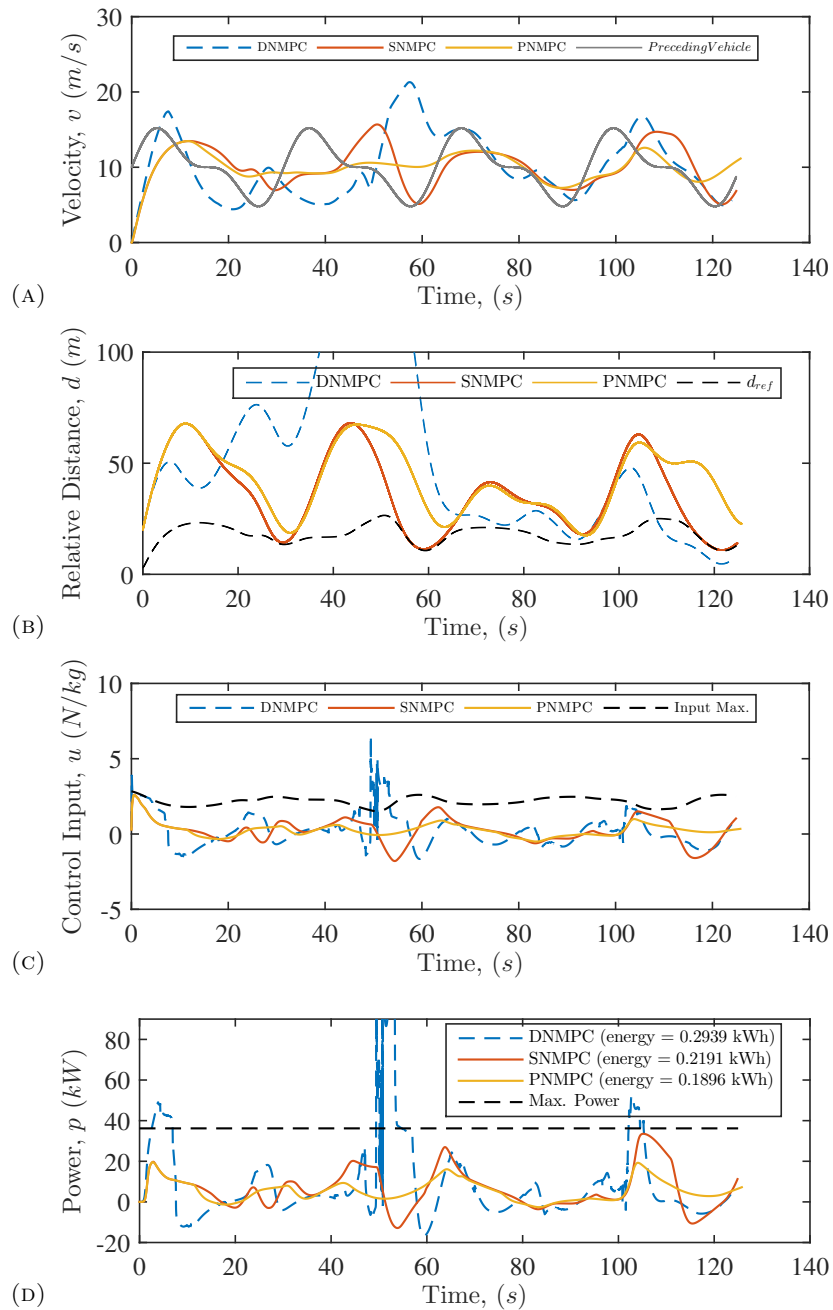
FIGURE 5.28: Performance of the DNMPC, SNMPC, and PNMPC in terms of (A) velocity, (B) relative safe distance, (C) control input, and (D) power, with total energy consumption.

namely Perfect NMPC (PNMPC). A trigonometric speed profile for the preceding vehicle is considered as the simulation scenario in order to demonstrate the capabilities of the controllers in state regulations, constraint fulfilment, and energy efficiency with their treatments to unpredicted preceding vehicle speed profile.

Figure 5.28. shows the results obtained by the DNMPC, risk-averse SNMPC, and PN-MPC for the Eco-ACC system. Figure5.28a shows the velocity profile of the host vehicle

with DNMPC, risk-averse SNMPC, and PNMPC setting as well as the preceding vehicle. The preceding vehicle has average velocity of $10\,m/s$, and it can be observed that the velocity profile generated by the SNMPC is closer to the PNMPC rather than the DNMPC. Figure 5.28b shows the relative distance regulation between the host and the preceding vehicles. Particularly, the risk-averse SNMPC fulfils the relative distance inequality constraint with less violation rather than conventional DNMPC with relatively large constraint violations from reference relative distance. Although the risk-averse SNMPC does not know the preceding vehicle velocity profile in advance, it is shown that it can effectively regulate the safe relative distance.

Figure 5.28c is related to the control input profile and it is shown that the DNMPC can significantly be sensitive to unpredicted events. This leads to a non-smooth control behaviour and the maximum input constraint violation. On the other hand, the risk-averse SNMPC demonstrates not only a robust behaviour against the uncertainties but also is capable of capturing similar behaviour to the PNMPC. It is shown that the risk-averse SNMPC generates better velocity profile than the DNMPC, which leads to a proper energy consumption profile. This can also be observed in Figure 5.28d that demonstrate the power and energy consumption of the DNMPC, SNMPC, and PNMPC with the maximum power of the host vehicle. It is shown that the DNMPC violates the maximum power constraint with higher energy consumption than the risk-averse SNMPC with relatively close to the PNMPC performance.

The OCP calculation time for the proposed risk-averse SNMPC is about $3\,ms$ in average on an Intel® Core™ i7 with memory of 7.7 GiB. Hence, the proposed risk-averse SNMPC could be a real-time capable controller for the proposed Eco-ACC system. For more details about the proposed risk-averse SNMPC for the Eco-ACC system, follow Seyed Amin Sajadi-Alamdari et al. (2017b).

### 5.3.4 RSNMPC with Open-loop EVaR for Extended Eco-ACC

The Eco-ADAS concept proposed in Figure 5.25 is provided with RSNMPC based on open-loop EVaR in this subsection. The EVaR is used as a coherent risk measure to quantify the risk involved in constraints violation.

The cost-per-stage function for Extended Eco-ACC system is defined as:

$$J_c(x_i, u_i) := \sum_{i=0}^{N-1} \parallel \hat{v}_{hi} - v_{h_{ref}} \parallel_q^2 + \parallel u_i - u_{ref} \parallel_r^2 + c\hat{e}_{hi}, \qquad (5.17)$$

with corresponding weights $q$, $r$, and $c$. The chance-constraints are based on the proposed RSNMPC for the semi-autonomous Eco-ACC system in Chapter 4.

The proposed Eco-ACC system has been evaluated with numerical simulations using realistic values of the parameters of the Smart-ED. The prediction horizon for the predictive controller is set to $T = 15\,s$ to cover upcoming road geometry, traffic speed limit zone and the preceding vehicle motion prediction with $N = 30$ discretised steps. The constants in performance index function are set as $q = 2$, $r = 110$, $c = 0.095$. The reference for the comfort lateral acceleration level is $\psi_{ref} = 3.7\,m/s^2$, and the confidence level for the relative distance chance-constraint is set to $\beta_3 = 0.95$ and quantified based the open-loop EVaR that is defined as follows:

$$EVaR_{1-\alpha_j}(h_j(\hat{x}_i)) := \inf_{z>0}\{z^{-1}ln(M_{h_j(\hat{x}_i)}(z)/\alpha_j)\}, \tag{5.18}$$

where $M_{h_j(\hat{x}_i)} = \mathbf{E}_{x_t}[\exp^{(zh_j(\hat{x}_i))}]$ is the moment-generating function of $h_j(\hat{x}_i)$. The control input box constraint and state inequality constraints are implemented based on the FB inequality handling method.

In order to compare the mentioned state-of-the-art methods with the proposed approach in a fair and informative manner, the European Urban Driving Cycle (EUDC) is used to represent the preceding vehicle velocity profile $(v_p)$. We have compared the proposed RSNMPC with the SMPC presented by Bichi et al. (2010), and the deterministic NMPC (DNMPC) introduced by Md Abdus Samad Kamal et al. (2013), to show the performance enhancements. The cruising velocity reference is fixed to $v_{h_{ref}} = 26\,m/s$ for all of the controllers with the same values for $d_0 = 4\,m$ and $t_{hw} = 3\,s$ considered by Bichi et al. (2010). Figure 5.29a shows the performance of various controllers in terms of velocity regulations. The DNMPC and RSNMPC track the preceding vehicle and cruising reference with less overshoot compared to the SMPC. The more steady velocity profile generated by RSNMPC provides the better drive comfort with lower energy consumption.

The proposed RSNMPC benefits from an improved penalty method to handle the soft inequality constraints in comparison to the DNMPC using the conventional soft penalty method (barrier method) and the SMPC using the quadratic cost function to handle the relative distance inequality constraint. Figure 5.29b and Figure 5.29c show the relative distance regulation performance and related histogram information around the violation region. The DNMPC hardly minimises the constraint violation while the SMPC regulates the relative distance irrespective of the violation of the reference tracking. On the other hand, the RSNMPC satisfies the chance-constraint lower bound requirement. Note that in Figure 5.29c, the positive values denotes the constraint satisfaction, while the negative values represent the constraint violation.
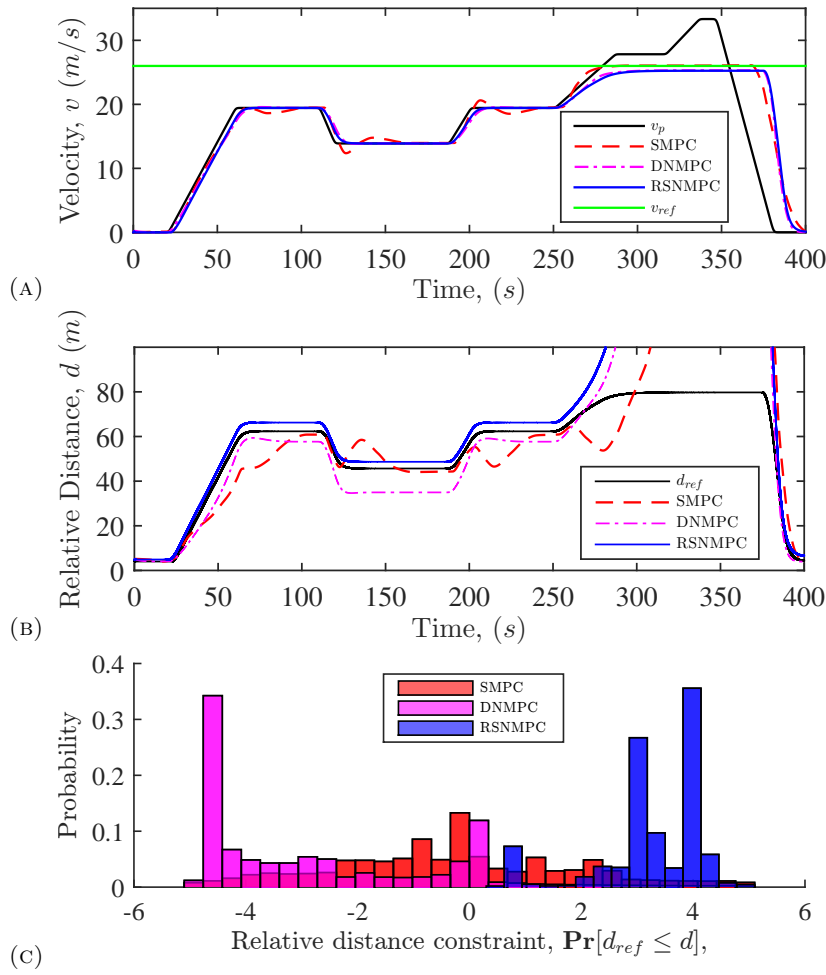
FIGURE 5.29: Performance of controllers for (A) Velocity regulation, and (B) Relative distance regulation, with (C) probability of chance-constraint around violation region

The OCP calculation time for the proposed RSNMPC is $1.1\,ms$ on the Intel® Core™ i7 with memory of 7.7 GiB, compared to the SMPC with $1\,s$ and DNMPC with $0.43\,ms$. Although the DNMPC is quicker than the RSNMPC, it has suffered from the low fidelity preceding vehicle motion model. The proposed RSNMPC is $+0.3\%$ more energy efficient than the DNMPC method, thanks to proper relative distance regulation. In the carried out simulations, the road is assumed to be flat and straight with no speed limit zones. Thus, there are few potentials to save energy which achieved by accounting the energy consumption dynamics. In other words, for longer trips with more hilly and curvy roads, our proposed method has higher potential to save energy.

### 5.3.5 Current-value Hamiltonian for Extended Eco-ACC

This subsection presents a real-time risk-averse SNMPC based on the current-value Hamiltonian to enhance the Eco-ACC system for the BEV. A discount factor is utilised

in the objective function to associate weights on costs at different stages within the prediction horizon. In addition, the open-loop EVaR as a coherent risk measure is used to quantify the risk involved in constraint violation and rear-ends collision by a tightest lower bound. It is resealable to assume that the predicted cost for long-term or infinite-time future prediction horizon is less costly in comparison to near-term future prediction horizon. Thus, the deterministic certainty equivalent cost function can be accomplished through the parameter $\rho$ that reduces the future cost to the present cost value. We investigate a certainty equivalent cost function with the discount factor on a long $N$. The cost-per-stage function for the Extended Eco-ACC system is defined as:

$$V_N(x_t, \boldsymbol{\pi}) := \sum_{i=0}^{N-1} (1 - \rho)^i (\parallel \hat{v_{hi}} - v_{h_{ref}} \parallel_q^2 + \parallel u_i - u_{ref} \parallel_r^2), \qquad (5.19)$$

where $\rho \in [0, 1)$ is the discount factor and $q, r$ are corresponding weights. It is noteworthy that $J_f(\hat{x}(t_f)) = 0$ which is know as the standard transversality conditions. In addition, the energy consumption of the BEV ($e_h$) is not considered to highlight the effect of the discount factor based SNMPC. Furthermore, the EVaR provides the tightest upper bound one can find using the Chernoff inequality for the VaR and CVaR with the same confidence levels. The chance-constraints are based on the proposed RSNMPC for the semi-autonomous Eco-ACC system in Chapter 4. In addition, the hard and soft inequality constraints is handled based on the FB method.

The prediction horizon for the predictive controller is set to $T = 10\,s$ with $N = 20$ discretised steps. The constants in performance index function are set as $Q = diag[0, 1, 0, 0, 0]$, $R = diag[40]$. The confidence level for the relative distance chance-constraint is set to $\beta_3 = 0.95$ with close spacing setting as $d_0 = 6\,m$ and $t_{hw} = 1.5\,s$, which improves traffic flow microscopically. The performance of the current-value Hamiltonian controller is simulated on the Colmar-Berg test track in Luxembourg. Figure 5.30a shows the performance of velocity regulations with the current-value Hamiltonian based RSNMPC in compare to Perfect NMPC (PNMPC), where the uncertainty is exactly known in advance along the prediction horizon.

The controllers speeding up until the BEV reaches the first and second curves ($20 \leq t \leq 40$) where the lateral acceleration constraint should be satisfied. As it is shown, the RSNMPC is faster than the PNMPC controller. However, during the first and second curves, the RSNMPC and PNMPC show similar behaviour. Figure 5.30b shows the relative distance regulation performance, where the RSNMPC is more conservative than PNMPC in this part of the test track. Afterwards, the controllers increase the velocity again up to the point the third and fourth curves are in their prediction horizon ($83 \leq t \leq 109$), where both controllers slow down to fulfil the lateral acceleration constraint
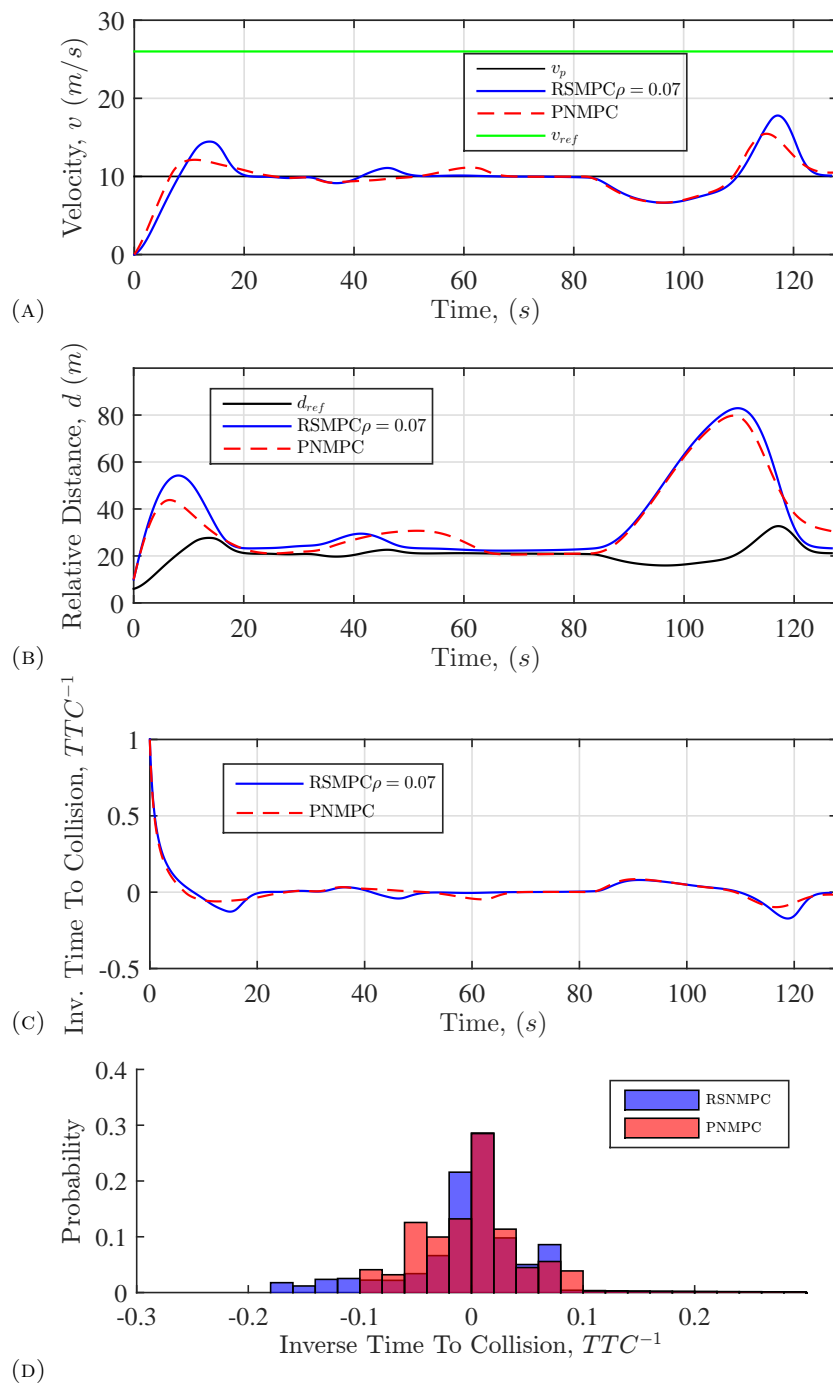
FIGURE 5.30: Performance of RSNMPC vs. PNMPC for (A) Velocity regulation, (B) Relative distance regulation, (C) and (D) Inverse Time To Collision

on curves. Since the RSNMPC is not aware of the future realised velocity profile of the preceding vehicle, it shows less optimum behaviour in compare to the PNMPC. However, the RSNMPC shows similar behaviour close to the PNMPC performance within $64 \leq t \leq 114$. Finally, the controllers speed up once more to reach the starting point while satisfying the relative distance safety constraint.

Figure 5.30c and Figure 5.30d show the performance of the RSNMPC in comparison to the PNMPC in terms of Inverse of Time To Collision ($TTC^{-1}$) which is defined as:

$$TTC^{-1} := \frac{v_p - v_h}{d} \tag{5.20}$$

The $TTC^{-1}$ probability distribution is a direct and continuous indicator of the collision risk. It is noteworthy that the lower values indicate the more dangerous situations, while zero implies the preserving trend. The RSNMPC shows sharp velocity and relative distance regulations, which increase its energy consumption. However, due to statistically accurate prediction model of the preceding vehicle and considering the upcoming road geometries with energy consumption map of the Smart-ED, the RSNMPC is +90% as energy-efficient as PNMPC on the test track despite unknown system uncertainty.

Furthermore, in order to compare the mentioned works of literature with the proposed RSNMPC approach in a fair and informative manner, the EUDC is used to represent the preceding vehicle velocity profile. The proposed RSNMPC has been compared with the SMPC presented by Bichi et al. (2010) and deterministic NMPC (DNMPC) introduced by Md Abdus Samad Kamal et al. (2013) to show the performance enhancements. The cruising velocity reference is fixed to $v_{h_{ref}} = 26 \, m/s$ with the same values for $d_0 = 4 \, m$ and $t_{hw} = 3 \, s$ considered by Bichi et al. (2010). Figure 5.31a shows the performance of controllers in terms of velocity regulations. The RSNMPC tracks the preceding vehicle and cruising reference with less over/under-shoot compared to the SMPC. Figure 5.31b shows the relative distance regulation performance. The DNMPC and SMPC hardly satisfy the safety constraint with large variance around the violation region. On the other hand, the RSNMPC fulfil the chance-constraint lower bound requirement with minimum variance. This is shown in Figure 5.31c by noting that the positive values are the constraint satisfaction, while the negative values represent the constraint violation.

The OCP calculation time for the proposed RSNMPC is around $5.7 \, ms$, compared to the SMPC with $1 \, s$ and DNMPC with $2.2 \, ms$ on the Intel$^{®}$ Core$^{TM}$ i7 with a memory of 7.7 GiB PC. The proposed RSNMPC is +0.5% more energy efficient than the DNMPC method which respects the OCP inequality constraints satisfaction. In the carried out simulations, the road is assumed to be flat and straight with no speed limit zones. Thus, there are few potentials to save energy, which is achieved by accounting the energy
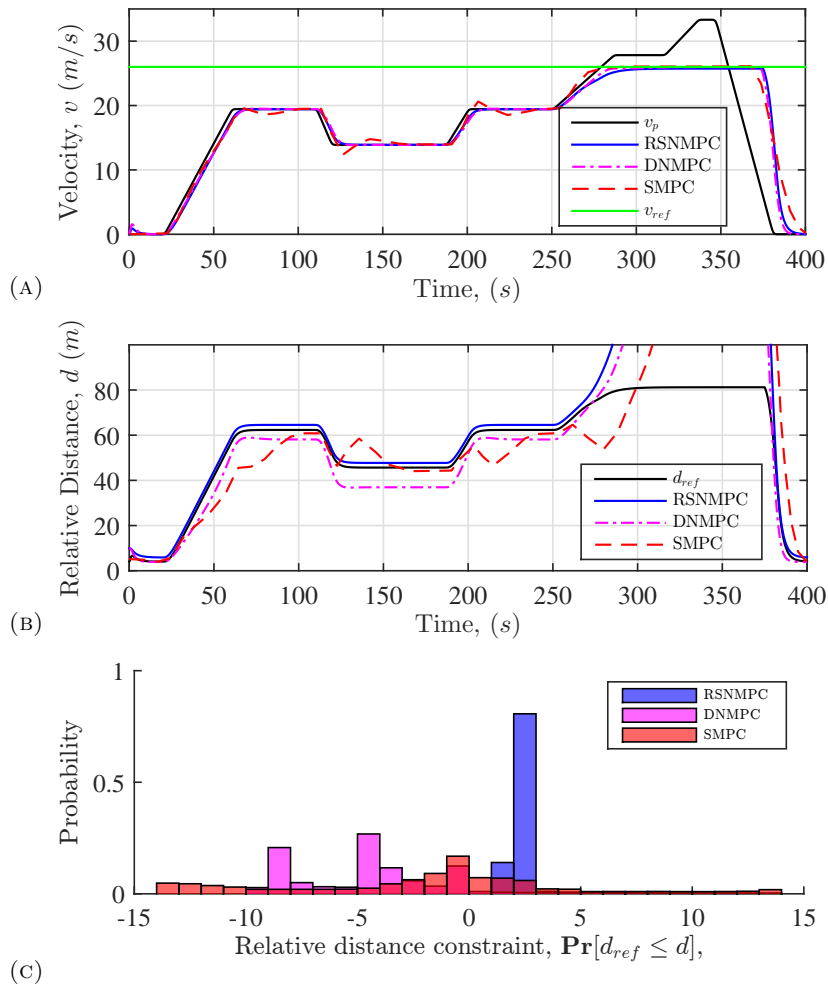
FIGURE 5.31: Performance of controllers for (A) Velocity regulation, and (B) Relative distance regulation, with (C) probability of chance-constraint around violation region

consumption dynamics. In other words, for longer trips with more hilly and curvy roads, the proposed method has higher potential to save energy.

### 5.3.6 RSNMPC with Closed-loop EVaR for Extended Eco-ACC

In this subsection, the Eco-ADAS concept proposed in Figure 5.25 is extended with RSNMPC based on closed-loop EVaR evaluation. The EVaR is used as a coherent risk measure to quantify the risk involved in constraints violation. The proposed closed-loop confidence level $\{\beta_i(t)\}_{m-1}^0$ is estimated based on a *Two-pass* algorithm to compute the standard deviation using the *Exponential Moving Average* of the past $M$-measurement vector. In this method, the samples moving average is calculated by:

$$\bar{p} = \frac{\sum_{j=0}^{m-1} x_j}{M}. \tag{5.21}$$

Afterwards, the unbiased estimation of the variance of samples can be computed based on the Bessel's correction given by:

$$\text{Var}(P) := \sigma^2 = \frac{\sum_{i=0}^{m-1}(p_i - \bar{p})^2}{M - 1}, \tag{5.22}$$

where $\sigma$ is the corrected sample standard deviation ($\sigma = \sqrt{\text{Var}(P)}$). This algorithm is numerically stable if $M$ is small (for more details see Einarsson (2005)). Generally, the standard deviation is considered as a tuning parameter in works of literature. A larger value results in conservative but robust behaviour, while a small value could lead to high performance but more frequent constraints violation. However, the proposed method to estimate the standard deviation utilises the advantages of feedback to reduce the conservative behaviours of the risk-averse chance-constraints and improves the tradeoff between the performance and robustness.

The cost-per-stage function for the Extended Eco-ACC system is defined as:

$$V_N(x_t, \boldsymbol{\pi}) := \sum_{i=0}^{N-1} \| \hat{v}_{hi} - v_{h_{ref}} \|_q^2 + \| u_i - u_{ref} \|_r^2 + c\hat{e}_{hi}, \tag{5.23}$$

with corresponding weights $q, r$, and $c$. The control input is limited by:

$$u_{min}(v) \leq u \leq u_{max}(v). \tag{5.24}$$

The chance-constraints are based on the proposed RSNMPC in Chapter 4.

Achieved simulation results demonstrate the effectiveness of the RSNMPC for the semi-autonomous BEV in terms of safe, energy-efficient states regulation and constraints satisfaction based on the Eco-ACC system. The prediction horizon for the predictive controller is set to $T = 10\,s$ to cover upcoming road geometry, traffic speed limit zones and the preceding vehicle motion prediction with $N = 20$ discretised steps. The constants in the performance index function are set to $q = 1$, $r = 110$, $c = 1$.

Figure 5.32 shows the simulation results of the proposed RSNMPC for the optimal energy management of the BEV on a realistic hilly and curvy road of the test track. In this setup, the BEV follows the preceding vehicle with the close spacing setting as $d_0 = 6\,m$ and $t_{hw} = 1.5\,s$ which could improve traffic flow microscopically. Performance of the RSNMPC is compared with a Perfect NMPC (PNMPC), which the behaviour of the preceding vehicle is exactly known in advance along the prediction horizon. Figure 5.32a shows the BEV velocity profile. The BEV speeds up to the first and second curves ($20 \leq t \leq 40$) where it has to slow down where the lateral acceleration constraint should be satisfied. As it is shown, the RSNMPC is faster than the PNMPC controller due to
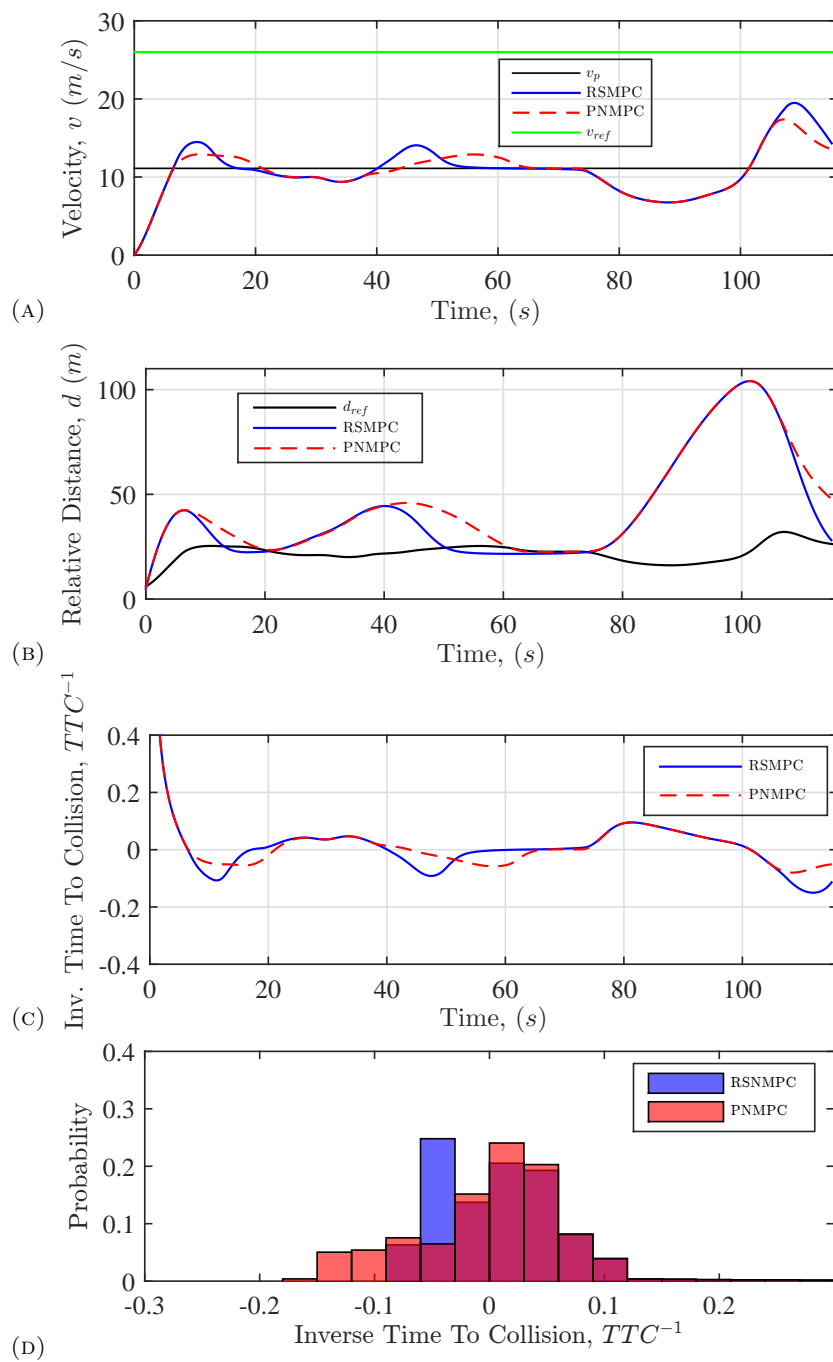
FIGURE 5.32: Performance of RSNMPC vs. PNMPC for (A) Velocity regulation, (B) Relative distance regulation, (C) and (D) Inverse Time To Collision

lack of knowledge from the preceding vehicle behaviour and assuming that the preceding vehicle will speed up. However, during the first and second curves, the RSNMPC and PNMPC show similar behaviour due to more accurate prediction. Figure 5.32b shows the relative distance regulation performance where the RSNMPC is more aggressive than PNMPC in this part of the test track. This is due to the constant velocity profile of the preceding vehicle with perfect measurement in a simulation environment leads to low variance estimation in relative distance measurement. Therefore, the EVaR evaluation causes the relative distance chance-constraint to be treated with low confidence level. Afterwards, the controllers increase the velocity again up to the point where the third and fourth curves are in its prediction horizon ($83 \leq t \leq 109$) where both controllers slow down to fulfil the relative distance and the lateral acceleration constraints on curves. Since the RSNMPC is not aware of the future realised velocity profile of the preceding vehicle, it shows less optimum behaviour in comparison to the PNMPC. However, the RSNMPC shows similar behaviour close to the PNMPC performance within $66 \leq t \leq 106$. Finally, both controllers speed up once more to reach the starting point while satisfying the relative distance safety constraint.

Figure 5.32c and Figure 5.32d show the performance of the RSNMPC in comparison to PNMPC in terms of $TTC^{-1}$ probability distribution. The $TTC^{-1}$ is a direct and continuous indicator of the collision risk. The lower values indicate the more dangerous situations while zero implies the preserving trend. The RSNMPC shows sharper velocity and relative distance regulations which could increase its energy consumption. However, due to the statistically accurate prediction model of the preceding vehicle and considering the upcoming road geometries with energy consumption map of the Smart-ED, the RSNMPC is approximately $+89\%$ as energy-efficient as the PNMPC on the test track despite unknown preceding vehicle behaviour.

In addition, to demonstrate the performance enhancements and compare the proposed approach with the mentioned state-of-the-art methods in a fair and informative manner, the EUDC is used to represent the preceding vehicle velocity profile ($v_p$). The proposed RSNMPC with closed-loop EVaR is compared with the deterministic NMPC (DNMPC) introduced by Md Abdus Samad Kamal et al. (2013), the SMPC presented by Bichi et al. (2010), and distributionally Robust SNMPC (RNMPC) presented in 5.3.2, which is configured with *worst case scenario*. The cruising velocity reference is fixed to $v_{h_{ref}} = 26\,m/s$ for all of the controllers with the same values for $d_0 = 4\,m$ and $t_{hw} = 3\,s$ considered by Bichi et al. (2010).

Figure 5.33a shows the performance of different controllers in terms of velocity regulations. The DNMPC, RNMPC, and RSNMPC track the preceding vehicle and cruising reference with less overshoot compared to the SMPC. The proposed RSNMPC benefits
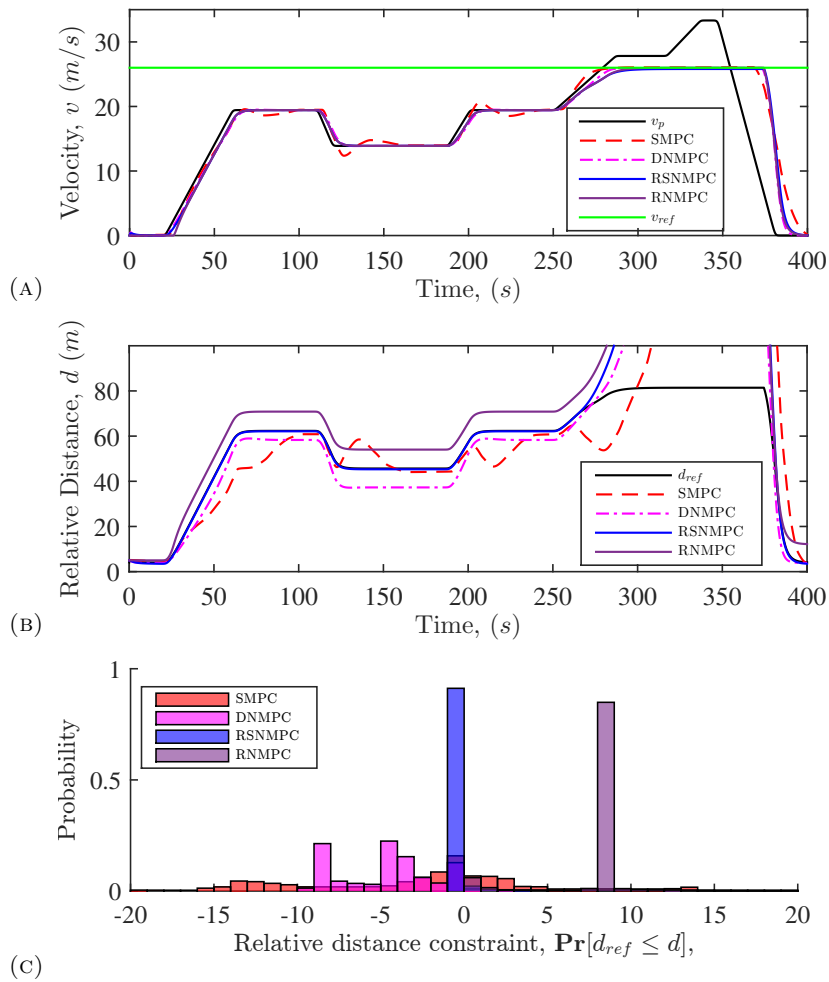
FIGURE 5.33: Performance of controllers for (A) Velocity and (B) Relative distance regulations, with (C) probability distribution of chance-constraint around violation region

from the closed-loop EVaR inequality constraints handling method, compared to the DNMPC using the conventional soft constrained penalty method as well as the SMPC using the quadratic cost function to handle the relative distance inequality. Figure 5.33b and Figure 5.33c show the relative distance regulation performance and related histogram information around the violation region. The DNMPC hardly minimises the constraint violation, while the SMPC regulates the relative distance irrespective of the violation of the reference tracking. The RNMPC shows a too conservative behaviour, where the RSNMPC satisfies the chance-constraint performance requirement. Note that in Figure 5.33c, the positive values denote the constraint satisfaction, while the negative values represent the constraint violation. The proposed RSNMPC is approximately +1% more energy efficient than the DNMPC method, thanks to proper relative distance regulation. In the carried out simulations, the road is assumed to be flat and straight with no speed limit zones. Thus, there are few potentials to save energy, which is achieved

|             | SMPC | DNMPC  | RNMPC  | RSNMPC |
|-------------|------|--------|--------|--------|
| Eco. (kWh)  | -    | 1.4778 | 1.4770 | 1.4680 |
| OCP (ms)    | 1000 | 2.2    | 3.5    | 5.3    |

TABLE 5.1: Energy consumption and computation time of OCPs

by accounting the energy consumption dynamics. In other words, for longer trips with more hilly and curvy roads, the proposed method has higher potential to save energy.

The OCP calculation time for the proposed RSNMPC is $5.3\,ms$ on the Intel® Core™ i7 with a memory of 7.7 GiB PC, in comparison to the SMPC with $1\,s$; the RNMPC with $3.5\,ms$, and the DNMPC with $2.2\,ms$. Although the DNMPC is faster than the RSNMPC and RNMPC, it has suffered from the low fidelity preceding vehicle motion model. Furthermore, the more steady velocity profile with proper constraints satisfaction, which is generated by the RSNMPC provides a better drive comfort with lower energy consumption. An overlay energy consumption and average computation time of the OCP is given in Table 5.1 to conclude this subsection.

## 5.4 Conclusions

In this chapter, it is found that the proposed RSNMPC is robust against the Smart-ED model parameters error and its energy consumption model mismatch. The proposed system is capable to track the desired reference without significant deviation. Various Eco-driving techniques such as taking advantage of the gravity, energy efficient velocity profile in road curvatures, taking the speed limit zones into account, and safe relative distance regulation to the preceding vehicle assessed. The capability of the RSNMPC with different settings such as the influence of the prediction horizon, confidence level of the chance-constraint, and discount factor evaluated in the numerical simulation environment. Performance of the RSNMPC for the semi-autonomous Eco-ACC system in different scenarios examined and the achieved results in terms of the safety and energy efficiency of the BEV compared with the state-of-the-art methods to demonstrate the capabilities of the proposed system. Based on these findings, the following chapter will evaluate the proposed RSNMPC applied on the semi-autonomous Eco-ACC system based on field experimental results.

# Chapter 6

# Practical Implementation

The proposed RSNMPC for the semi-autonomous Eco-ACC system is experimentally implemented to validate the results of this study for the BEV. The field experimental test is carried out on the test track located at Centre de Formation pour Conducteurs S.A. Colmar-Berg, Luxembourg. The RSNMPC is experimentally implemented on the Smart-ED as the host vehicle and a city vehicle *Peugeot 108* is chosen to represent the preceding vehicle. The required sensors, computation resource, and the actuators are installed on the Smart-ED. The localisation and position of the host BEV is calculated based on the GPS sensor. The states of the Smart-ED such as velocity and battery voltage are updated by the CAN through the OBD interface. The relative distance and relative velocity of the preceding vehicle is measured by a 77GHz RADAR. The onboard computational resource operated by the Linux based Robot Operating System (ROS) is foreseen to mount on the Smart-ED. A connection panel is developed for the sensor power supply and the actuators port connection. The control input of the proposed RSNMPC is realised by manipulating either the accelerator or the brake actuators.

This chapter is structured as follows. Section 6.1 presents the required setup including the sensors, computational resource, and actuators for the practical implementation of the RSNMPC on the Smart-ED. Section 6.2 provides the field experimental results, which are carried out on the test track aimed to cover different traffic situations including cruising, car-following, cut-in/out, and Stop&GO. Section 6.3 concludes the findings of this chapter.

## 6.1   Practical Implementation Setup

The RSNMPC is experimentally implemented on the Smart-ED as the host vehicle and a city vehicle *Peugeot 108* is chosen to represent the preceding vehicle. Figure 6.1 shows

FIGURE 6.1: Smart Fortwo Electric Drive and the *Peugeot 108* on the test track

the Smart-ED and the *Peugeot 108* on the test track located at Centre de Formation pour Conducteurs S.A. Colmar-Berg, Luxembourg (CFC, 2015). This section presents the detailed information about the sensors, computation resource, and the actuators installed on the Smart-ED.

### 6.1.1   Sensors

The localisation and position of the host BEV are calculated based on the GPS sensor. In order to localise the Smart-ED, the test track position $(s_h)$ is mapped based on lookup table with linear interpolation to the related GPS coordinates latitude and longitude. The Euclidean deviation of GPS measurement from latitude and longitude pairs is computed and the pair with the smallest deviations is taken as the current position of the Smart-ED (Tim Schwickart, Voos, Hadji-Minaglou, et al., 2016). The used GPS has a ROS interface with an output compatible with National Marine Electronics Association (NMEA) sentences. Figure 6.2 shows the used GPS sensor on the Smart-ED.

The CAN-bus data is accessible by a CAN reader through the OBD interface. The Smart-ED state information such as velocity, battery voltage, battery current, and etc are updated by having access to the CAN messages. The CAN adapter enables connection to the CAN network. Figure 6.3 shows the CAN adapter installed in the Smart-ED.

The CAN adapter is connected to the Smart-ED through the OBD interface (Figure 6.4).

FIGURE 6.2: GPS sensor installed on the Smart-ED



FIGURE 6.3: CAN adapter installed in Smart-ED



FIGURE 6.4: OBD interface of the Smart-ED

FIGURE 6.5: RADAR sensor installed on the Smart-ED

The ACC functionality succeeds or fails with the detection of the relevant target vehicle, which is the basis for the control (Eskandarian, 2012). The RADAR is successfully used as surrounding sensor technologies. The RADAR that is manufactured by the Delphi ESR has been used for the proposed Eco-ACC system. The detail and specification of this sensor to detect and track the preceding vehicle provided in the previous Chapter (3.1). Figure 6.5 shows the RADAR sensor that is installed on the Smart-ED.

Target selection strategy carries a great importance to the quality of the ACC system (Eskandarian, 2012). There are several target selection methods such as path prediction and the driving corridor, which was reviewed by Eskandarian (2012). In this study, the preceding vehicle is detected and tracked based on the driving corridor with the extra criteria for target selection. First, the driving corridor based on the Smart-ED is created. Second, any object within this corridor is considered as a candidate for the preceding vehicle. The closest object which has a positive velocity more than the $1\,m/s$ is selected as the preceding vehicle. It is noteworthy that any object lower than the $1\,m/s$ is chosen as a static object which is used for the Automatic Emergency Braking (AEB) system. Then, the selected target from the RADAR signal is smoothed based on the *Exponential Moving Average* of the past $M$-measurements. The moving average filter is used to overcome the target selection limits such as losing the target during the road curvatures variations.

### 6.1.2 Computation Resource and Port Connection Panel

The online solution of the OCP with the minimum computation delay is an essential requirement for the real-time RSNMPC. One of the effective methods to achieve a

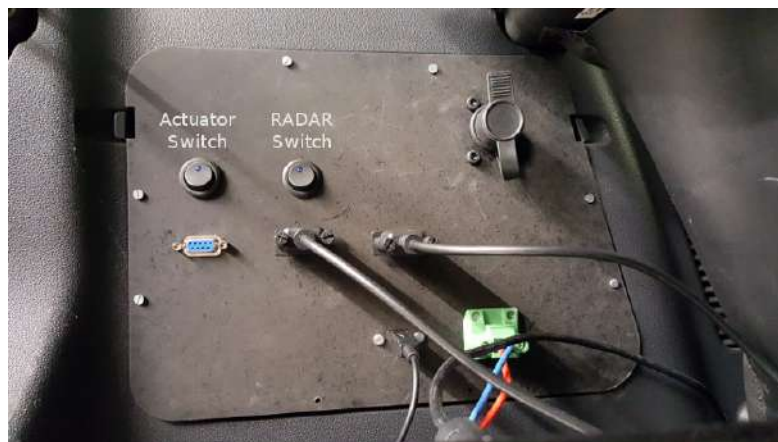FIGURE 6.6: In-vehicle computer by Acrosser installed on the Smart-ED



FIGURE 6.7: Port connection panel installed on the Smart-ED

fast RSNMPC is to have a powerful computation resource. In this study, the onboard computational resource for the Extended Eco-ACC system is foreseen by the Linux based ROS on the Intel® Core™ i7 with a memory of 7.7 GiB In-vehicle computer. The ROS is a flexible framework for writing robot software. It is a collection of tools, libraries, and conventions that aim to simplify the task of creating complex and robust robot behavior across a wide variety of robotic platforms (Willow Garage, 2017). Figure 6.6 shows a commercial In-vehicle computer provided by Acrosser installed on the Smart-ED. In addition, a connection panel is designed and developed for the Eco-ACC system for the RADAR power supply and actuators connection. Figure 6.7 shows the port connection panel installed on the Smart-ED.

### 6.1.3 Actuators

The actuators of the Smart-ED are modified in order to transform the control input signal into motion. The control input of the proposed RSNMPC is realised by actuating either the accelerator or brake pedals. The control input $u\,(N/Kg)$ is a high-level control

FIGURE 6.8: E-accelerator to manipulate the Smart-ED acceleration



FIGURE 6.9: E-accelerator installed on the Smart-ED

command, which is converted into two low-level control signals for the accelerator and brake pedals. The control input is considered as the reference value for the low-level controllers, which is a function of velocity and pedals position. The control input is mapped to the position of relative actuator pedals as well as velocity, which is measured on a dynamometer test bench. Given the high-level control input computed by the RSNMPC and the velocity of the Smart-ED provided by the CAN network, the relative position for the accelerator and brake pedals can be computed. This computation is based on the lookup tables with a linear interpolation.

The accelerator pedal is replaced by an electronic board (E-accelerator) to manipulate the required acceleration and to imitate the electric signals generated by the original accelerator pedal of the *Smart-ED*. Figure 6.8 shows the E-accelerator, which is the Arduino based microcontroller development kit provided by the *Teensy*. Figure 6.9 shows the accelerator pedal replaced by the E-accelerator. In addition, Figure 6.10 shows the accelerator transition response of the BEV. Figure 6.10a shows a full step response from initial value 0% to 100% with $130\,ms$ rise time. Furthermore, the step response from initial value 100% to 0% with $130\,ms$ rise time is shown in Figure 6.10b.

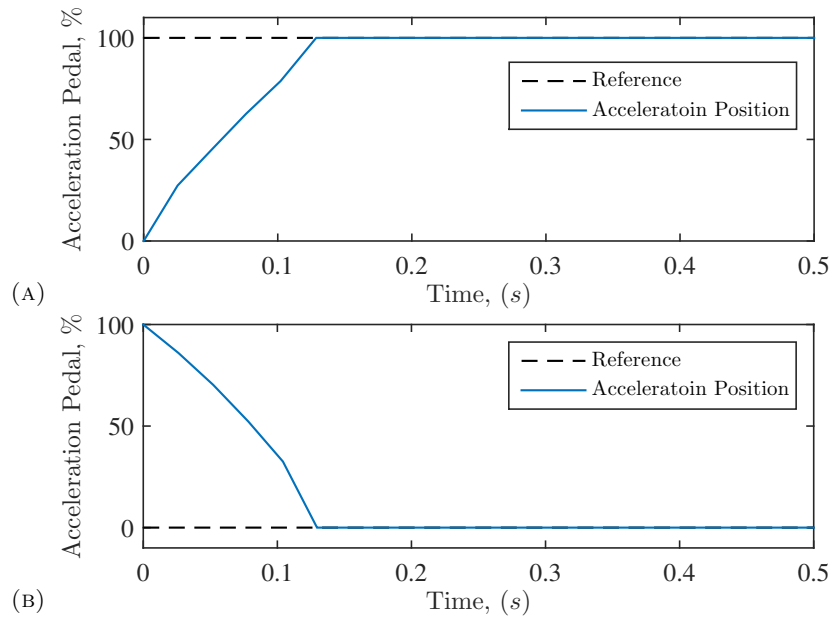In addition, the brake actuator of the Smart-ED is manipulated by an electric stepper

(A)

(B)

FIGURE 6.10: The Smart-ED acceleration transient response (A) $0 - 100\%$ Step response, (B) $100 - 0\%$ Step response.



FIGURE 6.11: Brake pedal actuator installed on the Smart-ED

motor that is connected to the brake pedal by a planetary gearbox and flexible cable. The electric stepper motor with a high-torque economy planetary gearbox is manufactured by the *Nanotec*. The flexible cable connects the rear brake pedal to a rotary disk. The automatic brake pedal actuation is designed in a way that preserves the possibility for the driver to apply brake in emergency cases. Figure 6.11 shows the configuration of the installed brake pedal actuator on the Smart-ED.

Figure 6.12 shows the brake transition response of the BEV. It is noteworthy that a two-degree-of-freedom PID controller (2 DOF) as the low level brake actuator controller is implemented. Figure 6.12a shows a full step response from initial value $0\%$ to $60\%$
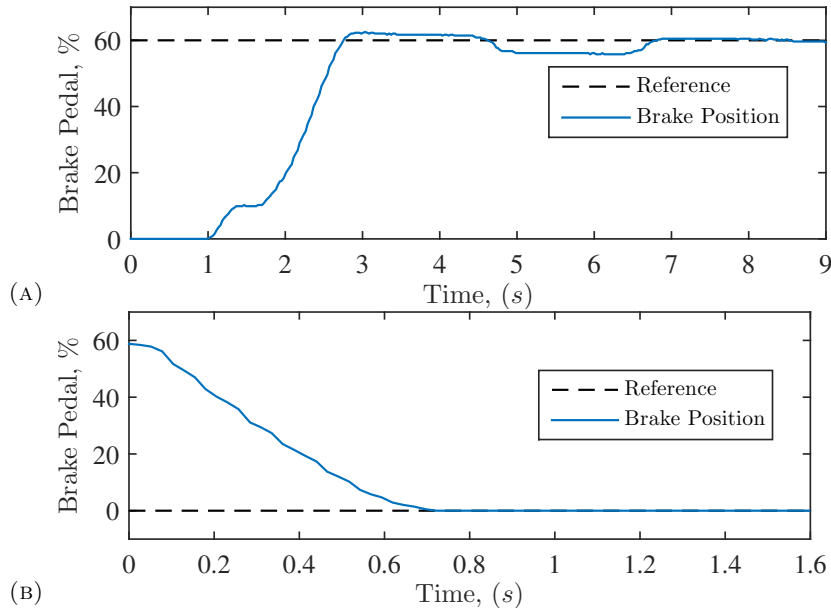
FIGURE 6.12: The Smart-ED brake transient response (A) $0-60\%$ Step response, (B) $60-0\%$ Step response.

with $2.7\,s$ rise time and $0.97\,s$ Dead-time. Furthermore, the step response from initial value $60\%$ to $0\%$ with $0.72\,s$ rise time is shown in Figure 6.12b. It is essential to account for the control input delay in the NMPC. The 6.1 represents the delay of the control input as follows:

$$\frac{u_p(t)}{dt} = k_p(u(t) - u_p(t)), \tag{6.1}$$

where $k_p$ is the constant the denotes the delay of the control input $u(t)$ (Yamaguchi et al., 2012).

## 6.2 Field Experimental Results

This section presents the overall performance of the SEDAS concept in terms of the states regulation, safety, and energy efficiency in various predictive control configurations and driving situations. The field experimental results of the deterministic NMPC applied on the Extended Eco-CC, in addition with the Risk-averse SNMPC, the current-value Hamiltonian SNMPC, and RSNMPC with open-loop and closed-loop EVaR for the Extended Eco-ACC are presented.

### 6.2.1 NMPC for Extended Eco-CC

The concept of the proposed Extended Eco-CC system based on the RSNMPC for the BEV on a hilly road with road curvatures and traffic speed limits (based on Figure 5.22)

are experimentally evaluated on the test track located at Centre de Formation pour Conducteurs S.A. Colmar-Berg, Luxembourg (CFC, 2015). In this study, the final cost function of the RSNMPC, $J_f$ is chosen as:

$$J_f(x_N) = \parallel \hat{v}_{hN} - v_{h_{ref}} \parallel_{q_f}^2 + c_f \hat{e}_{hN} \tag{6.2}$$

with the corresponding weights $q_f$ and $c_f$. The cost-per-stage function for the Extended Eco-ACC system is defined as:

$$J_c(x_i, \pi_i) := \sum_{i=0}^{N-1} \parallel \hat{v}_{hi} - v_{h_{ref}} \parallel_q^2 + \parallel u_i - u_{ref} \parallel_r^2 + c\hat{e}_{hi}, \tag{6.3}$$

with corresponding weights $q, r$, and $c$. The prediction horizon $T = 15\,s$ is chosen to cover upcoming road and traffic events. This prediction horizon is discretised into $N = 30$ steps of size $\Delta t = 0.5\,s$ based on the approximate vehicle's actuators maximum delay time. Achieved field experimental results demonstrate the effectiveness of the proposed method for the semi-autonomous BEV in terms of safe and energy-efficient states regulation and constraints satisfaction based on the Extended Eco-CC system. The constraints are handled based on barrier method and control input weight ($r = 550$).

Figure 6.13 shows the field experimental results of the proposed RSNMPC for the optimal energy management of the BEV on a realistic hilly and curvy road of the test track. In this setup, the BEV is set to cruise at the $v_{ref} = 50\,km/h$. Performance of the RSNMPC (Exp-RSNMPC) is compared with a simulation result (Sim-RSNMPC). Figure 6.13a shows the BEV velocity profile generated by RSNMPC for the both experimental and simulation. The controllers increase the velocity of the BEV from standstill to reach the desired velocity ($v_{ref}$). However, the velocity decreases as the vehicle approaches the first and second curves where the lateral acceleration constraint becomes active ($220 \leq s \leq 440$). After the second curve, the controllers increase the velocity of the BEV to reach the reference value ($550 \leq s \leq 700$) where it is the only opportunity to reach the desired velocity. By approaching to the third and forth curves, the velocity of the BEV has to be reduced to satisfy the lateral acceleration inequality constraint. Figure 6.13b shows the BEV power consumption profile of the BEV generated by the RSNMPC for both field experiment and simulation. Figure 6.14a and Figure 6.14b show the performance of the experimental RSNMPC in comparison to the simulation RSNMPC in terms of probability distribution.

In addition, a modified version of the RSNMPC with a low weight on the control input ($r = 40$) is tested with the prediction horizon $T = 10\,s$. The control input delay in this version is considered in the respective OCP. This prediction horizon is discretised into $N = 20$ steps and the constraints are handled based on the FB method. Figure 6.15
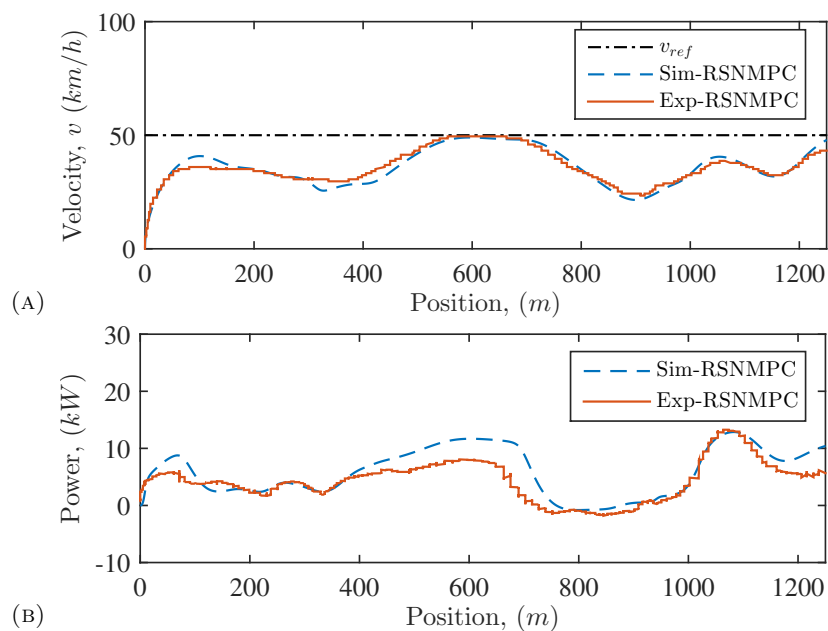
FIGURE 6.13: Performance of field experimental RSNMPC vs. simulation RSNMPC at $50\,km/h$ for (A) Velocity regulation, (B) Power consumption.
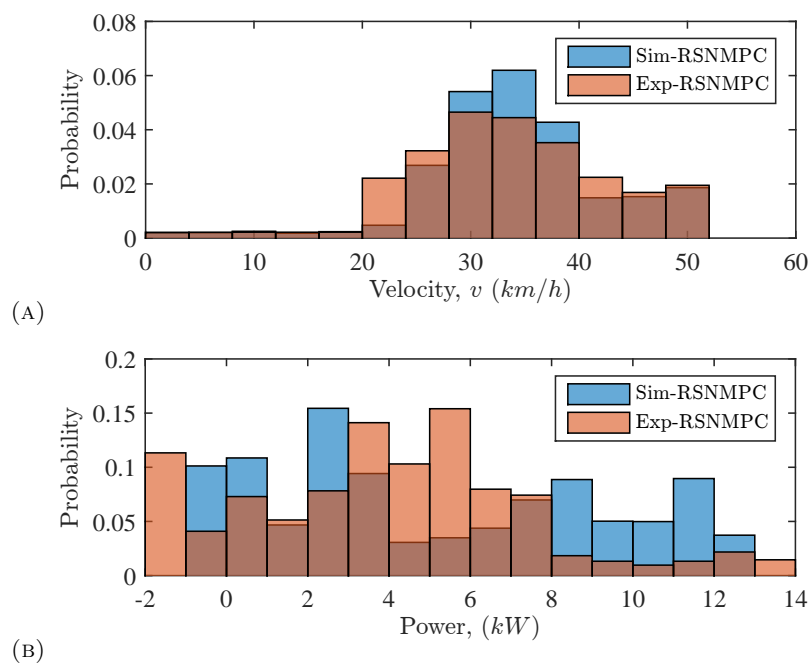


FIGURE 6.14: Performance distribution of field experimental RSNMPC vs. simulation RSNMPC at $50\,km/h$ for (A) Velocity regulation, (B) Power consumption.
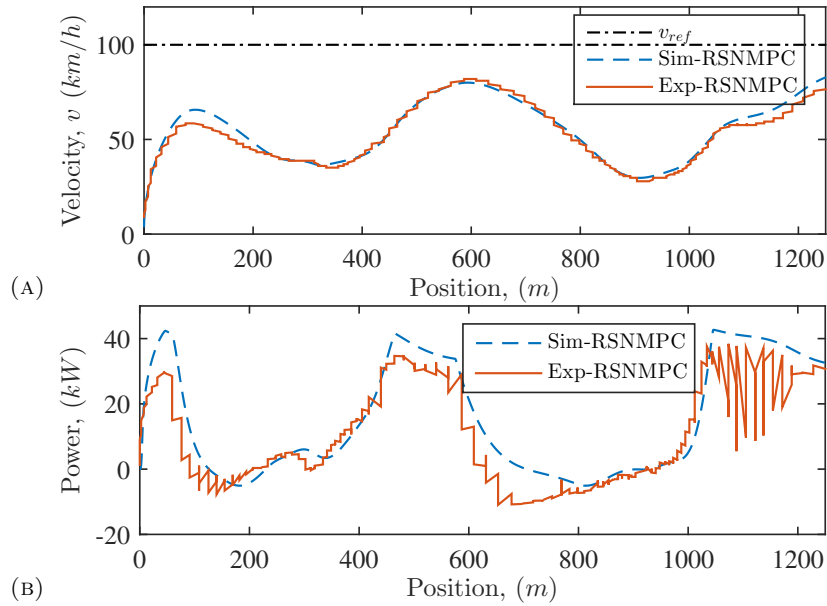
(A)

(B)

FIGURE 6.15: Performance of field experimental RSNMPC vs. simulation RSNMPC at $100\,km/h$ for (A) Velocity regulation, (B) Power consumption.

shows the field experimental results of the proposed RSNMPC for the optimal energy management of the BEV on a realistic hilly and curvy road of the test track. In this setup, the BEV is set to the maximum cruise velocity at the $v_{ref} = 100\,km/h$. Performance of the RSNMPC (Exp-RSNMPC) is compared with a simulation result (Sim-RSNMPC). Figure 6.15a shows the BEV velocity profile generated by the RSNMPC for both experiment and simulation. The controllers increase the velocity of the BEV from standstill to reach the desired velocity ($v_{ref}$). However, the velocity decreases as the vehicle approaches the first and second curves where the lateral acceleration constraint becomes active at ($220 \leq s \leq 440$). After the second curve, the controllers increase the velocity of the BEV to reach the reference value ($550 \leq s \leq 700$). However, the desired velocity is not reachable on time before approaching to the third and fourth curves, where the velocity of the BEV has to be reduced to satisfy the lateral acceleration inequality constraint. Figure 6.15b shows the BEV power consumption profile of the BEV generated by the RSNMPC for the both field experimental and simulation. It is shown that a low value on the weight of the control input can lead to frequent and agile behaviour of the BEV with the cost of non-smooth power consumption after the fourth curve on the large positive slope. Figure 6.16a and Figure 6.16b show the performance of the experimental RSNMPC in comparison to the simulation RSNMPC in terms of the probability distribution.
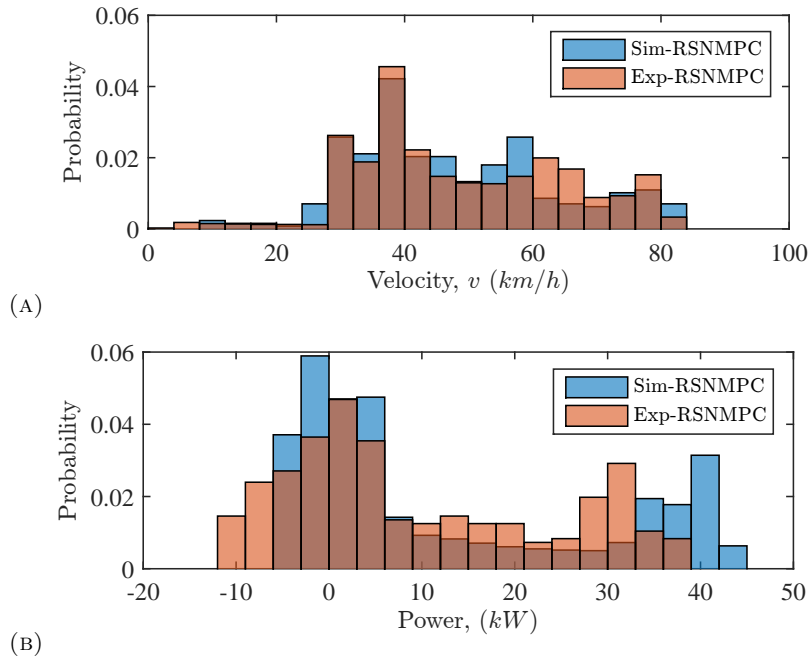
(A)



(B)

FIGURE 6.16: Performance distribution of field experimental RSNMPC vs. simulation RSNMPC at $100\,km/h$ for (A) Velocity regulation, (B) Power consumption.

## 6.2.2 NMPC for Extended Eco-CC with Deadzone Penalty Functions

The RSNMPC with proposed deadzone penalty functions is experimentally implemented on the Smart-ED and the extended Eco-CC system is tested on the test track. The control input of the proposed RSNMPC with deadzone-quadratic penalty function is realised by actuating either the accelerator pedal or brake actuator. The accelerator pedal is replaced by an electronic board (E-accelerator) to manipulate the required acceleration and imitates the electric signals generated by the original accelerator pedal of the Smart-ED.

A prediction horizon for the predictive controller is set to $T = 15\,s$, to cover upcoming road geometry, and traffic speed limit zone with $N = 30$ discretised steps. The constants in performance index function are set as $Q = diag[0, 1, 0]$, and $R = diag[450]$. Note the weight for energy-consumption is set to zero since the effectiveness of the deadzone-quadratic penalty function in energy efficiency is the main focus in this subsection. The proposed deadzone-quadratic RSNMPC (DQ-RSNMPC) is compared with the conventional RSNMPC with $\ell_2$-norm (RSNMPC) and human driver in terms of velocity regulation, travel time ($t$), power consumption profile and total energy-consumption ($e$). For the sake of fair comparison, all of the tests are started from the standstill and the maximum reference velocity value is chosen, $v_{ref} = 100\,km/h$, without imposing speed limit zone. The desired reference zone for velocity tracking is chosen as $z = 2\,m/s$. We have proposed the human driver to drive as fast and energy-efficient as possible.
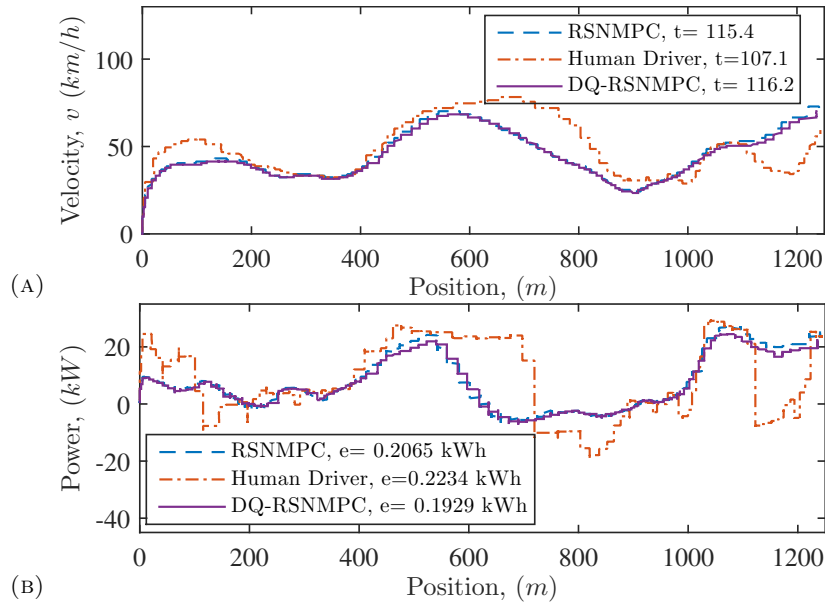
FIGURE 6.17: Experimental results of DQ-RSNMPC in comparison with RSNMPC and Human Driver for (A) Velocity regulation, and (B) Power consumption profile.

Figure 6.17a shows the performance of various tests in terms of velocity regulations and total travel time. The DQ-RSNMPC and RSNMPC increase the velocity up to reaching the first curve ($220 \leq s \leq 270$) where the lateral acceleration constraint should be satisfied. As it is shown, the human driver is faster than the controllers. However, during the first and second curves ($320 \leq s \leq 440$), the controllers and human driver show similar behaviour. Afterwards, the controllers increase over again the velocity up to the point the third curve ($860 \leq s \leq 930$) being in their prediction horizon. This leads to the beginning of slowing down predictively to satisfy the upcoming constraints in an energy-efficient way. The human driver shows late but sharper velocity reduction, which may not be an energy-efficient technique. Finally, the controllers keep the velocity during the fourth curve ($930 \leq s \leq 1045$) and speed up once more to reach the starting point on the test track. Thus, the presented result shows that the maximum reference velocity is not reachable, however, the reference velocity for less than $v_{ref} = 80\,km/h$ is reachable on the experimental tests carried out on the test track. Figure 6.17b shows the power consumption profile and total energy used. Note that negative power consumption refers to energy recovery mechanism.

Figure 6.18a and Figure 6.18b show the normalised histogram information of the velocity and power consumption. The proposed DQ-RSNMPC benefits from an improved penalty function which leads to a denser velocity and power consumption distribution in comparison to the RSNMPC and human driver. Based on achieved results, it is shown that the set-point value is not reachable on the test track by the controllers or the human driver. The DQ-RSNMPC leads to more steady velocity profile and consequently
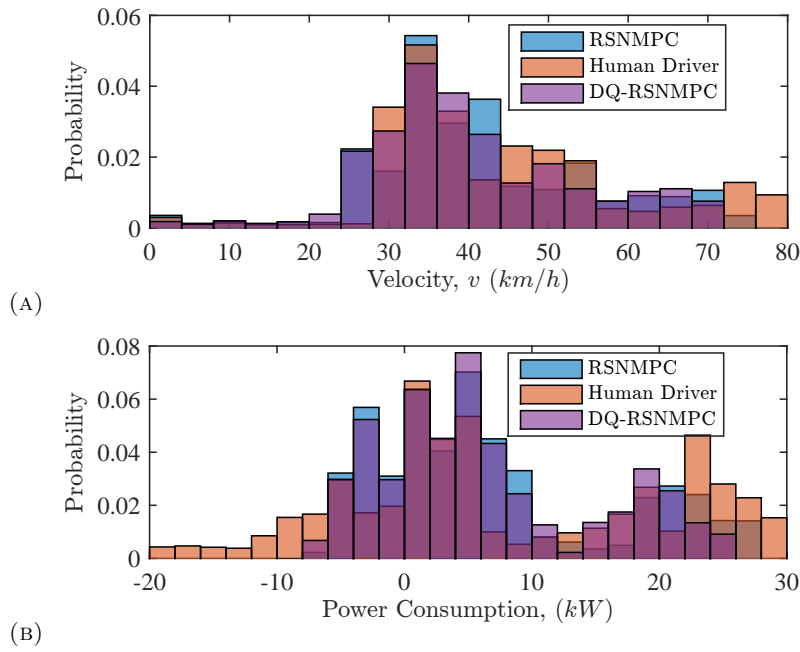
(A)

(B)

FIGURE 6.18: Experimental performance distribution of DQ-RSNMPC in comparison with RSNMPC and the Human Driver for (A) Velocity and (B) Power consumption.

the better drive comfort with relatively small increased travel time. The total energy consumption of DQ-RSNMPC is $+13.65\%$ more energy efficient than the human driver and $+6.58\%$ more energy efficient than the RSNMPC. In other words, for longer trips with more hilly and curvy roads, the proposed method has higher potential to be more energy-efficient. It is noteworthy that the OCP average calculation time for the DQ-RSNMPC is $2.35\,ms$, which indicates the real-time capability of the proposed controller.

Figure 6.19 shows the probability distribution of the accelerator and brake actuators. Figure 6.19a shows that the DQ-RSNMPC has relatively denser distribution in comparison to the RSNMPC and the human driver where Figure 6.19b demonstrates a similar brake pedal distribution for the DQ-RSNMPC, the RSNMPC, and the human driver. For more details about the proposed RSNMPC for the predictive extended CC system with experimental validation, follow Seyed Amin Sajadi-Alamdari et al. (2018).

### 6.2.3 RSNMPC with Open-loop EVaR for Extended Eco-ACC

The concept of the proposed semi-autonomous Eco-ACC system based on the RSNMPC for the BEV on a hilly road with curvatures and traffic speed limits (based on Figure 5.25) are experimentally evaluated on the test track located at Centre de Formation pour Conducteurs S.A. Colmar-Berg, Luxembourg (CFC, 2015). In this experiment,
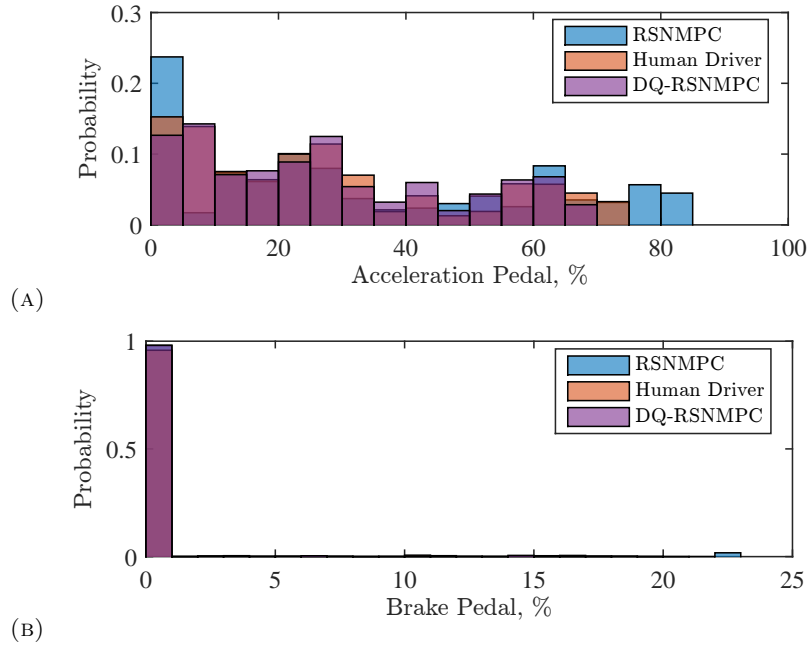
FIGURE 6.19: Experimental performance distribution of DQ-RSNMPC in comparison with RSNMPC and the Human Driver for (A) Acceleration pedal and (B) Brake pedal.

the final cost function of the RSNMPC, $J_f$ is chosen as:

$$J_f(x_N) = \parallel \hat{v}_{hN} - v_{h_{ref}} \parallel^2_{q_f} + c_f \hat{e}_{hN} \tag{6.4}$$

with the corresponding weights $q_f$ and $c_f$. The cost-per-stage function for the Eco-ACC system is defined as:

$$J_c(x_i, \pi_i) := \sum_{i=0}^{N-1} \parallel \hat{v}_{hi} - v_{h_{ref}} \parallel^2_q + \parallel u_i - u_{ref} \parallel^2_r + c\hat{e}_{hi}, \tag{6.5}$$

with corresponding weights $q, r$, and $c$. The relative distance should be larger than the reference space ($d_{ref} := d_0 + v_h t_{hw}$) with closed-loop $\beta_3$ confident level as follows:

$$\mathbf{Pr}_{d_t}[g_3(\hat{d}_i) := d_{ref} \leq \hat{d}_i] \geq \beta_3. \tag{6.6}$$

The prediction horizon for the predictive controller is set to $T = 15\,s$ to cover upcoming road geometry, traffic speed limit zone and the preceding vehicle motion prediction with $N = 30$ discretised steps. The confidence level for the relative distance chance constraint is set to $\beta_3 = 0.95$. In this setup, the desired reference velocity is set to maximum value ($v_{h_{ref}} = 100\,km/h$) and the preceding vehicle is asked to cruise with a constant velocity $v_p = 50\,km/h$ as often as possible.

Figure 6.20 shows the performance of the proposed RSNMPC with the open-loop EVaR chance-constraint evaluation. Figure 6.20a shows the performance of the human driver
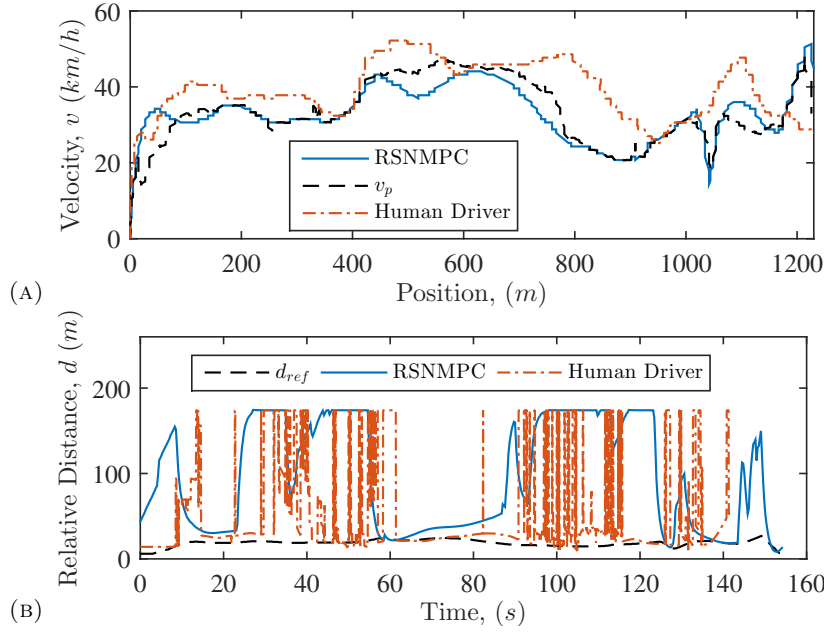
FIGURE 6.20: Experimental results of RSNMPC with open-loop EVaR in comparison with Human Driver for (A) Velocity regulation, and (B) Relative distance regulation.

in comparison to the RSNMPC in terms of velocity regulations. The BEV follows the preceding vehicle with close spacing setting as $d_0 = 6\,m$ and $t_{hw} = 1\,s$. The RSNMPC is speeding up until the vehicle reaches the first and second curves ($220 \le s \le 440$) where the lateral acceleration constraint should be satisfied. As it is shown, the human driver is faster than the controller. However, during the first and second curves, the RSNMPC and human driver show similar behaviour. Afterwards, the controller increases velocity again up to the point where the third and fourth curves are in its prediction horizon ($860 \le s \le 1045$). Finally, the controller speeds up once more to reach the starting point with maximum achievable velocity. The human driver shows sharp velocity and late relative distance regulations, which increase its energy consumption. However, due to statistically accurate prediction model of the preceding vehicle and considering the upcoming road geometries with energy consumption map of the Smart-ED, the RSNMPC is approximately $+18\%$ more energy-efficient on the test track in comparison to the human driver.

In addition, the velocity distribution is denser in comparison to the human driver which improves the energy-efficiency of Extended Eco-ACC system (Fig. 6.21a). Figure 6.21b shows the relative distance probability distribution. It is shown that the relative distance distribution is improved in comparison to the human driver who has a tendency for the close car-following. This could increase the risk of constraint violation or energy-consumption. Figure 6.21c shows the relative distance chance-constraint around the violation region. In other words, the negative values quantify the amount of violation and its frequency. It is shown that the chance-constraint satisfies the required lower
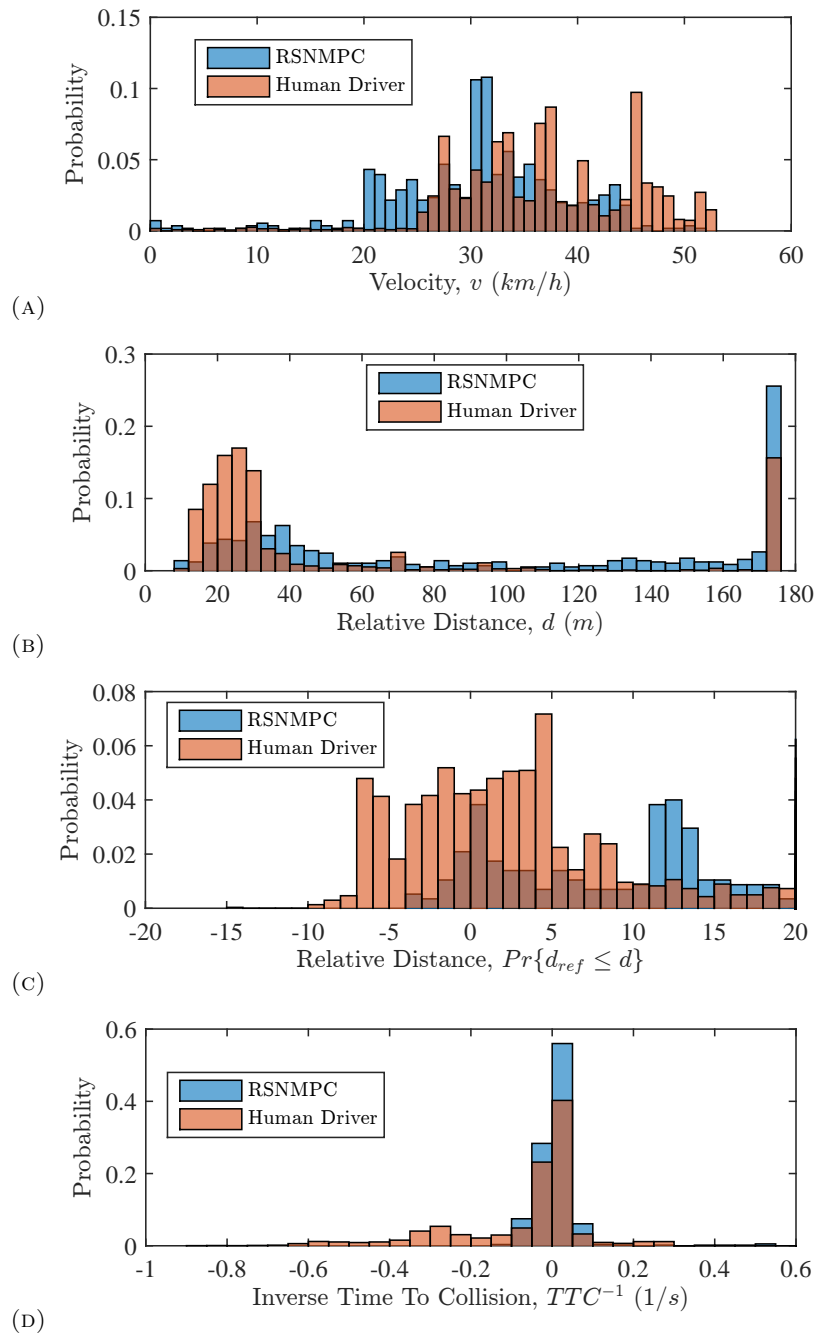
FIGURE 6.21: Experimental results of RSNMPC with open-loop EVaR in comparison with Human Driver for (A) Velocity, (B) relative distance, (C) Relative distance constraint violation, and (D) $TTC^{-1}$.

bound. Figure 6.21d shows the $TTC^{-1}$ probability distribution which is a direct and continuous indicator for the collision risk. It is noteworthy that the lower values indicate the more dangerous situations while zero implies the preserving trend.

### 6.2.4 RSNMPC with Closed-loop EVaR for Extended Eco-ACC

In this subsection, the proposed RSNMPC with open-loop EVaR evaluation of the chance-constraints is extended to the RSNMPC with the introduced closed-loop EVaR. Generally, the standard deviation is considered as a tuning parameter in works of literature. A larger value results in conservative but robust behaviour while a small value could lead to high performance but more frequent constraints violation. However, the proposed method to estimate the standard deviation utilises the advantages of feedback to reduce the conservative behaviours of the risk-averse chance-constraints and improves the tradeoff between the performance and robustness. In the case of the risk-averse control policy, the proposed closed-loop confidence level $\{\beta_i(t)\}_{m-1}^0$ is estimated based on a *Two-pass* algorithm to compute the standard deviation using the exponential moving average of the past $\{p(t_{m-1}), p(t_{m-2}), \ldots, p(0)\}$ $M$-measurement vector.

The prediction horizon for the predictive controller is set to $T = 10\,s$ to cover upcoming road geometry, traffic speed limit zone and the preceding vehicle motion prediction with $N = 20$ discretised steps. The reference velocity is fixed to maximum $v_{h_{ref}} = 100\,km/h$ with spacing setting $d_0 = 6\,m$ and $t_{hw} = 1.5\,s$. The human driver of the preceding vehicle is cruising at $v_p = 50\,km/h$ as often as possible. Figure 6.22a shows the performance of the human driver in comparison to the RSNMPC in terms of velocity regulations. Figure 6.22b shows the relative distance regulation. It is shown that the closed-loop EVaR evaluation of the chance-constraint has the tendency to violation for the sake of performance improvement. This improves the power and energy consumption of the BEV shown in Figure 6.22c.

Figure 6.23a shows the velocity distribution of the BEV during the car-following scenario. The violation of the chance-constraint is shown in Figure 6.21c. The relative distance chance-constraint is less satisfied with minimum violation in comparison to the human driver. The power consumption distribution of the BEV in this scenario is presented in Figure 6.23c. It is shown that the variance of the power consumption by the RSNMPC is lower than the human driver for similar situations which leads to approximately $+21\%$ more energy efficiency in comparison to the human driver. Figure 6.23d demonstrates the performance of the $TTC^{-1}$ as risk of rear-end collision and relative distance constraint violation.

Figure 6.24 shows the probability distribution of the accelerator and brake actuators. Figure 6.24a shows that the RSNMPC has relatively denser distribution in comparison to the human driver where Figure 6.24b demonstrates a similar brake pedal distribution for the RSNMPC and the human driver.
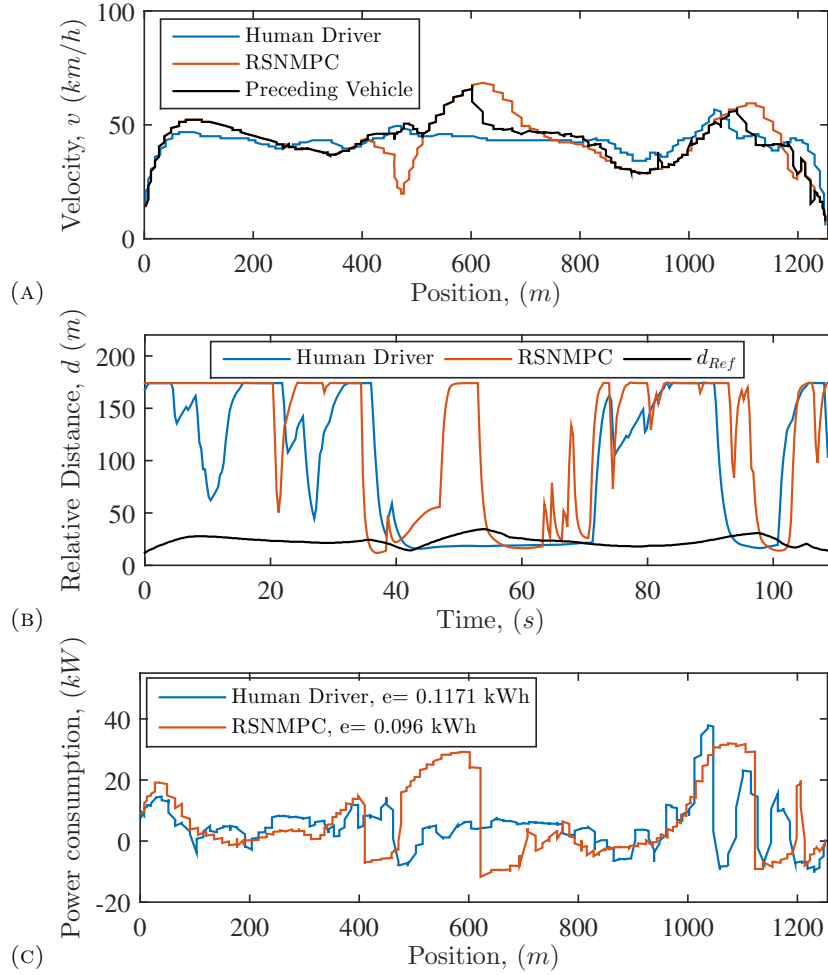
FIGURE 6.22: Performance of RSNMPC with closed-loop EVaR vs Human Driver for (A) Velocity regulation, (B) Relative distance, and (C) Power and total energy consumption.

### 6.2.5 Current-value Hamiltonian with Closed-loop EVaR

The performance of the RSNMPC based on current-value Hamiltonian is evaluated in this subsection. In addition to the proposed RSNMPC with the closed-loop EVaR evaluation, the final cost function of the RSNMPC, $J_f$ is modified based on the current-value Hamiltonian as follows:

$$J_f(x_N) = (1 - \rho)^N (\| \hat{v}_{hN} - v_{h_{ref}} \|_{q_f}^2 + c_f \hat{e}_{hN}) \tag{6.7}$$

with the corresponding weights $q_f$ and $c_f$. The cost-per-stage function for the Extended Eco-ACC system is defined as:

$$J_c(x_i, \pi_i) := \sum_{i=0}^{N-1} (1 - \rho)^i (\| \hat{v}_{hi} - v_{h_{ref}} \|_q^2 + \| u_i - u_{ref} \|_r^2 + c \hat{e}_{hi}), \tag{6.8}$$
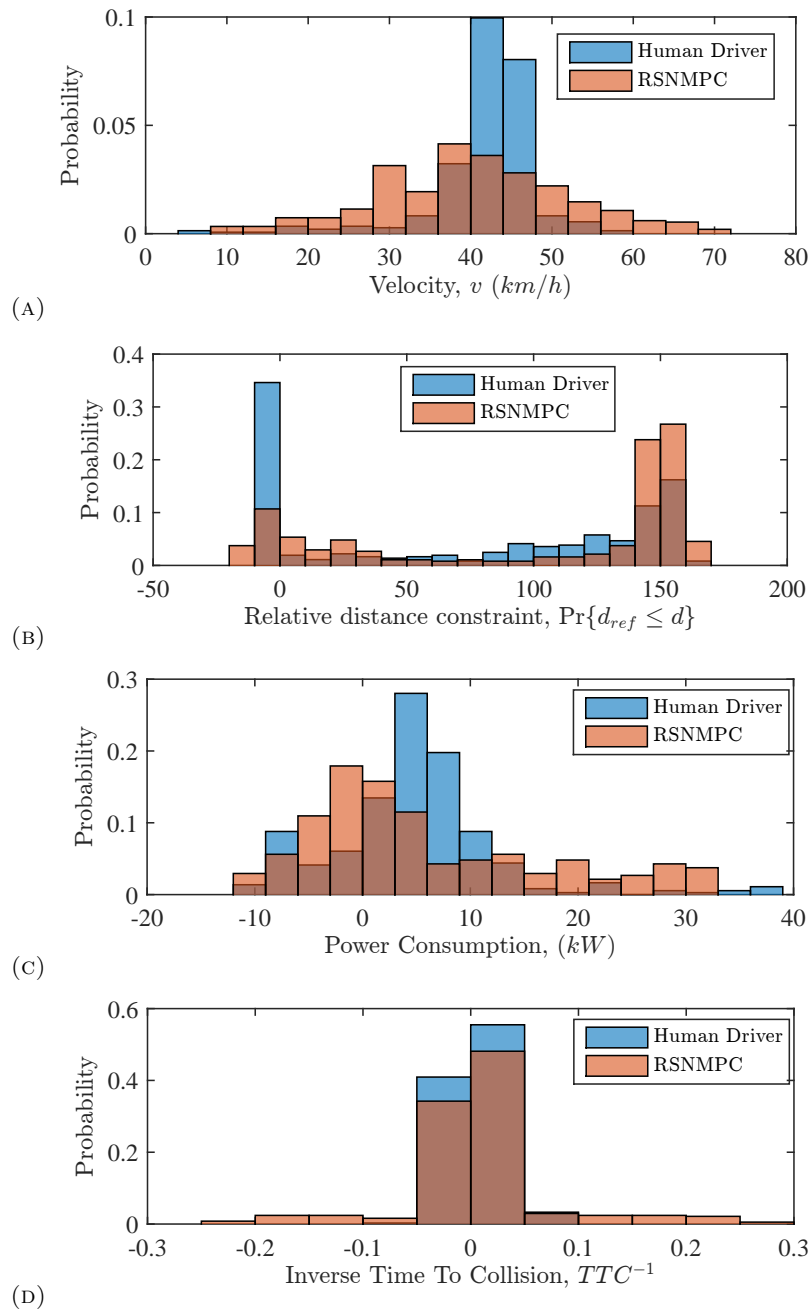
FIGURE 6.23: Experimental results of RSNMPC with closed-loop EVaR in comparison with Human Driver for (A) Velocity, (B) Relative distance constraint violation, (C) Power consumption, and (D) $TTC^{-1}$.
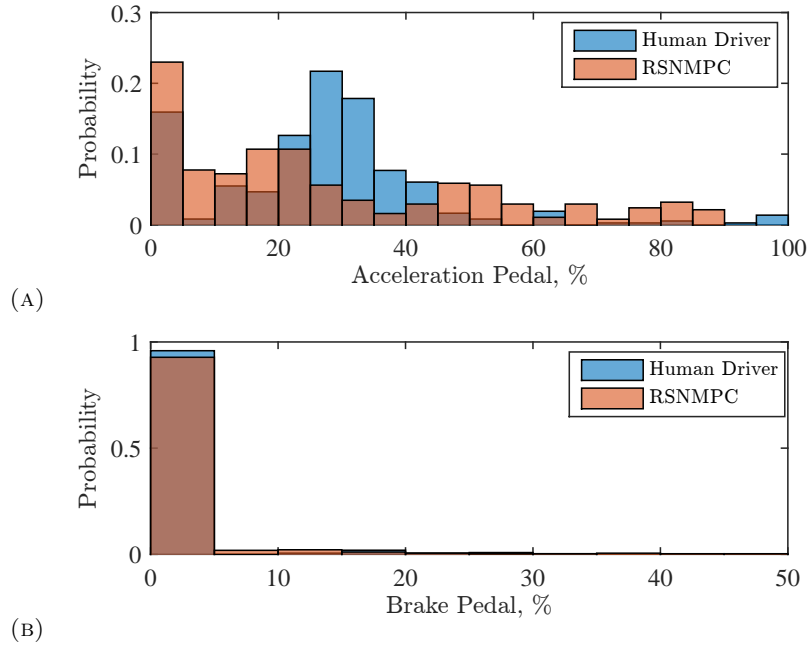
(A)



(B)

FIGURE 6.24: Performance distribution of RSNMPC with closed-loop EVaR in comparison with the Human Driver for (A) Acceleration pedal and (B) Brake pedal.

with corresponding weights $q, r$, and $c$. The prediction horizon for the predictive controller is set to $T = 10\,s$ to cover upcoming road geometry, traffic speed limit zone and the preceding vehicle motion prediction with $N = 20$ discretised steps. The confidence level for the relative distance chance constraint is set to $\beta_3 = 0.95$ and the discount factor is set to $\rho = 0.2$.

Figure 6.25a shows the performance of the human driver in comparison to the current-value Hamiltonian based RSNMPC in terms of velocity regulations. Figure 6.25b shows the relative distance regulation. The power and energy consumption of the BEV is shown in Figure 6.25c. Figure 6.26a shows the velocity distribution of the BEV during the car-following scenario. The violation of the chance-constraint is shown in Figure 6.26b. The relative distance chance-constraint is less satisfied with minimum violation in comparison to the human driver. The power consumption distribution of the BEV in this scenario is presented in Figure 6.26c. It is shown that the variance of the power consumption by the RSNMPC is lower than the one of the human driver for similar situations which leads to approximately $+13\%$ more energy efficiency in comparison to the human driver. Figure 6.26d demonstrates the performance of the $TTC^{-1}$ as risk of rear-end collision and the relative distance constraint violation.

Figure 6.27 shows the probability distribution of the accelerator and brake actuators. Figure 6.27a shows that the RSNMPC has relatively denser distribution in comparison to the human driver where Figure 6.27b demonstrates a similar brake pedal distribution for the RSNMPC and the human driver.
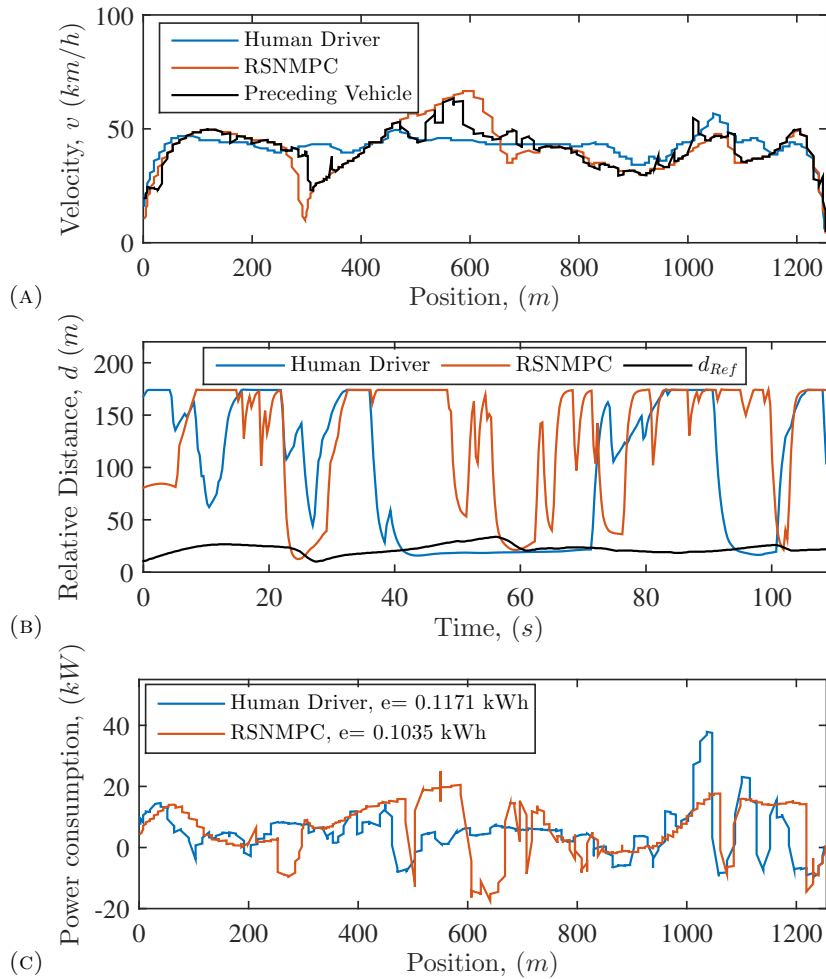
FIGURE 6.25: Performance of current-value Hamiltonian RSNMPC vs Human Driver for (A) Velocity regulation, (B) Relative distance, and (C) Power and total energy consumption.

## 6.2.6 Cut-in and Cut-out Situations

In order to demonstrate the performance of the RSNMPC for the unforeseen situation, the cut-in test scenario is carried out. In this practical test, the BEV is cruising along the track while the preceding vehicle cuts-in the lane of the BEV after having overtaken it. Figure 6.28 shows the velocity and relative distance regulations, receptively. It is shown that the RSNMPC can manage to control the relative distance during the unexpected cut-in situation. Figure 6.28a shows a smooth reduction in velocity of the BEV to adapt to the preceding vehicle. Furthermore, Figure 6.28 demonstrates the performance of relative distance regulation in order to preserve a safe distance to the preceding vehicle in an energy efficient manner.

In addition, the cut-out test scenario is carried out to demonstrate the performance of the RSNMPC for the unforeseen situation. In this practical test, the BEV is cruising in a car-following situation. The preceding vehicle cuts-out the lane of the BEV. Figure 6.29
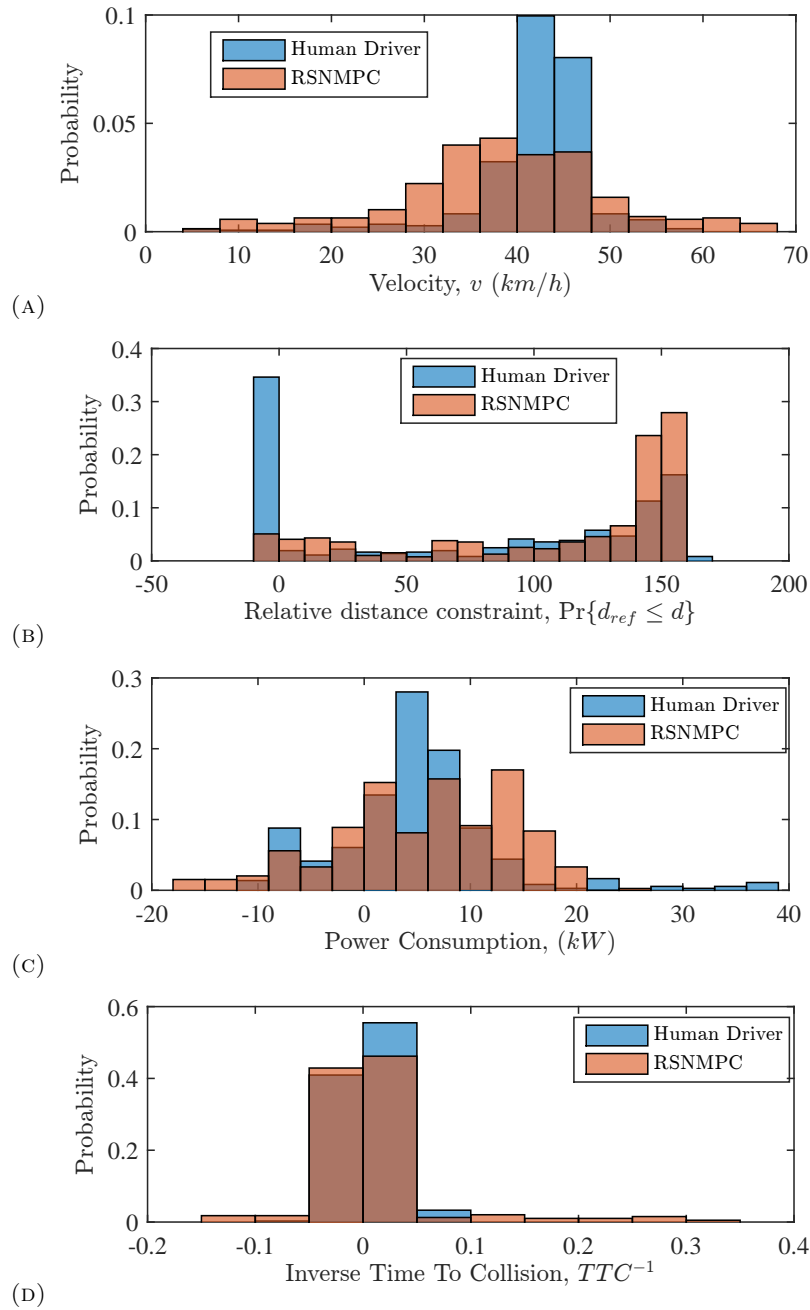
FIGURE 6.26: Experimental results of current-value Hamiltonian RSNMPC in comparison with Human Driver for (A) Velocity, (B) Relative distance constraint violation, (C) Power consumption, and (D) $TTC^{-1}$.
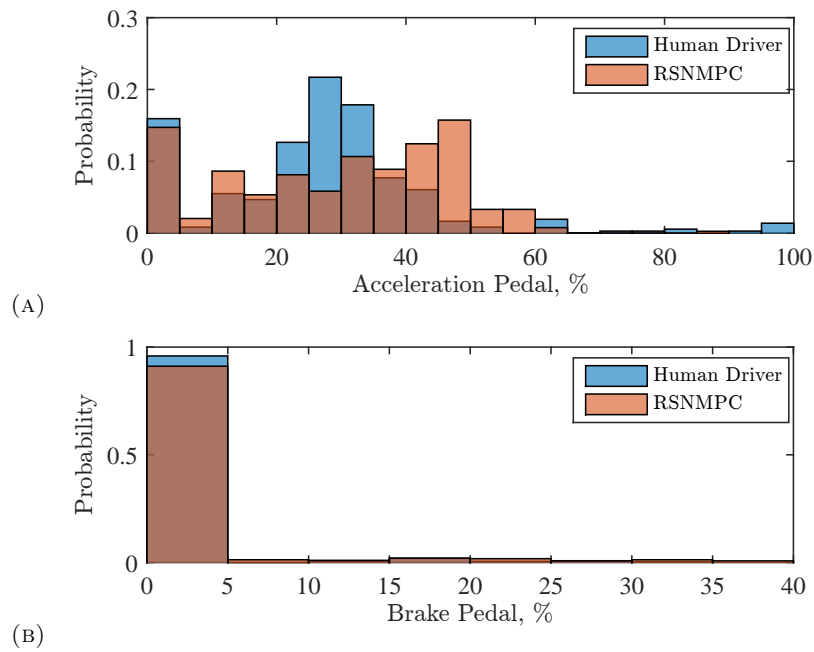
FIGURE 6.27: Experimental performance distribution of RSNMPC in comparison with the Human Driver for (A) Acceleration pedal and (B) Brake pedal.



FIGURE 6.28: Performance of RSNMPC for Cut-in test scenario (a) Velocity and (b) Relative distance regulations
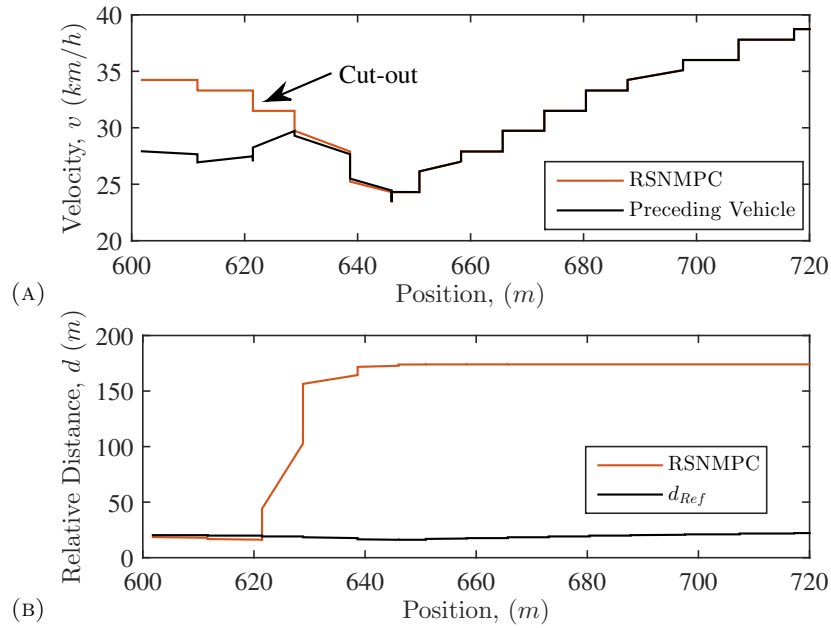
FIGURE 6.29: Performance of RSNMPC for Cut-out test scenario (a) Velocity and (b) Relative distance regulations

shows the velocity and relative distance regulations, receptively. It is shown that the RSNMPC can handle the unexpected cut-out situation. Figure 6.29a shows a smooth increase in velocity of the BEV to reach the desired velocity ($v_{ref} = 100 \, km/h$) after the cut-out situation.

### 6.2.7 Stop&Go Situation

In this subsection, the performance of the RSNMPC cooperating with a developed CAS for the AEB scenario is evaluated. In this case, the preceding vehicle slows down and stop. The preceding vehicle is detected and tracked if the candidate object of the RADAR signal has a positive velocity. Otherwise, the detected object is considered as static. The developed CAS is designed based on fixed time headway policy ($d_{emg} = d_0 + t_{emg_{hw}} v_h$) which generates the related emergency control input if $d_{emg} \leq d$. The control input generated by the CAS overwrites the RSNMPC control input as the final control command that influence on the actuators of the BEV. The CAS spacing setting is set to $d_0 = 6 \, m$ and $t_{emg_{hw}} = 0.5 \, s$.

Figure 6.30 shows the velocity and relative distance regulations in the AEB situation, receptively. It is shown that the RSNMPC with CAS can control the unexpected full stop. Figure 6.30a shows a smooth reduction in velocity of the BEV to stop behind the preceding vehicle. Furthermore, Figure 6.30b demonstrates the relative distance regulation aimed to preserve a safe distance to the preceding vehicle. It is noteworthy
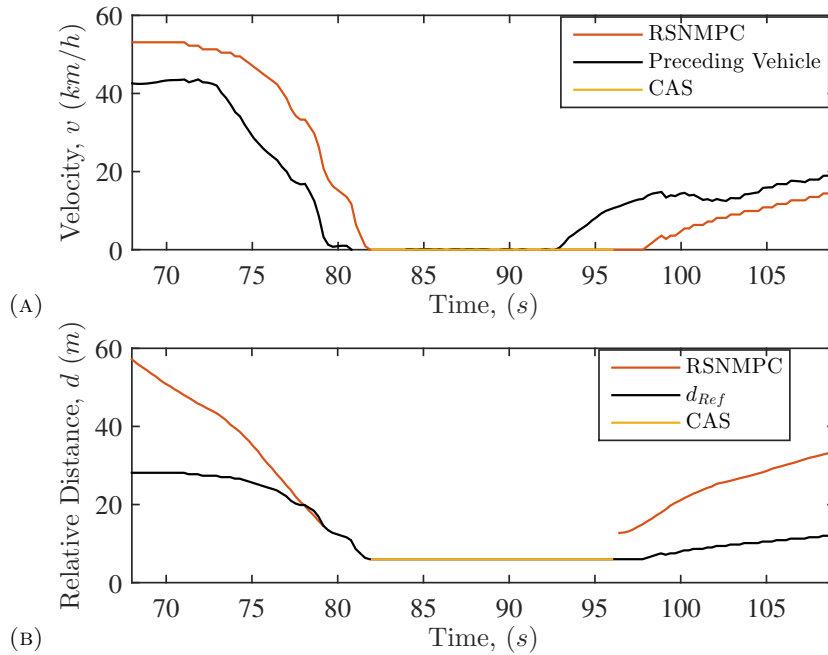
FIGURE 6.30: Performance of RSNMPC for Stop&Go test scenario (a) Velocity and (b) Relative distance regulations

that in Figure 6.30b, as soon as the velocity of the preceding vehicle is below the $v_p \leq 3.6\,m/s$, the relative distance signal for the preceding vehicle is not generated.

## 6.3 Conclusions

In this chapter, practical implementation and field experimental tests have been carried out to evaluate the performance of the optimal energy management system for the Smart-ED based on the Eco-ACC system. The required setup including the sensors, computational resource, and actuators for the practical implementation of the RSNMPC for the Smart-ED introduced. The field experimental tests carried out on the closed track have covered different traffic situations including cruising, car-following, cut-in/out, and Stop&Go. The capability of the RSNMPC in various traffic situations has been evaluated in terms of safety and energy efficiency. The proposed Eco-ACC system based on the RSNMPC found to be a robust and effective ADAS application for the Smart-ED in comparison to the conventional SNMPC and Human drivers. Based on these findings, the following chapter will conclude the thesis with the overall findings, a discussion of the contributions of the proposed RSNMPC applied to the semi-autonomous Eco-ACC system aimed to address the limited cruising range challenge of the BEVs, and research direction of future outlook.

# Chapter 7

# Findings, Conclusions, and Future Outlook

The motivation of this thesis is the challenge in the limited cruising range of the BEVs and the performance evaluation outlined in Chapter 1. The main objectives are to develop a RSNMPC for the ADAS applications that support the ecological driving as well as the performance assessment of the proposed concept on the safety and energy consumption of the BEVs. Several research questions to obtain the objectives of this study are answered throughout Chapter 2 to Chapter 6. This chapter is structured as follows. The main findings are summarised in Section 7.1 followed by Section 7.2 that draws a conclusion based on the findings and contributions of this thesis. Section 7.3 discusses potential areas for future research outlook.

## 7.1 Findings

The aim of this study is to develop a real-time RSNMPC for the Eco-ACC with extended functionalities to achieve an optimal energy management system for the BEV. The performance and impact of the proposed ADAS application combined with the ecological driving techniques on energy consumption of the BEV are examined. The main findings in this study are structured around the contributions that answer research questions mentioned in Chapter 1.

The review of the literature study answers the question of *what are the most effective factors that influence on the BEV's cruising range.* It turns out that the total resistive forces in longitudinal dynamics of the BEV at different ambient temperature are the most effective factors on the cruising range of the BEV. In addition, the review of the works

of literature also answers the question of *which ADAS concepts can be utilised to improve the safety and energy efficiency of the BEVs*. It turns out that the ADAS applications such as CC and ACC systems that automate the throttle and brake control of the vehicle to retain the pre-set longitudinal velocity while maintaining a safe distance from the preceding vehicles have high potential to improve the safety and energy efficiency of the BEVs. Furthermore, review of the ecological driving techniques answers the research question of *how to enhance the performance of the ACC systems for the BEVs*. It turns out that the combination of the ACC system with energy efficient driving techniques enables the system to take advantages of the road geometries which improves the performance of the ACC system for the BEVs. Besides, the ecological driving on the curvy roads and taking the behaviour of the preceding vehicle into account enhance the performance and energy efficiency of the conventional ACC systems.

It has been found out that there are multiple objectives in the proposed semi-autonomous Eco-ACC controller design where some of these objectives are contradictory. The constrained stochastic OCP is a flexible control framework that results in a constrained OCP to optimise multiple performance criteria under different design constraints and system uncertainties. The RSNMPC is proposed to answer the research question *how to formulate the controller of the proposed Eco-ACC system in the OCP*. It also turns out that the differentiable and continuous system and environment models play an important role in the formulation of the stochastic OCP which answer the question of *how should the control system be modelled*. Furthermore, the proposed economic Deadzone penalty functions improve the energy efficiency of the Eco-ACC system. The proposed physical-statistical dynamics for the preceding vehicle motion estimation turns out to be able to propagate the uncertainties along the prediction horizon and evaluation of the obtained scenario in a chance-constraint answer the question of *how to deal with uncertainties of the Eco-ACC system in the OCP*.

It has also been found out that the evaluation and reformulations of the probabilistic constraints with proper risk allocation provide the acceptable tradeoff between the performance and the robustness of the inequality constraints which answers the research question *how to enhance the tradeoff challenge between the performance and the robustness of the controller*. In addition to the distributionally robust chance-constraint evaluation, it is shown that EVaR provides the tightest upper bound. It is shown as well that utilising the EVaR with open-loop fixed risk allocations could have a conservative but robust reaction while the closed-loop EVaR with variable risk allocations exhibits relatively less conservative reaction but improves the performance of the system. Different approaches for the OCPs are reviewed and discussed. It is shown that the PMP solution approach based on C/GMRES numerical method is capable of providing the real-time online solution of the designed RSNMPC. It is shown that the time required

to solve the proposed RSNMPC with different settings are under the $6\,ms$ on the Linux based ROS PC with the Intel® Core™ i7 and a memory of 7.7 GiB. This answers the research question about *which approaches have prospects to solve the obtained OCP in a real-time manner*. In addition, it is shown that the PMP is capable to be extended to deal with stochastic OCP by using the current-value Hamiltonian approach while the proposed soft inequality constraints handling method based on the FB complementary function improves the capability of the PMP approach for the OCP with inequality constraints.

The performance of the RSNMPC against model mismatch and the capabilities of the proposed Eco-ACC system at the microscopic level in terms of driving comfort, safety, and energy efficiency are assessed, which answers the research question of *what are the performance indexes to evaluate the Eco-ACC system and its impact on the BEV's cruising range*. Taking advantage of the road slope profile and safe velocity profile on a curvy road demonstrates the ecological and safe driving of the Eco-ACC system under the RSNMPC algorithm. The energy efficient states regulation and constraints satisfaction such as the relative distance safety constraint fulfilment even during the unforeseen situations such as cut-in/out demonstrates the safe and energy efficient driving performance of the Eco-ACC system which answers the research question of *how does the proposed Eco-ACC system perform on the BEV under various driving and traffic situations*. Numerical simulation and field experimental results validate the capability of the proposed Eco-ACC system based on the RSNMPC algorithm for the BEV in terms of safety, energy efficiency, and comfortable driving performance despite the stochastic system uncertainties. This answers the question of *what are the impacts of the Eco-ACC system on safety and cruising range of the BEV*.

Under the chosen parameters and settings, the Eco-ACC system with the deadzone quadratic penalty function based on the RSNMPC algorithm is +13.65% more energy efficient in comparison to the human driver during the Eco-CC mode on the test track. It is also shown that the RSNMPC with open-loop EVaR is approximately +18% more energy-efficient on the test track where the RSNMPC with close-loop EVaR is approximately +21% more energy efficient both in comparison to the human driver for the similar car-following situations. The energy efficiency of Current-value Hamiltonian with closed-loop EVaR is validated with +13.14% in comparison to the human driver on the test track.

## 7.2    Conclusions

The primary goal of this thesis was to improve the cruising range of the BEVs based on the combination of the ecological driving techniques and the ADAS applications. This was accomplished by extending the functionality and performance of the conventional ACC system to the Eco-ACC system tailored for the BEVs to include the energy consumption characteristic map of the BEV, the road geometries model, and statistically accurate preceding vehicle motion model. The road geometry and traffic information were models based on the hyperfunctions proposed in this study to support the Eco-ACC system. Using the road geometry and traffic information, the uncertain behaviour of the preceding vehicle modelled based on a physical-statistical motion model robust to far-term future prediction was introduced.

The RSNMPC was the main competent of the Eco-ACC system with improved formulations including the extension of the deterministic OCP into real-time stochastic OCP. The real-time C/GMRES numerical method based on PMP was extended to the current-value Hamiltonian that is able to deal with stochastic OCPs. The expected quadratic cost function which is an interesting method to include risk during decision-making process was adapted in this study. A distributionally robust chance-constraint reformulation was utilised to convert the chance-constraints explicitly into convex second-order cone constraints. Furthermore, open-loop EVaR evaluation of the chance-constraints was formulated in the PMP approach. Since the open-loop EVaR could lead to a conservative behaviour, the RSNMPC with closed-loop EVaR was proposed which was able to deal with system uncertainties with an improved tradeoff between the conservativeness and performance of the system. Furthermore, the economic Deadzone penalty functions were proposed to improve the systems energy efficiency. The soft inequality constraint handling method based on the FB complementary function was introduced to extend the capabilities of the PMP solution approach.

This thesis presented numerical and practical implementations of the Eco-ACC system based on the proposed real-time RSNMPC algorithm for the commercial BEV (Smart-ED) evaluated on a closed test track located in Colmar-berg, Luxembourg. The proposed RSNMPC with different settings were solved in real-time to plan the safe and energy efficient velocity profile for the Smart-ED without the driver intervention in various driving situations. These methods enabled the Smart-ED to successfully improve its energy consumption and extend the limited cruising range. It is noteworthy that the proposed Eco-ACC system for the BEV with RSNMPC algorithm provides a new approach for the ITS with ADAS applications for the intelligent vehicles. This system established a new interdisciplinary research activity in the Grand Duchy of Luxembourg comprising the ADAS applications in electro-mobility.

## 7.3   Future Outlook

Several interesting areas and direction for the future research can be extended and recommended based on the research presented in this thesis.

First, the regenerative braking features in the BEVs have high potential to improve the cruising range in terms of taking any opportunities to capture and harvest the energy. This can be achieved by different settings of the regenerative braking in the various driving situations. For instance, the developed Eco-ACC system could be extended to modify the internal regenerative braking setting of the BEV based on the upcoming road and traffic situations in a way that the friction braking is used only for emergency circumstances.

Second, advanced sensors are the main feature of intelligent vehicles in sensing and situational awareness capabilities. Typical sensor systems used for the ADAS applications are RADAR, LIDAR, vision-based, and infra-red sensors systems. Robust algorithms that detect and track the objects properly lead to a more information from the sensed data and improve the performance of the ADAS consequently. For instance, machine learning methods have shown promising performance in autonomous vehicles with a sophisticated perception capabilities. Thus, it is recommended to conduct research in utilising the machine learning methods on the RADAR data to detect objects and track multi-vehicles in different traffic situations. Expected results of such a research not only could improve the performance of the proposed Eco-ACC system but also could be a proper platform for other ADAS applications. In addition, improvement in environmental perception capability of the Eco-ACC system such as vision-based sensor fusion with the RADAR in order to improve the detection and tracking of the preceding vehicles could have a significant enhancement in the performance of the system. In addition, such a sensor fusion system could also improve the localisation of the system which finally might enhance the performance and robustness of the Eco-ACC system.

Furthermore, the proposed RSNMPC have been applied to solve the stochastic OCP with individual chance-constraints. Extending the RSNMPC formulation to handle joint chance-constraints is one of the interesting areas of future outlook. This is also a challenging research direction since the solution of the stochastic OCP with joint chance-constraints could result in overly risky or conservative if it is not defined and designed carefully. Last but not least, improved actuation system with lower delays as well as the combination of the Eco-ACC system with other ADAS applications related to steering manoeuvres such as lane keeping system could improve the safety and energy efficiency of the BEVs.

# Bibliography

Ahmadi Javid, A (Dec. 2012). "Entropic Value-at-Risk: A New Coherent Risk Measure". In: *Journal of Optimization Theory and Applications* 155.3, pp. 1105–1123. ISSN: 0022-3239. DOI: 10.1007/s10957-011-9968-2. URL: http://link.springer.com/10.1007/s10957-011-9968-2.

Alam, Assad, Bart Besselink, Valerio Turri, Jonas Martensson, and Karl H. Johansson (Dec. 2015). "Heavy-Duty Vehicle Platooning for Sustainable Freight Transportation: A Cooperative Method to Enhance Safety and Efficiency". In: *IEEE Control Systems* 35.6, pp. 34–56. ISSN: 1066-033X. DOI: 10.1109/MCS.2015.2471046. URL: http://ieeexplore.ieee.org/document/7286902/.

Alam, Md Saniul and Aonghus McNabola (Sept. 2014). "A critical review and assessment of Eco-Driving policy & technology: Benefits & limitations". In: *Transport Policy* 35, pp. 42–49. ISSN: 0967070X. DOI: 10.1016/j.tranpol.2014.05.016. URL: http://linkinghub.elsevier.com/retrieve/pii/S0967070X14001152.

Ames, Aaron D., Jessy W. Grizzle, and Paulo Tabuada (Dec. 2014). "Control barrier function based quadratic programs with application to adaptive cruise control". In: *53rd IEEE Conference on Decision and Control*. IEEE, pp. 6271–6278. ISBN: 978-1-4673-6090-6. DOI: 10.1109/CDC.2014.7040372. URL: http://ieeexplore.ieee.org/document/7040372/.

Andrieu, Cindie and Guillaume Saint Pierre (Oct. 2012). "Comparing Effects of Eco-driving Training and Simple Advices on Driving Behavior". In: *Procedia - Social and Behavioral Sciences* 54.2011, pp. 211–220. ISSN: 18770428. DOI: 10.1016/j.sbspro.2012.09.740. URL: http://linkinghub.elsevier.com/retrieve/pii/S1877042812042024.

Asadi, Behrang and Ardalan Vahidi (May 2011). "Predictive Cruise Control: Utilizing Upcoming Traffic Signal Information for Improving Fuel Economy and Reducing Trip Time". In: *IEEE Transactions on Control Systems Technology* 19.3, pp. 707–714. ISSN:

1063-6536. DOI: 10.1109/TCST.2010.2047860. URL: http://ieeexplore.ieee.org/document/5454336/.

Asprion, Jonas, Oscar Chinellato, and Lino Guzzella (2014). "Optimal Control of Diesel Engines: Numerical Methods, Applications, and Experimental Validation". In: *Mathematical Problems in Engineering* 2014, pp. 1–21. ISSN: 1024-123X. DOI: 10.1155/2014/286538. URL: http://www.hindawi.com/journals/mpe/2014/286538/.

Bageshwar, V.L., W.L. Garrard, and Rajesh Rajamani (Sept. 2004). "Model Predictive Control of Transitional Maneuvers for Adaptive Cruise Control Vehicles". In: *IEEE Transactions on Vehicular Technology* 53.5, pp. 1573–1585. ISSN: 0018-9545. DOI: 10.1109/TVT.2004.833625. URL: http://ieeexplore.ieee.org/document/1337334/.

Bayar, Bilgehan, S. Amin Sajadi-Alamdari, Francesco Viti, and Holger Voos (June 2016). "Impact of different spacing policies for adaptive cruise control on traffic and energy consumption of electric vehicles". In: *2016 24th Mediterranean Conference on Control and Automation (MED)*. IEEE, pp. 1349–1354. ISBN: 978-1-4673-8345-5. DOI: 10.1109/MED.2016.7535939. URL: http://ieeexplore.ieee.org/document/7535939/.

Bayless, Steven H, Adrian Guan, Patrick Son, Sean Murphy, and Anthony J Shaw (2014). *Connected Vehicle Insights Trends in Roadway Domain Active Sensing*. Tech. rep. Research and Innovative Technology Administration, pp. 1–31. URL: http://connectedvehicle.itsa.wikispaces.net/file/view/Connected+Vehicle+Insights+Roadway+Domain+Active+Sensing+-+FINAL+-+081313+-+ITS+America.pdf/444780568/Connected%20Vehicle%20Insights%20Roadway%20Domain%20Active%20Sensing%20-%20FINAL%20-%20081313%20-%20ITS%20America.pdf.

Bengler, Klaus, Klaus Dietmayer, Berthold Farber, Markus Maurer, Christoph Stiller, and Hermann Winner (Jan. 2014). "Three Decades of Driver Assistance Systems: Review and Future Perspectives". In: *IEEE Intelligent Transportation Systems Magazine* 6.4, pp. 6–22. ISSN: 1939-1390. DOI: 10.1109/MITS.2014.2336271. URL: http://ieeexplore.ieee.org/lpdocs/epic03/wrapper.htm?arnumber=6936444.

Bertozzi, M., L. Bombini, P. Cerri, P. Medici, P. C. Antonello, and M. Miglietta (June 2008). "Obstacle detection and classification fusing radar and vision". In: *2008 IEEE Intelligent Vehicles Symposium*. IEEE, pp. 608–613. ISBN: 978-1-4244-2568-6. DOI: 10.1109/IVS.2008.4621304. URL: http://ieeexplore.ieee.org/lpdocs/epic03/wrapper.htm?arnumber=4621304.

Bianchi Piccinini, Giulio Francesco, Carlos Manuel Rodrigues, Miguel Leitão, and Anabela Simões (June 2014). "Driver's behavioral adaptation to Adaptive Cruise Control (ACC): The case of speed and time headway". In: *Journal of Safety Research*

49.February, 77.e1–84. ISSN: 00224375. DOI: 10.1016/j.jsr.2014.02.010. URL: http://linkinghub.elsevier.com/retrieve/pii/S0022437514000280.

Bichi, M., G. Ripaccioli, S. Di Cairano, D. Bernardini, A. Bemporad, and I.V. Kolmanovsky (Dec. 2010). "Stochastic model predictive control with driver behavior learning for improved powertrain control". In: *49th IEEE Conference on Decision and Control (CDC)*. IEEE, pp. 6077–6082. ISBN: 978-1-4244-7745-6. DOI: 10.1109/CDC.2010.5717791. URL: http://ieeexplore.ieee.org/document/5717791/.

Bifulco, Gennaro Nicola, Luigi Pariota, Fulvio Simonelli, and Roberta Di Pace (Apr. 2013). "Development and testing of a fully Adaptive Cruise Control system". In: *Transportation Research Part C: Emerging Technologies* 29, pp. 156–170. ISSN: 0968090X. DOI: 10.1016/j.trc.2011.07.001. URL: http://linkinghub.elsevier.com/retrieve/pii/S0968090X11001008.

Birge, John R. and François Louveaux (2011). *Introduction to Stochastic Programming*. Springer Series in Operations Research and Financial Engineering. New York, NY: Springer New York, p. 524. ISBN: 978-1-4614-0236-7. DOI: 10.1007/978-1-4614-0237-4. URL: http://link.springer.com/10.1007/978-1-4614-0237-4.

Blackmore, Lars and Masahiro Ono (Aug. 2009). "Convex Chance Constrained Predictive Control Without Sampling". In: *AIAA Guidance, Navigation, and Control Conference*. Reston, Virigina: American Institute of Aeronautics and Astronautics. ISBN: 978-1-60086-978-5. DOI: 10.2514/6.2009-5876. URL: http://arc.aiaa.org/doi/10.2514/6.2009-5876.

Bloch, Alexander (2009). *Leichtbau ist nicht das Wichtigste (in German)*. URL: http://www.auto-motor-und-sport.de/news/spritsparpotential-leichtbau-ist-nicht-das-wichtigste-1478244.html (visited on 03/04/2016).

Borrelli, F, A Bemporad, and M Morari (2014). *Predictive control for linear and hybrid systems*, p. 443. ISBN: 9781108158770. URL: http://www.mpc.berkeley.edu/mpc-course-material.

Boyd, Stephen and Lieven Vandenberghe (2004). *Convex optimization*. Cambridge University Press, p. 730. ISBN: 0521833787. DOI: 10.1017/CBO9780511804441. URL: https://web.stanford.edu/%7B~%7Dboyd/cvxbook/.

Buehler, Edward A., Joel A. Paulson, and Ali Mesbah (July 2016). "Lyapunov-based stochastic nonlinear model predictive control: Shaping the state probability distribution functions". In: *2016 American Control Conference (ACC)*. Section IV. IEEE, pp. 5389–5394. ISBN: 978-1-4673-8682-1. DOI: 10.1109/ACC.2016.7526514. arXiv: 1505.02871. URL: http://ieeexplore.ieee.org/document/7526514/.

Calafiore, G. C. and L. El Ghaoui (Dec. 2006). "On Distributionally Robust Chance-Constrained Linear Programs". In: *Journal of Optimization Theory and Applications* 130.1, pp. 1–22. ISSN: 0022-3239. DOI: 10.1007/s10957-006-9084-x. URL: http://link.springer.com/10.1007/s10957-006-9084-x.

Campbell, M., M. Egerstedt, J. P. How, and R. M. Murray (Oct. 2010). "Autonomous driving in urban environments: approaches, lessons and challenges". In: *Philosophical Transactions of the Royal Society A: Mathematical, Physical and Engineering Sciences* 368.1928, pp. 4649–4672. ISSN: 1364-503X. DOI: 10.1098/rsta.2010.0110. URL: http://rsta.royalsocietypublishing.org/cgi/doi/10.1098/rsta.2010.0110.

CFC (2015). *Centre de Formation pour Conducteurs*. URL: http://www.cfc.lu/ (visited on 01/01/2015).

Chao Sun, Xiaosong Hu, Scott J Moura, and Fengchun Sun (May 2015). "Velocity Predictors for Predictive Energy Management in Hybrid Electric Vehicles". In: *IEEE Transactions on Control Systems Technology* 23.3, pp. 1197–1204. ISSN: 1063-6536. DOI: 10.1109/TCST.2014.2359176. URL: http://ieeexplore.ieee.org/document/6917015/.

Chen, Yan, Xiaodong Li, Christopher Wiet, and Junmin Wang (Aug. 2014). "Energy Management and Driving Strategy for In-Wheel Motor Electric Ground Vehicles With Terrain Profile Preview". In: *IEEE Transactions on Industrial Informatics* 10.3, pp. 1938–1947. ISSN: 1551-3203. DOI: 10.1109/TII.2013.2290067. URL: http://ieeexplore.ieee.org/document/6657818/.

Corona, Daniele and Bart De Schutter (2007). "Comparison of a linear and a hybrid adaptive cruise controller for a SMART". In: *2007 46th IEEE Conference on Decision and Control*. 1. IEEE, pp. 4779–4784. ISBN: 978-1-4244-1497-0. DOI: 10.1109/CDC.2007.4434054. URL: http://ieeexplore.ieee.org/document/4434054/.

Dahl, K. R. and E. Stokkereit (June 2016). "Stochastic maximum principle with Lagrange multipliers and optimal consumption with Lévy wage". In: *Afrika Matematika* 27.3-4, pp. 555–572. ISSN: 1012-9405. DOI: 10.1007/s13370-015-0360-5. URL: http://link.springer.com/10.1007/s13370-015-0360-5.

Daniel, J., G. Pouly, A. Birouche, J-P. Lauffenburger, and M. Basset (2009). "Navigation based speed profile generation for an open road speed assistant". In: *IFAC Proceedings Volumes* 42.15, pp. 320–327. ISSN: 14746670. DOI: 10.3182/20090902-3-US-2007.0112. URL: http://linkinghub.elsevier.com/retrieve/pii/S1474667016318146.

Delis, A.I., I.K. Nikolos, and M. Papageorgiou (Oct. 2015). "Macroscopic traffic flow modeling with adaptive cruise control: Development and numerical solution". In:

*Computers & Mathematics with Applications* 70.8, pp. 1921–1947. ISSN: 08981221. DOI: 10.1016/j.camwa.2015.08.002. URL: http://www.sciencedirect.com/science/article/pii/S0898122115003703.

*Delphi Automotive Systems Luxembourg S.A.* (2016). URL: http://www.delphi.com/ (visited on 01/02/2016).

Dey, Kakan C., Li Yan, Xujie Wang, Yue Wang, Haiying Shen, Mashrur Chowdhury, Lei Yu, Chenxi Qiu, and Vivekgautham Soundararaj (Feb. 2016). "A Review of Communication, Driver Characteristics, and Controls Aspects of Cooperative Adaptive Cruise Control (CACC)". In: *IEEE Transactions on Intelligent Transportation Systems* 17.2, pp. 491–509. ISSN: 1524-9050. DOI: 10.1109/TITS.2015.2483063. URL: http://ieeexplore.ieee.org/lpdocs/epic03/wrapper.htm?arnumber=7314936.

Dib, Wissam, Alexandre Chasse, Philippe Moulin, Antonio Sciarretta, and Gilles Corde (Aug. 2014). "Optimal energy management for an electric vehicle in eco-driving applications". In: *Control Engineering Practice* 29, pp. 299–307. ISSN: 09670661. DOI: 10.1016/j.conengprac.2014.01.005. URL: http://linkinghub.elsevier.com/retrieve/pii/S0967066114000355.

Dickmann, Juergen, Nils Appenrodt, Hans-Ludwig Bloecher, C. Brenk, Thomas Hackbarth, Markus Hahn, Jens Klappstein, Marc Muntzinger, and Alfons Sailer (Oct. 2014). "Radar contribution to highly automated driving". In: *2014 11th European Radar Conference*. IEEE, pp. 412–415. ISBN: 978-2-8748-7037-8. DOI: 10.1109/EuRAD.2014.6991295. URL: http://ieeexplore.ieee.org/lpdocs/epic03/wrapper.htm?arnumber=6991295.

Diehl, Moritz, Hans Joachim Ferreau, and Niels Haverbeke (2009). "Efficient Numerical Methods for Nonlinear MPC and Moving Horizon Estimation". In: *Workshop on Assessment and Future Directions of NMPC*, pp. 391–417. ISBN: 978-3-642-01093-4. DOI: 10.1007/978-3-642-01094-1_32. URL: http://link.springer.com/10.1007/978-3-642-01094-1%7B%5C_%7D32.

Diehl, Moritz, Rolf Findeisen, and Frank Allgöwer (Jan. 2007). "A Stabilizing Real-Time Implementation of Nonlinear Model Predictive Control". In: *Real-Time PDE Constrained Optimization*. March. Society for Industrial and Applied Mathematics, pp. 25–52. ISBN: 9780898718935. DOI: 10.1137/1.9780898718935.ch2. URL: http://epubs.siam.org/doi/10.1137/1.9780898718935.ch2.

Dirk, Ehmanns and Spannheimer Helmut (2004). *Advanced driver assistance systems in Europe (ADASE) Roadmap*. Tech. rep. ADASE2 Consortium, p. 22. URL: http://www.imobilitysupport.eu/library/imobility-forum/working-groups/active/

`implementation-road-map/documents/1795-ir-wg-road-map-deliverable-d2d-roadmap-development-adase-jul-2004/file`.

Dokic, Jadranka, Beate Müller, and Gereon Meyer (2015). *European Roadmap Smart Systems for Automated Driving*. Tech. rep. Berlin, p. 39. URL: `http://www.smart-systems-integration.org/public/news-events/news/eposs-roadmap-smart-systems-for-automated-driving-now-published`.

Domahidi, Alexander, Aldo U. Zgraggen, Melanie N. Zeilinger, Manfred Morari, and Colin N. Jones (Dec. 2012). "Efficient interior point methods for multistage problems arising in receding horizon control". In: *2012 IEEE 51st IEEE Conference on Decision and Control (CDC)*. IEEE, pp. 668–674. ISBN: 978-1-4673-2066-5. DOI: `10.1109/CDC.2012.6426855`. URL: `http://ieeexplore.ieee.org/document/6426855/`.

Driel, Cornelie J G Van and Bart Van Arem (2010). "The Impact of a Congestion Assistant on Traffic Flow Efficiency and Safety in Congested Traffic Caused by a Lane Drop". In: *Journal of Intelligent Transportation Systems* 14.4, pp. 197–208. DOI: `10.1080/15472450.2010.516226`. URL: `http://www.tandfonline.com/doi/abs/10.1080/15472450.2010.516226`.

Dudek, Manuel, Ismail Nasr, Gabor Bozsik, Mohamed Hamouda, Dietmar Kissinger, and Georg Fischer (Jan. 2015). "System Analysis of a Phased-Array Radar Applying Adaptive Beam-Control for Future Automotive Safety Applications". In: *IEEE Transactions on Vehicular Technology* 64.1, pp. 34–47. ISSN: 0018-9545. DOI: `10.1109/TVT.2014.2321175`. URL: `http://ieeexplore.ieee.org/lpdocs/epic03/wrapper.htm?arnumber=6808509`.

Dudley, David (2014). *The Driverless Car Is (Almost) Here*. URL: `http://www.aarp.org/home-family/personal-technology/info-2014/google-self-driving-car.html` (visited on 04/07/2016).

Dugas, Charles, Yoshua Bengio, François Bélisle, Claude Nadeau, and René Garcia (2000). "Incorporating Second-order Functional Knowledge for Better Option Pricing". In: *Proceedings of the 13th International Conference on Neural Information Processing Systems*. NIPS'00. Cambridge, MA, USA: MIT Press, pp. 451–457. URL: `http://dl.acm.org/citation.cfm?id=3008751.3008817`.

Eberle, Dr Ulrich and Dr Rittmar von Helmolt (2010). "Sustainable transportation based on electric vehicle concepts: a brief overview". In: *Energy & Environmental Science* 3.6, p. 689. ISSN: 1754-5692. DOI: `10.1039/c001674h`. URL: `http://xlink.rsc.org/?DOI=c001674h`.

Ehsani, Mehrdad, Yimin Gao, and Ali Emadi (2009). *Modern Electric, Hybrid Electric, and Fuel Cell Vehicles: Fundamentals, Theory, and Design*. 2, illustr. CRC Press,

p. 557. ISBN: 1420054007, 9781420054002. URL: https://www.crcpress.com/Modern-Electric-Hybrid-Electric-and-Fuel-Cell-Vehicles-Fundamentals/Ehsani-Gao-Emadi/9781420053982.

Einarsson, Bo (Jan. 2005). *Accuracy and Reliability in Scientific Computing*. Ed. by Bo Einarsson. Society for Industrial and Applied Mathematics. ISBN: 978-0-89871-584-2. DOI: 10.1137/1.9780898718157. URL: http://epubs.siam.org/doi/book/10.1137/1.9780898718157.

Ellis, Matthew and Panagiotis D. Christofides (Feb. 2015). "Real-time economic model predictive control of nonlinear process systems". In: *AIChE Journal* 61.2, pp. 555–571. ISSN: 00011541. DOI: 10.1002/aic.14673. arXiv: 0201037v1 [arXiv:physics]. URL: http://doi.wiley.com/10.1002/aic.14673.

Ellis, Matthew, Helen Durand, and Panagiotis D. Christofides (Aug. 2014). "A tutorial review of economic model predictive control methods". In: *Journal of Process Control* 24.8, pp. 1156–1178. ISSN: 09591524. DOI: 10.1016/j.jprocont.2014.03.010. URL: http://linkinghub.elsevier.com/retrieve/pii/S0959152414000900.

Emadi, Ali (2014). *Advanced Electric Drive Vehicles*. CRC Press, p. 616. ISBN: 978-1-4665-9769-3. URL: https://www.crcpress.com/Advanced-Electric-Drive-Vehicles/Emadi/9781466597693.

Eom, Hwisoo and Sang Lee (June 2015). "Human-Automation Interaction Design for Adaptive Cruise Control Systems of Ground Vehicles". In: *Sensors* 15.6, pp. 13916–13944. ISSN: 1424-8220. DOI: 10.3390/s150613916. URL: http://www.mdpi.com/1424-8220/15/6/13916/.

ERTRAC Task Force (2015). *Automated Driving Roadmap*. Tech. rep., pp. 1–48. URL: http://www.ertrac.org/uploads/documentsearch/id38/ERTRAC%7B%5C_%7DAutomated-Driving-2015.pdf.

Eskandarian, Azim, ed. (2012). *Handbook of Intelligent Vehicles*. Vol. 2. London: Springer, pp. 1–1629. ISBN: 978-0-85729-084-7. DOI: 10.1007/978-0-85729-085-4. URL: http://link.springer.com/10.1007/978-0-85729-085-4.

*European Commission* (2018). URL: https://ec.europa.eu.

European, Commission (2016). *AUTOPILOT, the European Commission's Large-Scale Pilots*. DOI: http://autopilot-project.eu.

European, Commission (2018). *2018-2020 Digitising And Transforming European Industry And Services: Automated Road Transport*. DOI: https://ec.europa.eu/research/participants/portal/desktop/en/opportunities/h2020/calls/h2020-dt-art-2018-2019-2020.html#c,topics=callIdentifier/t/H2020-DT-

ART-2018-2019-2020/1/1/1/default-group&callStatus/t/Forthcoming/1/1/
0/default-group&callStatus/t/Open/1/1/0/default-group&callStatus/t/
Closed/1/1/0/default-group&+identifier/desc.

Fanping Bu, Han-Shue Tan, and Jihua Huang (June 2010). "Design and field testing of a Cooperative Adaptive Cruise Control system". In: *Proceedings of the 2010 American Control Conference*. IEEE, pp. 4616–4621. ISBN: 978-1-4244-7427-1. DOI: 10.1109/ ACC.2010.5531155. URL: http://ieeexplore.ieee.org/lpdocs/epic03/wrapper. htm?arnumber=5531155.

Ferreau, Hans Joachim, Christian Kirches, Andreas Potschka, Hans Georg Bock, and Moritz Diehl (Dec. 2014). "qpOASES: a parametric active-set algorithm for quadratic programming". In: *Mathematical Programming Computation* 6.4, pp. 327–363. ISSN: 1867-2949. DOI: 10.1007/s12532-014-0071-1. URL: http://link.springer.com/ 10.1007/s12532-014-0071-1.

Filho, Carlos Massera, Marco H. Terra, and Denis F. Wolf (2017). "Safe Optimization of Highway Traffic With Robust Model Predictive Control-Based Cooperative Adaptive Cruise Control". In: *IEEE Transactions on Intelligent Transportation Systems*, pp. 1– 11. ISSN: 1524-9050. DOI: 10.1109/TITS.2017.2679098. URL: http://ieeexplore. ieee.org/document/7932167/.

Fiori, Chiara, Kyoungho Ahn, and Hesham A. Rakha (Apr. 2016). "Power-based electric vehicle energy consumption model: Model development and validation". In: *Applied Energy* 168, pp. 257–268. ISSN: 03062619. DOI: 10.1016/j.apenergy.2016.01.097. URL: http://linkinghub.elsevier.com/retrieve/pii/S030626191630085X.

Fischer, A (1992). "A special newton-type optimization method". In: *Optimization* 24.3-4, pp. 269–284. DOI: 10.1080/02331939208843795. URL: https://doi.org/10. 1080/02331939208843795.

Franke, Thomas, Peter Cocron, Josef F. Krems, Franziska Bühler, and Isabel Neumann (Sept. 2015). "Eco-driving strategies in battery electric vehicle use – how do drivers adapt over time?" In: *IET Intelligent Transport Systems* 9.7, pp. 746–753. ISSN: 1751-956X. DOI: 10.1049/iet-its.2014.0221. URL: http://digital-library.theiet. org/content/journals/10.1049/iet-its.2014.0221.

Fukushima, Masao, Zhi-Quan Luo, and Jong-Shi Pang (1998). "A Globally Convergent Sequential Quadratic Programming Algorithm for Mathematical Programs with Linear Complementarity Constraints". In: *Computational Optimization and Applications* 10.1, pp. 5–34. ISSN: 09266003. DOI: 10.1023/A:1018359900133. URL: http: //link.springer.com/10.1023/A:1018359900133.

Fwa, T. F. (2006). *The Handbook of Highway Engineering*. CRC Press, Taylor & Francis Group, p. 848. ISBN: 0-8493-1986-2. URL: https://www.crcpress.com/The-Handbook-of-Highway-Engineering/Fwa/p/book/9780849319860.

Gagliardi, Davide, T. Othsuka, and L. del Re (2014). "Direct C/GMRES Control of The Air Path of a Diesel Engine". In: *IFAC Proceedings Volumes* 47.3, pp. 3000–3005. ISSN: 14746670. DOI: 10.3182/20140824-6-ZA-1003.02481. URL: http://linkinghub.elsevier.com/retrieve/pii/S1474667016420677.

Ganji, Behnam, Abbas Z Kouzani, Sui Yang Khoo, and Mojtaba Shams-Zahraei (Feb. 2014). "Adaptive cruise control of a HEV using sliding mode control". In: *Expert Systems with Applications* 41.2, pp. 607–615. ISSN: 09574174. DOI: 10.1016/j.eswa.2013.07.085. URL: http://linkinghub.elsevier.com/retrieve/pii/S0957417413005861.

Geringer, Bernhard and Werner K. Tober (2012). *Battery Electric Vehicles in Practice*. Tech. rep. Austrian Society of Automotive Engineers (OEVK), the Austrian Automobile, Motorcycle, and Touring Club (OEAMTC), p. 83. URL: http://www.%7B%5C%22%7Bo%7D%7Dvk.at/aktuelles/2012/Battery%20Electric%20Vehicles%20in%20Practice.pdf.

Gilbert, Elmer G. (Mar. 1976). "Vehicle cruise: Improved fuel economy by periodic control". In: *Automatica* 12.2, pp. 159–166. ISSN: 00051098. DOI: 10.1016/0005-1098(76)90079-0. URL: http://linkinghub.elsevier.com/retrieve/pii/0005109876900790.

Glaser, Sebastien, Olivier Orfila, Lydie Nouveliere, Roman Potarusov, Sagar Akhegaonkar, Frederic Holzmann, and Volker Scheuch (June 2013). "Smart and Green ACC, adaptation of the ACC strategy for electric vehicle with regenerative capacity". In: *2013 IEEE Intelligent Vehicles Symposium (IV)*. Iv. IEEE, pp. 970–975. ISBN: 978-1-4673-2755-8. DOI: 10.1109/IVS.2013.6629592. URL: http://ieeexplore.ieee.org/document/6629592/.

Gonzalez, Jhonny (2015). "Modelling and Controlling Risk in Energy Systems". Doctor of Philosophy. University of Manchester, p. 245. URL: http://eprints.maths.manchester.ac.uk/2406/1/PhDthesis%7B%5C_%7DJhonny%7B%5C_%7DGonzalez.pdf.

Gonzalez, Jhonny and John Moriarty (July 2014). "Risk-sensitive optimal switching and applications to district energy systems". In: *2014 International Conference on Probabilistic Methods Applied to Power Systems (PMAPS)*. IEEE, pp. 1–6. ISBN: 978-1-4799-3561-1. DOI: 10.1109/PMAPS.2014.6960649. URL: http://ieeexplore.ieee.org/document/6960649/.

Goodrich, M.A. and E.R. Boer (1998). "Semiotics and mental models: modeling automobile driver behavior". In: *Proceedings of the 1998 IEEE International Symposium on Intelligent Control (ISIC) held jointly with IEEE International Symposium on Computational Intelligence in Robotics and Automation (CIRA) Intelligent Systems and Semiotics (ISAS) (Cat. No.98CH36262)*. IEEE, pp. 771–776. ISBN: 0-7803-4423-5. DOI: 10.1109/ISIC.1998.713817. URL: http://ieeexplore.ieee.org/document/713817/.

Graichen, Knut, Andreas Kugi, Nicolas Petit, and Francois Chaplais (Nov. 2010). "Handling constraints in optimal control with saturation functions and system extension". In: *Systems & Control Letters* 59.11, pp. 671–679. ISSN: 01676911. DOI: 10.1016/j.sysconle.2010.08.003. URL: http://linkinghub.elsevier.com/retrieve/pii/S0167691110001076.

Grancharova, Alexandra and Tor Arne Johansen (2012). *Explicit Nonlinear Model Predictive Control*. Vol. 429. Lecture Notes in Control and Information Sciences. Berlin, Heidelberg: Springer Berlin Heidelberg. ISBN: 978-3-642-28779-4. DOI: 10.1007/978-3-642-28780-0. URL: http://link.springer.com/10.1007/978-3-642-28780-0.

Graser, Anita, Johannes Asamer, and Wolfgang Ponweiser (June 2015). "The elevation factor: Digital elevation model quality and sampling impacts on electric vehicle energy estimation errors". In: *2015 International Conference on Models and Technologies for Intelligent Transportation Systems (MT-ITS)*. Vol. 1. June. IEEE, pp. 81–86. ISBN: 978-9-6331-3140-4. DOI: 10.1109/MTITS.2015.7223240. URL: http://ieeexplore.ieee.org/lpdocs/epic03/wrapper.htm?arnumber=7223240.

Grüne, Lars and Jürgen Pannek (2011). *Nonlinear Model Predictive Control*. Communications and Control Engineering. London: Springer London. ISBN: 978-0-85729-500-2. DOI: 10.1007/978-0-85729-501-9. URL: http://link.springer.com/10.1007/978-0-85729-501-9.

Grüne, Lars and Marleen Stieler (Aug. 2014). "Asymptotic stability and transient optimality of economic MPC without terminal conditions". In: *Journal of Process Control* 24.8, pp. 1187–1196. ISSN: 09591524. DOI: 10.1016/j.jprocont.2014.05.003. URL: http://linkinghub.elsevier.com/retrieve/pii/S0959152414001401.

Guarnieri, Massimo (Sept. 2012). "Looking back to electric cars". In: *2012 Third IEEE HISTory of ELectro-technology CONference (HISTELCON)*. IEEE, pp. 1–6. ISBN: 978-1-4673-3078-7. DOI: 10.1109/HISTELCON.2012.6487583. URL: http://ieeexplore.ieee.org/lpdocs/epic03/wrapper.htm?arnumber=6487583.

Hajek, W., I. Gaponova, K.H. Fleischer, and J. Krems (Sept. 2013). "Workload-adaptive cruise control – A new generation of advanced driver assistance systems". In: *Transportation Research Part F: Traffic Psychology and Behaviour* 20, pp. 108–120. ISSN: 13698478. DOI: 10.1016/j.trf.2013.06.001. URL: http://linkinghub.elsevier.com/retrieve/pii/S1369847813000582.

Harris, Mark (2014). *How Google's Autonomous Car Passed the First U.S. State Self-Driving Test.* URL: http://spectrum.ieee.org/transportation/advanced-cars/how-googles-autonomous-car-passed-the-first-us-state-selfdriving-test (visited on 04/07/2016).

Hasch, Jürgen, Eray Topak, Raik Schnabel, Thomas Zwick, Robert Weigel, and Christian Waldschmidt (Mar. 2012). "Millimeter-Wave Technology for Automotive Radar Sensors in the 77 GHz Frequency Band". In: *IEEE Transactions on Microwave Theory and Techniques* 60.3, pp. 845–860. ISSN: 0018-9480. DOI: 10.1109/TMTT.2011.2178427. URL: http://ieeexplore.ieee.org/lpdocs/epic03/wrapper.htm?arnumber=6127923.

Hawkins, Andrew J. (2017). *Waymo is first to put fully self-driving cars on US roads without a safety driver.* URL: https://www.theverge.com/2017/11/7/16615290/waymo-self-driving-safety-driver-chandler-autonomous.

Heppeler, Gunter, Marcus Sonntag, and Oliver Sawodny (2014). "Fuel Efficiency Analysis for Simultaneous Optimization of the Velocity Trajectory and the Energy Management in Hybrid Electric Vehicles". In: *IFAC Proceedings Volumes* 47.3, pp. 6612–6617. ISSN: 14746670. DOI: 10.3182/20140824-6-ZA-1003.00286. URL: http://linkinghub.elsevier.com/retrieve/pii/S1474667016426510.

Herceg, Domagoj, Pantelis Sopasakis, Alberto Bemporad, and Panagiotis Patrinos (Apr. 2017). "Risk-averse model predictive control". In: arXiv: 1704.00342. URL: http://arxiv.org/abs/1704.00342.

Hessem, D.H. van and O.H. Bosgra (2003). "A full solution to the constrained stochastic closed-loop MPC problem via state and innovations feedback and its receding horizon implementation". In: *42nd IEEE International Conference on Decision and Control (IEEE Cat. No.03CH37475).* Vol. 1. IEEE, pp. 929–934. ISBN: 0-7803-7924-1. DOI: 10.1109/CDC.2003.1272686. URL: http://ieeexplore.ieee.org/document/1272686/.

Hof, Tineke, Luis Conde, Eva Garcia, Alessandro Iviglia, Samantha Jamson, Ann Jopson, Frank Lai, Natasha Merat, Jonna Nyberg, Samuel Rios, David Sanchez, Steffen Schneider, Philipp Seewald, Caroline van der Weerdt, Remco Wijn, and Adrian Zlocki

(2014). *D11.1: A state of the art review and user's expectations. ecoDriver Project.* Tech. rep., p. 202. URL: www.ecodriver-project.eu.

Hosseinpour, Shima, Hongyi Chen, and Hua Tang (Aug. 2015). "Barriers to the wide adoption of electric vehicles: A literature review based discussion". In: *2015 Portland International Conference on Management of Engineering and Technology (PICMET).* IEEE, pp. 2329–2336. ISBN: 978-1-8908-4331-1. DOI: 10.1109/PICMET.2015.7273259. URL: http://ieeexplore.ieee.org/lpdocs/epic03/wrapper.htm?arnumber=7273259.

Huang, Mike, Hayato Nakada, Ken Butts, and Ilya Kolmanovsky (2015). "Nonlinear Model Predictive Control of a Diesel Engine Air Path: A Comparison of Constraint Handling and Computational Strategies". In: *IFAC-PapersOnLine* 48.23, pp. 372–379. ISSN: 24058963. DOI: 10.1016/j.ifacol.2015.11.308. URL: http://linkinghub.elsevier.com/retrieve/pii/S2405896315025926.

Huang, Yanjun, Hong Wang, Amir Khajepour, Hongwen He, and Jie Ji (Feb. 2017). "Model predictive control power management strategies for HEVs: A review". In: *Journal of Power Sources* 341, pp. 91–106. ISSN: 03787753. DOI: 10.1016/j.jpowsour.2016.11.106. URL: http://linkinghub.elsevier.com/retrieve/pii/S0378775316316731.

INL (2014). *BEV Battery Testing Results, Smart Electric Drive - VIN 2457.* Tech. rep. Idaho National Laboratory, Advanced Vehicle Testing Activity, p. 4. URL: http://avt.inl.gov/pdf/fsev/batteryElectric2457.pdf.

ISO 15622 (2010). *Intelligent transport systems – Adaptive Cruise Control systems – Performance requirements and test procedures.* Tech. rep. ISO - International Organization for Standardization, p. 25. URL: http://www.iso.org/iso/iso%7B%5C_%7Dcatalogue/catalogue%7B%5C_%7Dtc/catalogue%7B%5C_%7Ddetail.htm?csnumber=50024.

ISO 22178 (2009). *Intelligent transport systems – Low speed following (LSF) systems – Performance requirements and test procedures.* Tech. rep. ISO - International Organization for Standardization, p. 28. URL: http://www.iso.org/iso/catalogue%7B%5C_%7Ddetail.htm?csnumber=40752.

Ito, Yuji, Kenji Fujimoto, Yukihiro Tadokoro, and Takayoshi Yoshimura (Dec. 2015). "On linear solutions to a class of risk sensitive control for linear systems with stochastic parameters". In: *2015 54th IEEE Conference on Decision and Control (CDC).* Vol. 4. Cdc. IEEE, pp. 6516–6523. ISBN: 978-1-4799-7886-1. DOI: 10.1109/CDC.2015.7403246. URL: http://ieeexplore.ieee.org/lpdocs/epic03/wrapper.htm?arnumber=7403246.

Izmailov, Alexey F and Mikhail V Solodov (2014). *Newton-Type Methods for Optimization and Variational Problems*. Springer Series in Operations Research and Financial Engineering. Cham: Springer International Publishing. ISBN: 978-3-319-04246-6. DOI: 10.1007/978-3-319-04247-3. URL: http://link.springer.com/10.1007/978-3-319-04247-3.

Jacobson, D. (Apr. 1973). "Optimal stochastic linear systems with exponential performance criteria and their relation to deterministic differential games". In: *IEEE Transactions on Automatic Control* 18.2, pp. 124–131. ISSN: 0018-9286. DOI: 10.1109/TAC.1973.1100265. URL: http://ieeexplore.ieee.org/document/1100265/.

Jeong, S. H., J. E. Lee, S. U. Choi, J. N. Oh, and K. H. Lee (Dec. 2012). "Technology analysis and low-cost design of automotive radar for adaptive cruise control system". In: *International Journal of Automotive Technology* 13.7, pp. 1133–1140. ISSN: 1229-9138. DOI: 10.1007/s12239-012-0116-2. URL: http://link.springer.com/10.1007/s12239-012-0116-2.

Jia, Dongyao, Kejie Lu, Jianping Wang, Xiang Zhang, and Xuemin Shen (Jan. 2016). "A Survey on Platoon-Based Vehicular Cyber-Physical Systems". In: *IEEE Communications Surveys & Tutorials* 18.1, pp. 263–284. ISSN: 1553-877X. DOI: 10.1109/COMST.2015.2410831. arXiv: arXiv:1011.1669v3. URL: http://ieeexplore.ieee.org/lpdocs/epic03/wrapper.htm?arnumber=7056505.

Jiang, Houyuan and Daniel Ralph (Jan. 2000). "Smooth SQP Methods for Mathematical Programs with Nonlinear Complementarity Constraints". In: *SIAM Journal on Optimization* 10.3, pp. 779–808. ISSN: 1052-6234. DOI: 10.1137/S1052623497332329. URL: http://epubs.siam.org/doi/10.1137/S1052623497332329.

Jones, W.D. (2001). "Keeping cars from crashing". In: *IEEE Spectrum* 38.9, pp. 40–45. ISSN: 00189235. DOI: 10.1109/6.946636. URL: http://ieeexplore.ieee.org/lpdocs/epic03/wrapper.htm?arnumber=946636.

Kamal, M A S, Masakazu Mukai, Junichi Murata, and Taketoshi Kawabe (Sept. 2011). "Ecological Vehicle Control on Roads With Up-Down Slopes". In: *IEEE Transactions on Intelligent Transportation Systems* 12.3, pp. 783–794. ISSN: 1524-9050. DOI: 10.1109/TITS.2011.2112648. URL: http://ieeexplore.ieee.org/document/5721826/.

Kamal, M. A S, Masakazu Mukai, Junichi Murata, and Taketoshi Kawabe (Sept. 2011). "Ecological Vehicle Control on Roads With Up-Down Slopes". In: *IEEE Transactions on Intelligent Transportation Systems* 12.3, pp. 783–794. ISSN: 1524-9050. DOI: 10.1109/TITS.2011.2112648. URL: http://ieeexplore.ieee.org/lpdocs/epic03/wrapper.htm?arnumber=5721826.

Kamal, Md Abdus Samad, Masakazu Mukai, Junichi Murata, and Taketoshi Kawabe (May 2013). "Model Predictive Control of Vehicles on Urban Roads for Improved Fuel Economy". In: *IEEE Transactions on Control Systems Technology* 21.3, pp. 831–841. ISSN: 1063-6536. DOI: 10.1109/TCST.2012.2198478. URL: http://ieeexplore.ieee.org/document/6214590/.

Kantas, N, J. M. Maciejowski, and A. Lecchini-Visintini (2009). "Sequential Monte Carlo for Model Predictive Control". In: *Nonlinear Model Predictive ...* Pp. 263–273. ISBN: 978-0-85729-500-2. DOI: 10.1007/978-3-642-01094-1\_21. URL: http://link.springer.com/chapter/10.1007/978-3-642-01094-1%7B%5C_%7D21%20http://link.springer.com/10.1007/978-3-642-01094-1%7B%5C_%7D21.

Kanzow, Christian and Heiko Pieper (Jan. 1999). "Jacobian Smoothing Methods for Nonlinear Complementarity Problems". In: *SIAM Journal on Optimization* 9.2, pp. 342–373. ISSN: 1052-6234. DOI: 10.1137/S1052623497328781. URL: http://epubs.siam.org/doi/10.1137/S1052623497328781.

Kelley, C T (Jan. 1995). *Iterative Methods for Linear and Nonlinear Equations*. Vol. 16. 11. Society for Industrial and Applied Mathematics, pp. 166. ISBN: 978-0-89871-352-7. DOI: 10.1137/1.9781611970944. URL: http://epubs.siam.org/doi/book/10.1137/1.9781611970944.

Khayyam, Hamid and Alireza Bab-Hadiashar (May 2014). "Adaptive intelligent energy management system of plug-in hybrid electric vehicle". In: *Energy* 69, pp. 319–335. ISSN: 03605442. DOI: 10.1016/j.energy.2014.03.020. URL: http://linkinghub.elsevier.com/retrieve/pii/S0360544214002825.

Khayyam, Hamid, Saeid Nahavandi, and Sam Davis (Feb. 2012). "Adaptive cruise control look-ahead system for energy management of vehicles". In: *Expert Systems with Applications* 39.3, pp. 3874–3885. ISSN: 09574174. DOI: 10.1016/j.eswa.2011.08.169. URL: http://linkinghub.elsevier.com/retrieve/pii/S0957417411013005.

Khodayari, Alireza, Ali Ghaffari, Sina Ameli, and Jamal Flahatgar (Sept. 2010). "A historical review on lateral and longitudinal control of autonomous vehicle motions". In: *2010 International Conference on Mechanical and Electrical Technology*. Icmet. IEEE, pp. 421–429. ISBN: 978-1-4244-8100-2. DOI: 10.1109/ICMET.2010.5598396. URL: http://ieeexplore.ieee.org/lpdocs/epic03/wrapper.htm?arnumber=5598396.

Kim, Beomjun and Kyongsu Yi (Oct. 2014). "Probabilistic and Holistic Prediction of Vehicle States Using Sensor Fusion for Application to Integrated Vehicle Safety Systems". In: *IEEE Transactions on Intelligent Transportation Systems* 15.5, pp. 2178–

2190. ISSN: 1524-9050. DOI: 10.1109/TITS.2014.2312720. URL: http://ieeexplore.ieee.org/document/6815699/.

Kim, Dongwook Kim Dongwook, Seungwuk Moon Seungwuk Moon, Jaemann Park Jaemann Park, H.J. Kim, and Kyongsu Yi Kyongsu Yi (2009). "Design of an Adaptive Cruise Control / Collision Avoidance with lane change support for vehicle autonomous driving". In: *ICCAS-SICE, 2009.* Fukuoka, pp. 2938–2943. ISBN: 978-4-907764-34-0. URL: http://ieeexplore.ieee.org/document/5333840/.

Knapp, Andreas, Markus Neumann, Martin Brockmann, Rainer Walz, and Thomas Winkle (2009). *Code of Practice for the Design and Evaluation of ADAS Revision chart and history log Deliverable of the RESPONSE 3 project.* Tech. rep., p. 115. URL: http://www.acea.be/uploads/publications/20090831_Code_of_Practice_ADAS.pdf.

Knyazev, Andrew and Alexander Malyshev (Jan. 2017). "Preconditioned warm-started Newton-Krylov methods for MPC with discontinuous control". In: *2017 Proceedings of the Conference on Control and its Applications.* Philadelphia, PA: Society for Industrial and Applied Mathematics, pp. 1–8. DOI: 10.1137/1.9781611975024.1. arXiv: arXiv:1704.06973v1. URL: http://epubs.siam.org/doi/10.1137/1.9781611975024.1.

Langson, W., I. Chryssochoos, S.V. Raković, and D.Q. Mayne (Jan. 2004). "Robust model predictive control using tubes". In: *Automatica* 40.1, pp. 125–133. ISSN: 00051098. DOI: 10.1016/j.automatica.2003.08.009. URL: http://linkinghub.elsevier.com/retrieve/pii/S0005109803002838.

LeCun, Yann, Yoshua Bengio, and Geoffrey Hinton (May 2015). "Deep learning". In: *Nature* 521.7553, pp. 436–444. ISSN: 0028-0836. URL: http://10.0.4.14/nature14539.

Li, Keqiang, Tao Chen, Yugong Luo, and Jianqiang Wang (Mar. 2012). "Intelligent Environment Friendly Vehicles: Concept and Case Studies". In: *IEEE Transactions on Intelligent Transportation Systems* 13.1, pp. 318–328. ISSN: 1524-9050. DOI: 10.1109/TITS.2011.2170680. URL: http://ieeexplore.ieee.org/document/6064893/.

Li, Shengbo Eben, Qiangqiang Guo, Shaobing Xu, Jingliang Duan, Shen Li, Chengjun Li, and Kuifeng Su (2017). "Performance Enhanced Predictive Control for Adaptive Cruise Control System Considering Road Elevation Information". In: *IEEE Transactions on Intelligent Vehicles* 8858.2, pp. 1–1. ISSN: 2379-8904. DOI: 10.1109/TIV.2017.2736246. URL: http://ieeexplore.ieee.org/document/8002647/.

Li, Shengbo Eben, Zhenzhong Jia, Keqiang Li, and Bo Cheng (June 2015). "Fast Online Computation of a Model Predictive Controller and Its Application to Fuel Economy-Oriented Adaptive Cruise Control". In: *IEEE Transactions on Intelligent Transportation Systems* 16.3, pp. 1199–1209. ISSN: 1524-9050. DOI: 10 . 1109 / TITS . 2014 . 2354052. URL: http://ieeexplore.ieee.org/document/6899598/.

Li, Shengbo Eben, Yang Zheng, Keqiang Li, Le-Yi Wang, and Hongwei Zhang (2017). "Platoon Control of Connected Vehicles from a Networked Control Perspective: Literature Review, Component Modeling, and Controller Synthesis". In: *IEEE Transactions on Vehicular Technology* 9545.2014, pp. 1–1. ISSN: 0018-9545. DOI: 10.1109/ TVT.2017.2723881. URL: http://ieeexplore.ieee.org/document/7970188/.

Li, Shengbo, Keqiang Li, Rajesh Rajamani, and Jianqiang Wang (May 2011). "Model Predictive Multi-Objective Vehicular Adaptive Cruise Control". In: *IEEE Transactions on Control Systems Technology* 19.3, pp. 556–566. ISSN: 1063-6536. DOI: 10 . 1109 / TCST . 2010 . 2049203. URL: http : / / ieeexplore . ieee . org / document / 5471064/.

Li, Xiaohui, Zhenping Sun, Dongpu Cao, Zhen He, and Qi Zhu (Apr. 2016). "Real-Time Trajectory Planning for Autonomous Urban Driving: Framework, Algorithms, and Verifications". In: *IEEE/ASME Transactions on Mechatronics* 21.2, pp. 740–753. ISSN: 1083-4435. DOI: 10.1109/TMECH.2015.2493980. URL: http://ieeexplore. ieee.org/document/7303933/.

Li, Yongfu, Li Zhang, Hong Zheng, Xiaozheng He, Srinivas Peeta, Taixiong Zheng, and Yinguo Li (Oct. 2015). "Evaluating the energy consumption of electric vehicles based on car-following model under non-lane discipline". In: *Nonlinear Dynamics* 82.1-2, pp. 629–641. ISSN: 0924-090X. DOI: 10 . 1007 / s11071 – 015 – 2183 – 1. URL: http : //link.springer.com/10.1007/s11071-015-2183-1.

Liang, Kuo-Yun, Jonas Mårtensson, and Karl Henrik Johansson (2013). "When is it Fuel Efficient for a Heavy Duty Vehicle to Catch Up With a Platoon?" In: *IFAC Proceedings Volumes* 46.21, pp. 738–743. ISSN: 14746670. DOI: 10.3182/20130904- 4 – JP – 2042 . 00071. URL: http : / / linkinghub . elsevier . com / retrieve / pii / S1474667016384622.

Lohse-Busch, Henning, Michael Duoba, Eric Rask, Kevin Stutenberg, Vivek Gowri, Lee Slezak, and David Anderson (Apr. 2013). "Ambient Temperature (20°F, 72°F and 95°F) Impact on Fuel and Energy Consumption for Several Conventional Vehicles, Hybrid and Plug-In Hybrid Electric Vehicles and Battery Electric Vehicle". In: DOI: 10.4271/2013-01-1462. URL: http://papers.sae.org/2013-01-1462/.

Lorenzen, Matthias, Fabrizio Dabbene, Roberto Tempo, and Frank Allgower (July 2017). "Constraint-Tightening and Stability in Stochastic Model Predictive Control". In: *IEEE Transactions on Automatic Control* 62.7, pp. 3165–3177. ISSN: 0018-9286. DOI: 10.1109/TAC.2016.2625048. URL: http://ieeexplore.ieee.org/document/7733074/.

Luenberger, David G. and Yinyu Ye (2008). *Linear and Nonlinear Programming*. Vol. 116. International Series in Operations Research & Management Science. Boston, MA: Springer US. ISBN: 978-0-387-74502-2. DOI: 10.1007/978-0-387-74503-9. URL: http://link.springer.com/10.1007/978-0-387-74503-9.

Ma, Yudong, Sergey Vichik, and Francesco Borrelli (Dec. 2012). "Fast stochastic MPC with optimal risk allocation applied to building control systems". In: *2012 IEEE 51st IEEE Conference on Decision and Control (CDC)*. IEEE, pp. 7559–7564. ISBN: 978-1-4673-2066-5. DOI: 10.1109/CDC.2012.6426251. URL: http://ieeexplore.ieee.org/lpdocs/epic03/wrapper.htm?arnumber=6426251.

Maciejowski, Jan Marian (2002). *Predictive Control: With Constraints*. Pearson Education. Prentice Hall, p. 331. ISBN: 0201398230, 9780201398236. URL: www-control.eng.cam.ac.uk/jmm/mpcbook/mpcbook.html.

Malakorn, Kristin J. and Byungkyu Park (May 2010). "Assessment of mobility, energy, and environment impacts of IntelliDrive-based Cooperative Adaptive Cruise Control and Intelligent Traffic Signal control". In: *Proceedings of the 2010 IEEE International Symposium on Sustainable Systems and Technology*. IEEE, pp. 1–6. ISBN: 978-1-4244-7094-5. DOI: 10.1109/ISSST.2010.5507709. URL: http://ieeexplore.ieee.org/lpdocs/epic03/wrapper.htm?arnumber=5507709.

MarkVollrath, Susanne Schleicher, and Christhard Gelau (May 2011). "The influence of Cruise Control and Adaptive Cruise Control on driving behaviour – A driving simulator study". In: *Accident Analysis & Prevention* 43.3, pp. 1134–1139. ISSN: 00014575. DOI: 10.1016/j.aap.2010.12.023. URL: http://linkinghub.elsevier.com/retrieve/pii/S0001457510004008.

Marsden, Greg, Mike McDonald, and Mark Brackstone (Feb. 2001). "Towards an understanding of adaptive cruise control". In: *Transportation Research Part C: Emerging Technologies* 9.1, pp. 33–51. ISSN: 0968090X. DOI: 10.1016/S0968-090X(00)00022-X. URL: http://linkinghub.elsevier.com/retrieve/pii/S0968090X0000022X.

Marzbanrad, Javad and Iman Tahbaz-zadeh Moghaddam (Sept. 2016). "Self-tuning control algorithm design for vehicle adaptive cruise control system through real-time estimation of vehicle parameters and road grade". In: *Vehicle System Dynamics* 54.9,

pp. 1291–1316. ISSN: 0042-3114. DOI: 10.1080/00423114.2016.1199886. URL: https://www.tandfonline.com/doi/full/10.1080/00423114.2016.1199886.

Maurer, Markus and Hermann Winner (2013). *Automotive Systems Engineering*. Ed. by Markus Maurer and Hermann Winner. Berlin, Heidelberg: Springer Berlin Heidelberg, p. 268. ISBN: 978-3-642-36454-9. DOI: 10.1007/978-3-642-36455-6. URL: http://www.springer.com/in/book/9783642364549.

Mayne, D.Q., J.B. Rawlings, C.V. Rao, and P.O.M. Scokaert (June 2000). "Constrained model predictive control: Stability and optimality". In: *Automatica* 36.6, pp. 789–814. ISSN: 00051098. DOI: 10.1016/S0005-1098(99)00214-9. URL: http://linkinghub.elsevier.com/retrieve/pii/S0005109899002149.

Mayne, David (2016). "Robust and stochastic model predictive control: Are we going in the right direction?" In: *Annual Reviews in Control* 41, pp. 184–192. ISSN: 13675788. DOI: 10.1016/j.arcontrol.2016.04.006. URL: http://linkinghub.elsevier.com/retrieve/pii/S1367578816300098.

Mayne, David Q. (Dec. 2014). "Model predictive control: Recent developments and future promise". In: *Automatica* 50.12, pp. 2967–2986. ISSN: 00051098. DOI: 10.1016/j.automatica.2014.10.128. URL: http://linkinghub.elsevier.com/retrieve/pii/S0005109814005160.

Mayne, David Q. and Eric C. Kerrigan (2007). "Tube-based Robust Nonlinear Model Predictive Control". In: *IFAC Proceedings Volumes* 40.12, pp. 36–41. ISSN: 14746670. DOI: 10.3182/20070822-3-ZA-2920.00006. URL: http://linkinghub.elsevier.com/retrieve/pii/S1474667016354994.

McDonough, K, I Kolmanovsky, D Filev, D Yanakiev, S Szwabowski, and J Michelini (June 2012). "Stochastic dynamic programming control policies for fuel efficient intraffic driving". In: *2012 American Control Conference (ACC)*. 734. IEEE, pp. 3986–3991. ISBN: 978-1-4577-1096-4. DOI: 10.1109/ACC.2012.6314889. URL: http://ieeexplore.ieee.org/document/6314889/.

Mesbah, Ali (Dec. 2016). "Stochastic Model Predictive Control: An Overview and Perspectives for Future Research". In: *IEEE Control Systems* 36.6, pp. 30–44. ISSN: 1066-033X. DOI: 10.1109/MCS.2016.2602087. URL: http://ieeexplore.ieee.org/document/7740982/.

Mesbah, Ali, Stefan Streif, Rolf Findeisen, and Richard D. Braatz (June 2014). "Stochastic nonlinear model predictive control with probabilistic constraints". In: *2014 American Control Conference*. IEEE, pp. 2413–2419. ISBN: 978-1-4799-3274-0. DOI: 10.1109/ACC.2014.6858851. arXiv: arXiv:1410.4535v1. URL: http://ieeexplore.ieee.org/lpdocs/epic03/wrapper.htm?arnumber=6858851.

Milanes, Vicente, Steven E. Shladover, John Spring, Christopher Nowakowski, Hiroshi Kawazoe, and Masahide Nakamura (Feb. 2014). "Cooperative Adaptive Cruise Control in Real Traffic Situations". In: *IEEE Transactions on Intelligent Transportation Systems* 15.1, pp. 296–305. ISSN: 1524-9050. DOI: 10.1109/TITS.2013.2278494. URL: http://ieeexplore.ieee.org/lpdocs/epic03/wrapper.htm?arnumber=6588305.

Milanes, Vicente, Jorge Villagra, Jorge Godoy, and Carlos Gonzalez (May 2012). "Comparing Fuzzy and Intelligent PI Controllers in Stop-and-Go Manoeuvres". In: *IEEE Transactions on Control Systems Technology* 20.3, pp. 770–778. ISSN: 1063-6536. DOI: 10.1109/TCST.2011.2135859. URL: http://ieeexplore.ieee.org/lpdocs/epic03/wrapper.htm?arnumber=5756467.

Miyata, Shigeharu, Takashi Nakagami, Sei Kobayashi, Tomoji Izumi, Hisayoshi Naito, Akira Yanou, Hitomi Nakamura, and Shin Takehara (2010). "Improvement of Adaptive Cruise Control Performance". In: *EURASIP Journal on Advances in Signal Processing* 2010.1, p. 295016. ISSN: 1687-6180. DOI: 10.1155/2010/295016. URL: http://asp.eurasipjournals.com/content/2010/1/295016.

Montanaro, Umberto, Manuela Tufo, Giovanni Fiengo, Mario di Bernardo, Alessandro Salvi, and Stefania Santini (June 2014). "Extended Cooperative Adaptive Cruise Control". In: *2014 IEEE Intelligent Vehicles Symposium Proceedings.* Iv. IEEE, pp. 605–610. ISBN: 978-1-4799-3638-0. DOI: 10.1109/IVS.2014.6856530. URL: http://ieeexplore.ieee.org/lpdocs/epic03/wrapper.htm?arnumber=6856530.

Moon, Seungwuk, Ilki Moon, and Kyongsu Yi (Apr. 2009). "Design, tuning, and evaluation of a full-range adaptive cruise control system with collision avoidance". In: *Control Engineering Practice* 17.4, pp. 442–455. ISSN: 09670661. DOI: 10.1016/j.conengprac.2008.09.006. URL: http://linkinghub.elsevier.com/retrieve/pii/S0967066108001548.

Moran, Kevin, Brendan Foley, Ulrich Fastenrath, and Jeff Raimo (Oct. 2010). "Digital Maps, Connectivity and Electric Vehicles - Enhancing the EV/PHEV Ownership Experience". In: *SAE International Journal of Passenger Cars - Electronic and Electrical Systems* 3.2, pp. 2010–01–2316. ISSN: 1946-4622. DOI: 10.4271/2010-01-2316. URL: http://papers.sae.org/2010-01-2316/.

Moser, Dominik (2015). "Stochastic Model Predictive Control Applied to Cooperative Adaptive Cruise Control". Master's thesis, Johannes Kepler University Linz, p. 111. URL: http://epub.jku.at/obvulihs/content/pageview/388428.

Moser, Dominik, Roman Schmied, Harald Waschl, and Luigi del Re (Jan. 2018). "Flexible Spacing Adaptive Cruise Control Using Stochastic Model Predictive Control".

In: *IEEE Transactions on Control Systems Technology* 26.1, pp. 114–127. ISSN: 1063-6536. DOI: 10.1109/TCST.2017.2658193. URL: http://ieeexplore.ieee.org/document/7862832/.

Moser, Dominik, Harald Waschl, Harald Kirchsteiger, Roman Schmied, and Luigi del Re (July 2015). "Cooperative adaptive cruise control applying stochastic linear model predictive control strategies". In: *2015 European Control Conference (ECC)*. IEEE, pp. 3383–3388. ISBN: 978-3-9524-2693-7. DOI: 10.1109/ECC.2015.7331057. URL: http://ieeexplore.ieee.org/document/7331057/.

Müller, Matthias A. and Karl Worthmann (Aug. 2017). "Quadratic costs do not always work in MPC". In: *Automatica* 82, pp. 269–277. ISSN: 00051098. DOI: 10.1016/j.automatica.2017.04.058. URL: http://linkinghub.elsevier.com/retrieve/pii/S0005109817302522.

Naranjo, J.E., C. Gonzalez, R. Garcia, and T. DePedro (June 2006). "ACC+Stop&Go Maneuvers With Throttle and Brake Fuzzy Control". In: *IEEE Transactions on Intelligent Transportation Systems* 7.2, pp. 213–225. ISSN: 1524-9050. DOI: 10.1109/TITS.2006.874723. URL: http://ieeexplore.ieee.org/lpdocs/epic03/wrapper.htm?arnumber=1637676.

Naus, G.J.L., J. Ploeg, M.J.G. Van de Molengraft, W.P.M.H. Heemels, and M. Steinbuch (Aug. 2010). "Design and implementation of parameterized adaptive cruise control: An explicit model predictive control approach". In: *Control Engineering Practice* 18.8, pp. 882–892. ISSN: 09670661. DOI: 10.1016/j.conengprac.2010.03.012. URL: http://linkinghub.elsevier.com/retrieve/pii/S0967066110000882.

Naus, Gerrit, Jeroen Ploeg, Rene van de Molengraft, and Maarten Steinbuch (June 2008). "Explicit MPC design and performance-based tuning of an Adaptive Cruise Control Stop&Go". In: *2008 IEEE Intelligent Vehicles Symposium*. IEEE, pp. 434–439. ISBN: 978-1-4244-2568-6. DOI: 10.1109/IVS.2008.4621248. URL: http://ieeexplore.ieee.org/document/4621248/.

Naz, Rehana (Jan. 2018). "A current value Hamiltonian Approach for Discrete time Optimal Control Problems arising in Economic Growth". In: pp. 1–10. arXiv: 1801.03637. URL: http://arxiv.org/abs/1801.03637.

Ngoduy, D. (Oct. 2013). "Instability of cooperative adaptive cruise control traffic flow: A macroscopic approach". In: *Communications in Nonlinear Science and Numerical Simulation* 18.10, pp. 2838–2851. ISSN: 10075704. DOI: 10.1016/j.cnsns.2013.02.007. URL: http://linkinghub.elsevier.com/retrieve/pii/S1007570413000713.

Noga, Rafal, Toshiyuki Ohtsuka, Cesar de Prada, Enrique Blanco, and Juan Casas (Jan. 2011). "Simulation Study on Application of Nonlinear Model Predictive Control to the

Superfluid Helium Cryogenic Circuit". In: *IFAC Proceedings Volumes* 44.1, pp. 3647–3652. ISSN: 14746670. DOI: 10.3182/20110828-6-IT-1002.02156. URL: http://linkinghub.elsevier.com/retrieve/pii/S1474667016441777.

Nowakowski, Christopher, Jessica O'Connell, Steven E Shladover, and Delphine Cody (Sept. 2010). "Cooperative Adaptive Cruise Control: Driver Acceptance of Following Gap Settings Less than One Second". In: *Proceedings of the Human Factors and Ergonomics Society Annual Meeting* 54.24, pp. 2033–2037. ISSN: 1541-9312. DOI: 10.1177/154193121005402403. URL: http://pro.sagepub.com/lookup/doi/10.1177/154193121005402403.

Ohsumi, Kohei and Toshiyuki Ohtsuka (Jan. 2011). "Particle Model Predictive Control for Probability Density Functions". In: *IFAC Proceedings Volumes* 44.1, pp. 7993–7998. ISSN: 14746670. DOI: 10.3182/20110828-6-IT-1002.01904. URL: http://linkinghub.elsevier.com/retrieve/pii/S1474667016448937.

Ohtsuka, Toshiyuki (Apr. 2004). "A continuation/GMRES method for fast computation of nonlinear receding horizon control". In: *Automatica* 40.4, pp. 563–574. ISSN: 00051098. DOI: 10.1016/j.automatica.2003.11.005. URL: http://linkinghub.elsevier.com/retrieve/pii/S0005109803003637.

Ohtsuka, Toshiyuki and Kohei Ozaki (2009). "Practical Issues in Nonlinear Model Predictive Control: Real-Time Optimization and Systematic Tuning". In: pp. 447–460. DOI: 10.1007/978-3-642-01094-1_35. URL: http://link.springer.com/10.1007/978-3-642-01094-1%7B%5C_%7D35.

Ojeda, Luis Leon, Jihun Han, Antonio Sciarretta, Giovanni De Nunzio, and Laurent Thibault (Dec. 2017). "A real-time eco-driving strategy for automated electric vehicles". In: *2017 IEEE 56th Annual Conference on Decision and Control (CDC)*. Cdc. IEEE, pp. 2768–2774. ISBN: 978-1-5090-2873-3. DOI: 10.1109/CDC.2017.8264061. URL: http://ieeexplore.ieee.org/document/8264061/.

Oldewurtel, Frauke, David Sturzenegger, Peyman Mohajerin Esfahani, Goran Andersson, Manfred Morari, and John Lygeros (June 2013). "Adaptively constrained Stochastic Model Predictive Control for closed-loop constraint satisfaction". In: *2013 American Control Conference*. IEEE, pp. 4674–4681. ISBN: 978-1-4799-0178-4. DOI: 10.1109/ACC.2013.6580560. URL: http://ieeexplore.ieee.org/document/6580560/.

Ondruska, Peter and Ingmar Posner (June 2014). "Probabilistic attainability maps: Efficiently predicting driver-specific electric vehicle range". In: *2014 IEEE Intelligent Vehicles Symposium Proceedings*. IEEE, pp. 1169–1174. ISBN: 978-1-4799-3638-0. DOI:

10.1109/IVS.2014.6856572. URL: http://ieeexplore.ieee.org/document/6856572/.

Ono, Masahiro (Dec. 2012). "Closed-loop chance-constrained MPC with probabilistic resolvability". In: *2012 IEEE 51st IEEE Conference on Decision and Control (CDC)*. IEEE, pp. 2611–2618. ISBN: 978-1-4673-2066-5. DOI: 10.1109/CDC.2012.6427393. URL: http://ieeexplore.ieee.org/document/6427393/.

Ossen, Saskia (2008). *Longitudinal Driving Behavior : Theory and Empirics*. The Netherlands TRIAL Research School, pp. 1–268. ISBN: 9789055841028. URL: http://repository.tudelft.nl/islandora/object/uuid:fe2291ad-185b-4813-a518-e13ed31994a3/?collection=research.

Pomerleau, Dean A. (1989). *Alvinn: An autonomous land vehicle in a neural network*. Ed. by D. S. Touretzky. Morgan-Kaufmann, pp. 305–313. ISBN: 1-558-60015-9. URL: http://papers.nips.cc/paper/95-alvinn-an-autonomous-land-vehicle-in-a-neural-network.pdf.

Porsche (2016). *Porsche Panamera - Porsche InnoDrive inkl. Abstandsregeltempostat*. URL: http://www.porsche.com/germany/models/panamera/panamera/assistance-systems/porsche-innodrive/ (visited on 11/23/2016).

Poullikkas, Andreas (Jan. 2015). "Sustainable options for electric vehicle technologies". In: *Renewable and Sustainable Energy Reviews* 41, pp. 1277–1287. ISSN: 13640321. DOI: 10.1016/j.rser.2014.09.016. URL: http://linkinghub.elsevier.com/retrieve/pii/S1364032114007898.

Raff, Tobias, Christian Ebenbauer, and Frank Allgower (2007). *Assessment and Future Directions of Nonlinear Model Predictive Control*. Ed. by Rolf Findeisen, Frank Allgöwer, and Lorenz T. Biegler. Vol. 358. Lecture Notes in Control and Information Sciences. Berlin, Heidelberg: Springer Berlin Heidelberg, pp. 151–162. ISBN: 978-3-540-72698-2. DOI: 10.1007/978-3-540-72699-9. URL: http://link.springer.com/10.1007/978-3-540-72699-9.

Rahman, Khwaja M., Sinisa Jurkovic, Constantin Stancu, John Morgante, and Peter J. Savagian (May 2015). "Design and Performance of Electrical Propulsion System of Extended Range Electric Vehicle (EREV) Chevrolet Volt". In: *IEEE Transactions on Industry Applications* 51.3, pp. 2479–2488. ISSN: 0093-9994. DOI: 10.1109/TIA.2014.2363015. URL: http://ieeexplore.ieee.org/document/6928443/.

Rajamani, R. and C. Zhu (Sept. 2002). "Semi-autonomous adaptive cruise control systems". In: *IEEE Transactions on Vehicular Technology* 51.5, pp. 1186–1192. ISSN: 0018-9545. DOI: 10.1109/TVT.2002.800617. URL: http://ieeexplore.ieee.org/lpdocs/epic03/wrapper.htm?arnumber=1105955.

Rajamani, Rajesh, Han-Shue Tan, Boon Kait Law, and Wei-Bin Zhang (July 2000). "Demonstration of integrated longitudinal and lateral control for the operation of automated vehicles in platoons". In: *IEEE Transactions on Control Systems Technology* 8.4, pp. 695–708. ISSN: 10636536. DOI: 10.1109/87.852914. URL: http://ieeexplore.ieee.org/lpdocs/epic03/wrapper.htm?arnumber=852914.

Rao, Singiresu S. (July 2009). *Engineering Optimization*. Hoboken, NJ, USA: John Wiley & Sons, Inc., p. 829. ISBN: 9780470549124. DOI: 10.1002/9780470549124. URL: http://doi.wiley.com/10.1002/9780470549124.

Rawlings, J. B. and K. R. Muske (Oct. 1993). "The stability of constrained receding horizon control". In: *IEEE Transactions on Automatic Control* 38.10, pp. 1512–1516. ISSN: 0018-9286. DOI: 10.1109/9.241565. URL: http://ieeexplore.ieee.org/document/241565/.

Rawlings, James B., David Angeli, and Cuyler N. Bates (Dec. 2012). "Fundamentals of economic model predictive control". In: *2012 IEEE 51st IEEE Conference on Decision and Control (CDC)*. IEEE, pp. 3851–3861. ISBN: 978-1-4673-2066-5. DOI: 10.1109/CDC.2012.6425822. URL: http://ieeexplore.ieee.org/document/6425822/.

Rawlings, James B. and David Q. Mayne (2009). *Model Predictive Control : Theory and Design*. Nob Hill Publishing, LLC, p. 723. URL: http://jbrwww.che.wisc.edu/home/jbraw/mpc/.

Rawlings, James B., David Q. Mayne, and Moritz M. Diehl (2015). *Model Predictive Control: Theory and Design*. 2nd ed. Madison, Wisconsin: Nob Hill Publishing, p. 724. ISBN: 978-0-975-93770-9. URL: http://jbrwww.che.wisc.edu/home/jbraw/mpc/.

Re, Luigi del, Frank Allgöwer, Luigi Glielmo, Carlos Guardiola, and Ilya Kolmanovsky, eds. (2010). *Automotive Model Predictive Control*. Vol. 402. Lecture Notes in Control and Information Sciences. London: Springer London, p. 284. ISBN: 978-1-84996-070-0. DOI: 10.1007/978-1-84996-071-7. URL: http://link.springer.com/10.1007/978-1-84996-071-7.

Richter, Michael, Sebastian Zinser, and Herbert Kabza (Oct. 2012). "Comparison of eco and time efficient routing of ICEVs, BEVs and PHEVs in inner city traffic". In: *2012 IEEE Vehicle Power and Propulsion Conference*. IEEE, pp. 1165–1169. ISBN: 978-1-4673-0954-7. DOI: 10.1109/VPPC.2012.6422511. URL: http://ieeexplore.ieee.org/document/6422511/.

Richter, S. and R. de Carlo (June 1983). "Continuation methods: Theory and applications". In: *IEEE Transactions on Circuits and Systems* 30.6, pp. 347–352. ISSN: 0098-4094. DOI: 10.1109/TCS.1983.1085373. URL: http://ieeexplore.ieee.org/document/1085373/.

Rommerskirchen, Christoph P., Magnus Helmbrecht, and Klaus J. Bengler (Jan. 2014). "The Impact of an Anticipatory Eco-Driver Assistant System in Different Complex Driving Situations on the Driver Behavior". In: *IEEE Intelligent Transportation Systems Magazine* 6.2, pp. 45–56. ISSN: 1939-1390. DOI: 10.1109/MITS.2014.2307078. URL: http://ieeexplore.ieee.org/lpdocs/epic03/wrapper.htm?arnumber=6803955.

Roth, M., T. Radke, M. Lederer, F. Gauterin, M. Frey, C. Steinbrecher, J. Schröter, and M Goslar (2011). "Porsche InnoDrive - An Innovative Approach for the Future of Driving". In: *20th Aachen Colloquium Automobile and Engine Technology*. Aachen, Germany, pp. 1453–1467.

Rouzikhah, Hossein, Mark King, and Andry Rakotonirainy (Jan. 2013). "Examining the effects of an eco-driving message on driver distraction". In: *Accident Analysis & Prevention* 50.June. Ed. by Intergovernmental Panel on Climate Change, pp. 975–983. ISSN: 00014575. DOI: 10.1016/j.aap.2012.07.024. arXiv: arXiv:1011.1669v3. URL: http://linkinghub.elsevier.com/retrieve/pii/S0001457512002862.

SAE International (2013). *Taxonomy and Definitions for Terms Related to On-Road Motor Vehicle Automated Driving Systems*. Tech. rep. On-Road Automated Vehicle Standards Committee, p. 12. URL: http://standards.sae.org/wip/j3016/.

Sajadi-Alamdari, S. Amin, Holger Voos, and Mohamed Darouach (June 2016). "Nonlinear model predictive extended eco-cruise control for battery electric vehicles". In: *2016 24th Mediterranean Conference on Control and Automation (MED)*. 7041503. IEEE, pp. 467–472. ISBN: 978-1-4673-8345-5. DOI: 10.1109/MED.2016.7535929. URL: http://ieeexplore.ieee.org/document/7535929/.

Sajadi-Alamdari, Seyed Amin, Holger Voos, and Mohamed Darouach (June 2017a). "Fast stochastic non-linear model predictive control for electric vehicle advanced driver assistance systems". In: *2017 IEEE International Conference on Vehicular Electronics and Safety (ICVES)*. IEEE, pp. 91–96. ISBN: 978-1-5090-5677-4. DOI: 10.1109/ICVES.2017.7991907. URL: http://ieeexplore.ieee.org/document/7991907/.

Sajadi-Alamdari, Seyed Amin, Holger Voos, and Mohamed Darouach (July 2017b). "Risk-averse Stochastic Nonlinear Model Predictive Control for Real-time Safety-critical Systems". In: *IFAC-PapersOnLine* 50.1, pp. 5991–5997. ISSN: 24058963. DOI: 10.1016/j.ifacol.2017.08.1431. URL: http://linkinghub.elsevier.com/retrieve/pii/S2405896317319973.

Sajadi-Alamdari, Seyed Amin, Holger Voos, and Mohamed Darouach (2018). "Deadzone-Quadratic Penalty Function for Predictive Extended Cruise Control with Experimental Validation". In: *ROBOT 2017: Third Iberian Robotics Conference*. Ed. by Anibal Ollero, Alberto Sanfeliu, Luis Montano, Nuno Lau, and Carlos Cardeira. Cham: Springer International Publishing, pp. 446–459. ISBN: 978-3-319-70836-2. DOI: 10.1007/978-3-319-70836-2_37.

Scania (2011). *Scania Active Prediction*. Tech. rep. Scania, p. 17. URL: http://www.scania.com.mm/trucks/safety-driver-support/driver-support-systems/active-prediction/.

Schaltz, Erik (Sept. 2011). "Electrical Vehicle Design and Modeling". In: *Electric Vehicles - Modelling and Simulations*. InTech, pp. 1–24. DOI: 10.5772/20271. URL: http://www.intechopen.com/books/electric-vehicles-modelling-and-simulations/electrical-vehicle-design-and-modeling.

Schmied, Roman, Harald Waschl, Rien Quirynen, Moritz Diehl, and Luigi del Re (2015). "Nonlinear MPC for Emission Efficient Cooperative Adaptive Cruise Control". In: *IFAC-PapersOnLine* 48.23, pp. 160–165. ISSN: 24058963. DOI: 10.1016/j.ifacol.2015.11.277. URL: http://linkinghub.elsevier.com/retrieve/pii/S2405896315025616.

Schroeder (2016). *Centre de Formation pour Conducteurs S.A.* URL: www.schroeder.lu (visited on 12/21/2016).

Schwickart, T., H. Voos, J.-R. Hadji-Minaglou, M. Darouach, and A. Rosich (Feb. 2015). "Design and simulation of a real-time implementable energy-efficient model-predictive cruise controller for electric vehicles". In: *Journal of the Franklin Institute* 352.2, pp. 603–625. ISSN: 00160032. DOI: 10.1016/j.jfranklin.2014.07.001. URL: http://linkinghub.elsevier.com/retrieve/pii/S0016003214001926.

Schwickart, Tim (2015). "Energy-Efficient Driver Assistance System for Electric Vehicle Using Model Predictive Control". PhD thesis. University of Luxembourg, p. 211. URL: https://orbilu.uni.lu/handle/10993/23467.

Schwickart, Tim, Holger Voos, and Mohamed Darouach (Oct. 2014). "A real-time implementable model-predictive cruise controller for electric vehicles and energy-efficient driving". In: *2014 IEEE Conference on Control Applications (CCA)*. Section IV. IEEE, pp. 617–622. ISBN: 978-1-4799-7409-2. DOI: 10.1109/CCA.2014.6981408. URL: http://ieeexplore.ieee.org/lpdocs/epic03/wrapper.htm?arnumber=6981408.

Schwickart, Tim, Holger Voos, Jean-Régis Hadji-Minaglou, and Mohamed Darouach (Jan. 2016). "A Fast Model-Predictive Speed Controller for Minimised Charge Consumption of Electric Vehicles". In: *Asian Journal of Control* 18.1, pp. 133–149. ISSN:

15618625. DOI: 10.1002/asjc.1251. URL: http://doi.wiley.com/10.1002/asjc.1251.

Sciarretta, Antonio, Giovanni De Nunzio, and Luis Leon Ojeda (Oct. 2015). "Optimal Ecodriving Control: Energy-Efficient Driving of Road Vehicles as an Optimal Control Problem". In: *IEEE Control Systems* 35.5, pp. 71–90. ISSN: 1066-033X. DOI: 10.1109/MCS.2015.2449688. URL: http://ieeexplore.ieee.org/lpdocs/epic03/wrapper.htm?arnumber=7265166.

Seaman, Aden, Thanh-Son Dao, and John McPhee (June 2014). "A survey of mathematics-based equivalent-circuit and electrochemical battery models for hybrid and electric vehicle simulation". In: *Journal of Power Sources* 256, pp. 410–423. ISSN: 03787753. DOI: 10.1016/j.jpowsour.2014.01.057. URL: http://linkinghub.elsevier.com/retrieve/pii/S0378775314000810.

Seki, Y., J. Ohya, and M. Miyoshi (1999). "Collision avoidance system for vehicles applying model predictive control theory". In: *Proceedings 199 IEEE/IEEJ/JSAI International Conference on Intelligent Transportation Systems (Cat. No.99TH8383)*. IEEE, pp. 453–458. ISBN: 0-7803-4975-X. DOI: 10.1109/ITSC.1999.821100. URL: http://ieeexplore.ieee.org/document/821100/.

Shakouri, Payman and Andrzej Ordys (May 2014). "Nonlinear Model Predictive Control approach in design of Adaptive Cruise Control with automated switching to cruise control". In: *Control Engineering Practice* 26.1, pp. 160–177. ISSN: 09670661. DOI: 10.1016/j.conengprac.2014.01.016. URL: http://linkinghub.elsevier.com/retrieve/pii/S096706611400046X.

Shakouri, Payman, Andrzej Ordys, and Mohamad R Askari (Sept. 2012). "Adaptive cruise control with stop&go function using the state-dependent nonlinear model predictive control approach". In: *ISA Transactions* 51.5, pp. 622–631. ISSN: 00190578. DOI: 10.1016/j.isatra.2012.05.001. URL: http://linkinghub.elsevier.com/retrieve/pii/S0019057812000742.

Shao, Yunli and Zongxuan Sun (May 2017). "Robust eco-cooperative adaptive cruise control with gear shifting". In: *2017 American Control Conference (ACC)*. IEEE, pp. 4958–4963. ISBN: 978-1-5090-5992-8. DOI: 10.23919/ACC.2017.7963723. URL: http://ieeexplore.ieee.org/document/7963723/.

Shengbo Li, Keqiang Li, Jianqiang Wang, Lei Zhang, Xiaomin Lian, Hiroshi Ukawa, and Dongsheng Bai (Sept. 2008). "MPC based vehicular following control considering both fuel economy and tracking capability". In: *2008 IEEE Vehicle Power and Propulsion Conference*. March. IEEE, pp. 1–6. ISBN: 978-1-4244-1848-0. DOI: 10.1109/VPPC.2008.4677689. URL: http://ieeexplore.ieee.org/document/4677689/.

Shimizu, Yuichi, Toshiyuki Ohtsuka, and Moritz Diehl (May 2009). "A real-time algorithm for nonlinear receding horizon control using multiple shooting and continuation/krylov method". In: *International Journal of Robust and Nonlinear Control* 19.8, pp. 919–936. ISSN: 10498923. DOI: 10.1002/rnc.1363. URL: http://doi.wiley.com/10.1002/rnc.1363.

Shladover, S.E., C.A. Desoer, J.K. Hedrick, M. Tomizuka, J. Walrand, W.-B. Zhang, D.H. McMahon, H. Peng, S. Sheikholeslam, and N. McKeown (Feb. 1991). "Automated vehicle control developments in the PATH program". In: *IEEE Transactions on Vehicular Technology* 40.1, pp. 114–130. ISSN: 0018-9545. DOI: 10.1109/25.69979. URL: http://ieeexplore.ieee.org/lpdocs/epic03/wrapper.htm?arnumber=69979.

Shuyou Yu, Christoph Bohm, Hong Chen, and Frank Allgower (June 2010). "Robust model predictive control with disturbance invariant sets". In: *Proceedings of the 2010 American Control Conference*. 14. IEEE, pp. 6262–6267. ISBN: 978-1-4244-7427-1. DOI: 10.1109/ACC.2010.5531520. URL: http://ieeexplore.ieee.org/document/5531520/.

Sivak, Michael and Brandon Schoettle (July 2012). "Eco-driving: Strategic, tactical, and operational decisions of the driver that influence vehicle fuel economy". In: *Transport Policy* 22, pp. 96–99. ISSN: 0967070X. DOI: 10.1016/j.tranpol.2012.05.010. URL: http://linkinghub.elsevier.com/retrieve/pii/S0967070X12000807.

Sivaraman, Sayanan and Mohan Manubhai Trivedi (Dec. 2013). "Looking at Vehicles on the Road: A Survey of Vision-Based Vehicle Detection, Tracking, and Behavior Analysis". In: *IEEE Transactions on Intelligent Transportation Systems* 14.4, pp. 1773–1795. ISSN: 1524-9050. DOI: 10.1109/TITS.2013.2266661. URL: http://ieeexplore.ieee.org/lpdocs/epic03/wrapper.htm?arnumber=6563169.

*Smart Automobile* (2016). URL: https://www.smart.com (visited on 02/01/2016).

Smart Automobile (2015). *Smart Fortwo Electric Drive Specifications Brochure*. URL: http://www.smartusa.com/resources/doc/2015-smart-electric-drive-brochure.pdf (visited on 03/12/2016).

Smith, Bryant Walker (2013). *SAE Levels of Driving Automation*. URL: http://cyberlaw.stanford.edu/blog/2013/12/sae-levels-driving-automation (visited on 03/30/2016).

Stanger, Thomas and Luigi del Re (June 2013). "A model predictive Cooperative Adaptive Cruise Control approach". In: *2013 American Control Conference*. IEEE, pp. 1374–1379. ISBN: 978-1-4799-0178-4. DOI: 10.1109/ACC.2013.6580028. URL: http://ieeexplore.ieee.org/document/6580028/.

Stanislas, Leo and Thierry Peynot (2015). "Characterisation of the Delphi Electronically Scanning Radar for robotics applications". In: *Australasian Conference on Robotics and Automation (ACRA 2015)*. Canberra, A.C.T, p. 10. URL: http://www.araa.asn.au/acra/acra2015/papers/pap167.pdf.

Tajeddin, Sadegh and Nasser L Azad (May 2017). "Ecological Cruise Control of a Plug-in Hybrid Electric Vehicle: A comparison of different GMRES-based Nonlinear Model Predictive Controls". In: *2017 American Control Conference (ACC)*. IEEE, pp. 3607–3612. ISBN: 978-1-5090-5992-8. DOI: 10.23919/ACC.2017.7963505. URL: http://ieeexplore.ieee.org/document/7963505/.

Tang, Jingyong, Li Dong, Jinchuan Zhou, and Liang Fang (Apr. 2013). "A smoothing Newton method for nonlinear complementarity problems". In: *Computational and Applied Mathematics* 32.1, pp. 107–118. ISSN: 0101-8205. DOI: 10.1007/s40314-013-0015-9. URL: http://link.springer.com/10.1007/s40314-013-0015-9.

Thomas, Julian, Kai Stiens, Sebastian Rauch, and Raul Rojas (June 2015). "Grid-based online road model estimation for advanced driver assistance systems". In: *2015 IEEE Intelligent Vehicles Symposium (IV)*. Vol. 2015-Augus. Iv. IEEE, pp. 71–76. ISBN: 978-1-4673-7266-4. DOI: 10.1109/IVS.2015.7225665. URL: http://ieeexplore.ieee.org/document/7225665/.

Thrun, Sebastian (Apr. 2010). "Toward Robotic Cars". In: *Commun. ACM* 53.4, pp. 99–106. ISSN: 0001-0782. DOI: 10.1145/1721654.1721679. URL: http://doi.acm.org/10.1145/1721654.1721679.

Tokoro, S., K. Kuroda, A. Kawakubo, K. Fujita, and H. Fujinami (2003). "Electronically scanned millimeter-wave radar for pre-crash safety and adaptive cruise control system". In: *IEEE IV2003 Intelligent Vehicles Symposium. Proceedings (Cat. No.03TH8683)*. IEEE, pp. 304–309. ISBN: 0-7803-7848-2. DOI: 10.1109/IVS.2003.1212927. URL: http://ieeexplore.ieee.org/lpdocs/epic03/wrapper.htm?arnumber=1212927.

Tremblay, Olivier and Louis A. Dessaint (2009). "Experimental validation of a battery dynamic model for EV applications". In: *World Electric Vehicle Journal* 3.1, pp. 1–10. ISSN: 20326653. URL: http://www.evs24.org/wevajournal/php/download.php?f=vol3/WEVJ3-2230080.pdf.

Tsai, Huai-Yin and Jein-Shan Chen (June 2014). "Geometric views of the generalized Fischer–Burmeister function and its induced merit function". In: *Applied Mathematics and Computation* 237.November, pp. 31–59. ISSN: 00963003. DOI: 10.1016/j.amc.2014.03.089. URL: http://linkinghub.elsevier.com/retrieve/pii/S0096300314004512.

Turne, Daniel S., Jr. Peter M. Briglia, and Kay Fitzpatrick (2011). *Modeling Operating Speed: Synthesis Report*. Tech. rep. July. Washington, DC, p. 136. URL: http://onlinepubs.trb.org/onlinepubs/circulars/ec151.pdf.

Ulsoy, A. Galip, Huei Peng, and Melih Cakmakci (2012). *Automotive Control Systems*. Cambridge: Cambridge University Press. ISBN: 9780511844577. DOI: 10.1017/CBO9780511844577. URL: http://ebooks.cambridge.org/ref/id/CBO9780511844577.

Vahidi, a. and A. Eskandarian (Sept. 2003). "Research advances in intelligent collision avoidance and adaptive cruise control". In: *IEEE Transactions on Intelligent Transportation Systems* 4.3, pp. 143–153. ISSN: 1524-9050. DOI: 10.1109/TITS.2003.821292. URL: http://ieeexplore.ieee.org/lpdocs/epic03/wrapper.htm?arnumber=1255576.

Vajedi, Mahyar and Nasser L. Azad (Jan. 2016). "Ecological Adaptive Cruise Controller for Plug-In Hybrid Electric Vehicles Using Nonlinear Model Predictive Control". In: *IEEE Transactions on Intelligent Transportation Systems* 17.1, pp. 113–122. ISSN: 1524-9050. DOI: 10.1109/TITS.2015.2462843. URL: http://ieeexplore.ieee.org/document/7225178/.

Veldman, Else and Remco A. Verzijlbergh (Jan. 2015). "Distribution Grid Impacts of Smart Electric Vehicle Charging From Different Perspectives". In: *IEEE Transactions on Smart Grid* 6.1, pp. 333–342. ISSN: 1949-3053. DOI: 10.1109/TSG.2014.2355494. URL: http://ieeexplore.ieee.org/lpdocs/epic03/wrapper.htm?arnumber=6905855.

Viti, Francesco, Serge P. Hoogendoorn, Tom P. Alkim, and Gerben Bootsma (June 2008). "Driving behavior interaction with ACC: results from a Field Operational Test in the Netherlands". In: *2008 IEEE Intelligent Vehicles Symposium*. IEEE, pp. 745–750. ISBN: 978-1-4244-2568-6. DOI: 10.1109/IVS.2008.4621199. URL: http://ieeexplore.ieee.org/lpdocs/epic03/wrapper.htm?arnumber=4621199.

Vitus, M.P., C.J. Tomlin, S.P. Boyd, S.M. Rock, Stanford University. Department of Aeronautics, and Astronautics (2012). *Stochastic Control Via Chance Constrained Optimization and Its Application to Unmanned Aerial Vehicles*. URL: https://books.google.lu/books?id=1wgungAACAAJ.

Wang, Jiquan, Igo Besselink, and Henk Nijmeijer (2015). "Electric vehicle energy consumption modelling and prediction based on road information". In: *EVS28 International Electric Vehicle Symposium and Exhibition*, pp. 1–12. URL: http://repository.tue.nl/dbdc9296-2437-4a58-aac0-2c98f6b122e7.

Wang, Junmin and Rajesh Rajamani (Sept. 2004). "Should Adaptive Cruise-Control Systems be Designed to Maintain a Constant Time Gap Between Vehicles?" In: *IEEE Transactions on Vehicular Technology* 53.5, pp. 1480–1490. ISSN: 0018-9545. DOI: 10.1109/TVT.2004.832386. URL: http://ieeexplore.ieee.org/lpdocs/epic03/wrapper.htm?arnumber=1337326.

Wang, M., W. Daamen, S.P. Hoogendoorn, and B. van Arem (Sept. 2012). "Driver assistance systems modeling by model predictive control". In: *2012 15th International IEEE Conference on Intelligent Transportation Systems*. December. IEEE, pp. 1543–1548. ISBN: 978-1-4673-3063-3. DOI: 10.1109/ITSC.2012.6338824. URL: http://ieeexplore.ieee.org/document/6338824/.

Wang, M., S. P. Hoogendoorn, W. Daamen, B. van Arem, B. Shyrokau, and R. Happee (Dec. 2016). "Delay-compensating strategy to enhance string stability of adaptive cruise controlled vehicles". In: *Transportmetrica B: Transport Dynamics* 0.0, pp. 1–19. ISSN: 2168-0566. DOI: 10.1080/21680566.2016.1266973. URL: https://www.tandfonline.com/doi/full/10.1080/21680566.2016.1266973.

Wang, Meng, Winnie Daamen, Serge P. Hoogendoorn, and Bart van Arem (Mar. 2014). "Rolling horizon control framework for driver assistance systems. Part I: Mathematical formulation and non-cooperative systems". In: *Transportation Research Part C: Emerging Technologies* 40, pp. 271–289. ISSN: 0968090X. DOI: 10.1016/j.trc.2013.11.023. URL: http://linkinghub.elsevier.com/retrieve/pii/S0968090X13002593.

Wang, Meng, Serge Hoogendoorn, Winnie Daamen, and Bart van Arem (Mar. 2014). "Potential impacts of ecological adaptive cruise control systems on traffic and environment". In: *IET Intelligent Transport Systems* 8.2, pp. 77–86. ISSN: 1751-956X. DOI: 10.1049/iet-its.2012.0069. URL: http://digital-library.theiet.org/content/journals/10.1049/iet-its.2012.0069.

Wang, Wenshuo, Junqiang Xi, and Huiyan Chen (2014). "Modeling and Recognizing Driver Behavior Based on Driving Data: A Survey". In: *Mathematical Problems in Engineering* 2014, pp. 1–20. ISSN: 1024-123X. DOI: 10.1155/2014/245641. URL: https://www.hindawi.com/journals/mpe/2014/245641/.

Watkins, Simon and Gioacchino Vino (June 2008). "The effect of vehicle spacing on the aerodynamics of a representative car shape". In: *Journal of Wind Engineering and Industrial Aerodynamics* 96.6-7, pp. 1232–1239. ISSN: 01676105. DOI: 10.1016/j.jweia.2007.06.042. URL: http://linkinghub.elsevier.com/retrieve/pii/S0167610507001687.

Weber, Marc (2014). *Where to? A History of Autonomous Vehicles*. URL: http://www.computerhistory.org/atchm/where-to-a-history-of-autonomous-vehicles/ (visited on 04/07/2016).

Whittle, P. and J. Kuhn (Jan. 1986). "A hamiltonian formulation of risk-sensitive Linear/quadratic/gaussian control". In: *International Journal of Control* 43.1, pp. 1–12. ISSN: 0020-7179. DOI: 10.1080/00207178608933445. URL: http://www.tandfonline.com/doi/abs/10.1080/00207178608933445.

Widmann, Glenn R., Michele K. Daniels, Lisa Hamilton, Lawrence Humm, Bryan Riley, Jan K. Schiffmann, David E. Schnelker, and William H. Wishon (Mar. 2000). "Comparison of Lidar-Based and Radar-Based Adaptive Cruise Control Systems". In: *SAE, Society of Automotive Engineers*. Vol. 109. 724, pp. 126–139. DOI: 10.4271/2000-01-0345. URL: http://papers.sae.org/2000-01-0345/.

Willow Garage (2017). *ROS: Robot Operating System*. URL: http://www.ros.org/.

Winter, Joost C.F. de, Riender Happee, Marieke H. Martens, and Neville A. Stanton (Nov. 2014). "Effects of adaptive cruise control and highly automated driving on workload and situation awareness: A review of the empirical evidence". In: *Transportation Research Part F: Traffic Psychology and Behaviour* 27.PB, pp. 196–217. ISSN: 13698478. DOI: 10.1016/j.trf.2014.06.016. URL: http://linkinghub.elsevier.com/retrieve/pii/S1369847814000904.

Worthmann, Karl, Mohamed W. Mehrez, George K.I. Mann, Raymond G. Gosine, and Jürgen Pannek (Aug. 2017). "Interaction of open and closed loop control in MPC". In: *Automatica* 82, pp. 243–250. ISSN: 00051098. DOI: 10.1016/j.automatica.2017.04.038. URL: http://linkinghub.elsevier.com/retrieve/pii/S0005109817302327.

Wu, Yuqing and Linda Ng Boyle (Aug. 2015). "Drivers' engagement level in Adaptive Cruise Control while distracted or impaired". In: *Transportation Research Part F: Traffic Psychology and Behaviour* 33, pp. 7–15. ISSN: 13698478. DOI: 10.1016/j.trf.2015.05.005. URL: http://linkinghub.elsevier.com/retrieve/pii/S1369847815000881.

Würth, Lynn, James B Rawlings, and Wolfgang Marquardt (2009). "Economic Dynamic Real-Time Optimization and Nonlinear Model-Predictive Control on Infinite Horizons". In: *IFAC Proceedings Volumes* 42.11, pp. 219–224. ISSN: 14746670. DOI: 10.3182/20090712-4-TR-2008.00033. URL: http://linkinghub.elsevier.com/retrieve/pii/S1474667015302767.

Xinkai Wu, Xiaozheng He, Guizhen Yu, Arek Harmandayan, and Yunpeng Wang (Oct. 2015). "Energy-Optimal Speed Control for Electric Vehicles on Signalized Arterials". In: *IEEE Transactions on Intelligent Transportation Systems* 16.5, pp. 2786–2796.

ISSN: 1524-9050. DOI: `10.1109/TITS.2015.2422778`. URL: `http://ieeexplore.ieee.org/lpdocs/epic03/wrapper.htm?arnumber=7097732`.

Xiong, Huimin and Linda Ng Boyle (Sept. 2012). "Drivers' Adaptation to Adaptive Cruise Control: Examination of Automatic and Manual Braking". In: *IEEE Transactions on Intelligent Transportation Systems* 13.3, pp. 1468–1473. ISSN: 1524-9050. DOI: `10.1109/TITS.2012.2192730`. URL: `http://ieeexplore.ieee.org/lpdocs/epic03/wrapper.htm?arnumber=6191353`.

Yamaguchi, Daisuke, M.A.S. Kamal, Masakazu Mukai, and Taketoshi Kawabe (2012). "Model Predictive Control for Automobile Ecological Driving Using Traffic Signal Information". In: *Journal of System Design and Dynamics* 6.3, pp. 297–309. ISSN: 1881-3046. DOI: `10.1299/jsdd.6.297`. URL: `http://japanlinkcenter.org/DN/JST.JSTAGE/jsdd/6.297?lang=en%7B%5C&%7Dfrom=CrossRef%7B%5C&%7Dtype=abstract`.

Yan, Xinping, Rui Zhang, Jie Ma, and Yulin Ma (2013). "Considering Variable Road Geometry in Adaptive Vehicle Speed Control". In: *Mathematical Problems in Engineering* 2013, pp. 1–12. ISSN: 1024-123X. DOI: `10.1155/2013/617879`. URL: `http://www.hindawi.com/journals/mpe/2013/617879/`.

Yang, Shichun, Cheng Deng, Tieqiao Tang, and Yongsheng Qian (Jan. 2013). "Electric vehicle's energy consumption of car-following models". In: *Nonlinear Dynamics* 71.1-2, pp. 323–329. ISSN: 0924-090X. DOI: `10.1007/s11071-012-0663-0`. URL: `http://link.springer.com/10.1007/s11071-012-0663-0`.

Yang, Xiaoke and Jan Maciejowski (2015). "Risk-Sensitive Model Predictive Control with Gaussian Process Models". In: *IFAC-PapersOnLine*. Vol. 48. 28. Elsevier B.V., pp. 374–379. DOI: `10.1016/j.ifacol.2015.12.156`. URL: `http://linkinghub.elsevier.com/retrieve/pii/S2405896315027809`.

Yong, Jia Ying, Vigna K Ramachandaramurthy, Kang Miao Tan, and N Mithulananthan (Sept. 2015). "A review on the state-of-the-art technologies of electric vehicle, its impacts and prospects". In: *Renewable and Sustainable Energy Reviews* 49, pp. 365–385. ISSN: 13640321. DOI: `10.1016/j.rser.2015.04.130`. URL: `http://linkinghub.elsevier.com/retrieve/pii/S1364032115004001`.

Yu, Kaijiang and Junqi Yang (2014). "Performance of a Nonlinear Real-Time Optimal Control System for HEVs/PHEVs during Car Following". In: *Journal of Applied Mathematics* 2014.1, pp. 1–14. ISSN: 1110-757X. DOI: `10.1155/2014/879232`. URL: `http://www.hindawi.com/journals/jam/2014/879232/`.

Zhang, Rui and Enjian Yao (Dec. 2015). "Electric vehicles' energy consumption estimation with real driving condition data". In: *Transportation Research Part D: Transport*

*and Environment* 41, pp. 177–187. ISSN: 13619209. DOI: `10.1016/j.trd.2015.10.010`. URL: `http://linkinghub.elsevier.com/retrieve/pii/S1361920915001625`.

Zhang, Xiaojing, Sergio Grammatico, Kostas Margellos, Paul Goulart, and John Lygeros (2014). "Randomized Nonlinear MPC for Uncertain Control-Affine Systems with Bounded Closed-Loop Constraint Violations". In: *IFAC Proceedings Volumes* 47.3, pp. 1649–1654. ISSN: 14746670. DOI: `10.3182/20140824-6-ZA-1003.02436`. URL: `http://linkinghub.elsevier.com/retrieve/pii/S1474667016418495`.

Zhao, Dongbin, Zhaohui Hu, Zhongpu Xia, Cesare Alippi, Yuanheng Zhu, and Ding Wang (Feb. 2014). "Full-range adaptive cruise control based on supervised adaptive dynamic programming". In: *Neurocomputing* 125, pp. 57–67. ISSN: 09252312. DOI: `10.1016/j.neucom.2012.09.034`. URL: `http://linkinghub.elsevier.com/retrieve/pii/S0925231213001422`.

Zhao, Dongbin, Bin Wang, and Derong Liu (Nov. 2013). "A supervised Actor–Critic approach for adaptive cruise control". In: *Soft Computing* 17.11, pp. 2089–2099. ISSN: 1432-7643. DOI: `10.1007/s00500-013-1110-y`. URL: `http://link.springer.com/10.1007/s00500-013-1110-y`.

Zhou, Jing and Huei Peng (June 2005). "Range Policy of Adaptive Cruise Control Vehicles for Improved Flow Stability and String Stability". In: *IEEE Transactions on Intelligent Transportation Systems* 6.2, pp. 229–237. ISSN: 1524-9050. DOI: `10.1109/TITS.2005.848359`. URL: `http://ieeexplore.ieee.org/lpdocs/epic03/wrapper.htm?arnumber=1438390`.

Zhou, Yang, Soyoung Ahn, Madhav Chitturi, and David A. Noyce (Oct. 2017). "Rolling horizon stochastic optimal control strategy for ACC and CACC under uncertainty". In: *Transportation Research Part C: Emerging Technologies* 83, pp. 61–76. ISSN: 0968090X. DOI: `10.1016/j.trc.2017.07.011`. URL: `http://linkinghub.elsevier.com/retrieve/pii/S0968090X17301997`.